

Lessons from the zebrafish

How to regenerate a heart

Dennis Eduard Maria de Bakker

Cover

Ward Groutars

Lay-Out

Ilse Modder | www.ilsemodder.nl

Printed by

Gildeprint, Enschede | www.gildeprint.nl

ISBN:

978-94-6419-341-1



© D.E.M. de Bakker, 2021

All rights reserved. No part of this thesis may be multiplied and/or published by means of print, photocopy, and microfilm or otherwise, without explicit permission of the author.

Lessons from the zebrafish: How to regenerate a heart

Lessen van de zebravis: Hoe regeneer je een hart

(met een samenvatting in het Nederlands)

Proefschrift

ter verkrijging van de graad van doctor aan de
Universiteit Utrecht
op gezag van de
rector magnificus, prof.dr. H.R.B.M. Kummeling,
ingevolge het besluit van het college voor promoties
in het openbaar te verdedigen op

donderdag 11 november 2021 des middags te 2.15 uur

door

Dennis Eduard Maria de Bakker

geboren op 4 juni 1991
te Middelburg

Promotor:

Prof. dr. J.P.W.M. Bakkers

Dit proefschrift werd (mede) mogelijk gemaakt met financiële steun van de Nederlandse Hartstichting als onderdeel van het COBRA3 consortium (NHS 2013T091).

Lessons from the zebrafish

How to regenerate a heart

Dennis Eduard Maria de Bakker

Promotor:

Prof. dr. Jeroen Bakkers

Hubrecht institute

Examination Committee:

Prof. dr. Wouter de Laat

Hubrecht institute

Prof. dr. Eva van Rooij

Hubrecht institute

Prof. dr. Jeroen den Hertog

Hubrecht institute

Prof. dr. Sander J.L van den Heuvel

Utrecht University

Prof. dr. Vincent Christoffels

AMC-UvA

The work described in this thesis was performed at the Hubrecht Institute for Developmental Biology and Stem Cell Research (the Royal Netherlands Academy of Arts and Sciences, KNAW) within the framework of the research school Cancer Stem cells & Developmental biology (CS&D), which is part of the Utrecht Graduate School of Life Sciences (Utrecht University). The work was funded by the Dutch heart foundation as part of the COBRA3 consortium (NHS 2013T091). Financial support by the Dutch Heart Foundation for the publication of this thesis is gratefully acknowledged.



CONTENTS

Summary		10
Samenvatting		12
Thesis outline		14
Chapter I	Introduction - Cardiac regenerative capacity: an evolutionary afterthought?	17
Chapter II	Single-cell analysis uncovers that metabolic reprogramming by ErbB2 signaling is essential for cardiomyocyte proliferation in the regenerating heart	45
Chapter III	Conserved NPPB+ border zone switches from MEF2- to AP-1–driven gene program	83
Chapter IV	Interspecies comparison reveals Hmga1 as a driver of cardiac regeneration	133
Chapter V	Prrx1b restricts fibrosis and promotes Nrg1-dependent cardiomyocyte proliferation during zebrafish heart regeneration	171
Chapter VI	Discussion	203
Appendices	Acknowledgements	216
	Curriculum vitae	224
	Publication list	226

SUMMARY

The human heart loses millions of cardiomyocytes after an ischemic injury but is unable to regenerate the lost tissue. In contrast, the injured zebrafish heart efficiently regenerates lost cardiomyocytes. During my PhD project in the lab of Jeroen Bakkers at the Hubrecht Institute (Utrecht), I investigated why the zebrafish heart can regenerate while the mammalian heart cannot, in order to identify novel factors that can be targeted to help regenerate the mammalian heart.

In this thesis, we first introduce the topic of heart regeneration by summarizing the most current literature of the field, as well as frame the regenerative capacity of the heart in an evolutionary context. We also touch upon the importance of the injury border zone during heart regeneration, which forms the source of the newly regenerated cardiomyocytes in the injured zebrafish heart. In contrast, the injury border zone of mice and humans does not efficiently yield newly formed cardiomyocytes, limiting the regenerative capacity of the mammalian heart. Therefore, to investigate this striking difference between the regenerative capacity of the zebrafish and mouse heart, we first characterized the processes that occur in the border zones of these species.

We characterized the regenerative zebrafish border zone using a single-cell-RNA-sequencing (scRNAseq) approach on sorted border zone cardiomyocytes. Through bioinformatical and histological analyses, we show that zebrafish border zone cardiomyocytes dedifferentiate to resemble an embryonic-like state. This includes metabolic reprogramming, which we show is vital to cardiomyocyte proliferation. Next, we characterized the non-regenerative mammalian border zone using RNA-sequencing and ATAC-sequencing. We found that mammalian border zone cardiomyocytes do not completely dedifferentiate back to an embryonic state, but instead replace a muscle-restricted gene program with a stress responsive program.

Next, we made a direct transcriptomic comparison between the zebrafish and mouse border zones using TOMO-sequencing to identify overlapping and species specific gene programs. We hypothesized that homologous-gene pairs showing upregulation in the zebrafish but not the mouse border zone could help explain the robust regenerative capacity of the zebrafish heart. To test this hypothesis, we created knock-out mutant lines for several of these genes through CRISPR/Cas9-mediated mutagenesis. Two of the four investigated knock-out lines, targeting the genes *hmga1a* or *prrx1b*, show a robust regeneration defect. This includes a lack of cardiomyocyte proliferation and permanent scar formation.

We show that the chromatin remodeler Hmga1a is important for cardiomyocyte proliferation in the injured zebrafish heart by initiating a broad gene program including chromatin

reorganization in cardiomyocytes. Furthermore, we found that overexpression of Hmga1a in zebrafish and mammalian cardiomyocytes stimulates cell cycle re-entry, both *in vivo* and *in vitro*.

In addition, we show that the transcription factor Prrx1b acts in epicardial (derived) cells. Using a combination of lineage tracing and scRNAseq, we identified that Prrx1b restricts fibrosis and promotes Nrg1-dependent cardiomyocyte proliferation during zebrafish heart regeneration.

Taken together, in this thesis we have characterized the zebrafish and mammalian injury border zone in detail, found key regulators of zebrafish heart regeneration and identified a novel factor that could be used to help stimulate heart regeneration in mammalian hearts.

SAMENVATTING

Het humane hart verliest miljoenen hartspiercellen na een ischemische beschadiging maar is niet in staat het verloren weefsel te regenereren. Het zebravis hart kan zich daarentegen wel efficiënt regenereren na schade. Tijdens mijn PhD project in de groep van Jeroen Bakkers in het Hubrecht Instituut (Utrecht) heb ik onderzocht waarom het zebravis hart kan regenereren terwijl het zoogdier hart dit niet kan, om zo nieuwe manieren te vinden om hart regeneratie te stimuleren in zoogdieren.

In deze thesis introduceren we eerst het onderwerp hart regeneratie door een samenvatting te geven van de meest recente literatuur uit het veld en door hart regeneratie te beschrijven in de context van evolutie. We beschrijven hierbij ook het belang van de regio in het hart grenzend aan de beschadiging, de zogeheten border zone, die de bron vormt van de nieuwe hartspiercellen in het beschadigde zebravis hart. In de border zone van muizen en mensen worden nauwelijks nieuwe hartspiercellen geproduceerd, wat het regeneratieve vermogen van het zoogdierhart limiteert. Om het opvallende verschil in regeneratief vermogen tussen het zebravis en muis hart te bestuderen, hebben we eerst de processen gekarakteriseerd die plaatsvinden in de border zones van deze soorten.

We hebben de regeneratieve border zone gekarakteriseerd door single-cell-RNA-sequencing (scRNAseq) technologie toe te passen op gesorteerde border zone hartspiercellen. Door middel van bioinformatische en histologische analyses hebben we laten zien dat hartspiercellen in de zebravis border zone dedifferentiëren richting een embryonale staat. Deze dedifferentiatie includeert de herprogrammering van het metabolisme en we laten zien dat deze herprogrammering van vitaal belang is voor de efficiënte celdeling van hartspiercellen. Vervolgens hebben we de niet-regeneratieve border zone van de muis gekarakteriseerd met behulp van RNA- en ATAC-sequencing. Hiermee hebben wij aangetoond dat zoogdier border zone hartspiercellen niet compleet dedifferentiëren naar een embryonale staat, maar in plaats daarvan een spier specifiek gen programma vervangen door een stress-responsief programma.

Vervolgens hebben we TOMO-sequencing gebruikt om een directe vergelijking te maken tussen het transcriptoom van de zebravis en muis border zones, om zo overlappende en soort specifieke gen-programma's te identificeren. Onze hypothese was dat de homologe gen-paren die toegenomen expressie laten zien in de zebravis maar niet de muis border zone, het robuuste regeneratieve vermogen van het zebravis hart kunnen helpen verklaren. Om deze hypothese te testen hebben we knock-out lijnen gecreëerd voor verschillende geïdentificeerde zebravis homologen door middel van CRISPR/Cas9-gemedieerde mutagenese. Twee van de vier onderzochte knock-out lijnen, namelijk de lijnen waarin *hmga1a* of *prx1b* werden uitgeschakeld, lieten een robuust regeneratie defect zien. We

vonden onder andere een tekort aan hartspier celdeling en permanente littekenvorming.

We laten zien dat de non-histone chromatine proteïne Hmga1a belangrijk is voor hartspier celdeling in het beschadigde zebravis hart door een breed gen programma te initiëren en chromatine te reorganiseren. Verder laten we zien dat over-expressie van Hmga1a in zebravis en muis hart hartspiercellen kan aanzetten tot deelname aan de celcyclus, zowel *in vitro* als *in vivo*.

Ook laten we zien dat Prrx1b tot expressie komt in epicardiale en epicardiaal afkomstige cellen. Vervolgens hebben we een combinatie van lineage tracing en scRNAseq gebruikt om te laten zien dat Prrx1b fibrose inhibeert en de Nrg1-afhankelijke hartspier celdeling stimuleert tijdens zebravis hart regeneratie.

Samengenomen hebben we in deze thesis de zebravis en muis border zone in detail gekarakteriseerd, belangrijke regulatoren van zebravis hart regeneratie gevonden en een factor geïdentificeerd die mogelijk gebruikt kan gaan worden om regeneratie te stimuleren in zoogdier harten.

THESIS OUTLINE

The results presented in this thesis help to elucidate the molecular mechanisms behind the striking difference in regenerative capacity between the zebrafish and mammalian heart. Previous work by the Bakkers lab and others has indicated that the injury border zone holds the regenerative capacity of the injured zebrafish heart. Therefore, the border zone forms the spatial focal point of the work presented here.

In **Chapter I (Introduction)**, we introduce the process of heart regeneration by framing it in an evolutionary context. We review the species specific traits known to impact heart regeneration, which could help explain the differences in regenerative capacity throughout the animal kingdom. We suggest to consider cardiac regenerative capacity as “an evolutionary afterthought”, only when no other traits take precedence, cardiac regeneration becomes an evolutionary priority to maintain.

In **Chapter II**, we characterize the regenerative zebrafish border zone using a single cell RNA sequencing approach on sorted border zone cardiomyocytes. Through bioinformatic- and histological analysis, we show that zebrafish border zone cardiomyocytes dedifferentiate to resemble an embryonic-like state. This includes metabolic reprogramming, which we show is vital to cardiomyocyte proliferation.

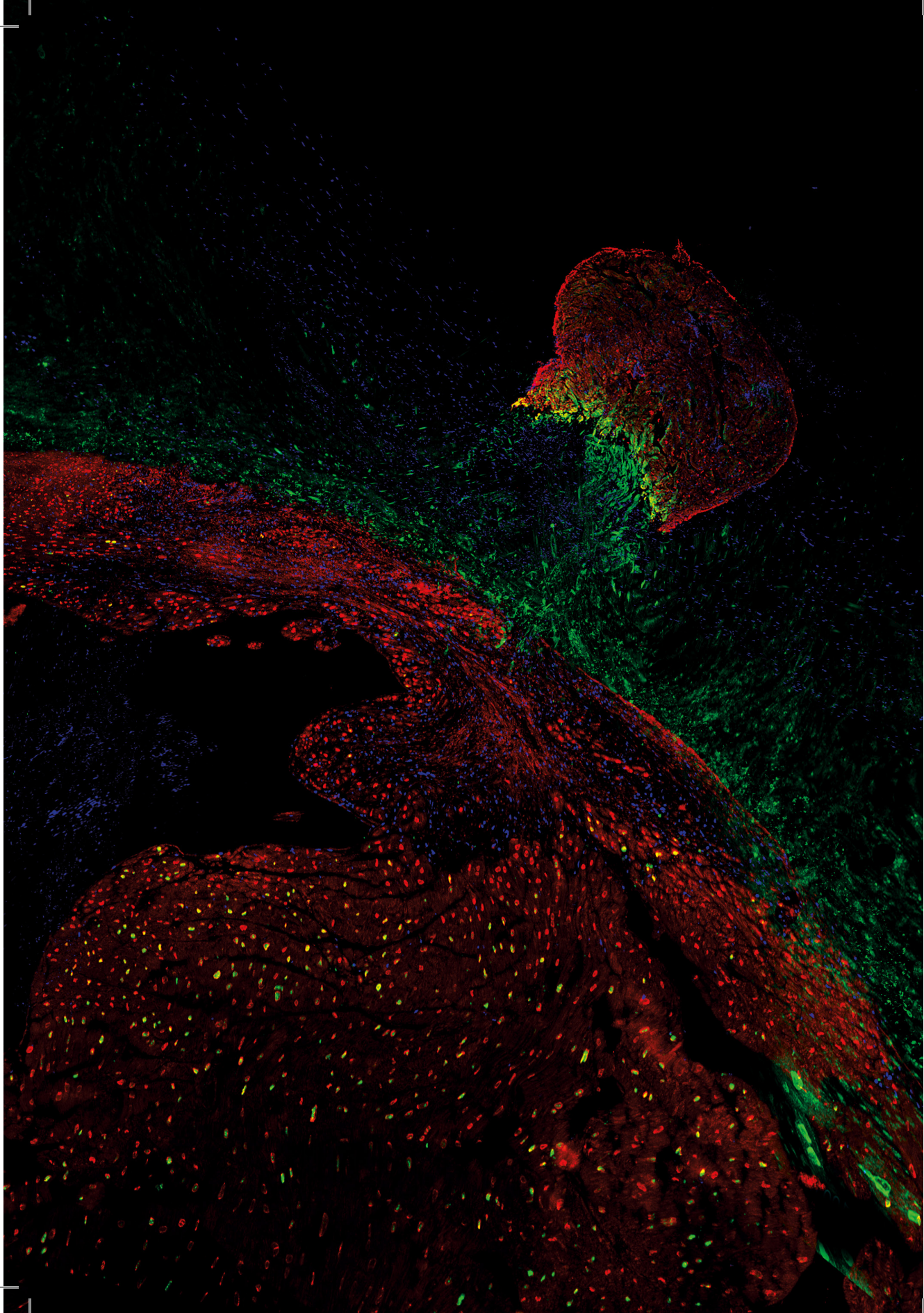
In **Chapter III**, we characterize the non-regenerative mammalian border zone using RNA-sequencing and ATAC-sequencing. We find that mammalian border zone cardiomyocytes do not completely dedifferentiate back to an embryonic state, but instead replace a muscle-restricted gene program with a stress responsive program. Importantly, we show that these findings are relevant to the injured human heart.

In **Chapter IV**, we perform a direct transcriptomic comparison between the zebrafish and mouse border zone and find *hmga1a/Hmga1* to be differentially expressed. We show that *hmga1a* is required for zebrafish heart regeneration. Furthermore, we show that overexpression of *hmga1a* can induce zebrafish cardiomyocyte proliferation *in vivo*, through the induction of a broad border zone-like program including changes in chromatin accessibility. Last, we provide evidence suggesting that *Hmga1* overexpression in injured murine hearts can induce cell cycle re-entry of border zone cardiomyocytes and help improve cardiac function after a myocardial infarction.

In **Chapter V**, we switch the focus from cardiomyocytes to epicardial cells, which play an important role in inducing proliferation in border zone cardiomyocytes through the secretion of mitogen Nrg1. We use a combination of histological analysis, lineage tracing and single cell RNA sequencing to identify that *Prrx1b* restricts fibrosis and promotes Nrg1-dependent

cardiomyocyte proliferation during zebrafish heart regeneration.

In **Chapter VI**, I put the findings presented in this thesis in the broader perspective of the main goal: to help elucidate the molecular mechanisms behind the striking difference in regenerative capacity between the zebrafish and mammalian heart. In addition, I discuss the various strategies explored to replenish the lost cardiomyocytes of the injured mammalian heart and share my outlook on the field of heart regeneration as a whole.



CHAPTER I

INTRODUCTION

Cardiac regenerative capacity: an evolutionary afterthought?

Phong D. Nguyen^{1#}, Dennis E.M. de Bakker^{1#}, Jeroen Bakkers^{1,2*}

¹ Hubrecht Institute-KNAW and University Medical Center Utrecht, Utrecht, Netherlands.

² Department of Pediatric Cardiology, Division of Pediatrics, University Medical Center Utrecht, Utrecht, Netherlands.

Contributed equally

* Corresponding author

Published in *Cellular and Molecular Life Sciences* (2021)

ABSTRACT

Cardiac regeneration is the outcome of the highly regulated interplay of multiple processes, including the immune response, cardiomyocyte dedifferentiation and proliferation, neovascularization and extracellular matrix turnover. Species-specific traits affect these injury-induced processes, resulting in a wide variety of cardiac regenerative potential between species. Indeed, while mammals are generally considered poor regenerators, certain amphibian and fish species like the zebrafish display robust regenerative capacity post heart injury. The species-specific traits underlying these differential injury responses are poorly understood. In this review, we will compare the injury induced processes of the mammalian and zebrafish heart, describing where these processes overlap and diverge. Additionally, by examining multiple species across the animal kingdom, we will highlight particular traits that either positively or negatively affect heart regeneration. Last, we will discuss the possibility of overcoming regeneration-limiting traits to induce heart regeneration in mammals.

INTRODUCTION

Regeneration is an injury induced process that can be considered as a combination of multiple synergistic processes that act not only to limit the injury, but also generate new cells to replace the loss of tissue. This regenerative response varies widely within the animal kingdom and can be viewed at multiple biological levels ranging from regeneration of a whole body part, a specific structure or organ, a tissue and to an individual cell [1]. When viewing organ regeneration, in particular the heart, there is considerable variation [2]. Mammalian hearts for example typically lack a regenerative response upon injury, and instead form a permanent scar. Other species, including the fish species Medaka (*Oryzias latipes*) [3,4] and cave-dwelling *Astyanax mexicanus* [5], show a similar limitation when it comes to cardiac regenerative capacity. In contrast, a wide range of species have been shown to contain robust cardiac regenerative capacity, including the giant danio (*Devario aequipinnatus*) [6], goldfish (*Carassius auratus*) [7], newts (*Notophthalmus viridescens*) [8,9], Mexican Axolotl (*Ambystoma mexicanum*) [10-12] and surface-dwelling *Astyanax mexicanus* [5]. However, the most commonly used animal to study cardiac regeneration is the zebrafish (*Danio rerio*), which was first reported in 2002 to contain a robust regenerative capacity from amputation of ventricular tissue [13]. Following this seminal study, there have been a plethora of studies examining the cellular and molecular mechanisms contributing to the regenerative response.

Interestingly, cardiac regenerative capacity does not only differ among species, or even sub-populations as is the case with *Astyanax mexicanus*, but also between genetically identical organisms at different life stages. Indeed, several mammalian species have been reported to have a short time-window after birth where they retain regenerative capacity of the heart. For example, neonatal mice can regenerate their heart from injury either via amputation [14] or myocardial infarction (MI) [15] during the first 7 days post birth, with some indication that the regenerative window is restricted to the first 2 days post birth [16]. The neonatal pig also displays this phenomenon whereby its regenerative window lies within their first 2 days post birth [17,18]. Additionally, there have been clinical reports of human newborns recovering from a MI to various degrees [19,20].

In this review, we will describe the heterogenous distribution of cardiac regenerative capacity between species. In doing so, we hope to shed light on the processes and traits which cumulatively allow for successful heart regeneration. To achieve this goal, we will first describe processes occurring in mammalian heart repair and zebrafish heart regeneration, indicating where the two process overlap or diverge. Next, we will broaden our scope to include additional species, identifying traits that either positively or negatively affect heart regeneration. Lastly, we will discuss whether these differential processes and traits can be overcome to allow for heart regeneration in mammals.

Repair vs Regeneration: Differences between poor and robust regenerators

The repair response following heart injury is shared between zebrafish and mammals. This includes processes involving regulation of cellular stress, the immune system and extracellular matrix deposition that limit the deleterious nature of the injury and secures immediate survival. There are some differences in this repair response when comparing between zebrafish and mammals. Meanwhile these differences become more apparent as time progresses, whereby non-regenerating hearts continue to form a mature and permanent scar while regenerating hearts enter a new phase to replace the lost tissue. Here, we will highlight the shared and differential processes between heart repair and regeneration.

Extracellular matrix (ECM) deposition

While the adult mammalian heart does not regenerate, it is quite efficient at repair. Indeed, patient fatality from the direct effects of a MI (e.g. heart rupture) is rare. Instead, patients often succumb to mortality from the long-term effects such as cardiomyocyte (CM) hypertrophy, chamber dilation and ultimately heart failure. One factor that contributes to the prevention of heart rupture and direct lethality post MI is the highly coordinated deposition of a dynamic extracellular matrix (ECM) network [21]. This reparative process can be divided into three distinct phases: The Inflammation, Proliferative and Maturation phase [21]. During the inflammation phase, necrotic tissue as well as the native ECM is broken down through the activity of matrix metalloproteases (MMPs) [22,23]. Simultaneously, increased permeability of vessels bordering the injured area allows for the influx of fibrinogen, forming a provisional fibrin-based matrix network [24,25]. Through the proliferation phase, which is marked by the proliferation of (myo)fibroblasts, the fibrin-based network is gradually replaced with fibronectin and collagenous type-III filaments secreted by myofibroblasts and macrophages [26-28]. Finally, in the maturation phase, the fibrinous collagen type-III network will be replaced by collagen type-I filaments, which are highly crosslinked and provide robust structural integrity and therefore increasing scar stiffness [29,30]. Although these ECM dynamics ensure the immediate survival and short-term integrity of heart morphology, the formation of a fully matured, permanent scar leads to adverse effects later in life [31,32].

ECM deposition during zebrafish heart regeneration also involves the formation of a provisional fibrinous network and consequent replacement by collagenous filaments similar to that seen during mammalian heart repair [33,34]. However, differences arise when addressing the origin of ECM in the regenerative heart. Besides activated fibroblasts, endocardial cells contribute to ECM production during zebrafish heart regeneration [35]. In addition, the source of pro-fibrotic fibroblasts differs between zebrafish and mammalian hearts. Upon injury, resident fibroblasts of the mammalian heart migrate to the injury site, proliferate and differentiate into pro-fibrotic myofibroblasts under the regulation of TGF- β [28]. In contrast, the pro-fibrotic fibroblasts of the regenerating zebrafish heart not only arise from resident fibroblasts but are also formed by trans-differentiation of epicardial cells [36-38].

Like mammalian fibroblasts, zebrafish fibroblasts are activated through TGF- β signalling to acquire a pro-fibrotic signature, referred to as activated fibroblasts [36]. However, as regeneration progresses these fibroblasts are gradually de-activated to prevent excessive fibrosis [38] and the produced ECM is ultimately replaced by new functional myocardium. The regression of the ECM is dependent on MMPs (such as *mmp2* and *mmp14a/b*) [39] cleaving the collagenous network. However, MMPs might have additional functions during the inflammation phase. Indeed at 4 days post cryoinjury, MMPs are highly expressed by vimentin+ fibroblasts (including *mmp9* and *mmp13*) [40]. In addition, *mmp2* and *mmp14a/b* have been shown to be expressed during the inflammation phase 3 days post cryoinjury. In contrast, the upregulation of *mmp2* and *mmp14a/b* only occurs at 7dpi in the apical resection model, which lacks necrotic tissue. This suggests that post cryo-injury, MMPs could play a role in clearance of the necrotic tissue during the inflammation phase. Whether differences in MMP expression could underly differential scar regression between the injured zebrafish and mouse hearts, or whether the difference is due to a change in deposition rate, remains to be elucidated. Besides differences in the origin and temporal dynamics of cardiac fibroblasts and fibrosis, differences in ECM composition are also observed between regenerating and non-regenerating hearts. Interestingly in neonatal mice, the ECM component Agrin is highly expressed during the regenerative window and is downregulated thereafter [41]. This enrichment of Agrin expression is important for promoting CM proliferation and injection of this proteoglycan following adult heart injury improves cardiac function [41,42]. Whether Agrin is expressed during zebrafish heart regeneration has not been reported however, administration of zebrafish ECM into the MI induced adult mouse hearts facilitated cardiac functional recovery [43]. This was similarly observed with injection of neonatal cardiac ECM [44]. Thus, showing that ECM components can possess a pro-regenerative role.

Taken together, ECM depositions like fibrin and collagen are shared between the repair and regeneration processes, albeit with differences in their establishment and clearance. Like in the injured mammalian heart, Collagen I is expressed in the injured zebrafish heart at 14 days post cryo-injury [45]. Differences between zebrafish and mammalian ECM maturation arise after the initial deposition of collagen I. Mammalian hearts maintain the production of collagen I fibres resulting in a stiff permanent scar. In contrast, the zebrafish heart shows a transient de-activation of pro-fibrotic fibroblasts, thereby limiting the amount of deposited fibrosis [38]. In addition, the zebrafish heart dissolves the initially deposited ECM (including the collagen I network) through the expression of MMPs. To which extend the reduced deposition and/or clearance of the deposited collagenous network determines the transient nature of the zebrafish fibrotic response remains unclear. In addition, it remains to be elucidated which specific differences arise between initial scar deposition between the zebrafish and mammalian heart. The differences in ECM scar composition between regenerating and non-regenerating hearts draw parallels to other forms of regeneration. Spinal cord regeneration in zebrafish for example display a transient stiff ECM that is

proposed to stabilize the injury and change to a less stiff ECM to facilitate neuron migration into the injury area [46, and reviewed in 47]. A similar mechanism may happen in cardiac regeneration to allow for CM to enter and repopulate the scar. Indeed, it has been shown that ECM stiffness correlates to the regenerative window in neonatal mice hearts. Whereby an increase in stiffness correlated with the lost regenerative capacity, while reducing stiffness by addition of an inhibitor at a stage when the regenerative window was closed resulted in the maintenance of regenerative competence [16]. Moreover, ECM production is important for regeneration and repair as ablating collagen producing cells from the injured zebrafish heart leads to impaired heart regeneration [38] and ablating myo-fibroblasts from the post-MI murine heart leads to decreased survival [48]. Furthermore, the composition of the ECM strongly influences the outcome of the heart regeneration and repair processes [49,50].

Innate immune system

The inflammatory response is a well-orchestrated, complex process that plays an indispensable role during cardiac repair in mammals. The start of the inflammation phase is marked by the recruitment of neutrophils to the infarct area, which secrete pro-inflammatory signals and attract monocytes to infiltrate the infarction. Resident cardiac macrophages have been shown to recruit monocytes originally derived from the spleen. These monocytes will differentiate into macrophages and play multiple roles while occupying the injury site [51,52]. This review will conveniently define these roles into 2 phases (M1 and M2), the separation of these states is much more complex and still not well understood. Nevertheless, these macrophages acquire pro-inflammatory properties (M1) [53] and together with neutrophils will secrete various MMPs that allow for the remodelling of the native ECM [54]. At the same time, damaged and dying cells in the infarct site will activate the complement system, marking necrotic cells for degradation and phagocytosis thereby clearing the infarcted area of dead and necrotic cells [53,55,56]. Next, during the proliferative phase, apoptotic neutrophils are cleared from the tissue through phagocytosis by the M1 macrophages, which now progress into a new state (also known as M2) that is marked by the secretion of anti-inflammatory signals [57]. During this phase, a collagenous ECM is produced that is rich in fibronectin. Although myofibroblasts are the main contributors to ECM deposition, it is thought that the M2 macrophages play a regulatory role in ECM turnover through the secretion of MMPs and their inhibitors, TIMPs (reviewed in [58]). In addition, M2 macrophages secrete TGF- β ligands, thereby activating the collagen production in myofibroblasts [59,28]. During the final maturation phase, collagen deposition is halted and the more loosely organized Collagen III is replaced with a tightly cross-linked type I collagen. The role of the innate immune system in this part remains largely unexplored. The role of resident cardiac macrophages has also been shown to play an important role in activating angiogenesis and CM proliferation in neonatal cardiac injury [52,60]. As well as modulating proinflammatory monocyte macrophages following adult cardiac injury [52].

During regeneration in zebrafish, a similar influx of neutrophils and a presence of various sub-populations of macrophages is observed [61,62,3]. A distinct Wt1+ macrophage sub-population, which at least partially arise from the hematopoietic niche was identified that displays a pro-regenerative transcriptomic signature [63]. It remains uncertain how the macrophage populations in the zebrafish compare with the mammalian macrophages. Besides the innate immune response, a recent study indicates that the acquired immune response plays an indispensable role during zebrafish heart regeneration and suggests that differences in the adaptive immune response might underlie differences in regenerative capacity [64]. It would be interesting to determine whether these unique macrophage cell states/subtypes found in zebrafish could be manipulated in mammalian macrophages to potentially improve regeneration.

Revascularization

During a myocardial infarction in patients, a blood clot restricts blood flow of a coronary artery. This limits the transport of nutrients and oxygen to the downstream region of the heart and cause massive ischemic tissue damage. There has been reports suggesting that injury-induced VEGF signalling leads to local neovascularization, which is a process detrimental to prolonged survival after MI [65-67]. Indeed, the initiation of angiogenesis starts as early as the inflammation phase and continues well into the proliferative phase [68,69,66]. First, newly formed vessels are hyper-permeable due to the lack pericytes and smooth muscle cells, allowing the infiltration of leukocytes into the ischemic area. Afterwards, under the influence of PDGF, these vessels obtain a mural coat existing of pericytes and smooth muscle cells reducing permeability [70,71]. Interestingly, supplying murine ischemic hearts with human pericytes reduced vessel permeability and leukocyte infiltration, which led to beneficial effects on cardiac remodelling. This indicates that targeting neovascularization could have beneficial effects post MI [72,73]. However, as the infarcted area is remodelled into a mature scar largely devoid of living cells, the demand for nutrients and oxygen plummets. Therefore, as the scar matures the newly generated vasculature becomes obsolete and diminishes accordingly [74,75].

During regeneration, like during repair, the revascularization is of vital importance. Indeed, revascularization as well as lymphangiogenesis of the injury area is important for efficient heart regeneration in zebrafish [76-78]. Both zebrafish and mammalian revascularization depends on VEGF-signalling, which is expressed in the injury area as early as 15 hours (zebrafish) and 6 hours (rats) post heart damage [76,65]. Indeed, injury-induced VEGF has been shown detrimental to prolonged survival after MI in mammals [65-67] and blocking angiogenesis through expression of a dominant-negative Vegfaa blocks cardiomyocyte proliferation and heart regeneration in the zebrafish [76]. The biggest difference is therefore not in the initiation, but in the maintenance of the regenerated vessels. Whereas in the non-regenerative hearts the new blood vessels have no function as the scar matures,

regenerated tissue retain their vasculature to support the newly formed high nutrient/oxygen dependent CMs. Taken together, revascularization plays a vital role during both repair and regeneration, but is only maintained following regeneration.

Cardiomyocytes

Cardiomyocyte proliferation in mammals is rare and occurs at a very low rate [79-81]. However, this does not increase nor significantly compensate for the millions of CMs that are permanently lost due to myocardial infarction. One strategy for the surviving CMs to counteract the reduced functionality of the heart is by growing in cell size. Although this hypertrophic response is rapid and quite efficient, it is often not sustainable in the long term. Indeed, many patients that suffered a myocardial infarction end up with pathogenic hypertrophy of the heart, ultimately resulting in heart failure [31,32]. CMs directly adjacent to the ischemic area, also called border zone CMs, respond in an even more dramatic manner. In order for them to survive the adjacent infarction, they partly dedifferentiate towards a more immature state [82,83]. This occurs through the replacement of a MEF2 driven gene program, defining adult CM cell fate, with a stress-responsive AP-1 driven gene program allowing for survival under ischemic conditions [84]. Indeed, knock-out of one of these border zone stress responsive factors, *Nppb*, results in acute death following myocardial infarction in mice [84].

Instead of displaying a hypertrophic response due to cardiac insult in mammals, regenerative species respond with a hyperplastic response. In the zebrafish heart, the CMs that are lost by the injury are replaced by proliferation of existing CMs in the border zone [85,86]. In doing so, the heart will be restored to its original properties and deposited fibrosis will be replaced by new functional myocardium [13,34]. Border zone CMs in the regenerating heart also dedifferentiate and activate a stress program indicated by the expression of stress induced genes such as members of the AP-1 complex (i.e. *junba*, *junbb*, *fosab*, *fosl1a*) as well as *nppa* and *nppb*, much like mammalian border zone CMs during heart repair [84,87]. However, this cellular reprogramming seems much more pronounced because it includes metabolic reprogramming from a fatty acid towards glycolysis dependent ATP production [88,89], as well as the re-activation of an embryonic gene program [37,85]. Indeed, a recent study has shown that the transcriptome of zebrafish border zone CMs is more similar to embryonic CMs than to remote myocardial CMs originating from the same hearts [88]. This reversion back to an embryonic state is likely key to unlock their proliferative potential as inhibiting their dedifferentiation, including the induction of glycolysis, prevents CMs from proliferating effectively [87,86,88,89].

Taken together, the reparative heart employs a hypertrophic response to deal with the loss of heart functionality, while the regenerative heart instead uses hyperplastic regrowth. Although the hypertrophic response forms an adequate short-term solution, it leads to severe problems

in the long term, including complete heart failure. Border zone CM of both the reparative and regenerative heart dedifferentiate and activate a stress response program. However, this response seems to deviate in the regenerative heart, where the dedifferentiation results in the initiation of an embryonic-like gene program and the induction of glycolysis, while in the mammalian BZ many genes with high expression in neonatal CMs are not induced [84]. The induction of the embryonic-like gene program, including the induction of glycolysis, might help explain why zebrafish BZ CMs proliferate while mammalian BZ CMs do not re-enter the cell-cycle. Another explanation for the limited proliferative capacity of mammalian BZ CMs might be due to the intrinsic properties of cardiomyocyte nuclei. While mammalian CMs are mainly polyploid (human) or multinuclear (mice), zebrafish CMs are mononuclear and diploid, which has been shown to be detrimental for efficient proliferation and zebrafish heart regeneration [90-92].

In summary, while the reparative and regenerative response show many similarities, distinct differences are observed as well (Figure 1, Table 1). Specifically targeting individual differences might help to stimulate the regenerative response in endogenously reparative species such as mammals.

TABLE 1. Comparing adult mammalian heart repair with zebrafish heart regeneration

Process	Repair	Regeneration
ECM deposition: Fibrin	Yes	Yes
ECM deposition: Collagen	Yes	Yes
ECM maturation	Yes	No
ECM clearance	No	Yes
Innate immune system: Neutrophils	Yes	Yes
Innate immune system: Inflammatory Macrophages (M1 phase)	Yes	No?
Innate immune system: Anti-inflammatory Macrophages (M2 phase)	Yes	Yes?
Neovascularization	Yes	Yes
Stress response border zone CMs	Yes	Yes
Reverting back to embryonic state / metabolic reprogramming	No	Yes
CM proliferation	No	Yes
CM hypertrophy	Yes	No

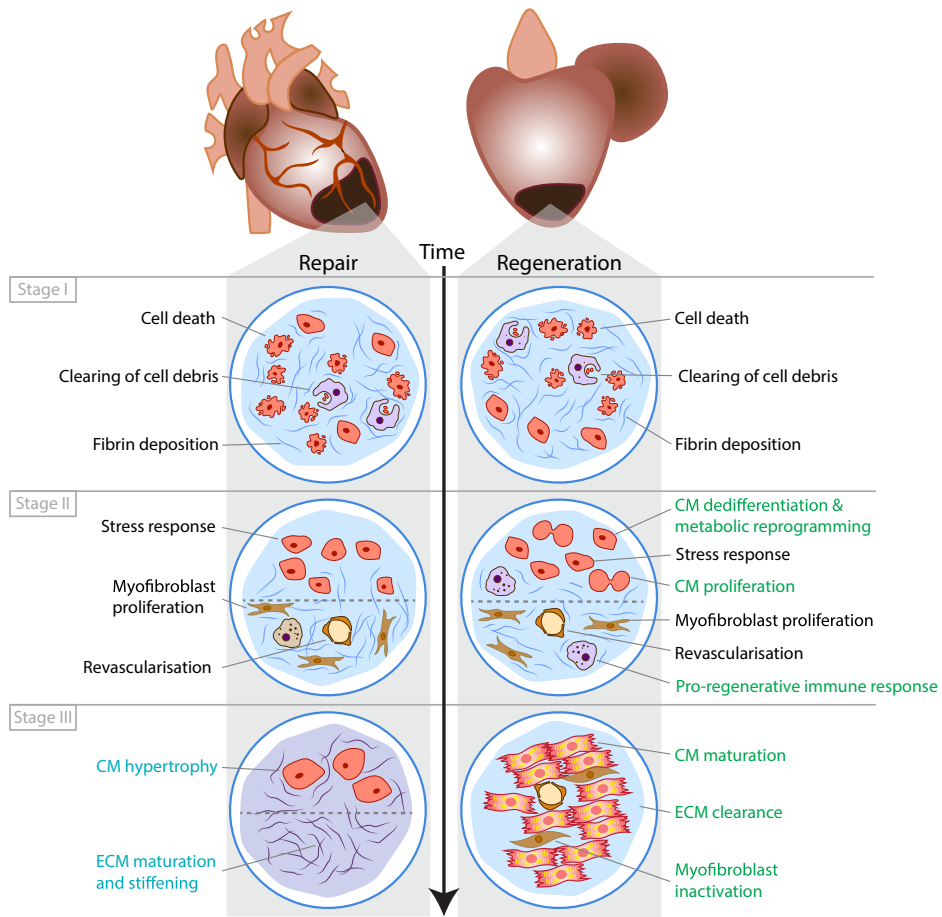


FIGURE 1. Comparison of repair vs regenerative response following cardiac injury

Schematic summary of the main processes and their response in animals that can either repair or regenerate following cardiac injury. This is also summarized in Table 1.

Regenerative Traits: Processes that facilitate a positive environment for regeneration

As discussed above, for cardiac regeneration to occur, many independent processes have to be precisely regulated and aligned. Recent studies have indicated the existence of regeneration-specific enhancers, which might have originated from repurposed injury responsive enhancers [93-95]. In fact, the loss of regeneration-specific enhancers might explain the lack of a regenerative response in some species [93]. While positive natural selection might occur on regeneration as a single unit, i.e. by maintaining regeneration specific enhancer elements, competition for selection will likely also occur on the level of the individual processes constituting regeneration. In other words, environmental changes

might force adaptations in a certain trait which is beneficial for the survival of the species, while being incompatible with cardiac regeneration. The second possibility is that a lack of evolutionary pressure (relaxed selection) would lead to the disappearance of cardiac regenerative capacity due to neutral evolution. The evolutionary mechanism leading to limited regenerative capacity is likely to differ between animal species and remains currently unresolved for mammals. In this section of the review, we will discuss the most prominent traits that impact cardiac regeneration. Furthermore, we will provide examples of species that have adapted these regeneration-compatible traits, likely losing the ability to regenerate their hearts in the process (Figure 2, Table 2).

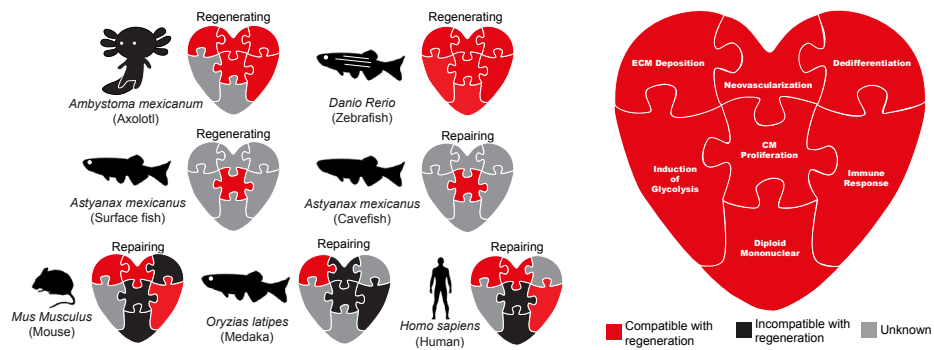


FIGURE 2. Regenerative traits viewed as pieces of a jigsaw that facilitates cardiac regenerative capacity. Summary of the current literature in regards to a specific regenerative trait and whether it can facilitate normal adult cardiac regeneration in Axolotl, Zebrafish, Human, Medaka, Mouse and Cavefish. Red represents confirmed trait involved in facilitating regeneration. Black represents confirmed trait that is incompatible with regeneration. Grey represents traits in which have not been directly tested. References for these traits are summarized in Table 2.

TABLE 2. Summary of the known and unknown literature of cardiac regenerative capacity in various species

	Ambystoma mexicanum (Axolotl)	Danio rerio (Zebrafish)	Homo sapiens (Humans)	Oryzias latipes (Medaka)	Mus musculus (Mouse)	Astyanax mexicanus (Cavefish)
ECM deposition	[10,11]	[33,34]	[84]	[3,4]	[84]	[5]
Neovascularization	[10,11]	[76]	[67]	[3,4]	[73]	unknown
Dedifferentiation	[10,11]	[85,37]	unknown	unknown	[84]	unknown
Metabolic reprogramming	unknown	[88,89]	unknown	unknown	unknown	unknown
CM proliferation	[10,11]	[13,96]	[79]	[3,4]	[14,15]	[5]
Immune Response	[10,11]	[97,98,63]	[99]	[3]	[100]	[5]
Diploid Mononuclear	unknown	[90]	[101]	unknown	[102,81]	unknown

Regeneration Trait: Cellular roles of macrophages

As mentioned above, the innate immune response, in particular the inflammatory response is one of the first responses to an injury. Aside from phagocytosing cellular debris at the injury area, macrophages also play multiple roles in the subsequent cellular responses. For example, they can mediate the fibrotic response and directly contribute to collagen deposition [103], promote neoangiogenesis [100,3,104,52] and initiate CM proliferation [52,105]. The importance of this cell population becomes apparent when overall depletion or ablation of specific macrophage subsets in zebrafish result in impaired regeneration with a decrease in CM proliferation and increase in scar formation [63,97,3,98,106].

The importance of macrophages during cardiac regeneration can also be observed in other species. In Medaka fish, heart regeneration does not occur and coincides with a delayed and reduced macrophage recruitment [3]. Meanwhile salamanders (axolotl), which are normally pro-regenerative display an inability to regenerate following macrophage depletion [10]. Likewise, macrophage depletion in neonatal mice following cardiac injury during the regenerative window resulted in an increase of fibrotic scar formation and decrease in cardiac output despite displaying a normal CM proliferation rate typically seen during regeneration [100]. All together these studies point to the positive role of macrophages in creating a permissive environment for regeneration.

The primary role of the innate immune system (and critically the M1 macrophages) is to defend from infection and repair damaged tissue. However, it appears that the M2 phase is an acquired state that plays a key role in the regenerative phase. One role for M2 macrophages is to secrete signals that stop the pro-inflammatory M1 phase through the release of many factors such as TGF- β and IL10 [107,108]. However, this regenerative phase depends on whether the initial injury persists or not. When there are chronic injury signals, M2 macrophages can instead activate and exacerbate fibrosis [109,103]. Additionally, comparisons between the transcriptomes of medaka and zebrafish macrophages showed the changes in gene expression profiles were similar, however the medaka profiles were less dynamic and consequently there was a reduced and delayed inflammation following injury. This again suggests that medaka macrophages still possess the ability to facilitate regeneration but the signal is not potent enough to induce this phase. Especially since exogenous activation of Toll-like receptors agonists (which elicits the acceleration of macrophage recruitment and neutrophil clearance) in injured medaka hearts boosted regeneration [3].

Taken together, it appears that medaka have lost the ability to regenerate their hearts through adaptations in their inflammatory response. These adaptations include less dynamic macrophages, delayed neutrophil clearance and delayed macrophage recruitment to the injury site [3]. This dampening of inflammation follows the theory that there is an

inverse relationship between organ and limb regenerative capacity and the strength of the inflammatory response within the innate immune system [110-112]. However, it remains unclear why medaka fish have evolved an altered innate immune system. A distinct difference from the regenerative zebrafish is that medaka stay longer in their chorions [113], thereby providing medaka embryos with a safe environment. Potentially, the prolonged protection by the chorion reduced the need for a strong injury response during early development. However, whether this resulted in the evolutionary adaptations seen in the medaka innate immune system, remains unclear.

Regeneration Trait: Modifying DNA content – polyploidy and polynucleation

Cells can exist with a varying amount of DNA material in the form of polyploidy (more than 2 sets of chromosomes per nuclei) and polynucleation (more than one nucleus). This phenomenon arises through the fusion of neighbouring cells or resulting from complete DNA replication without mitosis or cytokinesis (endoreplication) [114]. For example, adult hepatocytes, skeletal muscle, certain cell types in the lung, kidney, pancreas and CMs are typically polyploid [114]. In CMs, ploidy differs between species. CMs of non-mammalian species such as fish, amphibians and reptiles are mainly mononucleated and diploid. While at least 50% of the CMs in mammals such as humans, rodents, bats, livestock and even whales are multinucleated and polyploid [115]. Initially, mammalian CMs are predominately mononucleated and diploid, but this changes after birth. In the mouse heart, CM polyploidization commences during the first week after birth [102,116], after the loss of the cardiac regenerative potential period [16,14], while in humans, the persistence of polyploidy is maintained throughout life [101]. It is unclear why humans and mouse whom are both poor regenerators evolved to have different compositions of DNA content in their CMs (multinucleated vs polyploidy respectively). However, we have grouped these two events into one trait of modifying DNA content since as we will further discuss, the same end result in both contexts appears to modulate cardiac regeneration capacity.

The relation between ploidy and regenerative capacity of the heart was established in a survey of more than 120 genetically defined inbred mouse strains with variation in CMs ploidy. Furthermore, genetic experiments in mice confirmed such a correlation between the percentage of mononucleated CMs and regenerative capacity [91,92]. In zebrafish, a direct correlation between ploidy and regenerative capacity was also established. The majority of CMs in zebrafish are mononucleated and diploid [117,90], however increasing the percentage of polyploid CMs impaired regenerative capacity of the heart [90]. While in zebrafish and mice, a correlation between CM mononucleation and regenerative capacity was established, this correlation seems less clear in the porcine heart. In the porcine heart, polyploidization with multinucleation occurs over a 2-month period while loss of heart regeneration potential occurs at P3 [118].

The benefit of polyploidization is not well understood. One idea is that the polyploidy state prevents DNA damage [119] since the polyploidy state in hepatocytes have been shown to play a tumour-suppressive role in the liver [120]. Therefore, the stabilization of the nucleus facilitates the longevity of the organ and this trade-off for regenerative potential may allow cells to survive and maintain function. This would be important in the context of the heart as its function is regular contractions and unstable cells within the heart would compromise this role. Another explanation would be to support organ growth. It is theorized that the increase of polyploidy can support the growth of the cell via increased gene expression and therefore maintain higher cellular activity [121]. In the case of CMs, a larger cell would allow increased metabolic rates for energy production to support the metabolically intensive activity of contractions [122].

Taken together, mammals like mice and humans have adapted the nuclear content of cardiomyocytes, favouring multinucleated or polyploidy nuclei, respectively. While these adaptations might have resulted in distinct benefits such as a reduced risk of DNA-damage and potent regulation of cellular growth, it also limits cardiomyocyte proliferation and therefore heart regeneration.

Regeneration Trait: Energy consumption

Endothermal animals are able to self-regulate their body temperature as opposed to ectothermic animals that acquire the temperature of their environment. Thus, far adult heart regeneration capacity has only been reported in ectothermic fish and amphibians and not in endothermic birds or mammals and this may be attributed to difference in energy metabolism as endotherms have a higher resting rate metabolism [123]. This increase in resting rate metabolism is due to elevated aerobic metabolism, which is a very efficient process of energy production. Aerobic metabolism requires oxidative phosphorylation (OXPHOS) that occurs inside mitochondria. When less oxygen is available to cells, they can revert to glycolysis and lactate fermentation for energy metabolism, which generates lactate. While OXPHOS is much more efficient in producing energy as in ATP, it leads to the generation of reactive oxygen species (ROS), which can cause DNA damage. While the adult heart mainly utilizes fatty acids and OXPHOS for the generation of ATP, during mammalian development the foetus grows in an oxygen poor environment and the heart mainly utilizes glucose and glycolysis for energy metabolism. The transition from a low oxygen environment *in utero*, to an oxygen rich environment after birth coincidences with a shift in energy metabolism of cardiomyocytes from glycolysis towards the oxidation of fatty acids and OXPHOS [124,125] [126]. This also coincides with an increase in ROS production, DNA damage and a strong reduction in cardiomyocyte proliferation [126]. The increase in OXPHOS activity after birth impairs CM proliferation as reducing environmental oxygen after birth, inhibiting fatty acid utilization or promoting ROS scavenging prolongs the proliferative window of cardiomyocytes [127,126].

Besides the negative effects of OXPHOS and ROS production on CM proliferation, CM require glycolysis and lactate fermentation for efficient proliferation. In the regenerating zebrafish heart proliferating CMs in the border zone shift their energy metabolism from OXPHOS to glycolysis and when this is prevented CM proliferation and regeneration is impaired [88,89]. Conversely, stimulating glycolysis promotes CM proliferation [89]. The regulation of energy metabolism is highly complex and involves many pathways. Neuregulin 1 (Nrg1) is an agonist for the Epidermal Growth Factor Receptor Tyrosine Kinase family which includes ErbB1, 2, 3 and 4 [128]. There are several indications that in the heart this pathway plays an important role in controlling CM proliferation through regulation of energy metabolism. First, during development, Nrg1/ErbB2 signalling is important for cardiac development as knock out mice for these genes and zebrafish *erbb2* mutants are embryonically lethal as a result of a thinner myocardium due to reduced CM proliferation [129-134]. Second, CM specific expression of a constitutively active form of ErbB2 (caErbB2) results in cardiomegaly (large hearts) via increased CM proliferation [131]. In addition, when Nrg1 is overexpressed specifically in zebrafish CMs in an absence of injury, the fish also develop cardiomegaly by enhanced CM proliferation [135]. Third, activation of Nrg1/ErbB2 signalling in mouse and zebrafish hearts stimulates glycolysis in embryonic and adult CMs [136,88]. In the context of heart regeneration, Nrg1 expression is induced in the zebrafish heart upon injury, which again is required for the activation of glycolysis and induction of CM proliferation [88,135].

Why is a shift from fatty acid oxidation to glycolysis important for CM proliferation? One could argue that since mitochondrial OXPHOS generates ROS which is capable of inducing a DNA damage response and cell cycle arrest [126] [137], it may be better for the proliferative cell to revert to a lower energy producing state to reduce ROS production. Another argument could be that during proliferation, since there is a disassembly of the contractile apparatus [88,96], the high energy consumption is not needed as compared to a functionally contracting CM and therefore the more inefficient energy producing pathway would suffice. Finally, intermediate metabolites produced by aerobic glycolysis may be converted into precursors for the biosynthesis of amino acids and nucleotides that are essential for cell proliferation and growth [137,138]. In addition, there have been reports that components of the glycolytic pathway directly interact with cell cycle regulators, which is independent from their catalytic activity, [139,140] and therefore this pathway may be required to activate the proliferation programme.

The trade-off between regenerative potential and metabolism can also be seen in Mexican cavefish. This teleost species (*Astyanax mexicanus*) is a single species comprising of two populations. A cave-dwelling (Pachón) and surface-dwelling population. About 1.5 million years ago, these two populations diverged due to the changing environment of the Mexican rivers and caves and resulted in the Pachón population losing certain features such as their eyes and pigments [141], and instead acquire new traits such as highly sensitive taste

buds and lateral line neurons for navigating in the dark [141]. Interestingly, due to the food scarcity within the caves, the Pachón have adapted by changing its glucose metabolism [142,143]. In particular, RNA-seq between these fish populations indicate a downregulation of glycolysis related genes [5]. Moreover, the Pachón population cannot regenerate its heart following injury when compared to their surfacing dwelling counterparts [5]. While yet to be tested, if the surface dwelling fish also require a glycolytic switch in their CMs to facilitate CM proliferation, this would indicate the regeneration trade-off in the Pachón population may be beneficial for other functions that allow this species to survive.

Metabolism and endothermy are highly linked since endotherms have higher metabolic rates compared to ectotherms. The origin of endothermy in birds and mammals is a controversial topic in evolutionary biology. Several hypotheses have been proposed to explain its evolutionary origin of which the aerobic capacity model received most attention [123,144,145]. Physiological studies indicate that resting and maximal rate metabolism are linked so that one cannot increase without the other. The aerobic capacity model proposes that an increase in resting rate metabolism supported an increase in maximal rate metabolism to allow sustained muscle activities. High maximal oxygen consumption rates allow sustained workloads by aerobic metabolism, which is beneficial for many activities such as capturing prey or sustained flight. In addition, the increase in resting rate metabolism facilitated the regulation of body temperature. The increase in resting rate metabolism by mitochondrial OXPHOS requires higher oxygen consumption, which may have resulted in adaptations such as a more efficient ventilation system and an increase in blood circulation. Numerous adaptations seen in hearts of mammals and birds, such as separation of the chambers and increased wall thickness, accommodate a more efficient oxygen transportation to all tissues [146]. Therefore, heart regeneration, which depends on the ability of CMs to switch energy metabolism from a very efficient fatty acid oxidation to a more inefficient glucose metabolism by glycolysis and lactate fermentation, may have been a trade-off for an increase in energy demands in endotherms. This may not be restricted to only heart regeneration since a comparable metabolic switch towards glycolysis was also observed during appendage regeneration [147].

The higher availability of oxygen for energy production could in part be due to the aquatic to terrestrial transition which began approximately 500 to 400 million years ago [148]. Some possible reasons for this transition could be due to animals living during the Ordovician-Silurian extinction event, a period of marine O₂ deprivation [148]. Another reason an increase in atmospheric O₂ concentration allowed for bigger animals to form and therefore gain a competitive advantage against potential predators [149]. The link between animal size and atmospheric O₂ concentration is evident as giant animals became extinct when O₂ concentrations reduced [150,151]. While it is tempting to suggest that the transition from aquatic to terrestrial environment for vertebrates caused the loss of the regenerative trait, it

is possible this trait developed independently of this transition.

Inducing regenerative traits in species with a poor regenerative capacity

All vertebrates can regenerate to an extent, the difference lies in the capacity of the particular organ. Thus, one could view regeneration as a dormant process in organs that do not regenerate and manipulating this process can reactivate the organ's ability to proliferate. Following this reasoning, there have been attempts to boost CM proliferation in mammalian hearts. The modulation of both Hippo and ErbB2 signalling and most recently the interaction between these two pathways can robustly induce CM proliferation and regeneration following injury [152,153,131,154]. In all cases, when proliferation is induced, a number of cellular and molecular processes are activated that involve some of the above-mentioned regenerative traits. For example, mononucleated CMs preferentially undergo proliferation compared to binucleated CMs [155,131]. Meanwhile both zebrafish hearts via Nrg1 overexpression and mouse hearts via caErbB2 overexpression switch in metabolism towards glycolysis, which is required for CM proliferation [88]. In addition, ectopic expression of Pkm2, an isoenzyme of the glycolytic pyruvate kinase, in injured mouse hearts induces CM proliferation and restored cardiac function [156]. While the induction of the Nrg1/ErbB2 pathway appears to directly affect certain regeneration associated traits (e.g. metabolic reprogramming), it appears it can completely bypass others (e.g. polyploidy) by focussing on a specific subset of CMs (mononuclear, diploid). Understanding the factors that can overcome the regenerative block by examining interactions between pro-regenerative pathways (e.g. Nrg1/ErbB2 signalling) with the traits and processes affecting regenerative capacity, will help us develop novel methods of inducing CM proliferation and subsequent cardiac regeneration in mammals.

CONCLUDING REMARKS

Cardiac regeneration is a multimodal process that requires the precise regulation of numerous processes and cell types. It is unclear what the origin of cardiac regeneration is, but common features such as activation of CM proliferation suggest that it may have a common origin. How cardiac regeneration has been maintained or lost in specific animals is under extensive debate [1]. The loss of cardiac regenerative capacity can result from adaptations in any of the traits and processes described in this review, including the innate immune system, nuclear organization and metabolism. The heterogeneous distribution of cardiac regenerative capacity throughout the animal kingdom might therefore be a direct consequence of the complexity of the regeneration process. Here, we have summarized several examples of species that might have lost cardiac regenerative capacity through adaptations in distinctly different traits. Therefore, we might consider cardiac regenerative capacity as “an evolutionary afterthought”, only when no other traits take precedence, cardiac regeneration becomes an evolutionary priority to maintain, and this could be explained by

either the pleiotropy or adaptive hypothesis [1]. In the pleiotropy scenario, regeneration would be retained because it is developmentally tightly controlled to other adaptations. Cavefish for example changed their metabolism to adapt to the scarce food availability and this metabolomic state is also linked to CM proliferation. The adaptive hypothesis predicts that a trait is actively being maintained during selection and regeneration would be viewed to being negatively selected over repair. In general, the relative body size in poor vs. robust cardiac regenerators is anticorrelated, thus the energy and mechanical requirements for the heart to properly function and sustain the body is much higher in bigger and poor regenerators. Therefore, the need to quickly repair the injury and maintain heart function is being selected over the more slower regeneration process. The energy required to regenerate could also be expensive since the CMs themselves undergo dramatic changes in order to proliferate and mature, compared to a more simpler repair process. Thus, repair may be favoured in non-cardiac regenerators to divert energy expenditure to other energy intensive processes/organs. Alternatively, a phylogenetic inertia scenario could describe regeneration as this theory predicts the traits are being maintained for historical reasons and confer no selective advantage or disadvantage, therefore this trait was not yet been eliminated from the collection of traits an animal has acquired for survival [1]. Comparative studies between species allow us to identify differences and similarities between species and better understanding of the traits and processes underlying or limiting cardiac regeneration in these different species could potentially help overcome the limited regenerative capacity in mammalian hearts.

REFERENCES

1. Bely AE, Nyberg KG (2010) Evolution of animal regeneration: re-emergence of a field. *Trends Ecol Evol* 25 (3):161-170. doi:10.1016/j.tree.2009.08.005
2. Forbes SJ, Rosenthal N (2014) Preparing the ground for tissue regeneration: from mechanism to therapy. *Nat Med* 20 (8):857-869. doi:10.1038/nm.3653
3. Lai SL, Marín-Juez R, Moura PL, Kuenne C, Lai JKH, Tsedeke AT, Guenther S, Looso M, Stainier DY (2017) Reciprocal analyses in zebrafish and medaka reveal that harnessing the immune response promotes cardiac regeneration. *Elife* 6. doi:10.7554/eLife.25605
4. Ito K, Morioka M, Kimura S, Tasaki M, Inohaya K, Kudo A (2014) Differential reparative phenotypes between zebrafish and medaka after cardiac injury. *Dev Dyn* 243 (9):1106-1115. doi:10.1002/dvdy.24154
5. Stockdale WT, Lemieux ME, Killen AC, Zhao J, Hu Z, Riepsaame J, Hamilton N, Kudoh T, Riley PR, van Aerle R, Yamamoto Y, Mommersteeg MTM (2018) Heart Regeneration in the Mexican Cavefish. *Cell Rep* 25 (8):1997-2007.e1997. doi:10.1016/j.celrep.2018.10.072
6. Lafontant PJ, Burns AR, Grivas JA, Lesch MA, Lala TD, Reuter SP, Field LJ, Frounfelter TD (2012) The giant danio (*D. aequipinnatus*) as a model of cardiac remodeling and regeneration. *Anat Rec (Hoboken)* 295 (2):234-248. doi:10.1002/ar.21492
7. Grivas J, Haag M, Johnson A, Manalo T, Roell J, Das TL, Brown E, Burns AR, Lafontant PJ (2014) Cardiac repair and regenerative potential in the goldfish (*Carassius auratus*) heart. *Comp Biochem Physiol C Toxicol Pharmacol* 163:14-23. doi:10.1016/j.cbpc.2014.02.002
8. Laube F, Heister M, Scholz C, Borchardt T, Braun T (2006) Re-programming of newt cardiomyocytes is induced by tissue regeneration. *J Cell Sci* 119 (Pt 22):4719-4729. doi:10.1242/jcs.03252
9. Oberpriller JO, Oberpriller JC (1974) Response of the adult newt ventricle to injury. *J Exp Zool* 187 (2):249-253. doi:10.1002/jez.1401870208
10. Godwin JW, Debuque R, Salimova E, Rosenthal NA (2017) Heart regeneration in the salamander relies on macrophage-mediated control of fibroblast activation and the extracellular landscape. *NPJ Regen Med* 2. doi:10.1038/s41536-017-0027-y
11. Cano-Martínez A, Vargas-González A, Guarner-Lans V, Prado-Zayago E, León-Olea M, Nieto-Lima B (2010) Functional and structural regeneration in the axolotl heart (*Ambystoma mexicanum*) after partial ventricular amputation. *Arch Cardiol Mex* 80 (2):79-86
12. Vargas-González A, Prado-Zayago E, León-Olea M, Guarner-Lans V, Cano-Martínez A (2005) [Myocardial regeneration in *Ambystoma mexicanum* after surgical injury]. *Arch Cardiol Mex* 75 Suppl 3:S3-21-29
13. Poss KD, Wilson LG, Keating MT (2002) Heart regeneration in zebrafish. *Science* 298 (5601):2188-2190. doi:10.1126/science.1077857
14. Porrello ER, Mahmoud AI, Simpson E, Hill JA, Richardson JA, Olson EN, Sadek HA (2011) Transient regenerative potential of the neonatal mouse heart. *Science* 331 (6020):1078-1080. doi:10.1126/science.1200708
15. Porrello ER, Mahmoud AI, Simpson E, Johnson BA, Grinsfelder D, Canseco D, Mammen PP, Rothermel BA, Olson EN, Sadek HA (2013) Regulation of neonatal and adult mammalian heart regeneration by the miR-15 family. *Proc Natl Acad Sci U S A* 110 (1):187-192. doi:10.1073/pnas.1208863110
16. Notari M, Ventura-Rubio A, Bedford-Guaus SJ, Jorba I, Mulero L, Navajas D, Martí M, Raya Á (2018) The local microenvironment limits the regenerative potential of the mouse neonatal heart. *Sci Adv* 4 (5):eaa05553. doi:10.1126/sciadv.aao5553
17. Zhu W, Zhang E, Zhao M, Chong Z, Fan C, Tang Y, Hunter JD, Borovjagin AV, Walcott GP, Chen JY, Qin G, Zhang J (2018) Regenerative Potential of Neonatal Porcine Hearts. *Circulation* 138 (24):2809-2816. doi:10.1161/circulationaha.118.034886
18. Ye L, D'Agostino G, Loo SJ, Wang CX, Su LP, Tan SH, Tee GZ, Pua CJ, Pena EM, Cheng RB, Chen WC, Abdurrachim D, Lalic J, Tan RS, Lee TH, Zhang J, Cook SA (2018) Early Regenerative Capacity in the Porcine Heart. *Circulation* 138 (24):2798-2808. doi:10.1161/circulationaha.117.031542
19. Haubner BJ, Schneider J, Schweigmann U, Schuetz T, Dichtl W, Velik-Salchner C, Stein JI, Penninger JM (2016) Functional Recovery of a Human Neonatal Heart After Severe Myocardial Infarction. *Circ Res* 118 (2):216-221. doi:10.1161/circresaha.115.307017
20. Papneja K, Chan AK, Mondal TK, Paes B (2017) Myocardial Infarction in Neonates: A Review of an Entity with Significant Morbidity and Mortality. *Pediatr Cardiol* 38 (3):427-441. doi:10.1007/s00246-016-1556-7
21. Yang F, Liu YH, Yang XP, Xu J, Kapke A, Carretero

- OA (2002) Myocardial infarction and cardiac remodelling in mice. *Exp Physiol* 87 (5):547-555. doi:10.1113/eph8702385
22. Cannon RO, 3rd, Butany JW, McManus BM, Speir E, Kravitz AB, Bolli R, Ferrans VJ (1983) Early degradation of collagen after acute myocardial infarction in the rat. *Am J Cardiol* 52 (3):390-395. doi:10.1016/0002-9149(83)90145-5
 23. Whittaker P, Boughner DR, Kloner RA (1991) Role of collagen in acute myocardial infarct expansion. *Circulation* 84 (5):2123-2134. doi:10.1161/01.cir.84.5.2123
 24. Dobaczewski M, Bujak M, Zymek P, Ren G, Entman ML, Frangogiannis NG (2006) Extracellular matrix remodeling in canine and mouse myocardial infarcts. *Cell Tissue Res* 324 (3):475-488. doi:10.1007/s00441-005-0144-6
 25. Brown LF, Yeo KT, Berse B, Yeo TK, Senger DR, Dvorak HF, van de Water L (1992) Expression of vascular permeability factor (vascular endothelial growth factor) by epidermal keratinocytes during wound healing. *J Exp Med* 176 (5):1375-1379. doi:10.1084/jem.176.5.1375
 26. Brown LF, Dubin D, Lavigne L, Logan B, Dvorak HF, Van de Water L (1993) Macrophages and fibroblasts express embryonic fibronectins during cutaneous wound healing. *Am J Pathol* 142 (3):793-801
 27. Ulrich MM, Janssen AM, Daemen MJ, Rappaport L, Samuel JL, Contard F, Smits JF, Cleutjens JP (1997) Increased expression of fibronectin isoforms after myocardial infarction in rats. *J Mol Cell Cardiol* 29 (9):2533-2543. doi:10.1006/jmcc.1997.0486
 28. Ignatz RA, Massagué J (1986) Transforming growth factor-beta stimulates the expression of fibronectin and collagen and their incorporation into the extracellular matrix. *J Biol Chem* 261 (9):4337-4345
 29. Cleutjens JP, Verluyten MJ, Smiths JF, Daemen MJ (1995) Collagen remodeling after myocardial infarction in the rat heart. *Am J Pathol* 147 (2):325-338
 30. Wei S, Chow LT, Shum IO, Qin L, Sanderson JE (1999) Left and right ventricular collagen type I/III ratios and remodeling post-myocardial infarction. *J Card Fail* 5 (2):117-126. doi:10.1016/s1071-9164(99)90034-9
 31. Baudino TA, Carver W, Giles W, Borg TK (2006) Cardiac fibroblasts: friend or foe? *Am J Physiol Heart Circ Physiol* 291 (3):H1015-1026. doi:10.1152/ajpheart.00023.2006
 32. Travers JG, Kamal FA, Robbins J, Yutzey KE, Blaxall BC (2016) Cardiac Fibrosis: The Fibroblast Awakens. *Circ Res* 118 (6):1021-1040. doi:10.1161/circresaha.115.306565
 33. Garcia-Puig A, Mosquera JL, Jiménez-Delgado S, García-Pastor C, Jorba I, Navajas D, Canals F, Raya A (2019) Proteomics Analysis of Extracellular Matrix Remodeling During Zebrafish Heart Regeneration. *Mol Cell Proteomics* 18 (9):1745-1755. doi:10.1074/mcp.RA118.001193
 34. Chablais F, Veit J, Rainer G, Jaźwińska A (2011) The zebrafish heart regenerates after cryoinjury-induced myocardial infarction. *BMC Dev Biol* 11:21. doi:10.1186/1471-213x-11-21
 35. Münch J, Grivas D, González-Rajal Á, Torregrosa-Carrion R, de la Pompa JL (2017) Notch signalling restricts inflammation and serpine1 expression in the dynamic endocardium of the regenerating zebrafish heart. *Development* 144 (8):1425-1440. doi:10.1242/dev.143362
 36. Chablais F, Jazwinska A (2012) The regenerative capacity of the zebrafish heart is dependent on TGFβ signaling. *Development* 139 (11):1921-1930. doi:10.1242/dev.078543
 37. Lepilina A, Coon AN, Kikuchi K, Holdway JE, Roberts RW, Burns CG, Poss KD (2006) A dynamic epicardial injury response supports progenitor cell activity during zebrafish heart regeneration. *Cell* 127 (3):607-619. doi:10.1016/j.cell.2006.08.052
 38. Sánchez-Iranzo H, Galardi-Castilla M, Sanz-Morejón A, González-Rosa JM, Costa R, Ernst A, Sainz de Aja J, Langa X, Mercader N (2018) Transient fibrosis resolves via fibroblast inactivation in the regenerating zebrafish heart. *Proc Natl Acad Sci U S A* 115 (16):4188-4193. doi:10.1073/pnas.1716713115
 39. Gamba L, Amin-Javaheri A, Kim J, Warburton D, Lien CL (2017) Collagenolytic Activity Is Associated with Scar Resolution in Zebrafish Hearts after Cryoinjury. *J Cardiovasc Dev Dis* 4 (1). doi:10.3390/jcdd4010002
 40. Xu S, Webb SE, Lau TCK, Cheng SH (2018) Matrix metalloproteinases (MMPs) mediate leukocyte recruitment during the inflammatory phase of zebrafish heart regeneration. *Sci Rep* 8 (1):7199. doi:10.1038/s41598-018-25490-w
 41. Bassat E, Mutlak YE, Genzelinakh A, Shadrin IY, Baruch Umansky K, Yifa O, Kain D, Rajchman D, Leach J, Riabov Bassat D, Udi Y, Sarig R, Sagi I, Martin JF, Bursac N, Cohen S, Tzahor E (2017) The extracellular matrix protein agrin promotes heart regeneration in mice. *Nature* 547 (7662):179-184. doi:10.1038/nature22978
 42. Baehr A, Umansky KB, Bassat E, Jurisch V, Klett K, Bozoglu T, Hornaschewitz N, Solyanik O, Kain D, Ferraro B, Cohen-Rabi R, Krane M, Cyran C, Soehnlein O, Laugwitz KL, Hinkel R, Kupatt C, Tzahor E (2020) Agrin Promotes Coordinated

- Therapeutic Processes Leading to Improved Cardiac Repair in Pigs. *Circulation* 142 (9):868-881. doi:10.1161/circulationaha.119.045116
43. Chen WC, Wang Z, Missinato MA, Park DW, Long DW, Liu HJ, Zeng X, Yates NA, Kim K, Wang Y (2016) Decellularized zebrafish cardiac extracellular matrix induces mammalian heart regeneration. *Sci Adv* 2 (11):e1600844. doi:10.1126/sciadv.1600844
 44. Wang Z, Long DW, Huang Y, Chen WCW, Kim K, Wang Y (2019) Decellularized neonatal cardiac extracellular matrix prevents widespread ventricular remodeling in adult mammals after myocardial infarction. *Acta Biomater* 87:140-151. doi:10.1016/j.actbio.2019.01.062
 45. Marro J, Pfefferli C, de Preux Charles A-S, Bise T, Jaźwińska A (2016) Collagen XII Contributes to Epicardial and Connective Tissues in the Zebrafish Heart during Ontogenesis and Regeneration. *PLOS ONE* 11 (10):e0165497. doi:10.1371/journal.pone.0165497
 46. Möllmert S, Kharlamova MA, Hoche T, Taubenberger AV, Abuhattum S, Kuscha V, Kurth T, Brand M, Guck J (2020) Zebrafish Spinal Cord Repair Is Accompanied by Transient Tissue Stiffening. *Biophys J* 118 (2):448-463. doi:10.1016/j.bpj.2019.10.044
 47. Burnside ER, Bradbury EJ (2014) Manipulating the extracellular matrix and its role in brain and spinal cord plasticity and repair. *Neuropathol Appl Neurobiol* 40 (1):26-59. doi:10.1111/nan.12114
 48. Kanisicak O, Khalil H, Ivey MJ, Karch J, Maliken BD, Correll RN, Brody MJ, SC JL, Aronow BJ, Tallquist MD, Molkentin JD (2016) Genetic lineage tracing defines myofibroblast origin and function in the injured heart. *Nat Commun* 7:12260. doi:10.1038/ncomms12260
 49. Thavapalachandran S, Grieve SM, Hume RD, Le TYL, Raguram K, Hudson JE, Poulipoulos J, Figtree GA, Dye RP, Barry AM, Brown P, Lu J, Coffey S, Kesteven SH, Mills RJ, Rashid FN, Taran E, Kovoor P, Thomas L, Denniss AR, Kizana E, Asli NS, Xaymardan M, Feneley MP, Graham RM, Harvey RP, Chong JH (2020) Platelet-derived growth factor-AB improves scar mechanics and vascularity after myocardial infarction. *Sci Transl Med* 12 (524). doi:10.1126/scitranslmed.aay2140
 50. Yokota T, McCourt J, Ma F, Ren S, Li S, Kim TH, Kurmangaliyev YZ, Nasiri R, Ahadian S, Nguyen T, Tan XHM, Zhou Y, Wu R, Rodriguez A, Cohn W, Wang Y, Whitelegge J, Ryazantsev S, Khademhosseini A, Teitell MA, Chiou PY, Birk DE, Rowat AC, Crosbie RH, Pellegrini M, Seldin M, Lusic AJ, Deb A (2020) Type V Collagen in Scar Tissue Regulates the Size of Scar after Heart Injury. *Cell* 182 (3):545-562.e523. doi:10.1016/j.cell.2020.06.030
 51. Leid J, Carrelha J, Boukarabila H, Epelman S, Jacobsen SEW, Lavine KJ (2016) Primitive Embryonic Macrophages are Required for Coronary Development and Maturation. *Circulation research* 118 (10):1498-1511. doi:10.1161/CIRCRESAHA.115.308270
 52. Lavine KJ, Epelman S, Uchida K, Weber KJ, Nichols CG, Schilling JD, Ornitz DM, Randolph GJ, Mann DL (2014) Distinct macrophage lineages contribute to disparate patterns of cardiac recovery and remodeling in the neonatal and adult heart. *Proceedings of the National Academy of Sciences of the United States of America* 111 (45):16029-16034. doi:10.1073/pnas.1406508111
 53. Yan X, Anzai A, Katsumata Y, Matsushita T, Ito K, Endo J, Yamamoto T, Takeshima A, Shinmura K, Shen W, Fukuda K, Sano M (2013) Temporal dynamics of cardiac immune cell accumulation following acute myocardial infarction. *J Mol Cell Cardiol* 62:24-35. doi:10.1016/j.yjmcc.2013.04.023
 54. Rausch PG, Moore TG (1975) Granule enzymes of polymorphonuclear neutrophils: A phylogenetic comparison. *Blood* 46 (6):913-919
 55. Natarajan N, Abbas Y, Bryant DM, Gonzalez-Rosa JM, Sharpe M, Uygur A, Cocco-Delgado LH, Ho NN, Gerard NP, Gerard CJ, MacRae CA, Burns CE, Burns CG, Whited JL, Lee RT (2018) Complement Receptor C5aR1 Plays an Evolutionarily Conserved Role in Successful Cardiac Regeneration. *Circulation* 137 (20):2152-2165. doi:10.1161/circulationaha.117.030801
 56. Wysoczynski M, Solanki M, Borkowska S, van Hoose P, Brittain KR, Prabhu SD, Ratajczak MZ, Rokosh G (2014) Complement component 3 is necessary to preserve myocardium and myocardial function in chronic myocardial infarction. *Stem Cells* 32 (9):2502-2515. doi:10.1002/stem.1743
 57. Horckmans M, Ring L, Duchene J, Santovito D, Schloss MJ, Drechsler M, Weber C, Soehnlein O, Steffens S (2017) Neutrophils orchestrate post-myocardial infarction healing by polarizing macrophages towards a reparative phenotype. *Eur Heart J* 38 (3):187-197. doi:10.1093/eurheartj/ehw002
 58. Lindsey ML (2018) Assigning matrix metalloproteinase roles in ischaemic cardiac remodelling. *Nat Rev Cardiol* 15 (8):471-479. doi:10.1038/s41569-018-0022-z
 59. Chen B, Huang S, Su Y, Wu YJ, Hanna A, Brickshawana A, Graff J, Frangogiannis NG (2019) Macrophage Smad3 Protects the Infarcted Heart, Stimulating Phagocytosis and Regulating

- Inflammation. *Circ Res* 125 (1):55-70. doi:10.1161/circresaha.119.315069
60. Wang Z, Cui M, Shah AM, Ye W, Tan W, Min YL, Botten GA, Shelton JM, Liu N, Bassel-Duby R, Olson EN (2019) Mechanistic basis of neonatal heart regeneration revealed by transcriptome and histone modification profiling. *Proc Natl Acad Sci U S A* 116 (37):18455-18465. doi:10.1073/pnas.1905824116
 61. Xu S, Xie F, Tian L, Manno SH, Manno FAM, 3rd, Cheng SH (2019) Prolonged neutrophil retention in the wound impairs zebrafish heart regeneration after cryoinjury. *Fish Shellfish Immunol* 94:447-454. doi:10.1016/j.fsi.2019.09.030
 62. Nguyen-Chi M, Laplace-Builhe B, Travnickova J, Luz-Crawford P, Tejedor G, Phan QT, Duroux-Richard I, Levraud JP, Kissa K, Lutfalla G, Jorgensen C, Djouad F (2015) Identification of polarized macrophage subsets in zebrafish. *Elife* 4:e07288. doi:10.7554/eLife.07288
 63. Sanz-Morejón A, García-Redondo AB, Reuter H, Marques IJ, Bates T, Galardi-Castilla M, Große A, Manig S, Langa X, Ernst A, Piragyte I, Botos MA, González-Rosa JM, Ruiz-Ortega M, Briones AM, Salaices M, Englert C, Mercader N (2019) Wilms Tumor 1b Expression Defines a Pro-regenerative Macrophage Subtype and Is Required for Organ Regeneration in the Zebrafish. *Cell Rep* 28 (5):1296-1306.e1296. doi:10.1016/j.celrep.2019.06.091
 64. Hui SP, Sheng DZ, Sugimoto K, Gonzalez-Rajal A, Nakagawa S, Hesselson D, Kikuchi K (2017) Zebrafish Regulatory T Cells Mediate Organ-Specific Regenerative Programs. *Dev Cell* 43 (6):659-672.e655. doi:10.1016/j.devcel.2017.11.010
 65. Li J, Brown LF, Hibberd MG, Grossman JD, Morgan JP, Simons M (1996) VEGF, flk-1, and fit-1 expression in a rat myocardial infarction model of angiogenesis. *Am J Physiol* 270 (5 Pt 2):H1803-1811. doi:10.1152/ajpheart.1996.270.5.H1803
 66. Lin YD, Luo CY, Hu YN, Yeh ML, Hsueh YC, Chang MY, Tsai DC, Wang JN, Tang MJ, Wei EI, Springer ML, Hsieh PC (2012) Instructive nanofiber scaffolds with VEGF create a microenvironment for arteriogenesis and cardiac repair. *Sci Transl Med* 4 (146):146ra109. doi:10.1126/scitranslmed.3003841
 67. Lee SH, Wolf PL, Escudero R, Deutsch R, Jamieson SW, Thistlethwaite PA (2000) Early expression of angiogenesis factors in acute myocardial ischemia and infarction. *N Engl J Med* 342 (9):626-633. doi:10.1056/nejm200003023420904
 68. Kobayashi K, Maeda K, Takefuji M, Kikuchi R, Morishita Y, Hirashima M, Murohara T (2017) Dynamics of angiogenesis in ischemic areas of the infarcted heart. *Sci Rep* 7 (1):7156. doi:10.1038/s41598-017-07524-x
 69. Moccetti F, Brown E, Xie A, Packwood W, Qi Y, Ruggeri Z, Shentu W, Chen J, López JA, Lindner JR (2018) Myocardial Infarction Produces Sustained Proinflammatory Endothelial Activation in Remote Arteries. *J Am Coll Cardiol* 72 (9):1015-1026. doi:10.1016/j.jacc.2018.06.044
 70. Ren G, Michael LH, Entman ML, Frangogiannis NG (2002) Morphological characteristics of the microvasculature in healing myocardial infarcts. *J Histochem Cytochem* 50 (1):71-79. doi:10.1177/002215540205000108
 71. Zymek P, Bujak M, Chatila K, Cieslak A, Thakker G, Entman ML, Frangogiannis NG (2006) The role of platelet-derived growth factor signaling in healing myocardial infarcts. *J Am Coll Cardiol* 48 (11):2315-2323. doi:10.1016/j.jacc.2006.07.060
 72. Chen CW, Okada M, Proto JD, Gao X, Sekiya N, Beckman SA, Corselli M, Crisan M, Saparov A, Tobita K, Péault B, Huard J (2013) Human pericytes for ischemic heart repair. *Stem Cells* 31 (2):305-316. doi:10.1002/stem.1285
 73. Katare R, Riu F, Mitchell K, Gubernator M, Campagnolo P, Cui Y, Fortunato O, Avolio E, Cesselli D, Beltrami AP, Angelini G, Emanuelli C, Madeddu P (2011) Transplantation of human pericyte progenitor cells improves the repair of infarcted heart through activation of an angiogenic program involving micro-RNA-132. *Circ Res* 109 (8):894-906. doi:10.1161/circresaha.111.251546
 74. Nelissen-Vrancken HJ, Debets JJ, Snoeckx LH, Daemen MJ, Smits JF (1996) Time-related normalization of maximal coronary flow in isolated perfused hearts of rats with myocardial infarction. *Circulation* 93 (2):349-355. doi:10.1161/01.cir.93.2.349
 75. Desmoulière A, Redard M, Darby I, Gabbiani G (1995) Apoptosis mediates the decrease in cellularity during the transition between granulation tissue and scar. *Am J Pathol* 146 (1):56-66
 76. Marín-Juez R, Marass M, Gauvrit S, Rossi A, Lai SL, Materna SC, Black BL, Stainier DY (2016) Fast revascularization of the injured area is essential to support zebrafish heart regeneration. *Proc Natl Acad Sci U S A* 113 (40):11237-11242. doi:10.1073/pnas.1605431113
 77. Vivien CJ, Pichol-Thievend C, Sim CB, Smith JB, Bower NI, Hogan BM, Hudson JE, Francois M, Porrello ER (2019) Vegfc/d-dependent regulation of the lymphatic vasculature during cardiac regeneration is influenced by injury context. *NPJ Regen Med* 4:18. doi:10.1038/s41536-019-0079-2

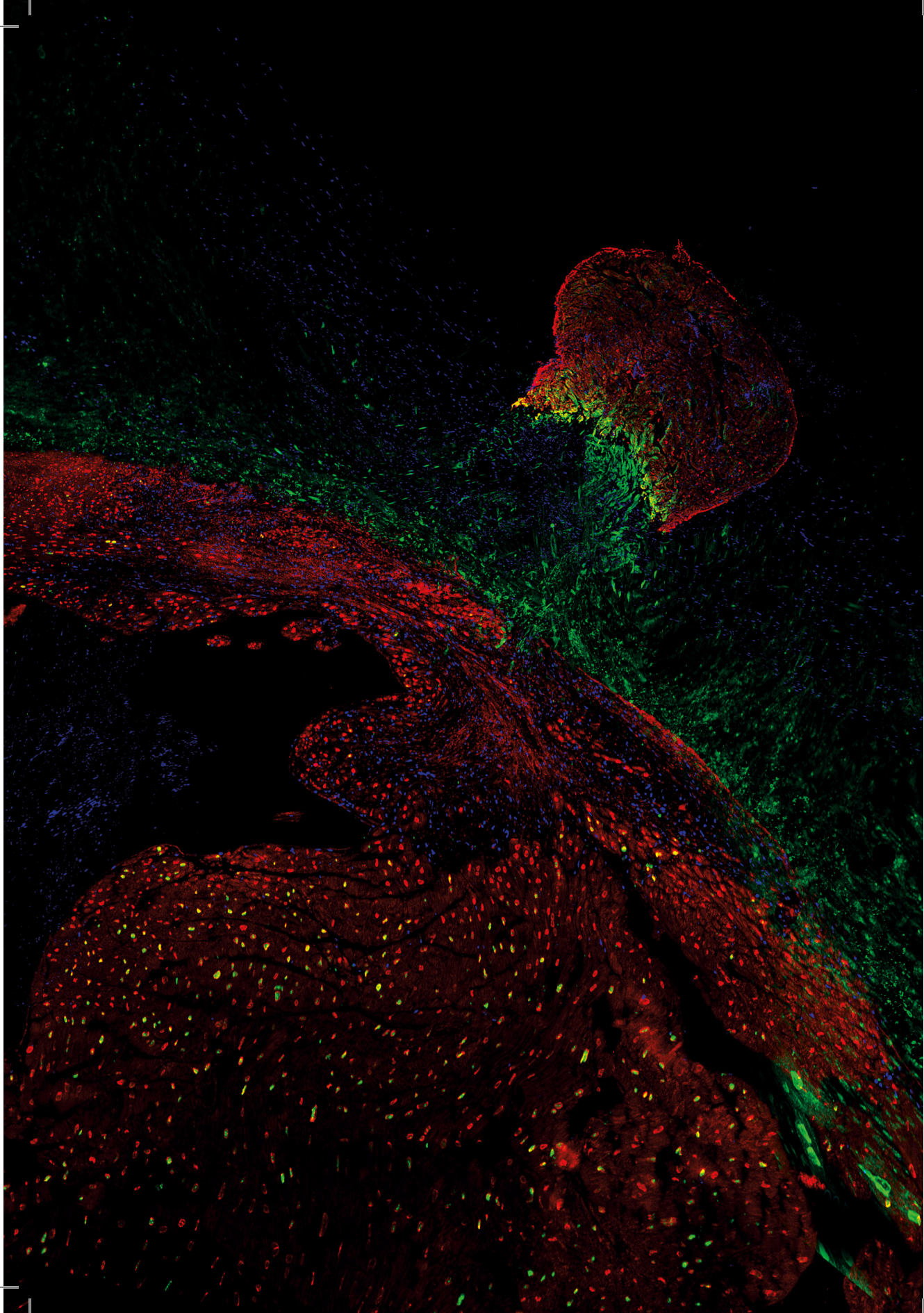
78. Harrison MR, Feng X, Mo G, Aguayo A, Villafuerte J, Yoshida T, Pearson CA, Schulte-Merker S, Lien CL (2019) Late developing cardiac lymphatic vasculature supports adult zebrafish heart function and regeneration. *Elife* 8. doi:10.7554/eLife.42762
79. Bergmann O, Bhardwaj RD, Bernard S, Zdunek S, Barnabé-Heider F, Walsh S, Zupicich J, Alkass K, Buchholz BA, Druid H, Jovinge S, Frisén J (2009) Evidence for cardiomyocyte renewal in humans. *Science* 324 (5923):98-102. doi:10.1126/science.1164680
80. Senyo SE, Steinhauser ML, Pizzimenti CL, Yang VK, Cai L, Wang M, Wu TD, Guerquin-Kern JL, Lechene CP, Lee RT (2013) Mammalian heart renewal by pre-existing cardiomyocytes. *Nature* 493 (7432):433-436. doi:10.1038/nature11682
81. Soonpaa MH, Field LJ (1997) Assessment of cardiomyocyte DNA synthesis in normal and injured adult mouse hearts. *Am J Physiol* 272 (1 Pt 2):H220-226. doi:10.1152/ajpheart.1997.272.1.H220
82. Dispersyn GD, Mesotten L, Meuris B, Maes A, Mortelmans L, Flameng W, Ramaekers F, Borgers M (2002) Dissociation of cardiomyocyte apoptosis and dedifferentiation in infarct border zones. *Eur Heart J* 23 (11):849-857. doi:10.1053/eurh.2001.2963
83. Sharov VG, Sabbah HN, Ali AS, Shimoyama H, Lesch M, Goldstein S (1997) Abnormalities of cardiocytes in regions bordering fibrous scars of dogs with heart failure. *Int J Cardiol* 60 (3):273-279. doi:10.1016/s0167-5273(97)00117-4
84. van Duijvenboden K, de Bakker DEM, Man JCK, Janssen R, Günthel M, Hill MC, Hooijkaas IB, van der Made I, van der Kraak PH, Vink A, Creemers EE, Martin JF, Barnett P, Bakkers J, Christoffels VM (2019) Conserved NPPB+ Border Zone Switches From MEF2- to AP-1-Driven Gene Program. *Circulation* 140 (10):864-879. doi:10.1161/circulationaha.118.038944
85. Kikuchi K, Holdway JE, Werdich AA, Anderson RM, Fang Y, Egnaczyk GF, Evans T, Macrae CA, Stainier DY, Poss KD (2010) Primary contribution to zebrafish heart regeneration by *gata4*(+) cardiomyocytes. *Nature* 464 (7288):601-605. doi:10.1038/nature08804
86. Jopling C, Sleep E, Raya M, Martí M, Raya A, Izpisua Belmonte JC (2010) Zebrafish heart regeneration occurs by cardiomyocyte dedifferentiation and proliferation. *Nature* 464 (7288):606-609. doi:10.1038/nature08899
87. Beisaw A, Kuenne C, Guenther S, Dallmann J, Wu CC, Bentsen M, Looso M, Stainier DYR (2020) AP-1 Contributes to Chromatin Accessibility to Promote Sarcomere Disassembly and Cardiomyocyte Protrusion During Zebrafish Heart Regeneration. *Circ Res* 126 (12):1760-1778. doi:10.1161/circresaha.119.316167
88. Honkoop H, de Bakker DE, Aharonov A, Kruse F, Shakked A, Nguyen PD, de Heus C, Garric L, Muraro MJ, Shoffner A, Tessadori F, Peterson JC, Noort W, Bertozzi A, Weidinger G, Posthuma G, Grün D, van der Laarse WJ, Klumperman J, Jaspers RT, Poss KD, van Oudenaarden A, Tzahor E, Bakkers J (2019) Single-cell analysis uncovers that metabolic reprogramming by ErbB2 signaling is essential for cardiomyocyte proliferation in the regenerating heart. *Elife* 8. doi:10.7554/eLife.50163
89. Fukuda R, Marín-Juez R, El-Sammak H, Beisaw A, Ramadass R, Kuenne C, Guenther S, Konzer A, Bhagwat AM, Graumann J, Stainier DY (2020) Stimulation of glycolysis promotes cardiomyocyte proliferation after injury in adult zebrafish. *EMBO Rep* 21 (8):e49752. doi:10.15252/embr.201949752
90. González-Rosa JM, Sharpe M, Field D, Soonpaa MH, Field LJ, Burns CE, Burns CG (2018) Myocardial Polyploidization Creates a Barrier to Heart Regeneration in Zebrafish. *Dev Cell* 44 (4):433-446.e437. doi:10.1016/j.devcel.2018.01.021
91. Patterson M, Barske L, Van Handel B, Rau CD, Gan P, Sharma A, Parikh S, Denholtz M, Huang Y, Yamaguchi Y, Shen H, Allayee H, Crump JG, Force T, Lien CL, Makita T, Lusic AJ, Kumar SR, Sucov HM (2017) Frequency of mononuclear diploid cardiomyocytes underlies natural variation in heart regeneration. *Nat Genet* 49 (9):1346-1353. doi:10.1038/ng.3929
92. Windmueller R, Leach JP, Babu A, Zhou S, Morley MP, Wakabayashi A, Petrenko NB, Viatour P, Morrissey EE (2020) Direct Comparison of Mononucleated and Binucleated Cardiomyocytes Reveals Molecular Mechanisms Underlying Distinct Proliferative Competencies. *Cell Rep* 30 (9):3105-3116.e3104. doi:10.1016/j.celrep.2020.02.034
93. Wang W, Hu CK, Zeng A, Alegre D, Hu D, Gotting K, Ortega Granillo A, Wang Y, Robb S, Schnittker R, Zhang S, Alegre D, Li H, Ross E, Zhang N, Brunet A, Sánchez Alvarado A (2020) Changes in regeneration-responsive enhancers shape regenerative capacities in vertebrates. *Science* 369 (6508). doi:10.1126/science.aaz3090
94. Kang J, Hu J, Karra R, Dickson AL, Tornini VA, Nachtrab G, Gemberling M, Goldman JA, Black BL, Poss KD (2016) Modulation of tissue repair by regeneration enhancer elements. *Nature* 532 (7598):201-206. doi:10.1038/nature17644
95. Goldman JA, Kuzu G, Lee N, Karasik J, Gemberling

- M, Foglia MJ, Karra R, Dickson AL, Sun F, Tolstorukov MY, Poss KD (2017) Resolving Heart Regeneration by Replacement Histone Profiling. *Dev Cell* 40 (4):392-404.e395. doi:10.1016/j.devcel.2017.01.013
96. Wu CC, Kruse F, Vasudevarao MD, Junker JP, Zebrowski DC, Fischer K, Noël ES, Grün D, Berezikov E, Engel FB, van Oudenaarden A, Weidinger G, Bakkers J (2016) Spatially Resolved Genome-wide Transcriptional Profiling Identifies BMP Signaling as Essential Regulator of Zebrafish Cardiomyocyte Regeneration. *Dev Cell* 36 (1):36-49. doi:10.1016/j.devcel.2015.12.010
 97. Bevan L, Lim ZW, Venkatesh B, Riley PR, Martin P, Richardson RJ (2020) Specific macrophage populations promote both cardiac scar deposition and subsequent resolution in adult zebrafish. *Cardiovasc Res* 116 (7):1357-1371. doi:10.1093/cvr/cvz221
 98. de Preux Charles AS, Bise T, Baier F, Marro J, Jazwińska A (2016) Distinct effects of inflammation on preconditioning and regeneration of the adult zebrafish heart. *Open Biol* 6 (7). doi:10.1098/rsob.160102
 99. Frangogiannis NG, Smith CW, Entman ML (2002) The inflammatory response in myocardial infarction. *Cardiovasc Res* 53 (1):31-47. doi:10.1016/s0008-6363(01)00434-5
 100. Aurora AB, Porrello ER, Tan W, Mahmoud AI, Hill JA, Bassel-Duby R, Sadek HA, Olson EN (2014) Macrophages are required for neonatal heart regeneration. *J Clin Invest* 124 (3):1382-1392. doi:10.1172/jci72181
 101. Brodsky V, Sarkisov DS, Arefyeva AM, Panova NW, Gvasava IG (1994) Polyploidy in cardiac myocytes of normal and hypertrophic human hearts; range of values. *Virchows Arch* 424 (4):429-435. doi:10.1007/bf00190566
 102. Soonpaa MH, Kim KK, Pajak L, Franklin M, Field LJ (1996) Cardiomyocyte DNA synthesis and binucleation during murine development. *Am J Physiol* 271 (5 Pt 2):H2183-2189. doi:10.1152/ajpheart.1996.271.5.H2183
 103. Simões FC, Cahill TJ, Kenyon A, Gavriouchkina D, Vieira JM, Sun X, Pezzolla D, Ravaud C, Masmanian E, Weinberger M, Mayes S, Lemieux ME, Barnette DN, Gunadasa-Rohling M, Williams RM, Greaves DR, Trinh LA, Fraser SE, Dallas SL, Choudhury RP, Sauka-Spengler T, Riley PR (2020) Macrophages directly contribute collagen to scar formation during zebrafish heart regeneration and mouse heart repair. *Nat Commun* 11 (1):600. doi:10.1038/s41467-019-14263-2
 104. Ferraro B, Leoni G, Hinkel R, Ormanns S, Paulin N, Ortega-Gomez A, Viola JR, de Jong R, Bongiovanni D, Bozoglu T, Maas SL, D'Amico M, Kessler T, Zeller T, Hristov M, Reutelingsperger C, Sager HB, Döring Y, Nahrendorf M, Kupatt C, Soehnlein O (2019) Pro-Angiogenic Macrophage Phenotype to Promote Myocardial Repair. *J Am Coll Cardiol* 73 (23):2990-3002. doi:10.1016/j.jacc.2019.03.503
 105. Liu B, Zhang HG, Zhu Y, Jiang YH, Luo GP, Tang FQ, Jian Z, Xiao YB (2017) Cardiac resident macrophages are involved in hypoxia-induced postnatal cardiomyocyte proliferation. *Mol Med Rep* 15 (6):3541-3548. doi:10.3892/mmr.2017.6432
 106. Huang WC, Yang CC, Chen IH, Liu YM, Chang SJ, Chuang YJ (2013) Treatment of Glucocorticoids Inhibited Early Immune Responses and Impaired Cardiac Repair in Adult Zebrafish. *PLoS One* 8 (6):e66613. doi:10.1371/journal.pone.0066613
 107. Fadok VA, Bratton DL, Konowal A, Freed PW, Westcott JY, Henson PM (1998) Macrophages that have ingested apoptotic cells in vitro inhibit proinflammatory cytokine production through autocrine/paracrine mechanisms involving TGF-beta, PGE2, and PAF. *The Journal of clinical investigation* 101 (4):890-898. doi:10.1172/JCI1112
 108. Voll RE, Herrmann M, Roth EA, Stach C, Kalden JR, Girkontaite I (1997) Immunosuppressive effects of apoptotic cells. *Nature* 390 (6658):350-351. doi:10.1038/37022
 109. Thompson RW, Pesce JT, Ramalingam T, Wilson MS, White S, Cheever AW, Ricklefs SM, Porcella SF, Li L, Ellies LG, Wynn TA (2008) Cationic amino acid transporter-2 regulates immunity by modulating arginase activity. *PLoS Pathog* 4 (3):e1000023-e1000023. doi:10.1371/journal.ppat.1000023
 110. Han C, Nie Y, Lian H, Liu R, He F, Huang H, Hu S (2015) Acute inflammation stimulates a regenerative response in the neonatal mouse heart. *Cell Res* 25 (10):1137-1151. doi:10.1038/cr.2015.110
 111. Lörchner H, Pöling J, Gajawada P, Hou Y, Polyakova V, Kostin S, Adrian-Segarra JM, Boettger T, Wietelmann A, Warnecke H, Richter M, Kubin T, Braun T (2015) Myocardial healing requires Reg3β-dependent accumulation of macrophages in the ischemic heart. *Nature medicine* 21 (4):353-362. doi:10.1038/nm.3816
 112. Wan E, Yeap XY, Dehn S, Terry R, Novak M, Zhang S, Iwata S, Han X, Homma S, Drosatos K, Lomasney J, Engman DM, Miller SD, Vaughan DE, Morrow JP, Kishore R, Thorp EB (2013) Enhanced efferocytosis of apoptotic cardiomyocytes through myeloid-epithelial-reproductive tyrosine kinase

- links acute inflammation resolution to cardiac repair after infarction. *Circ Res* 113 (8):1004-1012. doi:10.1161/circresaha.113.301198
113. Furutani-Seiki M, Wittbrodt J (2004) Medaka and zebrafish, an evolutionary twin study. *Mech Dev* 121 (7-8):629-637. doi:10.1016/j.mod.2004.05.010
 114. Gan P, Patterson M, Sucov HM (2020) Cardiomyocyte Polyploidy and Implications for Heart Regeneration. *Annu Rev Physiol* 82:45-61. doi:10.1146/annurev-physiol-021119-034618
 115. Hirose K, Payumo AY, Cutie S, Hoang A, Zhang H, Guyot R, Lunn D, Bigley RB, Yu H, Wang J, Smith M, Gillett E, Muroy SE, Schmid T, Wilson E, Field KA, Reeder DM, Maden M, Yartsev MM, Wolfgang MJ, Grützner F, Scanlan TS, Szweda LI, Buffenstein R, Hu G, Flamant F, Olgin JE, Huang GN (2019) Evidence for hormonal control of heart regenerative capacity during endothermy acquisition. *Science* 364 (6436):184-188. doi:10.1126/science.aar2038
 116. Li F, Wang X, Capasso JM, Gerdes AM (1996) Rapid transition of cardiac myocytes from hyperplasia to hypertrophy during postnatal development. *J Mol Cell Cardiol* 28 (8):1737-1746. doi:10.1006/jmcc.1996.0163
 117. Wills AA, Holdway JE, Major RJ, Poss KD (2008) Regulated addition of new myocardial and epicardial cells fosters homeostatic cardiac growth and maintenance in adult zebrafish. *Development* 135 (1):183-192. doi:10.1242/dev.010363
 118. Velayutham N, Alfieri CM, Agnew EJ, Riggs KW, Baker RS, Ponny SR, Zafar F, Yutzey KE (2020) Cardiomyocyte cell cycling, maturation, and growth by multinucleation in postnatal swine. *J Mol Cell Cardiol* 146:95-108. doi:10.1016/j.yjmcc.2020.07.004
 119. Otto SP (2007) The evolutionary consequences of polyploidy. *Cell* 131 (3):452-462. doi:10.1016/j.cell.2007.10.022
 120. Zhang S, Zhou K, Luo X, Li L, Tu HC, Sehgal A, Nguyen LH, Zhang Y, Gopal P, Tarlow BD, Siegwart DJ, Zhu H (2018) The Polyploid State Plays a Tumor-Suppressive Role in the Liver. *Dev Cell* 44 (4):447-459.e445. doi:10.1016/j.devcel.2018.01.010
 121. Frawley LE, Orr-Weaver TL (2015) Polyploidy. *Curr Biol* 25 (9):R353-358. doi:10.1016/j.cub.2015.03.037
 122. Orr-Weaver TL (2015) When bigger is better: the role of polyploidy in organogenesis. *Trends Genet* 31 (6):307-315. doi:10.1016/j.tig.2015.03.011
 123. Bennett AF, Ruben JA (1979) Endothermy and activity in vertebrates. *Science* 206 (4419):649-654. doi:10.1126/science.493968
 124. Lopaschuk GD, Collins-Nakai RL, Itoi T (1992) Developmental changes in energy substrate use by the heart. *Cardiovasc Res* 26 (12):1172-1180. doi:10.1093/cvr/26.12.1172
 125. Menendez-Montes I, Escobar B, Palacios B, Gómez MJ, Izquierdo-García JL, Flores L, Jiménez-Borreguero LJ, Aragonés J, Ruiz-Cabello J, Torres M, Martín-Puig S (2016) Myocardial VHL-HIF Signaling Controls an Embryonic Metabolic Switch Essential for Cardiac Maturation. *Dev Cell* 39 (6):724-739. doi:10.1016/j.devcel.2016.11.012
 126. Puente BN, Kimura W, Muralidhar SA, Moon J, Amatrua JF, Phelps KL, Grinsfelder D, Rothermel BA, Chen R, Garcia JA, Santos CX, Thet S, Mori E, Kinter MT, Rindler PM, Zacchigna S, Mukherjee S, Chen DJ, Mahmoud AI, Giacca M, Rabinovitch PS, Aroumougame A, Shah AM, Szweda LI, Sadek HA (2014) The oxygen-rich postnatal environment induces cardiomyocyte cell-cycle arrest through DNA damage response. *Cell* 157 (3):565-579. doi:10.1016/j.cell.2014.03.032
 127. Cardoso AC, Lam NT, Savla JJ, Nakada Y, Pereira AHM, Elnwasany A, Menendez-Montes I, Ensley EL, Petric UB, Sharma G, Sherry AD, Malloy CR, Khemtong C, Kinter MT, Tan WLW, Anene-Nzelu CG, Foo RS, Nguyen NUN, Li S, Ahmed MS, Elhelaly WM, Abdisalaam S, Asaithamby A, Xing C, Kanchwala M, Vale G, Eckert KM, Mitsche MA, McDonald JG, Hill JA, Huang L, Shaul PW, Szweda LI, Sadek HA (2020) Mitochondrial Substrate Utilization Regulates Cardiomyocyte Cell Cycle Progression. *Nat Metab* 2 (2):167-178
 128. Fuller SJ, Sivarajah K, Sugden PH (2008) ErbB receptors, their ligands, and the consequences of their activation and inhibition in the myocardium. *J Mol Cell Cardiol* 44 (5):831-854. doi:10.1016/j.yjmcc.2008.02.278
 129. Gassmann M, Casagrande F, Orioli D, Simon H, Lai C, Klein R, Lemke G (1995) Aberrant neural and cardiac development in mice lacking the ErbB4 neuregulin receptor. *Nature* 378 (6555):390-394. doi:10.1038/378390a0
 130. Lee KF, Simon H, Chen H, Bates B, Hung MC, Hauser C (1995) Requirement for neuregulin receptor erbB2 in neural and cardiac development. *Nature* 378 (6555):394-398. doi:10.1038/378394a0
 131. D'Uva G, Aharonov A, Lauriola M, Kain D, Yahalom-Ronen Y, Carvalho S, Weisinger K, Bassat E, Rajchman D, Yifa O, Lysenko M, Konfino T, Hegesh J, Brenner O, Neeman M, Yarden Y, Leor J, Sarig R, Harvey RP, Tzahor E (2015) ERBB2 triggers mammalian heart regeneration by promoting cardiomyocyte dedifferentiation and proliferation. *Nat Cell Biol* 17 (5):627-638.

- doi:10.1038/ncb3149
132. Meyer D, Birchmeier C (1995) Multiple essential functions of neuregulin in development. *Nature* 378 (6555):386-390. doi:10.1038/378386a0
 133. Liu J, Bressan M, Hassel D, Huisken J, Staudt D, Kikuchi K, Poss KD, Mikawa T, Stainier DY (2010) A dual role for ErbB2 signaling in cardiac trabeculation. *Development* 137 (22):3867-3875. doi:10.1242/dev.053736
 134. Uribe V, Ramadass R, Dogra D, Rasouli SJ, Gunawan F, Nakajima H, Chiba A, Reischauer S, Mochizuki N, Stainier DYR (2018) In vivo analysis of cardiomyocyte proliferation during trabeculation. *Development* 145 (14). doi:10.1242/dev.164194
 135. Gemberling M, Karra R, Dickson AL, Poss KD (2015) Nrg1 is an injury-induced cardiomyocyte mitogen for the endogenous heart regeneration program in zebrafish. *Elife* 4. doi:10.7554/eLife.05871
 136. Fukuda R, Aharonov A, Ong YT, Stone OA, El-Brolosy M, Maischein HM, Potente M, Tzahor E, Stainier DY (2019) Metabolic modulation regulates cardiac wall morphogenesis in zebrafish. *Elife* 8. doi:10.7554/eLife.50161
 137. Salazar-Roa M, Malumbres M (2017) Fueling the Cell Division Cycle. *Trends Cell Biol* 27 (1):69-81. doi:10.1016/j.tcb.2016.08.009
 138. Vander Heiden MG, Cantley LC, Thompson CB (2009) Understanding the Warburg effect: the metabolic requirements of cell proliferation. *Science* 324 (5930):1029-1033. doi:10.1126/science.1160809
 139. Yang W, Xia Y, Ji H, Zheng Y, Liang J, Huang W, Gao X, Aldape K, Lu Z (2011) Nuclear PKM2 regulates β -catenin transactivation upon EGFR activation. *Nature* 480 (7375):118-122. doi:10.1038/nature10598
 140. Dasgupta S, Rajapakshe K, Zhu B, Nikolai BC, Yi P, Putluri N, Choi JM, Jung SY, Coarfa C, Westbrook TF, Zhang XH, Foulds CE, Tsai SY, Tsai MJ, O'Malley BW (2018) Metabolic enzyme PFKFB4 activates transcriptional coactivator SRC-3 to drive breast cancer. *Nature* 556 (7700):249-254. doi:10.1038/s41586-018-0018-1
 141. Jeffery WR (2009) Regressive evolution in *Astyanax* cavefish. *Annu Rev Genet* 43:25-47. doi:10.1146/annurev-genet-102108-134216
 142. Aspiras AC, Rohner N, Martineau B, Borowsky RL, Tabin CJ (2015) Melanocortin 4 receptor mutations contribute to the adaptation of cavefish to nutrient-poor conditions. *Proc Natl Acad Sci U S A* 112 (31):9668-9673. doi:10.1073/pnas.1510802112
 143. Riddle MR, Aspiras AC, Gaudenz K, Peuß R, Sung JY, Martineau B, Peavey M, Box AC, Tabin JA, McGaugh S, Borowsky R, Tabin CJ, Rohner N (2018) Insulin resistance in cavefish as an adaptation to a nutrient-limited environment. *Nature* 555 (7698):647-651. doi:10.1038/nature26136
 144. Hayes JP, Garland T, Jr. (1995) THE EVOLUTION OF ENDOTHERMY: TESTING THE AEROBIC CAPACITY MODEL. *Evolution* 49 (5):836-847. doi:10.1111/j.1558-5646.1995.tb02320.x
 145. Nespolo RF, Solano-Iguaran JJ, Bozinovic F (2017) Phylogenetic Analysis Supports the Aerobic-Capacity Model for the Evolution of Endothermy. *Am Nat* 189 (1):13-27. doi:10.1086/689598
 146. Moorman AF, Christoffels VM (2003) Cardiac chamber formation: development, genes, and evolution. *Physiol Rev* 83 (4):1223-1267. doi:10.1152/physrev.00006.2003
 147. Sinclair J, Hoying D, Bresciani E, Nogare DD, Needle C, Wu W, Bishop K, Elkahoun A, Chitnis A, Liu P, Burgess S (2020) A metabolic shift to glycolysis promotes zebrafish tail regeneration through TGF- β dependent dedifferentiation of notochord cells to form the blastema. *bioRxiv*. doi:10.1101/2020.03.03.975318
 148. Benton MJ (1995) Diversification and extinction in the history of life. *Science* 268 (5207):52-58. doi:10.1126/science.7701342
 149. Falkowski PG, Katz ME, Milligan AJ, Fennel K, Cramer BS, Aubry MP, Berner RA, Novacek MJ, Zapol WM (2005) The rise of oxygen over the past 205 million years and the evolution of large placental mammals. *Science* 309 (5744):2202-2204. doi:10.1126/science.1116047
 150. Hsia CCW, Schmitz A, Lambertiz M, Perry SF, Maina JN (2013) Evolution of air breathing: oxygen homeostasis and the transitions from water to land and sky. *Comprehensive Physiology* 3 (2):849-915. doi:10.1002/cphy.c120003
 151. Payne JL, Boyer AG, Brown JH, Finnegan S, Kowalewski M, Krause RA, Jr., Lyons SK, McClain CR, McShea DW, Novack-Gottshall PM, Smith FA, Stempien JA, Wang SC (2009) Two-phase increase in the maximum size of life over 3.5 billion years reflects biological innovation and environmental opportunity. *Proc Natl Acad Sci U S A* 106 (1):24-27. doi:10.1073/pnas.0806314106
 152. Heallen T, Morikawa Y, Leach J, Tao G, Willerson JT, Johnson RL, Martin JF (2013) Hippo signaling impedes adult heart regeneration. *Development* 140 (23):4683-4690. doi:10.1242/dev.102798
 153. Leach JP, Heallen T, Zhang M, Rahmani M, Morikawa Y, Hill MC, Segura A, Willerson JT, Martin JF (2017) Hippo pathway deficiency reverses systolic heart failure after infarction. *Nature* 550 (7675):260-264. doi:10.1038/nature24045
 154. Aharonov A, Shakked A, Umansky KB, Savidor A,

- Genzelinakh A, Kain D, Lendengolts D, Revach OY, Morikawa Y, Dong J, Levin Y, Geiger B, Martin JF, Tzahor E (2020) ERBB2 drives YAP activation and EMT-like processes during cardiac regeneration. *Nat Cell Biol* 22 (11):1346-1356. doi:10.1038/s41556-020-00588-4
155. Bersell K, Arab S, Haring B, Kühn B (2009) Neuregulin1/ErbB4 signaling induces cardiomyocyte proliferation and repair of heart injury. *Cell* 138 (2):257-270. doi:10.1016/j.cell.2009.04.060
156. Magadum A, Singh N, Kurian AA, Munir I, Mehmood T, Brown K, Sharkar MTK, Chepurko E, Sassi Y, Oh JG, Lee P, Santos CXC, Gaziel-Sovran A, Zhang G, Cai CL, Kho C, Mayr M, Shah AM, Hajjar RJ, Zangi L (2020) Pkm2 Regulates Cardiomyocyte Cell Cycle and Promotes Cardiac Regeneration. *Circulation* 141 (15):1249-1265. doi:10.1161/circulationaha.119.043067



CHAPTER II

Single-cell analysis uncovers that metabolic reprogramming by ErbB2 signaling is essential for cardiomyocyte proliferation in the regenerating heart

Hessel Honkoop^{1#}, Dennis E.M. de Bakker^{1#}, Alla Aharonov², Fabian Kruse¹, Avraham Shakked², Phong D. Nguyen¹, Cecilia de Heus³, Laurence Garric¹, Mauro J Muraro¹, Adam Shoffner⁴, Federico Tessadori¹, Joshua C. Peterson⁵, Wendy Noort⁵, Alberto Bertozzi⁶, Gilbert Weidinger⁶, George Posthuma³, Dominic Grün⁷, Willem J. van der Laarse⁸, Judith Klumperman⁹, Richard T. Jaspers⁵, Kenneth D. Poss⁴, Alexander van Oudenaarden¹, Eldad Tzahor² and Jeroen Bakkers^{1,9*}

¹Hubrecht Institute and University Medical Center Utrecht, 3584 CT, Utrecht, The Netherlands

²Weizmann Institute of Science, Department of Molecular Cell Biology, Rehovot 7610001, Israel

³Department of Cell Biology and Institute of Biomembranes, Center for Molecular Medicine, University Medical Center Utrecht, 3584 CX, Utrecht, The Netherlands

⁴Regeneration Next, Department of Cell Biology, Duke University Medical Center, Durham NC 27710 USA

⁵Laboratory for Myology, Department of Human Movement Sciences, Faculty of Behavioural and Movement Sciences, Vrije Universiteit Amsterdam, 1081 BT Amsterdam, The Netherlands.

⁶Institute of Biochemistry and Molecular Biology, Ulm University, Ulm, Germany

⁷Max Planck Institute of Immunobiology and Epigenetics, 79108 Freiburg, Germany

⁸Department of Physiology, Institute for Cardiovascular Research, VU University Medical Center, 1007 MB Amsterdam, The Netherlands

⁹Department of Medical Physiology, Division of Heart and Lungs, University Medical Center Utrecht, 3584 CT Utrecht, the Netherlands.

Contributed equally

* Corresponding author

Published in *Elife* (2019)

ABSTRACT

While the heart regenerates poorly in mammals, efficient heart regeneration occurs in certain amphibian and fish species. Zebrafish has been used extensively to study heart regeneration, resulting in a model in which preexisting cardiomyocytes dedifferentiate and reinitiate proliferation to replace the lost myocardium. However, there is limited knowledge about the cellular processes that occur in this rare population of proliferating cardiomyocytes during heart regeneration. To identify such processes, we generated a transgenic line based on *nppa* expression that marks proliferating cardiomyocytes located at the wound border zone. Next, we have used a single-cell RNA-sequencing approach in the regenerating adult zebrafish heart and we uncovered that proliferating border zone cardiomyocytes have very distinct transcriptomes compared to the non-proliferating remote cardiomyocytes and that they resemble embryonic cardiomyocytes. Moreover, these cells have reduced expression of mitochondrial genes and reduced mitochondrial oxidative phosphorylation activity, while glycolysis gene expression and glucose uptake are increased, indicative for metabolic reprogramming. Furthermore, we find that inhibiting glycolysis impairs cardiomyocyte proliferation. Mechanistically, we find that the metabolic reprogramming of border zone cardiomyocytes is induced by Nrg1/ErbB2 signaling. This mechanism is conserved in murine hearts in which cardiomyocyte proliferation is induced by activating ErbB2 signaling. Together these results reveal a new mechanism in which glycolysis regulates cardiomyocyte proliferation during heart regeneration, which ultimately could help to develop novel methods to promote mammalian heart repair.

INTRODUCTION

Within the animal kingdom, regenerative capacity of damaged organs and body parts differs widely. While regenerative capacity is generally low in mammalian species, this can be very efficient in specific fish and amphibians (Poss, 2010). Even amongst animals of the same species, such as *Astyanax mexicanus* a teleost fish like the zebrafish, regenerative capacity can vary significantly (Stockdale et al., 2018). A better understanding of these differences and the cellular and molecular processes during tissue regeneration might ultimately help to improve the regenerative capacity of organs and tissues with poor intrinsic regenerative capacity.

The mammalian adult heart has very little regenerative capacity. The myocardium lost after an injury is replaced by scar tissue, which does not contribute to cardiac contraction resulting in reduced pumping efficiency and ultimately heart failure. Although a low level of cardiomyocyte turnover has been observed, there is no evidence of a stem cell population in the mammalian heart (Kretzschmar et al., 2018; van Berlo et al., 2014). Instead, a rare population of endogenous cardiomyocytes retains the capacity to proliferate to maintain cardiac homeostasis (Bergmann et al., 2009; 2015; Kimura et al., 2015; Senyo et al., 2012). Contrary to the adult heart, the neonatal mouse and potentially human heart still have the capacity to regenerate after injury (Haubner et al., 2016; Porrello et al., 2011). This regenerative capacity of the neonatal heart involves proliferation of pre-existing cardiomyocytes and is lost soon after birth most likely due to a sharp decrease in cardiomyocyte proliferation (Porrello et al., 2011; Soonpaa et al., 1996). Recent efforts to enhance proliferation of cardiomyocytes by either inhibiting Hippo signaling or activating the *Nrg1/ErbB2* signaling pathway in the adult mammalian heart have been successful and show the potential of existing cardiomyocytes to reenter the cell cycle. (Bersell et al., 2009; D'Uva et al., 2015; Heallen et al., 2011).

The zebrafish heart regenerates very efficiently and will regrow cardiac muscle without scarring (Poss et al., 2002). Lineage tracing experiments revealed a model in which proliferation of preexisting cardiomyocytes replaces the myocardium that was lost during the injury (Jopling et al., 2010; Kikuchi et al., 2010). While cardiomyocyte proliferation in the uninjured adult zebrafish heart is very low, 3 days after the injury (dpi) cardiomyocytes near the injury area (so-called border zone) start to reenter the cell cycle as observed by the induction PCNA expression, phosphorylated histone 3 and BrdU incorporation and proliferation peaks at 7 dpi (Jopling et al., 2010; Kikuchi et al., 2010), (Chablais et al., 2011; Gonzalez-Rosa et al., 2011; Schnabel et al., 2011; Wu et al., 2016). At the time when proliferation is observed, cardiomyocytes located in the border zone start to express cardiac transcription factors known for their role in embryonic heart development such as *nkx2.5* and *tbx20* and activate *gata4* enhancer elements (Kikuchi et al., 2010; Lepilina et al., 2006). In addition, border

zone cardiomyocytes show signs of dedifferentiation such as disorganization of sarcomere structures and the reexpression of embryonic myosins (Jopling et al., 2010; Wu et al., 2016). There is increasing evidence that other (non-muscle) cells in the heart secrete growth factors that stimulate cardiomyocyte proliferation including retinoic acid, TGF- β ligands, insulin-like growth factor, Hedgehog, and Neuregulin (Chablais and Jazwinska, 2012; Choi et al., 2013; Dogra et al., 2017; Gemberling et al., 2015; Lepilina et al., 2006; Wu et al., 2016; Zhao et al., 2019; 2014). In addition to these growth factors, prolonged hypoxia stimulates cardiomyocyte proliferation (Jopling et al., 2012; Marques et al., 2007).

The proliferating cardiomyocytes exist within a heterogeneous cell population including non-proliferating cardiomyocytes, endothelial cells and immune cells, hampering the discovery of genetic programs specific for these proliferating cardiomyocytes using whole tissue or spatially resolved RNA-sequencing (RNA-seq) approaches (Kang et al., 2016; Lien et al., 2006; Sleep et al., 2010). To identify molecular processes that differ between proliferating and non-proliferating cardiomyocytes, we explored a single-cell RNA-seq approach using the regenerating zebrafish heart. We found that upon injury, adult border zone cardiomyocytes dedifferentiate and resemble embryonic cardiomyocytes on a transcriptomic level. In addition, while adult cardiomyocytes mainly rely on fatty acid metabolism and mitochondrial oxidative phosphorylation (OXPHOS), border zone cardiomyocytes have reduced mitochondrial OXPHOS activity while genes encoding enzymes for glycolysis are induced and glucose uptake is enhanced. Importantly, Nrg1/ErbB2 signaling is sufficient to induce metabolic reprogramming in adult cardiomyocytes of both zebrafish as well as the murine hearts. In addition, the metabolic reprogramming from mitochondrial OXPHOS to glycolysis is required for efficient cardiomyocyte proliferation.

Together, these data support a model in which cardiomyocytes located in the border zone of the regenerating zebrafish heart undergo metabolic reprogramming, which is essential for cardiomyocyte proliferation and that this mechanism is conserved in a murine model with Nrg1/ErbB2 induced regeneration.

RESULTS

Single-cell RNA-seq reveals transcriptionally distinct border zone cardiomyocytes

The border zone comprises only a small fraction of the total number of cardiomyocytes in the injured ventricle (Wu et al., 2016). Several genes and regulatory sequencing have been identified that mark border zone cardiomyocytes, including *nppa*, which encodes for the cardiac stress hormone ANF (Kikuchi et al., 2010; Wu et al., 2016). To mark these borderzone cardiomyocytes we generated a transgenic zebrafish *nppa* reporter line (*TgBAC(nppa:mCitrine)*) in which mCitrine expression recapitulates endogenous cardiac

expression of *nppa* (Figure S1a-e). While low *nppa:mCitrine* expression was observed in trabecular cardiomyocytes of the remote area, higher expression was detected in the trabecular and cortical cardiomyocytes close to the injured area (Figures 1a and S1e). Moreover, expression of *nppa* correlates with previously reported border zone activity of *gata4* regulatory elements (Figure S1f) (Kikuchi et al., 2010). Histochemical analysis of cryo-injured adult hearts revealed that 75% (\pm 7%, n=3) of the cardiomyocytes expressing high levels of *nppa:mCitrine* reentered the cell cycle (Figure 1a). To obtain border zone (proliferating) and remote (non-proliferating) cardiomyocytes from the same tissue for further analysis, we cryo-injured *nppa:mCitrine* hearts followed by cell dissociation and FACS sorting for both mCitrine^{high} and mCitrine^{low} cells (Figure 1b). Individual, living cells were sorted, followed by single-cell mRNA-sequencing using the SORT-seq (SORTing and Robot-assisted Transcriptome SEQuencing) platform (Muraro et al., 2016) (Supplementary Data 1). In total 768 cells were sequenced in which we detected 19257 genes. We detected an average of 10,443 reads per cell and we introduced a cutoff at minimally 3500 reads per cell before further analysis, which resulted in the analysis of 352 cells. To identify the cardiomyocytes amongst the other cell types, we first identified the different cell types based on their transcriptomes. k-medoids clustering of the single cell transcriptomes by the RaceID clustering algorithm was used (Grün et al., 2015) (Figure 1c and Supplementary Data 2), and visualized in two dimensions using *t*-distributed stochastic neighbor embedding (*t*-SNE) (Figure 1d). A total of 12 cell clusters were identified, including a large group of cardiomyocytes (clusters 1,2,4,7 and 9), a smaller group of endothelial cells (clusters 5,6,8,10 and 12), and some fibroblasts (cluster 3) and immune cells (cluster 11) using the expression of marker genes for specific cell types (Figure S2). Based on the transcriptome clustering, the cardiomyocytes fell into four main transcriptionally-defined clusters (1, 2, 4 and 7), indicating that the injured heart contained subgroups of cardiomyocytes. To address whether the border zone cardiomyocytes were enriched in one of the four cardiomyocyte clusters we compared the mCitrine fluorescence intensity (recorded during FACS sorting) of the cardiomyocyte and found that the average intensity was highest in cluster 7 and lowest in cluster 2 (Figure S3). In addition, we analysed the single-cell transcriptome data for the expression of *nppa* and compared this to the expression of *vmhc* and *mustn1*, which mark border zone cardiomyocytes, and again found that cells expressing these genes were mostly in cluster 7 (Figure 1e and S4). Together, these results indicate two things: first, the border zone cardiomyocytes (grouped in cluster 7) can be identified as a separate group in the single-cell RNA-seq data. Secondly, these border zone cardiomyocytes are transcriptionally distinct from remote cardiomyocytes (grouped in cluster 2), while two intermediate cardiomyocyte clusters lie in between.

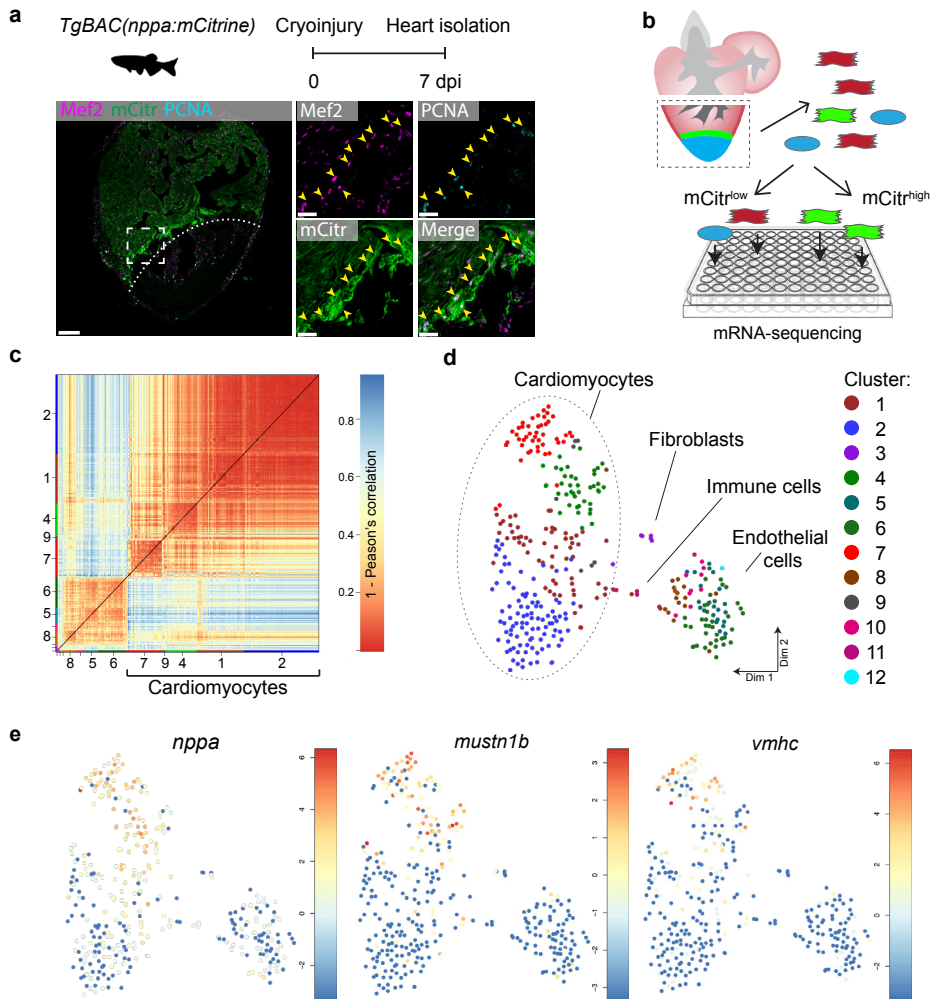


FIGURE 1. Single-cell mRNA sequencing identifies different cardiomyocyte-populations in the injured zebrafish heart.

(a) Schematic of cryoinjury procedure on adult *TgBAC(nppa:mCitrine)* fish and immunohistochemistry on section of injured *TgBAC(nppa:mCitrine)* heart 7 days post injury (dpi). Overview image on left and zoom-in of boxed region on the right. *Mef2* (in magenta) labels cardiomyocytes, *nppa:mCitrine* (in green) marks the borderzone, and *PCNA* (in cyan) marks proliferating cells. Arrows indicate triple-positive cells. Dashed line indicates injury site. Scale bar in overview 50 μm . Scale bar in zoom-ins 20 μm . (b) Experimental outline of the single-cell mRNA-sequencing of injured zebrafish hearts (blue, injury area; green, border zone) (c) Pairwise correlation between individual cells across all genes detected. Color-code indicates cell-to-cell distances measured by [1 - Pearson's correlation coefficient]. StemID clusters are indicated by color and number on the x- and y-axis. (d) t-distributed stochastic neighbor embedding (tSNE) map representation of transcriptome similarities between individual cells. (e) tSNE maps visualizing log₂-transformed read-counts of the border zone marker genes *nppa*, *mustn1b* and *vmhc*.

Border zone cardiomyocytes resemble embryonic cardiomyocytes

Cardiomyocytes in the border zone disassemble sarcomeric structures and re-express markers of embryonic cardiomyocytes suggesting their dedifferentiation. We therefore wanted to address the level of dedifferentiation of cluster 7 cardiomyocytes by comparing their transcriptome with embryonic cardiomyocytes. To obtain embryonic cardiomyocytes we performed FACS sorting on embryos expressing the cardiomyocyte specific marker *Tg(myf7:GFP)*. Single-cell mRNA-sequencing was performed and combined with the single-cell data from the injured adult hearts (Figure 2a). The RaceID algorithm identified several cell clusters with separate clusters for the embryonic and adult cardiomyocytes (Figure 2b, 2c and 2d). Importantly, the cluster 7 cardiomyocytes identified in the adult data analysis had a transcriptome that was highly similar to embryonic cardiomyocytes, as shown by pairwise correlation of the differentially expressed genes between the cardiomyocyte clusters: only 257 genes (p -value <0.01), out of 23,786 total detected genes, were differentially expressed between the embryonic and the cluster 7 (border zone) adult cardiomyocytes (Figure 2d and Supplementary Data 8) suggesting a dedifferentiation of border zone cardiomyocytes to embryonic-like cells. In contrast, over 1000 genes (p -value <0.01) were differentially expressed between embryonic and cluster 2 (remote zone) adult cardiomyocytes. A heatmap with unbiased hierarchical clustering on the 500 most differentially expressed genes between the 3 clusters confirmed that cluster 7 cardiomyocytes were more closely related to embryonic than cluster 2 cardiomyocytes (Figure 2e). Corroborating the observation that border zone cardiomyocytes resemble embryonic cardiomyocytes we found that genes encoding sarcomere proteins and cardiac-specific factors highly expressed in the embryo were re-expressed in cluster 7 (border zone) cardiomyocytes (Figure 2f, 2g and 2h).

To identify cellular events that occur during this dedifferentiation we used part of the RaceID algorithm (StemID) that uses the single cell transcriptome data and cell clustering to derive a branched lineage tree (Grün et al., 2016). The algorithm is based on the premise that stem cells and less differentiated cells tend to exhibit more uniform transcriptomes than differentiated cells, which express smaller numbers of genes at higher rates (Banerji et al., 2013). Using this approach, we found large differences in transcriptome entropy, resulting in low (cluster 2), intermediate (clusters 1 and 4) and high (cluster 7) StemID scores (Figure 3a). This gradual increase suggests a dedifferentiation axis from cells in cluster 2 (remote myocardium) to cells in cluster 7 (border zone myocardium) and is in good agreement with our finding that the transcriptome of cluster 7 cardiomyocytes resembles an embryonic cardiomyocyte transcriptome (Fig. 3b). Together, these results indicate that clusters 4 and 7 are enriched for dedifferentiated and proliferative border zone cardiomyocytes while clusters 1 and 2 are enriched for differentiated remote cardiomyocytes.

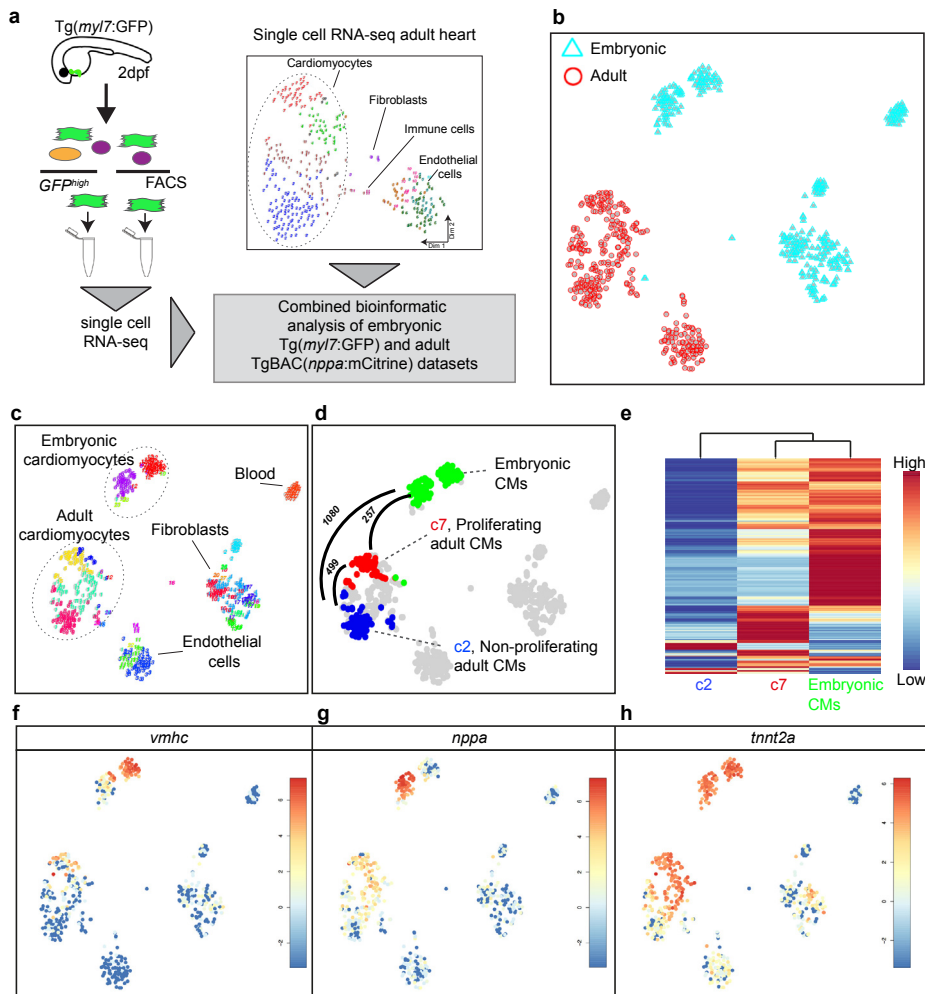


FIGURE 2. Single-cell transcriptome of border zone cardiomyocytes resembles that of embryonic cardiomyocytes.

(a) Cartoon to illustrate the experimental procedure for single cell analysis of embryonic and adult cardiac cells. (b) tSNE map of combined adult (red) and embryonic datasets (light blue). (c) tSNE map indicating the different cell types based on marker gene expression. (d) tSNE map with the adult cardiomyocytes of the injured heart (cluster 7 in red, cluster 2 in blue and clusters 1 and 4 in grey) and embryonic (2 dpf) cardiomyocytes (in green), with number of pairwise differentially expressed genes (p -value<0.01) indicated between cardiomyocyte clusters. (e) Heatmap with hierarchical clustering based on the 500 most differentially expressed genes between clusters. Red color represents high expression, blue color represents low expression. Rows represent individual genes. (f-h) tSNE maps visualizing \log_2 -transformed read-counts of *vmhc* (f), *nppa* (g) and *tnnt2a* (h).

Border zone cardiomyocytes induce glycolysis, which is required for proliferation.

While cardiomyocytes undergo a well-defined sequence of morphological and transcriptional changes during differentiation, very little is known about the reverse process. Ordering whole-transcriptome profiles of single cells with an unsupervised algorithm can resolve the temporal resolution during differentiation by identifying intermediate stages of differentiation without a priori knowledge of marker genes (Trapnell et al., 2014). In this manner, the single-cell mRNA-seq experiment will constitute an in-silico time series, with each cell representing a distinct state of differentiation along a continuum. To analyze the transcriptional changes occurring during this apparent dedifferentiation, the most likely dedifferentiation path, based on the StemID scores, was chosen starting at cluster 2 and progressing through clusters 1, 4 and 7. Next, gene expression profiles along this pseudo-temporal order were computed for all detected genes using the single-cell transcriptomes. These gene expression profiles were grouped into modules of co-expressed genes using self-organizing maps (SOMs), resulting in 14 modules (Figure 3c, Supplementary Data 7). Corroborating our hypothesis of varying differentiation states, we observed that gene expression within these modules changed smoothly over pseudo time. We next analyzed the temporally-ordered expression profiles and identified four groups of genes that shared the same dynamics of expression during this differentiation trajectory. The first group (modules 1, 2) contained genes that were most highly expressed only in cells at the very beginning of the pseudo time line and their expression rapidly declined in cells that were positioned later. This group contained many genes transcribed from mitochondrial DNA and with a role in energy metabolism, which indicates that the cells at the start of the pseudo time line are mature cardiomyocytes. The second group (module 6) contained genes that are expressed early and stay constant in cells further along the pseudo time line. Many genes involved in translation and cell cycle regulation follow this expression pattern. The third group showed an exponential increase in expression with the highest expression at the end of the pseudo time line (module 10). This group contained genes with a function in cardiac muscle fiber development and heart contraction. The fourth group (modules 11 and 14) contained genes with a rapid increase in expression that peaks before the end of the pseudo time, suggestive for an early role during the dedifferentiation process. Interestingly this group contained many genes with a known role in glycolysis. Together, these data suggest that border zone cardiomyocytes undergo profound metabolic changes. This was confirmed by GO-term analysis between cluster 7 and cluster 2 cells (Figure S5a and S5b)

To validate the functional consequences of the observed changes in mitochondrial gene expression, we measured succinate dehydrogenase (SDH) enzyme activity, located in the inner mitochondrial membrane that functions in both the citric acid cycle and electron transport chain. We observed a 40% reduction in SDH activity specifically in the border zone cardiomyocytes as compared to the remote cardiomyocytes (Figure 4a). In agreement with the reduced mitochondrial OXPHOS activity, transmission electron microscopy (TEM)

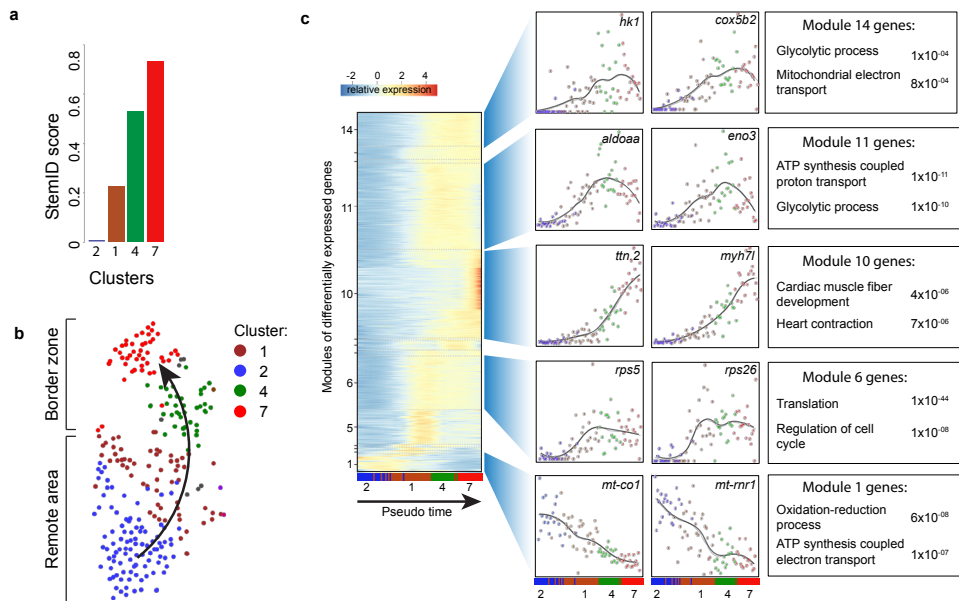


FIGURE 3. Pseudo time analysis reveals dedifferentiation and metabolic changes in border zone cardiomyocytes.

(a) Bar plot of StemID scores for the cardiomyocyte clusters (clusters #2, 1, 4 and 7) calculated by the formula: number of significant links for each cluster multiplied by the median transcriptome entropy across all cells in a cluster. (b) Cardiomyocyte clusters from adult injured heart. Arrow indicates the dedifferentiation path derived from the StemID scores. (c) Pseudo time analysis. Left; one-dimensional SOM of z-score transformed expression profiles along the differentiation trajectory incurred by StemID analysis. Y-axis represents the fourteen modules with differentially expressed genes. X-axis represents the pseudo time in which the cells were ordered. Middle; expression profiles of representative genes of the major modules. Y-axis shows transcript counts. X-axis represents the pseudo time. Right; Major gene ontology terms derived from all genes expressed in the module with p-values.

imaging revealed more immature mitochondria in border zone cardiomyocytes evidenced by their altered morphology and reduced cristae density (Figure 4b), which is consistent with previous reports linking mitochondrial function with morphology (Giraud et al., 2002; Paumard et al., 2002). Since the pseudotime analysis suggested an upregulation of glycolytic gene expression in the border zone cluster (#7), we performed gene set enrichment analysis (GSEA) for glycolysis genes. The GSEA revealed a strong and significant enrichment in the expression of glycolytic genes in cluster 7 cells compared to cluster 2 cells (Figure S5c). By in situ hybridization we confirmed the induced expression in border zone cardiomyocytes of the rate-limiting enzymes hexokinase (*hk1*), pyruvate kinase M1/M2a (*pkma*) and pyruvate dehydrogenase kinase (*pdk2a*), which diverts pyruvate away from the TCA cycle (Figure 4c and S4b). Corroborating the suggested enhanced glycolysis, we observed induced expression of glucose importer genes (*glut1a/slc2a1a* and *glut1b/slc2a1b*) in cluster 7 cells (Figure S5d) and enhanced *in vivo* glucose uptake of border zone cardiomyocytes (Figure 4d).

Furthermore, genes encoding lactate transporters and their proteins were upregulated in cluster 7 and border zone cardiomyocytes (Figure 4e and S5d). Together, these data indicate that during regeneration border zone cardiomyocytes switch energy metabolism from mitochondrial OXPHOS to glycolysis and lactate fermentation.

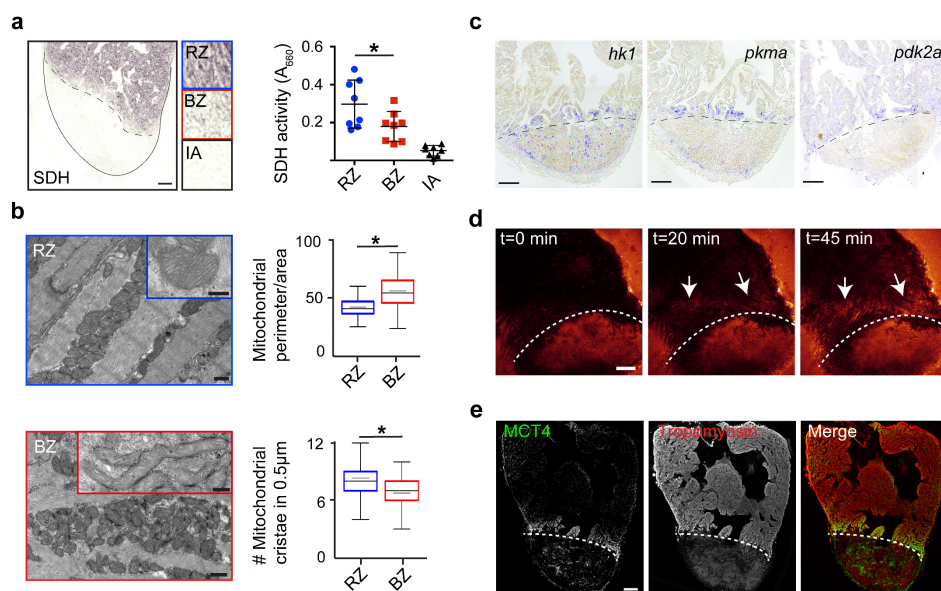


FIGURE 4. Border zone cardiomyocytes undergo a metabolic switch from mitochondrial OXPHOS to glycolysis.

(a) Succinate dehydrogenase (SDH) enzyme staining on a 7 dpi heart section with injury area separated by dashed line. Quantification of SDH activity in remote zone (RZ), border zone (BZ) and injury area (IA). Scale bar indicates 100 μ m. Error bars indicate mean and standard deviation. (b) Transmission electron microscopy (TEM) images of mitochondria in cardiomyocytes from the remote zone and the border zone of a 7 dpi injured heart. Note the disorganized and irregular shaped mitochondria in the border zone cardiomyocyte. Scale bar 500 nm (200 nm in inserts). Graphs show quantification of mitochondrial perimeter-to-area as a measurement for roundness and quantification of mitochondrial cristae density. * P-value<0.05. (c) In situ hybridizations for glycolytic genes *hk1*, *pkma* and *pdk2a* on sections of injured zebrafish hearts at 7 dpi. Dashed line indicates injury site. Scale bars indicate 100 μ m. (d) Time-lapse multi-photon confocal images of whole heart. The heart was isolated at 7 dpi and incubated with 2-NBDG, a fluorescent glucose analogue, at t=0. Dotted line indicates injury area. Arrows point to regions of the border zone. Scale bar represents 100 μ m. (e) Confocal image of injured zebrafish hearts at 7 dpi stained for the lactate transporter MCT4 (green) and Tropomyosin (red). Dashed line indicates injury site.

The pseudo time line analysis suggested that glycolysis genes induction precedes the induction of embryonic cardiac gene expression. Indeed, ISH analysis showed that glycolysis gene expression is already induced at 3 dpi and thereby precedes expression of embryonic cardiac gene expression and cardiomyocyte proliferation, which peaks at 7 dpi (Figure S6).

To address the functional importance of glycolysis we inhibited glycolysis in injured fish with the glucose analogue 2-Deoxyglucose (2-DG), a general inhibitor of glycolysis, and analyzed its effect on cardiomyocyte proliferation (Figure 5a). We observed that repeated injections of 2-DG in the adult zebrafish with a cryoinjured heart significantly impaired cardiomyocyte proliferation in the border zone (Figure 5b,c), suggesting that glycolysis is necessary for cell cycle reentry.

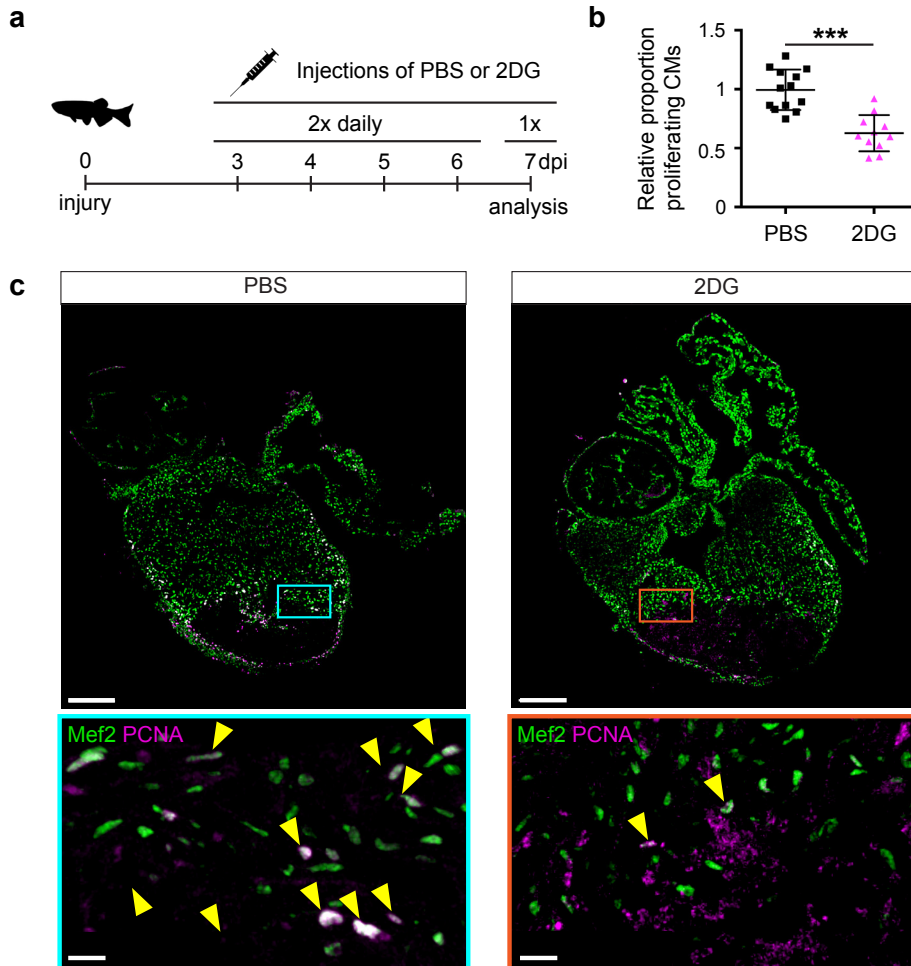


FIGURE 5. 2-Deoxy glucose impairs cardiomyocyte proliferation

(a) Experimental design for the 2-DG injections to inhibit glycolysis in injured zebrafish hearts. (b) Confocal image of injured zebrafish hearts at 7 dpi either injected with PBS or 2-DG stained for Mef2c (green) and PCNA (magenta). Zoom-in images of the borderzone are shown below overview pictures for both PBS (cyan box) and 2-DG (orange box). Arrowheads indicate nuclei positive for Mef2c and PCNA. Scale bar indicates 200 μ m (overview) or 20 μ m (zoom-in). (c) Quantification of the proliferating cardiomyocytes (double Mef2c/PCNA positive) in the border zone of PBS and 2-DG treated hearts represented as the proportion of proliferating cardiomyocytes compared to the average percentage in the PBS injected group. Each dot represents a single heart (3 sections per heart analyzed). Hearts were pooled from two separate experiments. Error bars represent mean \pm standard deviation. ***, $p < 0.0001$

Nrg1/ErbB2 signaling induces glycolytic gene expression in border zone cardiomyocytes

Next, we investigated the upstream signals that drive the observed metabolic reprogramming in border zone cardiomyocytes during cell cycle reentry. Hypoxia is a well-known stimulus for metabolic reprogramming during cancer and promotes cardiomyocyte proliferation during cardiac regeneration (Jopling et al., 2012; Nakada et al., 2016; Vander Heiden et al., 2009). The responses to hypoxia are induced by the transcription factor, hypoxia inducible factor (HIF), whose activity can be visualized using the *Tg(phd3:GFP)* reporter line (Santhakumar et al., 2012; Wang and Semenza, 1993). When analysing cryo-injured hearts of *Tg(phd3:GFP)* fish 7 days post injury we did not observe a good correlation between *phd3:GFP* reporter activity and the induction of *ldha* expression in border zone cardiomyocytes suggesting that HIF signaling is not required for the observed induction of glycolysis gene expression in border zone cardiomyocytes (Figure S7). Injury-induced Neuregulin 1 (Nrg1) expression is another potent mitogen that induces cardiomyocyte dedifferentiation and cell cycle reentry by activating ErbB2 receptor signaling (Gemberling et al., 2015). Furthermore, *in vitro* experiments suggest that Nrg1 can induce glucose metabolism (Cote et al., 2005; Suárez et al., 2001). To address whether Nrg1 can induce metabolic reprogramming *in vivo*, we used a previously described transgenic zebrafish model in which Nrg1 overexpression (OE) can be induced in a heart specific manner, *tg(cmlc2:CreER; β -act2:BSNrg1)* (Gemberling et al., 2015). In this model especially cortical cardiomyocytes start to divide after tamoxifen injection leading to thickening of this layer. We observed a profound and consistent upregulation of glycolysis genes in the cortical myocardium coinciding with the reported cardiomyocyte dedifferentiation and proliferation in this layer (Figure 6a). Expression of *ldha* and *hk1*, encoding the rate limiting glycolytic enzyme hexokinase, was strongly induced in the ventricular wall of Nrg1 OE hearts, which correlates well with the observed induction of cardiomyocyte dedifferentiation and proliferation in this region (Gemberling et al., 2015). Next, we assessed whether blocking Nrg1/ErbB2 signaling impairs glycolytic upregulation in the zebrafish border zone after cryoinjury. qPCR confirmed the profound upregulation of glycolytic genes in border zone cardiomyocytes compared to their expression in cardiomyocytes from uninjured hearts (Figure 6b). Importantly the ErbB2 inhibitor AG1478 inhibited the induction of glycolytic gene expression in border zone cardiomyocytes (Figure 6b). In contrast to the other glycolysis genes, *hk1* expression was not reduced after AG1478 treatment likely as a result of redundant signaling pathways in the border zone. From these results, we conclude that glycolysis gene expression can be induced by Nrg1/ErbB2 signaling even in the absence of cardiac injury and that endogenous Nrg1/ErbB2 signaling is an important mediator of metabolic rewiring during zebrafish heart regeneration.

Activating ErbB2 signaling induces a metabolic switch from OXPHOS to glycolysis and lactate fermentation in murine cardiomyocytes

The regenerative capacity of the adult murine heart is very low, but cardiomyocyte

dedifferentiation and proliferation can be stimulated by cardiomyocyte specific overexpression of a constitutively active ErbB2 receptor (caErbB2 OE) (D'Uva et al., 2015). To address whether this is correlated with metabolic changes we performed qPCRs for metabolic genes on cardiac tissue from caErbB2 mice. Indeed, we observed that critical glycolysis genes (e.g. *Pfkfb*, *Pdk3* and *Pkm2*) including glucose and lactate transporters (*Slc16A3* and *Slc2A1*) were significantly upregulated in caErbB2 OE cardiomyocytes while genes transcribed from mitochondrial DNA were downregulated (Figure 6c). *Pdk3* encodes a pyruvate dehydrogenase kinase, which phosphorylates pyruvate dehydrogenase (PDH). PDH is a mitochondrial multi-enzyme complex that converts pyruvate to Acetyl-CoA and provides a primary link between glycolysis and the TCA cycle. Upon phosphorylation by PDK, p-PDH is inactivated and pyruvate is diverted away from the TCA cycle resulting in enhanced lactate production. Consistent with the increase in *pdk3* expression, an increased phosphorylation of PDH was observed in the inner myocardial layer of caErbB2 OE hearts (Figure 6d).

Next, we addressed whether the observed switch in metabolic gene expression correlated with enhanced regenerative capacity after injury. Therefore, we performed myocardial infarction (MI) in wild type and caErbB2 OE hearts. Even though glucose uptake and glycolytic enzyme activity in the ischemic area are increased by MI (Schelbert and Buxton, 1988) (Owen et al., 1969), we observed a stronger upregulation of glycolytic gene expression and decreased mitochondrial gene expression in caErbB2 OE hearts with MI compared to wild type hearts with MI (Figure S8). This stronger and consistent upregulation of glycolytic gene expression in caErbB2 OE hearts correlates with the reported enhanced cardiomyocyte proliferation and improved regeneration (D'Uva et al., 2015). These findings imply that the enhanced glucose uptake and anaerobic glycolysis observed after MI might be sufficient for cell survival, but that a stronger induction of glycolysis gene expression is required to fully stimulate cardiomyocyte proliferation and regeneration.

CaErbB2 induced cardiomyocyte proliferation depends on glycolysis

Finally, we addressed whether the observed metabolic switch to glycolysis in caErbB2 OE cardiomyocytes is required for their reentry into the cell cycle (Figure 7a). Corroborating our model, we indeed observed that treating caErbB2 OE cardiomyocytes *in vitro* with the glycolysis inhibitors 2-DG or lonidamine strongly and significantly impaired cell cycle reentry (Figure 7b and 7c) and cytokinesis (Figure 7d and 7e). Together these results indicate that in murine cardiomyocytes, ErbB2 signaling drives a metabolic switch towards glycolysis, which is required for their cell cycle reentry. These results suggest that this metabolic switch in cardiomyocytes is beneficial for heart regeneration.

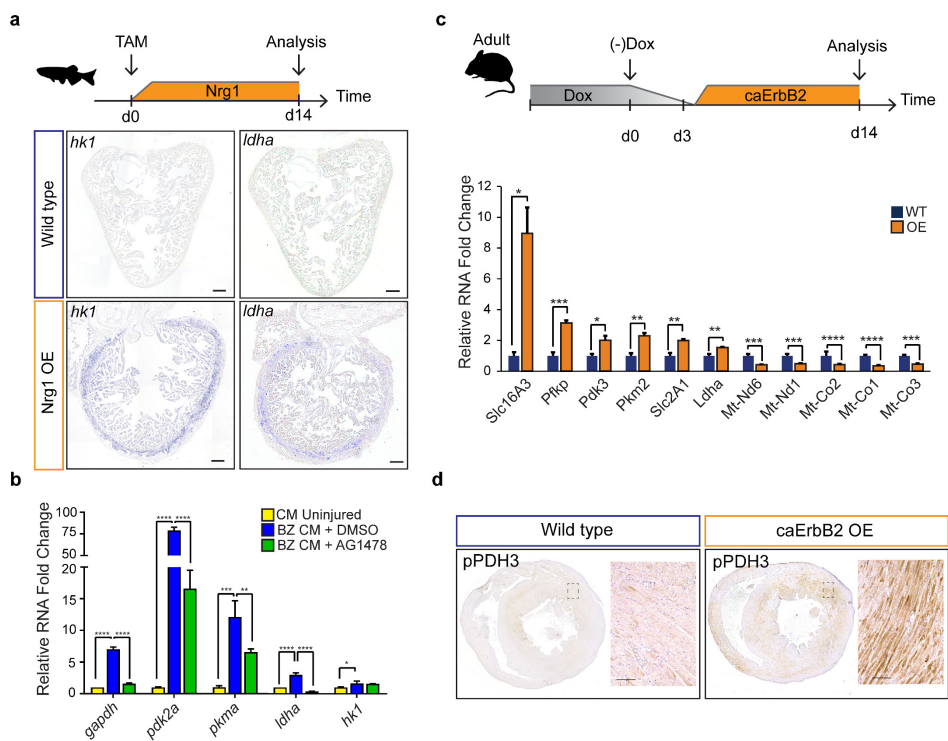


FIGURE 6. Nrg1/ErbB2 signaling induces glycolysis genes in zebrafish and mouse.

(a) Cartoon showing experimental procedure to induce cardiomyocyte specific Nrg1 expression in zebrafish. Panels show in situ hybridization for *hexokinase 1* (*hk1*) and *lactate dehydrogenase a* (*ldha*) expression on sections of control hearts (β -act2:*BSNrg1*) and Nrg1 OE hearts (*cm1c2:CreER*; β -act2:*BSNrg1*). Scale bars represent 100 μ m. (b) qPCR results for glycolytic genes showing their relative fold change in DMSO treated (n=9) (blue) and AG1478 treated (n=9) (green) *nppa*:mCitrine high border zone cardiomyocytes at 3dpi compared to uninjured adult cardiomyocytes (n=4) (yellow). Error bars represent standard deviation. (c) Upper panel: Cartoon showing the experimental procedure to analyse metabolic gene expression after activating ErbB2 signaling in the murine heart. Lower panel: qPCR results for metabolic genes showing their relative fold change in caErbB2 OE (n=4) heart compared to control WT hearts (n=4). Error bars represent standard deviation. (d) Immunohistochemistry for phospho-PDH3 on sections of control and caErbB2 OE hearts. Scale bars represent 100 μ m.

* = $p < 0.05$, ** = $p < 0.01$, *** = $p < 0.001$, **** = $p < 0.0001$

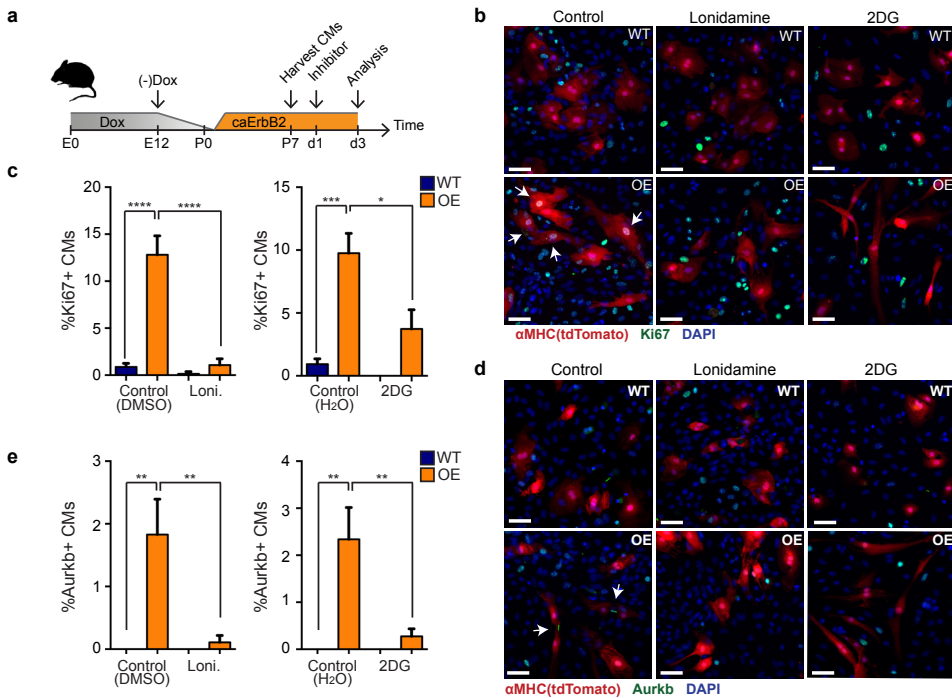


Figure 7. Glycolysis inhibitors impair mitogenic effect of ErbB2 activation in cardiomyocytes. (a) Cartoon showing the experimental procedure to analyse the effects of glycolysis inhibitors (2-DG and lonidamine) on cardiomyocyte proliferation. (b) Immunofluorescence analysis on P7 cardiac cultures derived from WT and caErbB2 OE hearts that are endogenously fluorescent for tdTomato under the α MHC promoter, stained for the cell-cycle marker Ki67. Arrows point at Ki67+ CMs. (c) Quantification of % Ki67+ CMs from WT and caErbB2 OE derived from P7 cardiac cultures treated with the glycolysis inhibitors 2-DG (n=4 for WT and n=4 for OE), and lonidamine (n=7 for WT and n=4 for OE) or their diluents as controls. (d) Immunofluorescence analysis on P7 cardiac cultures derived from WT and caErbB2 OE hearts that are endogenously fluorescent for tdTomato under the α MHC promoter, stained for the cytokinesis marker Aurora kinase B. Arrows point at Aurkb+ CMs. (e) Quantification of % Aurkb+ CMs from WT and caErbB2 OE derived from P7 cardiac cultures treated with the glycolysis inhibitors 2-DG (n=4 for WT and n=4 for OE), and lonidamine (n=7 for WT and n=4 for OE) or their diluents as controls. In all panels, bars represent the mean, and error bars represent s.e.m * p<0.05, ** p<0.01, *** p<0.001, **** p<0.0001, Scale bars represent 50 μ m

DISCUSSION

Heart regeneration in zebrafish is very efficient and relies on the proliferation of preexisting cardiomyocytes. The number of proliferating cardiomyocytes that is induced by injury is very small and they comprise only a small portion of the total cardiomyocytes, which has hampered their characterization. Thus far, RNA-seq data sets and differential gene analysis was based on whole tissue preparations or cryosections of uninjured and injured hearts (Goldman et al., 2017; Kang et al., 2016; Lai et al., 2017; Lien et al., 2006; Sleep et al., 2010; Wu et al., 2016). Not only cardiomyocytes but other cell types in the heart

such as epicardial and endocardial cells respond to the injury by the upregulation of injury-induced genes (Lepilina et al., 2006). Furthermore, the injured heart is infiltrated by immune cells and fibroblasts appear (Gonzalez-Rosa et al., 2011; Lai et al., 2017). Together, this complicates the detection of cardiomyocyte specific gene responses. The use of single cell transcriptomics can overcome these limitations and has allowed us to identify and characterize the different cardiomyocyte populations in the regenerating zebrafish heart. Here we have generated a unique RNA-seq dataset at single-cell resolution of cardiomyocytes during heart regeneration, which can be used as a resource to study and identify novel mechanisms.

Activation of Yap signaling in the murine heart promotes cardiomyocyte proliferation, which involves a partial reprogramming and dedifferentiation of adult cardiomyocytes towards a neonatal fate (Monroe et al., 2019). Interestingly, single-cell RNA-seq analysis of connective tissue cells during limb blastema formation revealed that their transcriptome is highly similar to embryonic limb precursor cells (Gerber et al., 2018). Together with our results that a similar reprogramming takes place during injury induced heart regeneration in zebrafish it suggests a common theme in which adult tissues that lack a clear stem cell use an alternative strategy to regenerate the missing tissue by reprogramming differentiated cells into embryo-like cells. This might involve different mechanisms since Yap signaling is not required for cardiomyocyte proliferation during zebrafish heart regeneration (Flinn et al., 2018). The presence of embryo-like cardiomyocytes in the border zone after injury can explain the observed switch from trabecular cardiomyocytes into cortical cardiomyocytes during zebrafish heart regeneration, since embryonic cardiomyocytes give rise to both trabecular and cortical cardiomyocytes (Sánchez-Iranzo et al., 2018; Staudt et al., 2014).

Increased mitochondrial OXPHOS activity promotes cardiomyocyte maturation and reduces the proliferative capacity of cardiomyocytes (Mills et al., 2017). This correlates well with the loss of regenerative capacity of the murine heart in the first week after birth at which time the metabolism in cardiomyocytes changes from predominantly glycolysis to mitochondrial OXPHOS (Lopaschuk et al., 1992; Menendez-Montes et al., 2016; Porrello et al., 2011). Reactive oxygen species (ROS) generated by mitochondrial OXPHOS induce DNA damage causing cardiomyocyte cell-cycle arrest (Nakada et al., 2016; Puente et al., 2014; Tao et al., 2016). Our pseudo time line analysis shows a rapid downregulation of mitochondrial gene expression together with an increase in genes encoding glucose transporters, glycolytic enzymes and lactate transporters. A direct role for glycolysis and lactate fermentation in cardiomyocyte proliferation had not been addressed and our results that pharmacological inhibition of glycolysis impairs cardiomyocyte proliferation suggest that activation of glycolysis can drive the reprogramming of cardiomyocytes. It also raises the question why cardiomyocytes need to switch their metabolism to glycolysis to reenter the cell cycle? Interestingly, a similar metabolic shift from mitochondrial OXPHOS to glycolysis and lactate

fermentation occurs in proliferating tumor cells, and was first described by Otto Warburg (Warburg et al., 1927). Since this glucose to lactate transformation occurs regardless of whether oxygen is present it is referred to as aerobic glycolysis. While glycolysis generates much less ATP compared to fatty acid oxidation, it is thought that glycolysis and the connected pentose-phosphate pathway provides essential metabolites that are needed to create sufficient biomass to sustain proliferation of the tumor cells (Vander Heiden et al., 2009). Furthermore, progenitor cells in the developing embryo as well as induced pluripotent stem cells depend on glycolysis to maintain proliferation and their potency (Folmes et al., 2011; Gu et al., 2016) (Mathieu and Ruohola-Baker, 2017). In addition, glycolytic enzymes such as PKM2 and PFKFB4 can also directly interact with cell cycle regulators to promote proliferation (Yang et al., 2011) (Dasgupta et al., 2018). The precise role for glycolysis in driving the cellular reprogramming during heart regeneration needs to be further investigated using genetic loss- and gain-of-function experiments combined with metabolomics, which is challenging given the low number of proliferating cardiomyocytes in the regenerating heart.

Activation of Nrg1/ErbB2 signaling in either zebrafish or mouse hearts induces cardiomyocyte dedifferentiation and proliferation (D'Uva et al., 2015; Gemberling et al., 2015). Our results build upon these observations and indicate that Nrg1/ErbB2 signaling induces profound metabolic reprogramming in cardiomyocytes and that this is required for efficient cardiomyocyte proliferation. Future work should address how Nrg1/ErbB2 signaling induces metabolic reprogramming in cardiomyocytes, which could have important implications for stimulating mammalian heart regeneration (Polizzotti et al., 2015).

METHODS

Transgenic zebrafish lines and cryoinjury

All procedures involving animals were approved by the local animal experiments committees and performed in compliance with animal welfare laws, guidelines and policies, according to national and European law.

The following fish lines were used: TL, Tg(*phd3*:GFP), Tg(*gata4*:EGFP)^{ae1} and myl7:GFP^{twu34Tg} (Huang et al., 2003) (Kikuchi et al., 2010; Santhakumar et al., 2012). The Tg(*cm1c2*:*CreER*; β -*act2*:*BSNrg1*) line was used as described before (Gemberling et al., 2015). The TgBAC(*nppa*:mCitrine) line was generated essentially as described previously (Bussmann and Schulte-Merker, 2011). In short, an iTOL2_amp cassette for pTarBAC was inserted in the vector sequence of bacterial artificial chromosome (BAC) CH211-70L17, which contains the full *nppa* locus. Subsequently, a mCitrine_kan cassette was inserted at the ATG start codon of the first exon of the *nppa* gene. Amplification from a pCS2+mCitrine_kanR plasmid

was achieved with primers :

FWD_NPPA_HA1_GFP

5'-gagccaagccagttcagagggcaagaaaacgcattcagagacactcagagACCATGGTGAGCAAGGG-CGAGG-3' and REV_NPPA_HA2_NEO

5'-gtctgctgccaaccaggagcagcagtcctgtcagaattagtccccggcTCAGAAGAACTCGT-CAAGAAGGCGATAGAA -3'.

Sequences homologous to the BAC are shown in lower case. Recombineering was performed following the manufacturer's protocol (Red/ET recombination; Gene Bridges GmbH, Heidelberg, Germany) with minor modifications. BAC DNA isolation was carried out using a Midiprep kit (Life Technologies BV, Bleiswijk, The Netherlands). BAC DNA was injected at a concentration of 300 ng/μl in the presence of 25ng Tol2 mRNA. At 3 dpf, healthy embryos displaying robust nppa-specific fluorescence in the heart were selected and grown to adulthood. Subsequently, founder fish were identified by outcrossing and their progeny grown to adulthood to establish the transgenic line.

Zebrafish of ~ 4 to 18 months of age (males and females, TL strain) were used for regeneration experiments. Cryoinjuries were performed as previously described (Schnabel et al., 2011), except that a liquid nitrogen-cooled copper filament of 0.3 mm diameter was used instead of dry ice.

Sample sizes were chosen to accommodate the generally accepted standards in the field: 5 or more cryoinjured hearts per condition.

Animals were only excluded from experiments in case of severe sickness/infection/aberrant behavior (according to animal experiment guidelines).

Transgenic mouse lines and animal procedures.

Doxycycline-inducible CM-restricted overexpression of a constitutively active ErbB2 (caErbB2) was generated by crossing the TetRE-caErbB2 (Xie et al., 1999) mouse line with αMHC-tTA which expresses the tetracycline-responsive transcriptional activator (tTA) under the control of the human alpha myosin heavy chain promoter (αMHC) (Yu et al., 1996). Doxycycline (DOX, Harlan Laboratories, TD02503) was administered in the food to repress transgene expression. For cultures derived of OE/WT hearts, we additionally intercrossed the αMHC-cre ROSA26-tdTomato transgenes in order to visualize CMs.

For myocardial infarction, mice were sedated with isoflurane (Abbott Laboratories) and were artificially ventilated following tracheal intubation. Experimental myocardial infarction was induced by ligation of the left anterior descending coronary artery (LAD ligation). Following

the closure of the thoracic wall mice were warmed for several minutes until recovery.

Immunofluorescence

ADULT: For immunofluorescence, hearts were extracted, fixed in 4% PFA at room temperature for 1,5 h and cryosectioned into 10 μm sections. Heart sections were equally distributed onto seven serial slides so each slide contained sections representing all areas of the ventricle.

Primary antibodies used were anti-AuroraB kinase (BD Transduction laboratories #611082, 1:200), anti-Ki67 (Cell Marque #275R, 1:200), anti-MCT4 (Santa Cruz #SC50329, 1:200), anti-PCNA (Dako #M0879, 1:800), anti-GFP (aves #GFP-1010, 1:1000), and anti-Mef2c (Santa Cruz #SC313, Biorbyt #orb256682 both 1:1000). Antigen retrieval was performed by heating slides containing heart sections at 85°C in 10 mM sodium citrate buffer (pH 6) for 10 minutes. Secondary antibodies conjugated to Alexa 488 (ThermoFisher Scientific), Cy3 or Cy5 (Jackson Laboratories) were used at a dilution of 1:1000. Nuclei were shown by DAPI (4',6-diamidino-2-phenylindole) staining. Images of immunofluorescence stainings are single optical planes acquired with a Leica Sp8 or Sp5 confocal microscope. Quantifications of PCNA, Mef2, and mCitrine expression were performed in cardiomyocytes situated within 150 μm from the wound border on 3 sections of >4 hearts. Sections were masked before quantification.

EMBRYONIC: Live embryos were immobilized using ms222 and embedded in nitrocellulose + E3 to be mounted on a Leica SPE confocal microscope, followed by a Z-stack maximum projection (step size 2 μm).

MAMMALIAN P7 CARDIAC CULTURES: For immunofluorescence, cardiac cultures were fixed with 4% PFA for 10 minutes on room temperature on the shaker, followed by permeabilization with 0.5% Triton X-100 in PBS for 5min, and blocking with 5% bovine serum albumin (BSA) in PBS containing 0.1% Triton for 1h at room temperature. Masking was performed before quantification.

Quantitative PCR

ADULT ZEBRAFISH: *nppa*:mCitrine zebrafish were cryoinjured and received two overnight pulses of DMSO (1:2000) or 5 μM AG1478 (10mM stock in DMSO; Selleck Chemical, Houston, TX) from 1dpi to 2dpi and from 2dpi to 3dpi. Then, hearts were extracted for both conditions (n=9) as well as uninjured *cmIc2*:dsRED controls (n=4), dissociated and single cells were FACS sorted for mCitrine and dsRED expression respectively. RNA was isolated from sorted cells using Trizol (Life Technologies BV, Bleiswijk, The Netherlands). RNA was quantified using a NanoDrop spectrophotometer. Superscript III First Strand Synthesis System (ThermoFisher Scientific) was used to reverse transcribe 200ng of purified RNA per

condition following manufacturer's protocol. qPCR reactions were performed using Fast SYBR Green PCR Master Mix (Applied Biosystems). Oligonucleotide sequences for real-time PCR analysis performed in this study are listed in Supplementary Table1.

MOUSE: RNA from whole hearts was isolated using the MiRNeasy kit (Qiagen, 217004), according to the manufacturer's instructions. RNA was quantified using a NanoDrop spectrophotometer. A High Capacity cDNA Reverse transcription kit (Applied Biosystems, 4374966) was used to reverse transcribe 1 µg of purified RNA according to the manufacturer's instructions. qPCR reactions were performed using Fast SYBR Green PCR Master Mix (Applied Biosystems). Oligonucleotide sequences for real-time PCR analysis performed in this study are listed in Supplementary Table1.

***In situ* hybridization**

PARAFFIN: After o/n fixation in 4% PFA, hearts were washed in PBS twice, dehydrated in EtOH, and embedded in paraffin. Serial sections were made at 10 µm. *In situ* hybridization was performed on paraffin-sections as previously described (Moorman et al., 2001) except that the hybridization buffer used did not contain heparin and yeast total RNA.

CRYOSECTIONS: Sections were obtained as described earlier. *In situ* hybridization was performed as for paraffin, however sections were pre-fixed for 10 minutes in 4% PFA + 0.25% glutaraldehyde before Proteinase K treatment. Moreover, slides were fixed for 1 hour in 4% PFA directly after staining. When *in situ* hybridization was combined with immunofluorescence, Fast Red staining solution was used instead of NBT-BCIP.

SUPPLEMENTARY TABLE 1.

Gene	Forward Primer	Reverse Primer
<i>gapdh</i>	CGAGCTGTCTCCCATCC	TCACCAACGTAGCTGTCTTTCTG
<i>pdk2a</i>	CCAATGTGCCTCATCACATC	TCTCGCATGCATTGGTAGAG
<i>pkma</i>	CATAGCTCGAACACTGGAA	TTCGGATTTCTGGTCCTTTG
<i>ldha</i>	TCACCCGGTTTCTACTTTGG	GGTCATGTGGACGACATCTG
<i>hk1</i>	AAATGACACAGTGGGCACAA	GTTTCGCATTTCTCCATGT
<i>Slc16a3</i>	TCACGGGTTTCTCCTACGC	GCCAAAGCGGTTACACAC
<i>Pfkp</i>	GAAACATGAGGCGTTCTGTGT	CCCGGCACATTGTTGGAGA
<i>Pdk3</i>	TCCTGGACTTCGGAAGGGATA	GAAGGGCGGTTCAACAAGTTA
<i>Pkm2</i>	TGCGATGCAGCACCTGATT	CCTCGAATAGCTGCAAGTGGTA
<i>Slc2a1</i>	AACTGGGCAAGTCCTTTG	TTCTTCTCCCGCATCATCTG
<i>Ldha</i>	TGTCTCCAGCAAAGACTACTGT	GACTGTACTTGACAATGTTGGGA
<i>mt-nd6</i>	AATACCCGCAAACAAGATCACCCAG	TGTTGGGGTTATGTTAGAGGGAGGGA
<i>mt-nd1</i>	CCCATTGCGGTTAATCTT	AAGTTGATCGTAACGGAAGC
<i>mt-co2</i>	AGTTGATAACCGAGTCGTTCTGCCA	TCGGCCTGGGATGGCATCAGT
<i>mt-co1</i>	CCAGTGCTAGCCGCAAGCAT	TCTGGGTGCCCAAGAATCAGAACA
<i>mt-co3</i>	ACCTACCAAGGCCACCACACTCC	GCAGCCTCTAGATCATGTGTTGGT

Isolation of single cells from cryoinjured hearts

Cryoinjured hearts (n=13) were extracted at 7 dpi. Cells were dissociated according to (Tessadori et al., 2012). For cell sorting, viable cells were gated by negative DAPI staining and positive YFP-fluorescence. In brief, the FACS gating was adjusted to sort cells for nppa:mCitrine^{high} (to enrich for proliferating cardiomyocytes) and nppa:mCitrine^{low} (remote cardiomyocytes and other cell types) cells. In total n=576 mCitrine^{high} and n=192 mCitrine^{low} cells were sorted into 384-well plates and processed for mRNA sequencing as described below.

Isolation of single cells from embryonic zebrafish

Transgenic *tg(myl7:GFP)* 2-day-old embryos (n=200) were dechorionated and digested in HBSS Ca²⁺/Mg²⁺ free media containing 0.1% collagenase type II (Gibco) at 32°C for 30-40 minutes followed by 1X TrypLE Express (Gibco) for 15-30 minutes at 32°C with agitation. Dissociated cells were then FACSsorted and subjected to single-cell mRNA-seq.

Single-cell mRNA sequencing

Single-cell sequencing libraries were prepared using SORT-seq (Muraro et al., 2016). Live cells were sorted into 384-well plates with Vapor-Lock oil containing a droplet with barcoded primers, spike-in RNA and dNTPs, followed by heat-induced cell lysis and cDNA syntheses using a robotic liquid handler. Primers consisted of a 24 bp polyT stretch, a 4bp random molecular barcode (UMI), a cell-specific 8bp barcode, the 5' Illumina TruSeq small RNA kit adapter and a T7 promoter. After cell-lysis for 5 minutes at 65°C, RT and second strand mixes were distributed with the Nanodrop II liquid handling platform (Inovadyne). After pooling all cells in one library, the aqueous phase was separated from the oil phase, followed by IVT transcription. The CEL-Seq2 protocol was used for library prep (Hashimshony et al., 2016). Illumina sequencing libraries were prepared with the TruSeq small RNA primers (Illumina) and paired-end sequenced at 75 bp read length on the Illumina NextSeq platform. Mapping was performed against the zebrafish reference assembly version 9 (Zv9).

Bioinformatic analysis

To analyze the single-cell RNA-seq data we used the previously published RaceID algorithm (Grün et al., 2015). For the adult hearts we had a dataset consisting of two different libraries of 384 cells each for a combined dataset of 768 cells, in which we detected 19257 genes. We detected an average of 10,443 reads per cell. Based on the distribution of the log₁₀ total reads plotted against the frequency, we introduced a cutoff at minimally 3500 reads per cell before further analysis. This reduced the number of cells used in the analysis to 352. Next, we downsampled reads to 3500 unique (UMI corrected) transcripts per cell, as means of normalization. Moreover, we discarded genes that were not detected at >3 transcripts in >1 cell and These cutoffs is a stringent normalization method that allows us to directly compare detected transcripts between cells from different cell types and libraries. Batch-

effects were analyzed and showed no plate-specific clustering of certain clusters.

For embryonic cardiomyocytes, two libraries of 384 cells were combined to obtain a set of 768 cells, in which 22271 genes could be detected. An average of 4412 reads per cell was detected. After downsampling of this library to 3500 reads per cell 302 cells were included for further analysis. Further analysis was performed by combining the embryonic heart data with the injured adult heart data.

The StemID algorithm were used as previously published (Grün et al., 2016). In short, StemID is an approach developed for inferring the existence of stem cell populations from single-cell transcriptomics data. StemID calculates all pairwise cell-to-cell distances ($1 - \text{Pearson correlation}$) and uses this to cluster similar cells into clusters that correspond to the cell types present in the tissue. The StemID algorithm calculates the number of links between clusters. This is based on the assumption that cell types with less links are more canalized while cell types with a higher number of links have a higher diversity of cell fates. Besides the number of links, the StemID algorithm also calculates the change in transcriptome entropy. Differentiated cells usually express a small number of genes at high levels in order to perform cell specific functions, which is reflected by a low entropy. Stem cells and progenitor cells display a more diverse transcriptome reflected by high entropy (Banerji et al., 2013). By calculating the number of links of one cluster to other clusters and multiplying this with the change in entropy, it generates a StemID score, which is representative to “stemness” of a cell population.

Differential gene expression analysis was performed using the “diffexpnb”, which makes use of the DESeq algorithm. P-values were Benjamini-Hochberg corrected for false discovery rate to make the cutoff.

For the comparison between the embryonic and adult cardiomyocyte clusters, the number of differentially expressed genes between two clusters was calculated as described above and this was used as a measure of similarity between clusters.

Inference of co-expressed gene modules

To identify modules of co-expressed genes along a specific differentiation trajectory (defined as a succession of significant links between clusters as identified by StemID) all cells assigned to these links were assembled in pseudo-temporal order based on their projection coordinate. Next, all genes that are not present with at least two transcripts in at least a single cell are discarded from the sub-sequent analysis. Subsequently, a local regression of the z-transformed expression profile for each gene is computed along the differentiation trajectory. These pseudo-temporal gene expression profiles are topologically ordered by computing a one-dimensional self-organizing map (SOM) with 1,000 nodes. Due

to the large number of nodes relative to the number of clustered profiles, similar profiles are assigned to the same node. Only nodes with more than 3 assigned profiles are retained for visualization of co-expressed gene modules. Neighboring nodes with average profiles exhibiting a Pearson's correlation coefficient >0.9 are merged to common gene expression modules. These modules are depicted in the final map. Analyses were performed as previously published (Grün et al., 2016).

Accession numbers

mRNA-seq data are deposited on Gene Expression Omnibus, accession number GSE139218. Samples FK1 and FK2 represent adult cardiomyocytes. Samples LG-A and LG-B represent embryonic cardiomyocytes.

Transmission Electron Microscopy

Hearts were excised and immediately chemically fixated at room temperature with 2,5% glutaraldehyde and 2% formaldehyde (EMS, Hainfield USA) in 0.1M phosphate buffer pH 7.4 for 2 hr. Next, hearts were post fixed with 1 % OsO_4 (EMS, Hainfield USA) / 1.5 % $\text{K}_3\text{Fe}(\text{CN})_6$ in 0.065 M phosphate buffer for 2 h at 4 °C and finally 1 h with 0,5% uranyl acetate. After fixation, hearts were dehydrated in a graded series of acetone and embedded in Epon epoxy resin (Polysciences). Ultrathin sections of 60 nm were cut on a Leica Ultracut T (Leica, Vienna, Austria) and contrasted with uranyl acetate (0.4% in AD, EMS, Hainfield USA) and lead citrate (Leica Vienna, Austria) using the AC20 (Leica Vienna, Austria) and examined with a Jeol 1010 electron microscope (Jeol Europe, Nieuw Venneep, The Netherlands).

Quantification of mitochondrial parameters.

In every heart, each in the borderzone and remote myocardial region, 100 well-delineated mitochondria with clearly visible outer and inner membranes were selected. Mitochondrial perimeter and surface were measured using the freehand tool of Image J. The perimeter to surface ratio was calculated and used as a factor that describes the pluriformity of mitochondria. The amount of cristae was estimated by counting the number of cristae intersected by a line of 0.5 μm length in 40 mitochondria per region.

Histology and enzyme histochemistry

Serial cryosections of the heart were cut 7 μm thick and either fixed in formalin, stained with Meyer's hematoxylin and eosin (HE), dehydrated and mounted in Entellan, or incubated for enzyme histochemistry. Chemicals for histochemistry of succinate dehydrogenase (SDH) activity were obtained from Sigma Aldrich. Sections for SDH activity were incubated for 20 min at 28°C in 37.5 mM sodium phosphate buffer pH 7.60, 70 mM sodium succinate, 5 mM sodium azide and 0.4 mM tetranitro blue tetrazolium (TNBT). The reaction was stopped in 10mM HCl. Controls without succinate did not stain. The incubated sections were mounted in glycerine gelatin. The absorbances of the SDH-reaction product in the sections were

determined at 660 nm using a calibrated microdensitometer and ImageJ.

Pharmacological inhibition of glycolysis

ZEBRAFISH: Zebrafish were injured and received intraperitoneal (i.p.) injections twice daily with either PBS or 2-Deoxy-D-Glucose (Sigma-Aldrich, 1 mg/g) from days 3 to 6 and one more injection on day 7 after injury, two hours before fish were euthanized and hearts harvested. I.p. injections were performed using a Hamilton Syringe (gauge 30) as described in literature (Kinkel et al., 2010). Injection volumes were corrected to body weight (30 μ l/g).

MAMMALIAN P7 CARDIAC CULTURES: Primary cardiac cultures were isolated from P7 mice using a neonatal dissociation kit (Miltenyi Biotec, 130-098-373) using the gentleMACS homogenizer, according to the manufacturer's instructions and cultured in Gelatin-coated (0.1%, G1393, Sigma) wells with DMEM/F12 medium supplemented with L-glutamine, Na-pyruvate, nonessential amino acids, penicillin, streptomycin, 5% horse serum and 10% FBS ('complete-medium') at 37°C and 5% CO₂ for 24h. Afterwards, medium was replaced with FBS-depleted medium (otherwise same composition) for additional 48hours of culture in either 3mM 2DG (Sigma-Aldrich) or 80 μ M Ionidamine (Sigma-Aldrich) before further processing.

Ex vivo glucose uptake

Fish were euthanized on ice water before hearts were extracted in PBS + heparin and were allowed to bleed out for 15 minutes. Hearts were then transferred into fresh PBS + 10%KCl to stop the heart from beating and mounted directly on a glass bottom cell culture dish in 1% agarose. Thereafter, 2NBDG (Caymanchem #11046, 400 μ M) was added to the dish and the hearts were taken directly for imaging. Imaging was performed using a Leica SP5 multiphoton microscopy using 930nm laser excitation wavelength. 150 μ m z-stacks were made with z-step size 5 μ m every 5 minutes for 2 hours.

Gene set enrichment analysis (GSEA)

GSEA (Genepattern, Broad Institute) was performed to assess enrichment for glycolytic genes upregulated between cluster 7 and 2. A list of genes involved in zebrafish glycolysis was obtained from KEGG. As number of permutations 1000 was used, which means $p=0$ indicates $p<0.001$.

Statistical analysis of data

All statistical testing was performed by unpaired T-tests besides zebrafish qPCR data for which a one-way ANOVA was performed.

REFERENCES

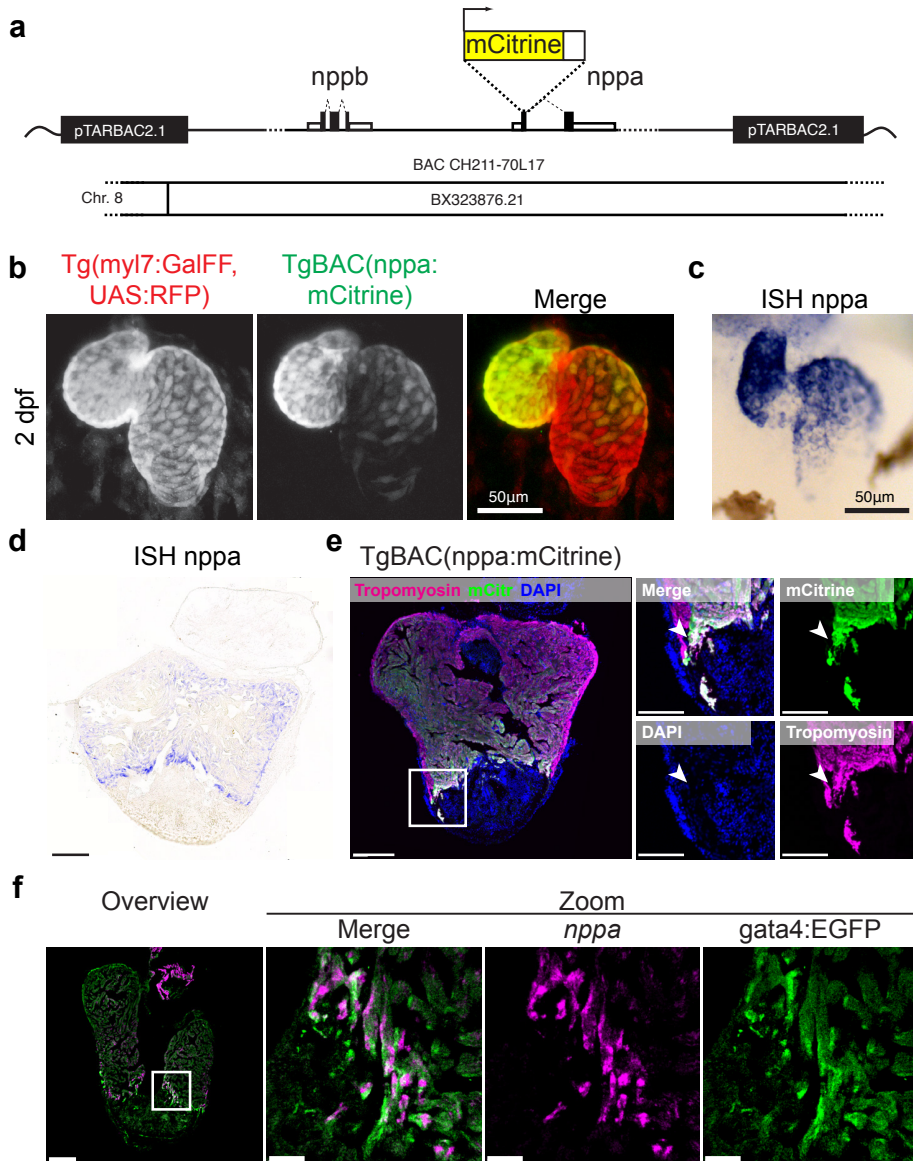
- Banerji, C.R.S., Miranda-Saavedra, D., Severini, S., Widschwendter, M., Enver, T., Zhou, J.X., Teschendorff, A.E., 2013. Cellular network entropy as the energy potential in Waddington's differentiation landscape. *Sci. Rep.* 3, 1129–7. doi:10.1038/srep03039
- Bergmann, O., Bhardwaj, R.D., Bernard, S., Zdunek, S., Barnabe-Heider, F., Walsh, S., Zupicich, J., Alkass, K., Buchholz, B.A., Druid, H., Jovinge, S., Frisen, J., 2009. Evidence for Cardiomyocyte Renewal in Humans. *Science* 324, 98–102. doi:10.1126/science.1164680
- Bergmann, O., Zdunek, S., Felker, A., Salehpour, M., Alkass, K., Bernard, S., Sjöström, S.L., Szewczykowska, M., Jackowska, T., Remedios, dos, C., Malm, T., Andrä, M., Jashari, R., Nyengaard, J.R., Possnert, G., Jovinge, S., Druid, H., Frisén, J., 2015. Dynamics of Cell Generation and Turnover in the Human Heart. *Cell* 161, 1566–1575. doi:10.1016/j.cell.2015.05.026
- Bersell, K., Arab, S., Haring, B., KUhn, B., 2009. Neuregulin1/ErbB4 Signaling Induces Cardiomyocyte Proliferation and Repair of Heart Injury. *Cell* 138, 257–270. doi:10.1016/j.cell.2009.04.060
- Busmann, J., Schulte-Merker, S., 2011. Rapid BAC selection for tol2-mediated transgenesis in zebrafish. *Development* 138, 4327–4332. doi:10.1242/dev.068080
- Chablais, F., Jazwinska, A., 2012. The regenerative capacity of the zebrafish heart is dependent on TGF signaling. *Development* 139, 1921–1930. doi:10.1242/dev.078543
- Chablais, F., Veit, J., Rainer, G., Jaźwińska, A., 2011. The zebrafish heart regenerates after cryoinjury-induced myocardial infarction. *BMC Dev Biol* 11, 21. doi:10.1186/1471-213X-11-21
- Choi, W.Y., Gemberling, M., Wang, J., Holdway, J.E., Shen, M.C., Karlstrom, R.O., Poss, K.D., 2013. In vivo monitoring of cardiomyocyte proliferation to identify chemical modifiers of heart regeneration. *Development* 140, 660–666. doi:10.1242/dev.088526
- Cote, G.M., Miller, T.A., LeBrasseur, N.K., Kuramochi, Y., Sawyer, D.B., 2005. Neuregulin-1 α and β isoform expression in cardiac microvascular endothelial cells and function in cardiac myocytes in vitro. *Exp Cell Res* 311, 135–146. doi:10.1016/j.yexcr.2005.08.017
- Dasgupta, S., Rajapakshe, K., Zhu, B., Nikolai, B.C., Yi, P., Putluri, N., Choi, J.M., Jung, S.Y., Coarfa, C., Westbrook, T.F., Zhang, X.H.F., Foulds, C.E., Tsai, S.Y., Tsai, M.-J., O'Malley, B.W., 2018. Metabolic enzyme PFKFB4 activates transcriptional coactivator SRC-3 to drive breast cancer. *Nature* 556, 249–254. doi:10.1038/s41586-018-0018-1
- Dogra, D., Ahuja, S., Kim, H.-T., Rasouli, S.J., Stainier, D.Y.R., Reischauer, S., 2017. Opposite effects of Activin type 2 receptor ligands on cardiomyocyte proliferation during development and repair. *Nature Communications* 8, 1–15. doi:10.1038/s41467-017-01950-1
- D'Uva, G., Aharonov, A., Lauriola, M., Kain, D., Yahalom-Ronen, Y., Carvalho, S., Weisinger, K., Bassat, E., Rajchman, D., Yifa, O., Lysenko, M., Konfino, T., Hegesh, J., Brenner, O., Neeman, M., Yarden, Y., Leor, J., Sarig, R., Harvey, R.P., Tzahor, E., 2015. ERBB2 triggers mammalian heart regeneration by promoting cardiomyocyte dedifferentiation and proliferation. *Nat Cell Biol* 17, 627–638. doi:10.1038/ncb3149
- Flinn, M.A., Jeffery, B.E., O'Meara, C.C., Link, B.A., 2018. Yap is required for scar formation but not myocyte proliferation during heart regeneration in zebrafish. *Cardiovascular Research* 115, 570–577. doi:10.1093/cvr/cvy243
- Folmes, C.D.L., Nelson, T.J., Martinez-Fernandez, A., Arrell, D.K., Lindor, J.Z., Dzeja, P.P., Ikeda, Y., Perez-Terzic, C., Terzic, A., 2011. Short Article. *Cell Metabolism* 14, 264–271. doi:10.1016/j.cmet.2011.06.011
- Gemberling, M., Karra, R., Dickson, A.L., Poss, K.D., 2015. Nrg1 is an injury-induced cardiomyocyte mitogen for the endogenous heart regeneration program in zebrafish. *eLife Sciences* 4. doi:10.7554/eLife.05871
- Gerber, T., Murawala, P., Knapp, D., Masselink, W., Schuez, M., Hermann, S., Gac-Santel, M., Nowoshilow, S., Kageyama, J., Khattak, S., Currie, J.D., Camp, J.G., Tanaka, E.M., Treutlein, B., 2018. Single-cell analysis uncovers convergence of cell identities during axolotl limb regeneration. *Science* 20, eaaq0681–19. doi:10.1126/science.aaq0681
- Giraud, M.-F., Paumard, P., Soubannier, V., Vaillier, J., Arselin, G., Salin, B., Schaeffer, J., Brêthes, D., di Rago, J.-P., Velours, J., 2002. Is there a relationship between the supramolecular organization of the mitochondrial ATP synthase and the formation of cristae? *Biochim. Biophys. Acta* 1555, 174–180.
- Gonzalez-Rosa, J.M., Martin, V., Peralta, M., Torres, M., Mercader, N., 2011. Extensive scar formation and regression during heart regeneration after cryoinjury in zebrafish. *Development* 138, 1663–

1674. doi:10.1242/dev.060897
- Grün, D., Lyubimova, A., Kester, L., Wiebrands, K., Basak, O., Sasaki, N., Clevers, H., van Oudenaarden, A., 2015. Single-cell messenger RNA sequencing reveals rare intestinal cell types. *Nature* 525, 251–255. doi:10.1038/nature14966
- Grün, D., Muraro, M.J., Boisset, J.-C., Wiebrands, K., Lyubimova, A., Dharmadhikari, G., van den Born, M., van Es, J., Jansen, E., Clevers, H., de Koning, E.J.P., van Oudenaarden, A., 2016. De Novo Prediction of Stem Cell Identity using Single-Cell Transcriptome Data. *Cell Stem Cell* 19, 266–277. doi:10.1016/j.stem.2016.05.010
- Gu, W., Gaeta, X., Sahakyan, A., Chan, A.B., Hong, C.S., Kim, R., Braas, D., Plath, K., Lowry, W.E., Christofk, H.R., 2016. Glycolytic Metabolism Plays a Functional Role in Regulating Human Pluripotent Stem Cell State. *Stem Cell* 19, 476–490. doi:10.1016/j.stem.2016.08.008
- Hashimshony, T., Senderovich, N., Avital, G., Klochendler, A., de Leeuw, Y., Anavy, L., Gennert, D., Li, S., Livak, K.J., Rozenblatt-Rosen, O., Dor, Y., Regev, A., Yanai, I., 2016. CEL-Seq2: sensitive highly-multiplexed single-cell RNA-Seq. *Genome biology* 17, 1–7. doi:10.1186/s13059-016-0938-8
- Haubner, B.J., Schneider, J., Schweigmann, U., Schuetz, T., Dichtl, W., Velik-Salchner, C., Stein, J.-I., Penninger, J.M., 2016. Functional Recovery of a Human Neonatal Heart After Severe Myocardial Infarction. *Circ Res* 118, 216–221. doi:10.1161/CIRCRESAHA.115.307017
- Heallen, T., Zhang, M., Wang, J., Bonilla-Claudio, M., Klysiak, E., Johnson, R.L., Martin, J.F., 2011. Hippo Pathway Inhibits Wnt Signaling to Restrain Cardiomyocyte Proliferation and Heart Size. *Science* 332, 458–461. doi:10.1126/science.1199010
- Huang, C.-J., Tu, C.-T., Hsiao, C.-D., Hsieh, F.-J., Tsai, H.-J., 2003. Germ-line transmission of a myocardium-specific GFP transgene reveals critical regulatory elements in the cardiac myosin light chain 2 promoter of zebrafish. *Dev Dyn* 228, 30–40. doi:10.1002/dvdy.10356
- Jopling, C., Sleep, E., Raya, M., Martí, M., Raya, A., Izpisua Belmonte, J.C., 2010. Zebrafish heart regeneration occurs by cardiomyocyte dedifferentiation and proliferation. *Nature* 464, 606–609. doi:10.1038/nature08899
- Jopling, C., Suñé, G., Faucherre, A., Fabregat, C., Izpisua Belmonte, J.C., 2012. Hypoxia induces myocardial regeneration in zebrafish. *Circulation* 126, 3017–3027. doi:10.1161/CIRCULATIONAHA.112.107888
- Kang, J., Hu, J., Karra, R., Dickson, A.L., Tornini, V.A., Nachtrab, G., Gemberling, M., Goldman, J.A., Black, B.L., Poss, K.D., 2016. Modulation of tissue repair by regeneration enhancer elements. *Nature* 532, 201–206. doi:10.1038/nature17644
- Kikuchi, K., Holdway, J.E., Werdich, A.A., Anderson, R.M., Fang, Y., Egnaczyk, G.F., Evans, T., MacRae, C.A., Stainier, D.Y.R., Poss, K.D., 2010. Primary contribution to zebrafish heart regeneration by gata4. *Nature* 464, 601–605. doi:10.1038/nature08804
- Kimura, W., Xiao, F., Canseco, D.C., Muralidhar, S., Thet, S., Zhang, H.M., Abderrahman, Y., Chen, R., Garcia, J.A., Shelton, J.M., Richardson, J.A., Ashour, A.M., Asaithamby, A., Liang, H., Xing, C., Lu, Z., Zhang, C.C., Sadek, H.A., 2015. Hypoxia fate mapping identifies cycling cardiomyocytes in the adult heart. *Nature* 523, 226–230. doi:10.1038/nature14582
- Kinkel, M.D., Eames, S.C., Philipson, L.H., Prince, V.E., 2010. Intraperitoneal injection into adult zebrafish. *J Vis Exp*. doi:10.3791/2126
- Kretzschmar, K., Post, Y., Bannier-Hélaouët, M., Mattiotti, A., Drost, J., Basak, O., Li, V.S.W., van den Born, M., Gunst, Q.D., Versteeg, D., Kooijman, L., van der Elst, S., van Es, J.H., van Rooij, E., van den Hoff, M.J.B., Clevers, H., 2018. Profiling proliferative cells and their progeny in damaged murine hearts. *Proc Natl Acad Sci USA* 555, 201805829–E12254. doi:10.1073/pnas.1805829115
- Lai, S.-L., Marín-Juez, R., Moura, P.L., Kuenne, C., Lai, J.K.H., Tsedek, A.T., Guenther, S., Looso, M., Stainier, D.Y., 2017. Reciprocal analyses in zebrafish and medaka reveal that harnessing the immune response promotes cardiac regeneration. *eLife Sciences* 6, 1382. doi:10.7554/eLife.25605
- Lepilina, A., Coon, A.N., Kikuchi, K., Holdway, J.E., Roberts, R.W., Burns, C.G., Poss, K.D., 2006. A dynamic epicardial injury response supports progenitor cell activity during zebrafish heart regeneration. *Cell* 127, 607–619. doi:10.1016/j.cell.2006.08.052
- Lien, C.-L., Schebesta, M., Makino, S., Weber, G.J., Keating, M.T., 2006. Gene expression analysis of zebrafish heart regeneration. *PLoS Biol* 4, e260. doi:10.1371/journal.pbio.0040260
- Lopaschuk, G.D., Collins-Nakai, R.L., Itoi, T., 1992. Developmental changes in energy substrate use by the heart. *Cardiovascular Research* 26, 1172–1180.
- Marques, I.J., Leito, J.T.D., Spaink, H.P., Testerink, J., Jaspers, R.T., Witte, F., van den Berg, S., Bagowski, C.P., 2007. Transcriptome analysis of the response to chronic constant hypoxia in zebrafish hearts. *J Comp Physiol B* 178, 77–92. doi:10.1007/s00360-007-0201-4

- Mathieu, J., Ruohola-Baker, H., 2017. Metabolic remodeling during the loss and acquisition of pluripotency. *Development* 144, 541–551. doi:10.1242/dev.128389
- Menendez-Montes, I., Escobar, B., Palacios, B., Gómez, M.J., Izquierdo-García, J.L., Flores, L., Jiménez-Borreguero, L.J., Aragones, J., Ruiz-Cabello, J., Torres, M., Martín-Puig, S., 2016. Myocardial VHL-HIF Signaling Controls an Embryonic Metabolic Switch Essential for Cardiac Maturation. *Dev Cell* 39, 724–739. doi:10.1016/j.devcel.2016.11.012
- Mills, R.J., Titmarsh, D.M., Koenig, X., Parker, B.L., Ryall, J.G., Quaipe-Ryan, G.A., Voges, H.K., Hodson, M.P., Ferguson, C., Drowley, L., Plowright, A.T., Needham, E.J., Wang, Q.-D., Gregorevic, P., Xin, M., Thomas, W.G., Parton, R.G., Nielsen, L.K., Launikonis, B.S., James, D.E., Elliott, D.A., Porrello, E.R., Hudson, J.E., 2017. Functional screening in human cardiac organoids reveals a metabolic mechanism for cardiomyocyte cell cycle arrest. *Proc Natl Acad Sci USA* 72, 201707316. doi:10.3791/2511
- Monroe, T.O., Hill, M.C., Morikawa, Y., Leach, J.P., Heallen, T., Cao, S., Krijger, P.H.L., de Laat, W., Wehrens, X.H.T., Rodney, G.G., Martin, J.F., 2019. YAP Partially Reprograms Chromatin Accessibility to Induce Adult Cardiogenesis In Vivo. *Dev Cell* 48, 1–23. doi:10.1016/j.devcel.2019.01.017
- Moorman, A., Houweling, A., de Boer, P., Christoffels, V., 2001. Sensitive nonradioactive detection of mRNA in tissue sections: novel application of the whole-mount in situ hybridization protocol. *Journal of Histochemistry & Cytochemistry* 49, 1.
- Muraro, M.J., Dharmadhikari, G., Grün, D., Groen, N., Dielen, T., Jansen, E., van Gorp, L., Engelse, M.A., Carlotti, F., de Koning, E.J.P., van Oudenaarden, A., 2016. A Single-Cell Transcriptome Atlas of the Human Pancreas. *Cell Systems* 3, 385–394.e3. doi:10.1016/j.cels.2016.09.002
- Nakada, Y., Canseco, D.C., Thet, S., Abdisalaam, S., Asaithamby, A., Santos, C.X., Shah, A.M., Zhang, H., Faber, J.E., Kinter, M.T., Szweda, L.I., Xing, C., Hu, Z., Deberardinis, R.J., Schiattarella, G., Hill, J.A., Oz, O., Lu, Z., Zhang, C.C., Kimura, W., Sadek, H.A., 2016. Hypoxia induces heart regeneration in adult mice. *Nature* 541, 222–227. doi:10.1038/nature20173
- Owen, P., Thomas, M., Opie, L., 1969. Relative changes in free-fatty-acid and glucose utilisation by ischaemic myocardium after coronary-artery occlusion. *Lancet* 1, 1187–1190.
- Paumard, P., Vaillier, J., Couly, B., Schaeffer, J., Soubannier, V., Mueller, D.M., Brèthes, D., di Rago, J.-P., Velours, J., 2002. The ATP synthase is involved in generating mitochondrial cristae morphology. *EMBO J* 21, 221–230. doi:10.1093/emboj/21.3.221
- Polizzotti, B.D., Ganapathy, B., Walsh, S., Choudhury, S., Ammanamanchi, N., Bennett, D.G., Remedios, C.G., Haubner, B.J., Penninger, J.M., Kühn, B., 2015. Neuregulin stimulation of cardiomyocyte regeneration in mice and human myocardium reveals a therapeutic window. *Science Translational Medicine* 7, 281ra45–281ra45. doi:10.1126/scitranslmed.aaa5171
- Porrello, E.R., Mahmoud, A.I., Simpson, E., Hill, J.A., Richardson, J.A., Olson, E.N., Sadek, H.A., 2011. Transient regenerative potential of the neonatal mouse heart. *Science* 331, 1078–1080. doi:10.1126/science.1200708
- Poss, K.D., 2010. Advances in understanding tissue regenerative capacity and mechanisms in animals. *Nat Rev Genet* 11, 710–721. doi:10.1038/nrg2879
- Poss, K.D., Wilson, L.G., Keating, M.T., 2002. Heart regeneration in zebrafish. *Science* 298, 2188–2190. doi:10.1126/science.1077857
- Puente, B.N., Kimura, W., Muralidhar, S.A., Moon, J., Amatruza, J.F., Phelps, K.L., Grinsfelder, D., Rothermel, B.A., Chen, R., Garcia, J.A., Santos, C.X., Thet, S., Mori, E., Kinter, M.T., Rindler, P.M., Zacchigna, S., Mukherjee, S., Chen, D.J., Mahmoud, A.I., Giacca, M., Rabinovitch, P.S., Asaithamby, A., Shah, A.M., Szweda, L.I., Sadek, H.A., 2014. The Oxygen-Rich Postnatal Environment Induces Cardiomyocyte Cell-Cycle Arrest through DNA Damage Response. *Cell* 157, 565–579. doi:10.1016/j.cell.2014.03.032
- Santhakumar, K., Judson, E.C., Elks, P.M., McKee, S., Elworthy, S., van Rooijen, E., Walmsley, S.S., Renshaw, S.A., Cross, S.S., Van Eeden, F.J.M., 2012. A Zebrafish Model to Study and Therapeutically Manipulate Hypoxia Signaling in Tumorigenesis. *Cancer Research* 72, 4017–4027. doi:10.1158/0008-5472.CAN-11-3148
- Sánchez-Iranzo, H., Galardi-Castilla, M., Mingullón, C., Sanz-Morejón, A., González-Rosa, J.M., Felker, A., Ernst, A., Guzmán-Martínez, G., Mosimann, C., Mercader, N., 2018. Tbx5a lineage tracing shows cardiomyocyte plasticity during zebrafish heart regeneration. *Nature Communications* 9, 1–13. doi:10.1038/s41467-017-02650-6
- Schelbert, H.R., Buxton, D., 1988. Insights into coronary artery disease gained from metabolic imaging. *Circulation* 78, 496–505.
- Schnabel, K., Wu, C.-C., Kurth, T., Weidinger, G., 2011. Regeneration of Cryoinjury Induced Necrotic Heart Lesions in Zebrafish Is Associated with Epicardial Activation and Cardiomyocyte Proliferation. *PLoS ONE* 6, e18503. doi:10.1371/journal.

- pone.0018503.g006
- Senyo, S.E., Steinhäuser, M.L., Pizzimenti, C.L., Yang, V.K., Cai, L., Wang, M., Wu, T.-D., Guerquin-Kern, J.-L., Lechene, C.P., Lee, R.T., 2012. Mammalian heart renewal by pre-existing cardiomyocytes. *Nature* 493, 433–436. doi:10.1038/nature11682
- Sleep, E., Boué, S., Jopling, C., Raya, M., Raya, A., Belmonte, J.C.I., 2010. Transcriptomics approach to investigate zebrafish heart regeneration. *Journal of Cardiovascular Medicine* 11, 369–380. doi:10.2459/JCM.0b013e3283375900
- Soonpaa, M.H., Kim, K.K., Pajak, L., Franklin, M., Field, L.J., 1996. Cardiomyocyte DNA synthesis and binucleation during murine development. *Am. J. Physiol.* 271, H2183–9.
- Staudt, D.W., Liu, J., Thorn, K.S., Stuurman, N., Liebling, M., Stainier, D.Y.R., 2014. High-resolution imaging of cardiomyocyte behavior reveals two distinct steps in ventricular trabeculation. *Development* 141, 585–593. doi:10.1242/dev.098632
- Stockdale, W.T., Lemieux, M.E., Killen, A.C., Zhao, J., Hu, Z., Riepsaame, J., Hamilton, N., Kudoh, T., Riley, P.R., van Aerle, R., Yamamoto, Y., Mommersteeg, M.T.M., 2018. Heart Regeneration in the Mexican Cavefish. *CellReports* 25, 1997–2007.e7. doi:10.1016/j.celrep.2018.10.072
- Suárez, E., Bach, D., Cadefau, J., Palacín, M., Zorzano, A., Gumà, A., 2001. A Novel Role of Neuregulin in Skeletal Muscle. *J Biol Chem* 276, 18257–18264. doi:10.1074/jbc.M008100200
- Tao, G., Kahr, P.C., Morikawa, Y., Zhang, M., Rahmani, M., Heallen, T.R., Li, L., Sun, Z., Olson, E.N., Amendt, B.A., Martin, J.F., 2016. Pitx2 promotes heart repair by activating the antioxidant response after cardiac injury. *Nature* 534, 119–123. doi:10.1038/nature17959
- Tessadori, F., van Weerd, J.H., Burkhard, S.B., Verkerk, A.O., de Pater, E., Boukens, B.J., Vink, A., Christoffels, V.M., Bakkers, J., 2012. Identification and Functional Characterization of Cardiac Pacemaker Cells in Zebrafish. *PLoS ONE* 7, e47644. doi:10.1371/journal.pone.0047644.t001
- Trapnell, C., Cacchiarelli, D., Grimsby, J., Pokharel, P., Li, S., Morse, M., Lennon, N.J., Livak, K.J., Mikkelsen, T.S., Rinn, J.L., 2014. The dynamics and regulators of cell fate decisions are revealed by pseudotemporal ordering of single cells. *Nat Biotechnol* 32, 381–386. doi:doi:10.1038/nbt.2859
- van Berlo, J.H., Kanisicak, O., Maillet, M., Vagnozzi, R.J., Karch, J., Lin, S.-C.J., Middleton, R.C., Marbán, E., Molkentin, J.D., 2014. c-kit⁺ cells minimally contribute cardiomyocytes to the heart. *Nature* 509, 337–341. doi:10.1038/nature13309
- Vander Heiden, M.G., Cantley, L.C., Thompson, C.B., 2009. Understanding the Warburg effect: the metabolic requirements of cell proliferation. *Science* 324, 1029–1033. doi:10.1126/science.1160809
- Wang, G.L., Semenza, G.L., 1993. General involvement of hypoxia-inducible factor 1 in transcriptional response to hypoxia. *Proc Natl Acad Sci USA* 90, 4304–4308. doi:10.1073/pnas.90.9.4304
- Warburg, O., Wind, F., Negelein, E., 1927. The metabolism of tumors in the body. *J. Gen. Physiol.* 8, 519–530.
- Wu, C.-C., Kruse, F., Vasudevarao, M.D., Junker, J.P., Zebrowski, D.C., Fischer, K., Noël, E.S., Grün, D., Berezikov, E., Engel, F.B., van Oudenaarden, A., Weidinger, G., Bakkers, J., 2016. Spatially Resolved Genome-wide Transcriptional Profiling Identifies BMP Signaling as Essential Regulator of Zebrafish Cardiomyocyte Regeneration. *Dev Cell* 36, 36–49. doi:10.1016/j.devcel.2015.12.010
- Xie, W., Chow, L.T., Paterson, A.J., Chin, E., Kudlow, J.E., 1999. Conditional expression of the ErbB2 oncogene elicits reversible hyperplasia in stratified epithelia and up-regulation of TGF α expression in transgenic mice. *Oncogene* 18, 3593–3607. doi:10.1038/sj.onc.1202673
- Yang, W., Xia, Y., Ji, H., Zheng, Y., Liang, J., Huang, W., Gao, X., Aldape, K., Lu, Z., 2011. Nuclear PKM2 regulates β -catenin transactivation upon EGFR activation. *Nature* 480, 118–122. doi:10.1038/nature10598
- Yu, Z., Redfern, C.S., Fishman, G.I., 1996. Conditional transgene expression in the heart. *Circ Res* 79, 691–697.
- Zhao, L., Ben-Yair, R., Burns, C.E., Burns, C.G., 2019. Endocardial Notch Signaling Promotes Cardiomyocyte Proliferation in the Regenerating Zebrafish Heart through Wnt Pathway Antagonism. *CellReports* 26, 546–554.e5. doi:10.1016/j.celrep.2018.12.048
- Zhao, L., Borikova, A.L., Ben-Yair, R., Guner-Ataman, B., Macrae, C.A., Lee, R.T., Burns, C.G., Burns, C.E., 2014. Notch signaling regulates cardiomyocyte proliferation during zebrafish heart regeneration. *Proc Natl Acad Sci USA* 111, 1403–1408. doi:10.1073/pnas.1311705111

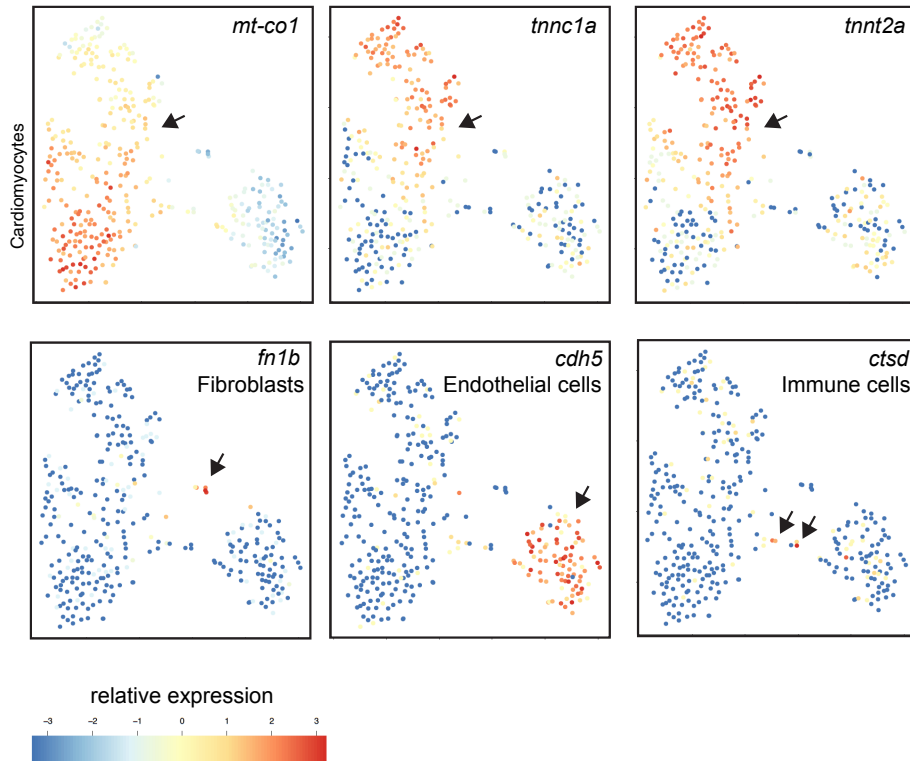
SUPPLEMENTARY INFORMATION



SUPPLEMENTAL FIGURE 1. TgBAC(*nppa*:mCitrine) expression recapitulates endogenous *nppa* gene expression.

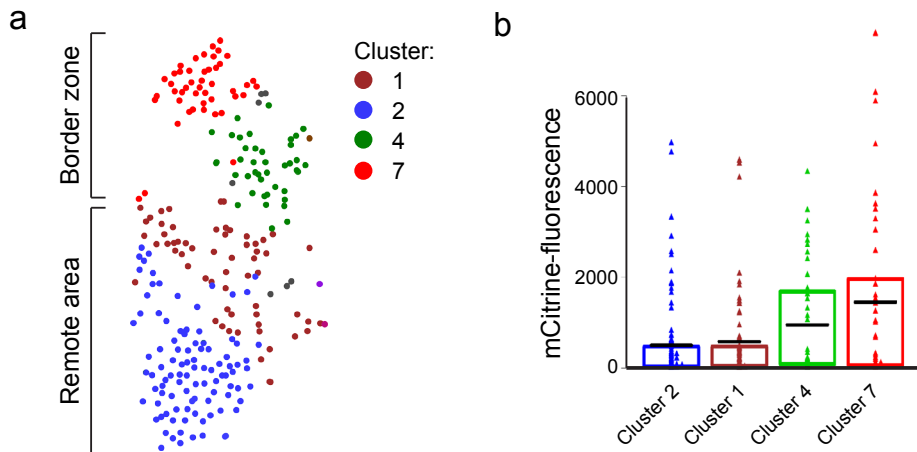
(a) Design of the bacterial artificial chromosome (BAC) used for generation of the transgenic line TgBAC(*nppa*:mCitrine). (b) Transgenic mCitrine expression in the heart in relation to RFP expression in the whole myocardium of Tg(*myl7*:GFF, UAS:RFP, *nppa*:mCitrine) in embryos at 2-days post-fertilization (dpf). (c) Whole mount *in situ* hybridization for endogenous *nppa* expression in embryos at 2 dpf. Note the specific expression in ventricle and atrium and absence of expression in atrioventricular canal of the *nppa*:mCitrine transgene expression (in panel b) as well as for the endogenous *nppa* expression (in

panel c). (d, e) Endogenous *nppa* expression (d) and *nppa*:mCitrine expression (e) in the adult heart at 7 days post-injury (dpi). Note expression of *nppa*:mCitrine in the cortical borderzone (arrowheads). (f) Fluorescent *in situ* hybridization for *nppa* performed on *gata4*:EGFP hearts 7dpi. Note the overlap of *nppa* and *gata4*:EGFP in trabecular borderzone cardiomyocytes.



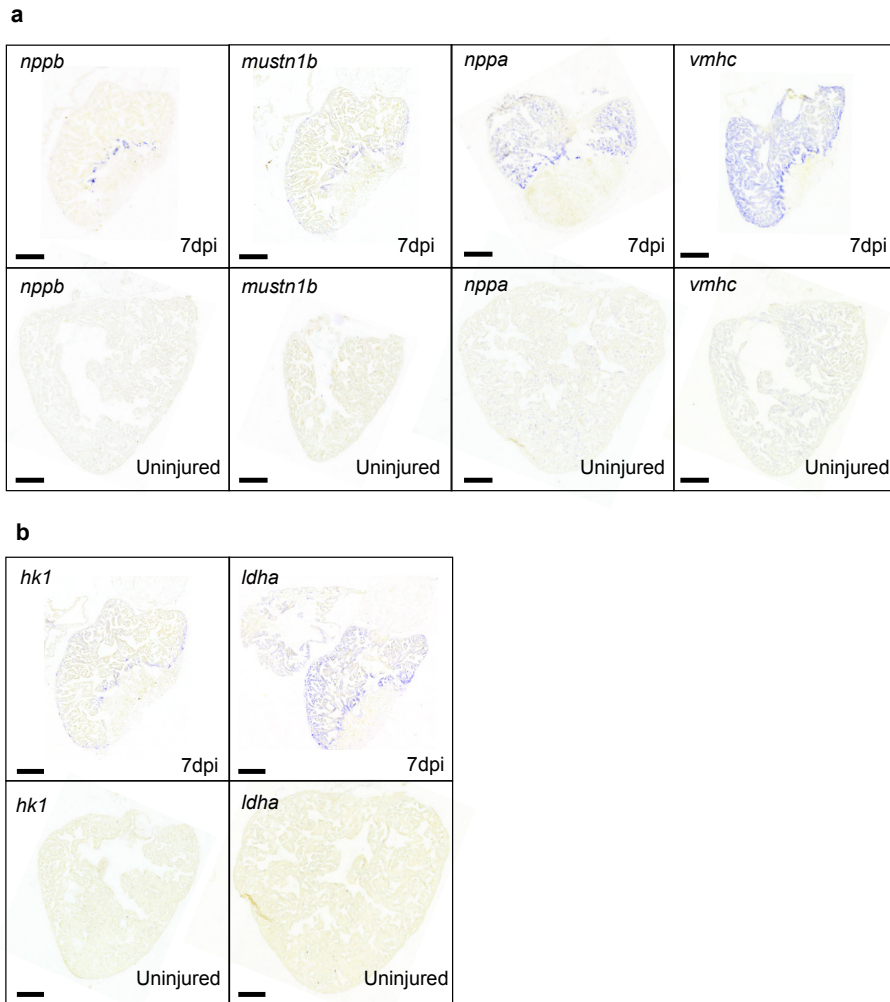
SUPPLEMENTAL FIGURE 2. Single-cell mRNA sequencing identifies different cell-populations in the injured zebrafish heart.

tSNE maps visualizing log₂-transformed read-counts of genes with high expression in cardiomyocytes (*mt-co1*, *tnnc1a*, *tnnt2a*), in fibroblasts (*fn1b*), in endothelial cells (*cdh5*) and immune cells (*ctsd*). Arrow indicates positive cell populations.



SUPPLEMENTAL FIGURE 3. Cluster 7 cells display highest npa:mCitrine expression.

(a) tSNE map of the cardiomyocyte clusters derived from the single-cell mRNA-sequencing. (b) mCitrine fluorescence levels of the npa:mCitrine FACS sorted cells from injured hearts that were used for the single-cell RNA-sequencing. Triangles represent individual cells of the four cardiomyocyte clusters. The box indicates the 25-75% quartiles, black lines indicate mean-fluorescence per cluster.

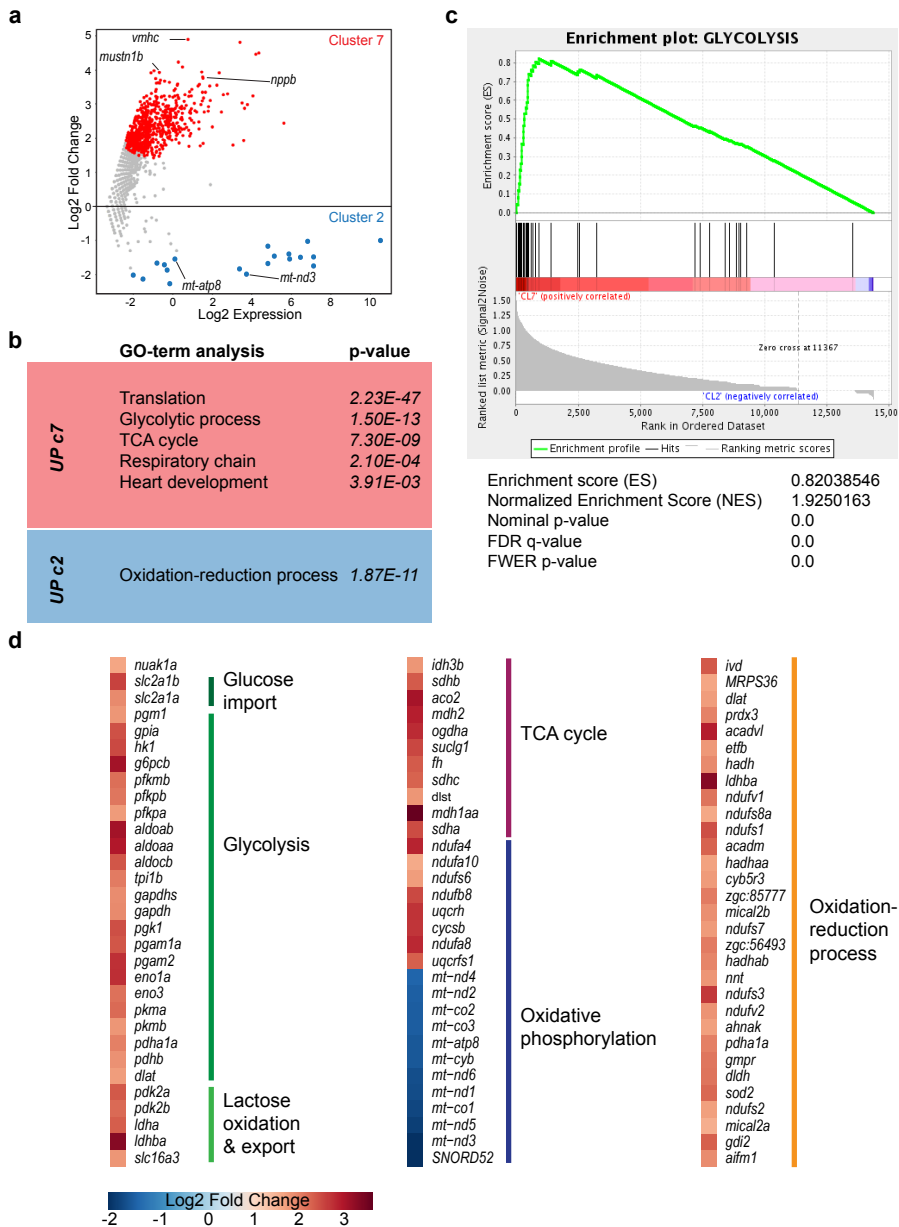


SUPPLEMENTAL FIGURE 4. Enhanced expression of genes elevated in cluster 7 versus cluster 2 is absent injury induced

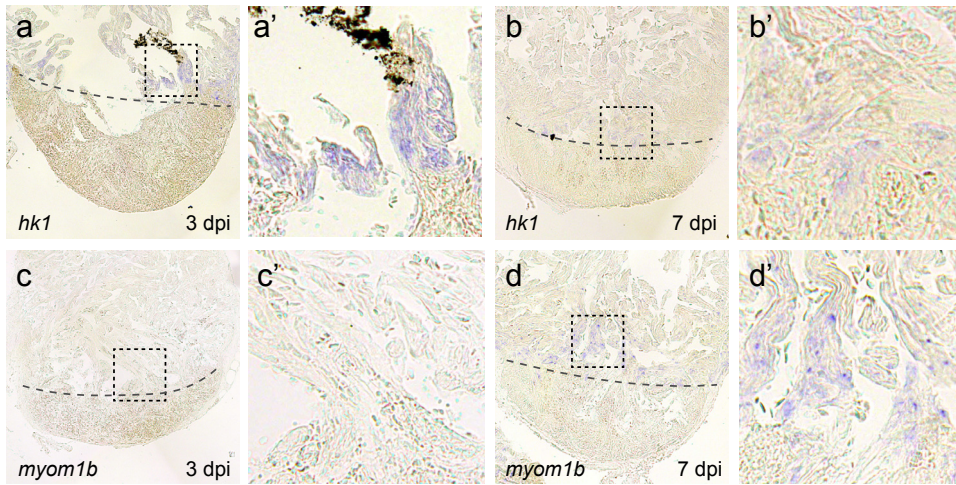
(a) *In situ* hybridizations for border zone genes *nppb*, *mustn1*, *nppa* and *vmhc* in zebrafish hearts at 7 dpi compared to uninjured hearts.

(b) *In situ* hybridizations for glycolysis genes *hk1* and *ldha* in zebrafish hearts at 7 dpi compared to uninjured hearts.

Staining for injured and uninjured hearts was stopped simultaneously. Scale bars indicate 200 μ m. (n=3 per condition)

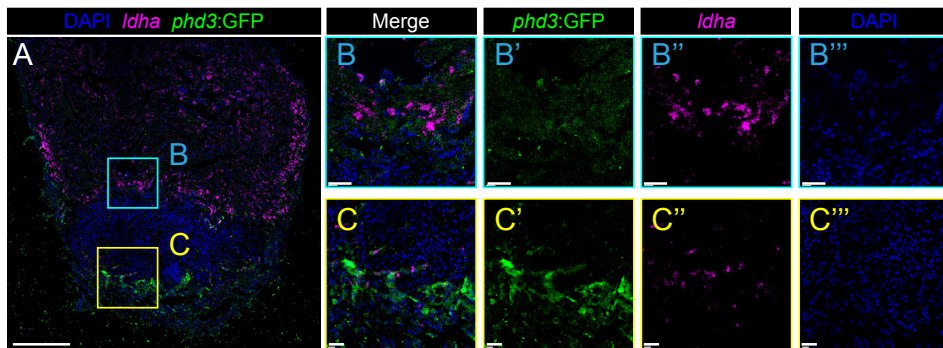


SUPPLEMENTAL FIGURE 5. Energy metabolism genes are differentially expressed between cluster 7 and cluster 2 cells. (a) Plot showing differentially expressed genes between cluster 7 versus cluster 2 cells. Differentially expressed genes (p -value <0.05) are highlighted in red (upregulated in cluster 7 cells) and blue (upregulated in cluster 2 cells). Complete gene list can be found in Supplementary Data8. 771 genes were differentially expressed ($p < 0.05$; adjusted p -value after Benjamini-Hochberg correction), of which 752 were specifically upregulated in cluster 7 cardiomyocytes, including the border zone genes, *nppa*, *nppb* and *mustn1b*. (b) GO-terms for upregulated genes in cluster 7 and cluster 2 respectively ($p < 0.01$). (c) Gene set enrichment analysis for glycolysis genes on all genes with differential expression between cluster 7 versus cluster 2 cells ($p < 0.05$). (d) Log2 fold change of differentially expressed genes (cluster 7 vs cluster 2) with a function in energy metabolism. High relative expression in cluster 7 depicted in red, high expression in cluster 2 depicted in blue.

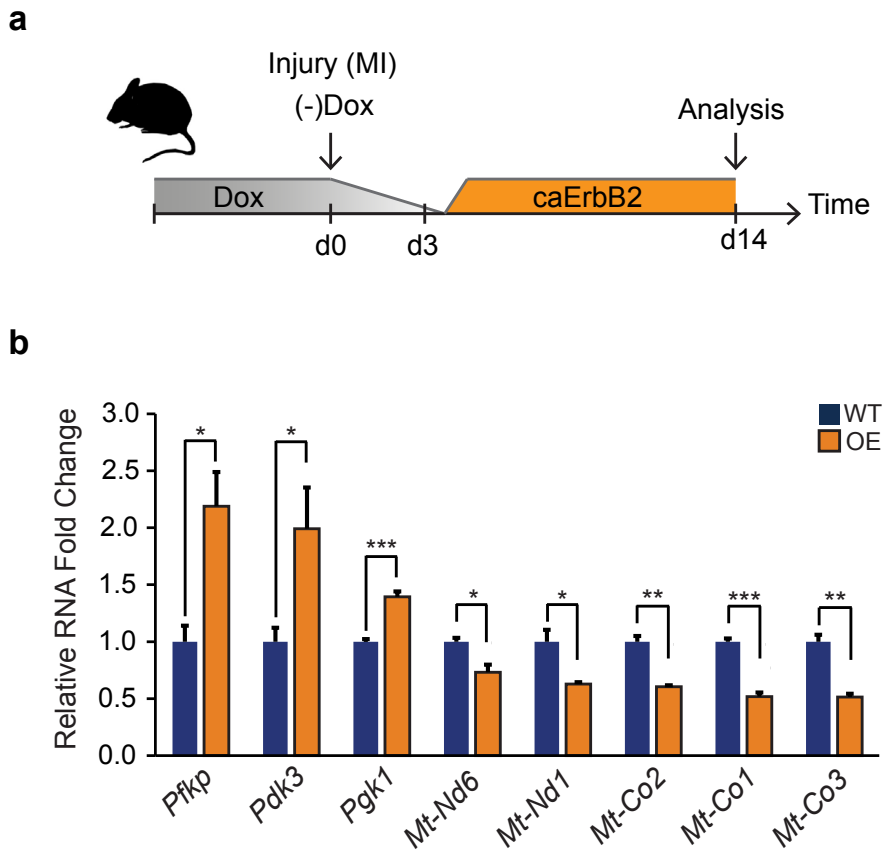


SUPPLEMENTAL FIGURE 6. Induction of *hexokinase1* expression precedes expression of *myomesin1b*.

In situ hybridization for the glycolysis gene *hexokinase1* (a,b) and the embryonic cardiac gene *myomesin1b* (c,d) on sections of injured zebrafish hearts at 3 dpi (a,c) and 7 dpi (b,d). While *hk1* expression in border zone cardiomyocytes was visible at 3 dpi and 7 dpi, *myom1b* expression was visible at 7 dpi but undetectable at 3dpi. (a',b',c' and d') show zoom-in of boxed areas in corresponding panels. Dashed line indicates the injury site.



SUPPLEMENTARY FIGURE 7. Hypoxia sensor *phd3:GFP* expression does not correlate with expression of the glycolytic gene *ldha*. (a) Overview picture of *phd3:GFP* heart 7dpi co-stained for expression of *ldha* by fluorescent ISH. (b) Zoom-ins of trabecular border zone cardiomyocytes. Note high *ldha* expression and low expression of *phd3:GFP*. (c) Zoom-ins of the apical region of the injury. Note the abundance of *phd3:GFP* signal in this region, while *ldha* expression is low.



SUPPLEMENTAL FIGURE 8. Activation of ErbB2 signaling in murine MI model induces glycolytic gene expression while repressing mitochondrial genes.

(a) Cartoon showing experimental procedure. Myocardial infarction (MI) was induced by left anterior descending coronary artery ligation at the same day when Dox was removed to induce cardiomyocyte specific caErbB2 overexpression (OE). Whole hearts were isolated for mRNA extraction 14 days after the MI and caErbB2 induction. (b) qPCR results with relative mRNA fold changes comparing wild type (WT, blue bars) with caErbB2 OE (OE, orange bars). Note the significant upregulation of glycolytic genes (*Pfkfb*, *Pdk3* and *Pgk1*) and significant downregulation of genes transcribed from the mitochondrial DNA (*Mt-Nd1*, *Mt-Co2*, *Mt-Co1* and *Mt-Co3*). Bars represent mean values and error bars represent standard deviation. * $p < 0,05$; ** $p < 0,01$; *** $p < 0,001$

Acknowledgements

We would like to thank V. Christoffels for critical reading of the manuscript and Life Science Editors for editing support.

Funding

J.B. acknowledges support from the Netherlands Cardiovascular Research Initiative and the Dutch Heart Foundation (grants CVON2011-12 HUSTCARE and Cobra³) and ERA-CVD grant CARDIO-PRO JCT2016-40-080. L.G. was supported by an EMBO long-term fellowship. P.D.N. is supported by an EMBO Long Term Fellowship ALTF1129-2015, HFSP Fellowship (LT001404/2017-L) and a NWO-ZonMW Veni grant (016.186.017-3). G.W. was funded by the Deutsche Forschungsgemeinschaft (SFB 1149, project number 251293561; SFB 1279, project number 316249678; WE 4223/6-1, project number 414077062) and by the BMBF (EU ERA-CVD “Cardio-Pro”, grant number 01KL1704). K.D.P. acknowledges support from the American Heart Association, Foundation Leducq, and NIH (R01 HL081674, R01 HL131319, and R01 HL136182).

Author contributions

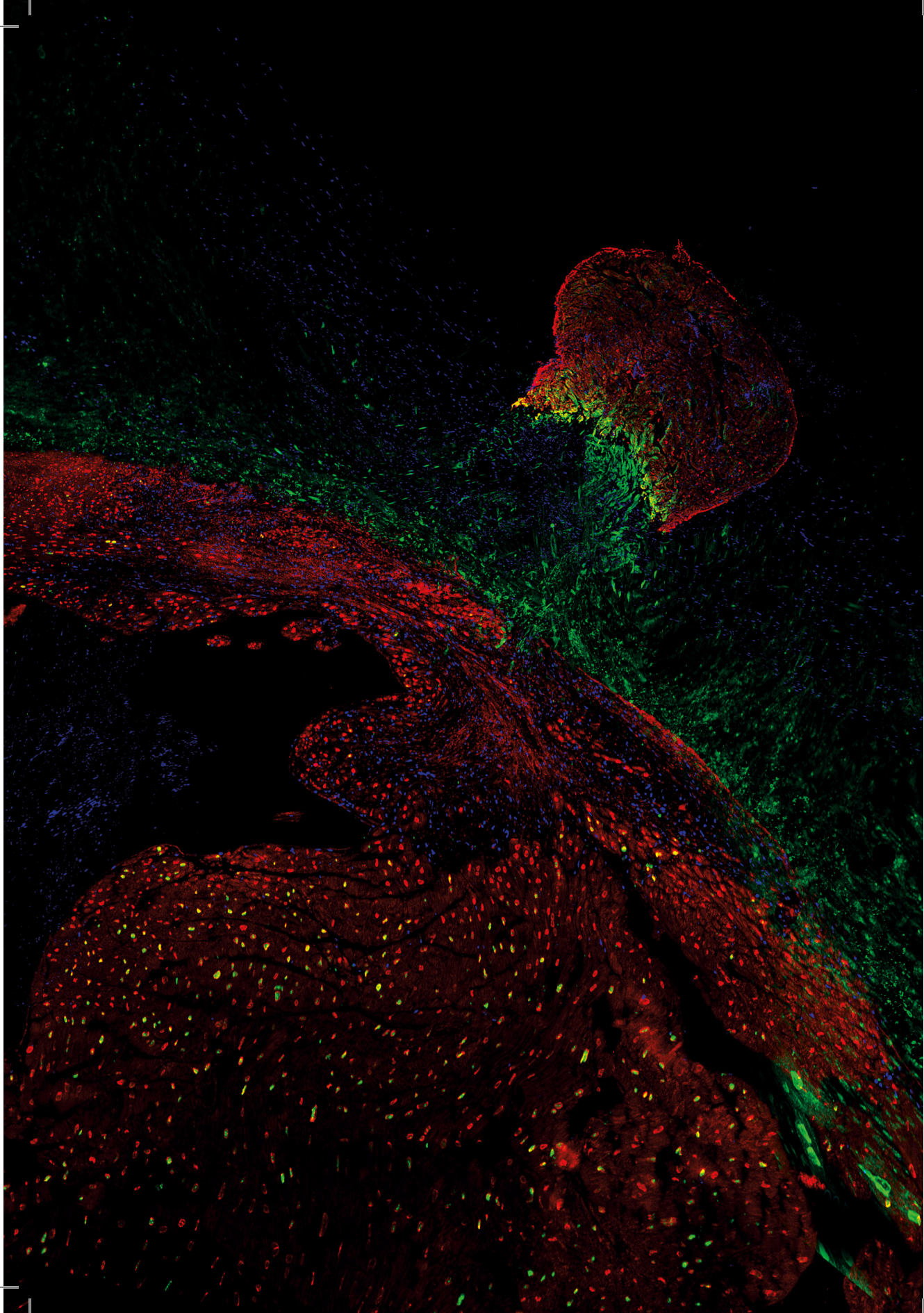
J.B. and E.T. conceived and designed the project. F.T. and J.C.P. generated the nppa-reporter line. F.K., D.E.M.d.B, P.N., M.J.M., D.G. and A.v.O. performed the single cell sequencing and helped with bioinformatics analyses. L.G. performed embryonic zebrafish work. D.E.M.d.B., H.H. and F.K. performed cryoinjuries, immunohistochemical analysis and in situ hybridizations. C.d.H, G.P. and J.K. performed and analyzed the electron microscopy data. W.N., W.J.v.d.L. and R.T.J. performed and analyzed enzymatic stainings. A.A. and A.S. performed and analysed mouse experiments. J.B., H.H., D.E.M.d.B, F.K and P.N. all helped writing the manuscript. A.B. and G.W. provided *gata4*:GFP samples. All authors approved the manuscript.

Competing interests

None

Data Availability

mRNA-seq data are deposited on Gene Expression Omnibus, accession number GSE139218.



CHAPTER III

Conserved NPPB+ border zone switches from MEF2- to AP-1-driven gene program

Karel van Duijvenboden^{#,1}, Dennis E. M. de Bakker^{#,2}, Joyce C. K. Man^{#,1}, Rob Janssen^{#,1}, Marie Günthel^{#,1}, Dipl.-Ing¹, Matthew, C. Hill³, Ingeborg B. Hooijkaas¹, Ingeborg van der Made⁶, Petra H. van der Kraak, BS⁴, Aryan Vink⁴, Esther E. Creemers⁶, James F. Martin^{3,5}, Phil Barnett¹, Jeroen Bakkers², Vincent M. Christoffels^{1,*}

¹ Department of Medical Biology, Academic Medical Center, Amsterdam, The Netherlands

² Hubrecht Institute, University Medical Centre Utrecht, Utrecht, The Netherlands

³ Program in Developmental Biology, Baylor College of Medicine, Houston, TX, USA

⁴ Department of Pathology, University Medical Centre Utrecht, Utrecht, the Netherlands

⁵ Department of Molecular Physiology and Biophysics, Baylor College of Medicine, Houston, TX, USA

⁶ Department of Experimental Cardiology, Academic Medical Center, Amsterdam, The Netherlands.

[#] Contributed equally

^{*} Corresponding author

Published in *Circulation* (2019)

ABSTRACT

Background

Surviving cells in the post-infarction border zone are subjected to intense fluctuations of their microenvironment. Recently, border zone cardiomyocytes have been specifically implicated in cardiac regeneration. Here, we defined their unique transcriptional and regulatory properties, and comprehensively validated new molecular markers, including *Nppb*, encoding B-type natriuretic peptide, after infarction.

Methods

Transgenic reporter mice were used to identify the *Nppb*-positive border zone after myocardial infarction. Transcriptome analysis of remote, border and infarct zones and of purified cardiomyocyte nuclei was performed using RNA-sequencing. Top candidate genes displaying border zone spatial specificity were histologically validated in ischemic human hearts. Mice in which *Nppb* was deleted by genome editing were subjected to myocardial infarction. Chromatin accessibility landscapes of border zone and control cardiomyocyte nuclei were assessed using ATAC-sequencing.

Results

We identified the border zone as a spatially confined region transcriptionally distinct from the remote myocardium. The transcriptional response of the border zone was much stronger than that of the remote ventricular wall, involving acute downregulation of mitochondrial oxidative phosphorylation, fatty acid metabolism, calcium handling and sarcomere function, and the activation of a stress response program. Analysis of infarcted human hearts revealed that the transcriptionally discrete border zone is conserved in humans, and led to the identification of novel conserved border zone markers including *NPPB*, *ANKRD1*, *DES*, *UCHL1*, *JUN* and *FOXP1*. Homozygous *Nppb* mutant mice developed acute and lethal heart failure after myocardial infarction, indicating B-type natriuretic peptide is required to preserve post-infarct heart function. ATAC-seq revealed thousands of cardiomyocyte lineage-specific MEF2-occupied regulatory elements that lost accessibility in the border zone. Putative injury-responsive enhancers that gained accessibility were highly associated with AP-1 binding sites. Nuclear c-Jun, a component of AP-1, was observed specifically in border zone cardiomyocytes.

Conclusion

Cardiomyocytes in a discrete zone bordering the infarct switch from a MEF2-driven homeostatic lineage-specific to an AP-1-driven injury-induced gene expression program. This program is conserved between mouse and human, and includes *Nppb* expression, which is required to prevent acute heart failure after infarction.

Keywords

Myocardial infarction, border zone, remote myocardium, epigenetics, ATAC-seq, RNA-seq

Non-standard Abbreviations and Acronyms

MI = myocardial infarction

CM = cardiomyocyte

IZ = infarct zone

BZ = border zone

RM = remote zone / remote myocardium

FDR = false discovery rate

LAD = left anterior descending coronary artery

CLINICAL PERSPECTIVE**What is new?**

- Mouse myocardial infarctions are surrounded by an *Nppb*-positive border zone, which contains cardiomyocytes that are transcriptionally and epigenetically distinct from remote myocardium.
- Infarcted human hearts contain similar border zone cardiomyocytes that share expression of novel border zone markers including *NPPB*, *JUN*, *DES* and *ANKRD1*, and are mainly located at the sub-endocardium adjacent to the infarction.
- *Nppb* knock-out mice are unable to recover from an ischemic injury, illustrating the importance of processes that occur in the border zone.
- *Nppb*-positive border zone cardiomyocytes undergo a profound transcriptional and epigenetic reprogramming, switching from a MEF2 to an AP-1-responsive gene program.

What are the clinical implications?

- Using *Nppb* knock-out mouse we illustrate that processes activated in the border zone are required for recovery after myocardial infarction, which may be applicable to patients that suffered an ischemic injury.
- Here, we present novel border zone markers that can be used in clinical research and are candidate biomarkers for assessing infarction severity and state.
- Since border zone cardiomyocytes have recently been implicated as a source for cardiomyocyte regeneration, the identification of the human sub-endocardial border zone might lead to novel strategies focusing on stimulating these cardiomyocytes to regenerate the injured heart.



INTRODUCTION

After acute myocardial infarction (MI), the compromised ischemic muscle is lost and replaced by scar tissue, impairing heart function. The mammalian heart is considered to be an essentially post mitotic organ with negligible regenerative capacity,¹ with cardiomyocyte (CM) hypertrophy serving as the principle adaptive response to injury. The infarct zone is usually highly irregular in shape, infiltrating the adjacent spared myocardium,² which is comprised of a mixture of viable, though severely affected CMs.³ The increase in CM cell size and reduction in capillary density is greater in the region bordering the infarct zone than in the remote area. CMs closer to the injury show hallmarks of dedifferentiation, sarcomere depletion and decrease in mitochondrial volume compared to remote CMs.^{4, 5} Molecular analyses of samples taken from different locations of the infarcted wall have consistently shown the existence of transcriptional differences between myocardium proximal and distal to the infarct.⁶⁻⁹

Pragmatically, the proximal-distal axis of the infarcted ventricular wall has been divided in an infarct zone (IZ), an infarct boundary zone or border zone (BZ; perfused but hypocontractile), and a remote zone (RM; perfused).¹⁰ The BZ remodels electrophysiologically and can be the origin of ventricular tachycardia, which are a common cause of sudden cardiac arrest in patients after MI, which originate from the BZ.¹¹⁻¹³ Furthermore, the BZ may be more susceptible to additional ischemic episodes, and its hypocontractile property seemingly expands after MI to involve contiguous myocardium that progressively loses contractile function as the heart remodels.¹⁰ Recently, the BZ myocardium received renewed attention with respect to its potential role in post-injury cardiac regeneration. Zebrafish efficiently regenerates the heart after injury, replacing the infarcted tissue by proliferating CMs, which are mainly located in the zone bordering the injury.¹⁴ Furthermore, in transgenic mouse models of enhanced regeneration, CM proliferation is primarily seen in the region proximal to the infarct, i.e. the putative BZ.¹⁵⁻¹⁸ Here, we identified and characterized a transcriptionally distinctive *NPPB*-expressing BZ conserved in mouse and human, and observed a role for *Nppb* in the survival after MI. Our findings indicate a CM lineage-specific MEF2-driven regulatory program is replaced by an AP-1-driven stress-responsive program in BZ CMs.

RESULTS

Identification of three transcriptionally distinct zones in the injured ventricular wall

To assess the spatial distribution of the transcriptome in the injured heart, we permanently ligated the left anterior descending coronary artery (LAD) in 10-12 week old mice. *Col1a1* and *Tnni3* expression patterns typically marked the infarct zone (IZ) and myocardium, respectively. *Nppa* expression, marking a border zone (BZ) region¹⁹ was evident in the area

adjacent the infarcted area and overlapping the spared myocardium (Figure 1A, B). The *Nppa*-negative myocardium was considered to be the remote myocardium (RM). The spatial analysis of the *Katushka* and *Nppa/Nppb* patterns in *BAC-Nppb-Katushka* mice 7 days post infarction (dpi) revealed that the transition of expression between the BZ and RM was relatively sharp rather than gradual, indicating the BZ is a discrete region adjacent to the infarct. Moreover, the size of the BZ was relatively constant across varying infarct sizes (Figure 1C). The thickness (from IZ to RM) of the *Nppa/Nppb*-positive zone was between 0.2 and 0.7 mm (Figure 1B, C and data not shown). The discreteness and sizes of the zones made it possible to isolate each zone by microdissection for characterization by RNA-seq analysis. Three independent samples of RM, BZ and IZ of 3, 7, and 14 dpi hearts were microdissected and the *Nppa* expression level in the microdissected tissues was compared to sham-operated left ventricular tissue to confirm correct dissection and isolation of the respective zones (Figure 1D). Using unsupervised principal component analysis, segregation between samples by time-points and zones was observed. Based on overall expression patterns, all sham samples clustered together, followed by RM, BZ and IZ. Interestingly, samples harvested three days after LAD were separated from both other time points, which were more similar to each other (Figure 1E).

Characterization of the transcriptional response of the BZ

Comparison of the transcriptomes of the BZ and RM at different time points to those of sham tissue showed that the majority of differentially expressed genes (3563) originated from the BZ (2983 genes), whereas the contribution of differentially expressed genes solely in the remote ventricular wall was minor (Figure 1F and Supplemental Figure 1). The direction of change of differentially expressed genes in RM and BZ was the same, i.e. either up in both zones or down in both zones, indicating that the injury response of the BZ and RM are comparable, but much more extensive in the BZ (Supplemental Figure 1). The early response involved the highest number of genes and stabilized thereafter as shown by increased gene overlap (Figure 1G). Analysis of changes in KEGG pathways and GO terms between different time points and zones was concordant with the course of pathology, for example at three days post-injury a dominant inflammatory response was noted (Figure 1H, clusters 3-5). In the BZ downregulated genes were enriched for CM-specific genes (sarcomere, calcium handling), whereas upregulated genes were enriched for those known to be expressed in non-CMs, compatible with the invasion of immune cells and activation of fibroblasts after injury.^{12, 23, 24} Moreover, a strong cell-cycle activation response, probably derived from activated fibroblasts and immune cells, was observed at 3 dpi, (Figure 1H, cluster 5).

Cluster analysis revealed a set of 165 transcription factor encoding genes induced in the BZ (Supplemental Figure 2 and Supplemental Table 1). These include *Jun* and *Fosl2*, encoding components of the activator protein 1 (AP-1) complex that regulates a wide range of cellular

processes, including cell proliferation, death, survival and differentiation.²⁵⁻²⁷ Furthermore, a number of genes (587) encoding excreted proteins were induced in the BZ that are candidate biomarkers (e.g. *Clu*, *Gpx3*; Supplemental Table 2).

The (post-MI) ventricular wall is composed of many different cell-types.^{9, 12, 23, 24, 28} To gain insight into the CM-specific response to injury, we purified CM nuclei from the BZ and RM using PCM-1-mediated purification (Figure 2 and Supplemental Figure 3A, B). Compared to whole tissue samples, PCM-1 sorted samples were enriched for cardiac genes and showed a low expression of genes specifically expressed by fibroblasts, endothelial cells and leukocytes (Supplemental Figure 3C). As also seen for the RNA-seq of whole tissue, the majority of significantly differentially expressed genes originates from cells of the BZ (Figure 2A). Genes upregulated in BZ CMs include the known markers *Nppa* and *Nppb*.

We compared the BZ and RM PCM-1+ nuclear RNA-seq data with those obtained from adult CMs from uninjured hearts²⁹ using unsupervised hierarchical clustering (Figure 2C). Samples from the RM clustered together with CMs from uninjured heart, whereas the BZ samples cluster alone. GO term analysis of each gene cluster revealed that CMs in the BZ downregulate genes involved in processes like oxidative phosphorylation, citrate cycle and lipid metabolism, while they upregulate genes involved in regulating transcriptional regulation, cell-cell adhesion junctions and hypertrophy. Cross-analysis with dissected BZ and PCM-1 sorted BZ samples indicated that *Clu*, *Gpx3*, *Finc*, *Des*, *Fhl1*, *Serpine1*, *Synpo2l* and *Ankrd1* are bona fide BZ markers confirmed in both experiments (Figure 2B). Using *in situ* hybridization (ISH), the BZ CM-specific induction of several markers at 7 dpi was validated (Figure 2D). Information regarding their function is provided in the Supplemental Material. Taken together, we present a rich dataset analysis which can be used as a starting point for future studies on BZ restricted processes.

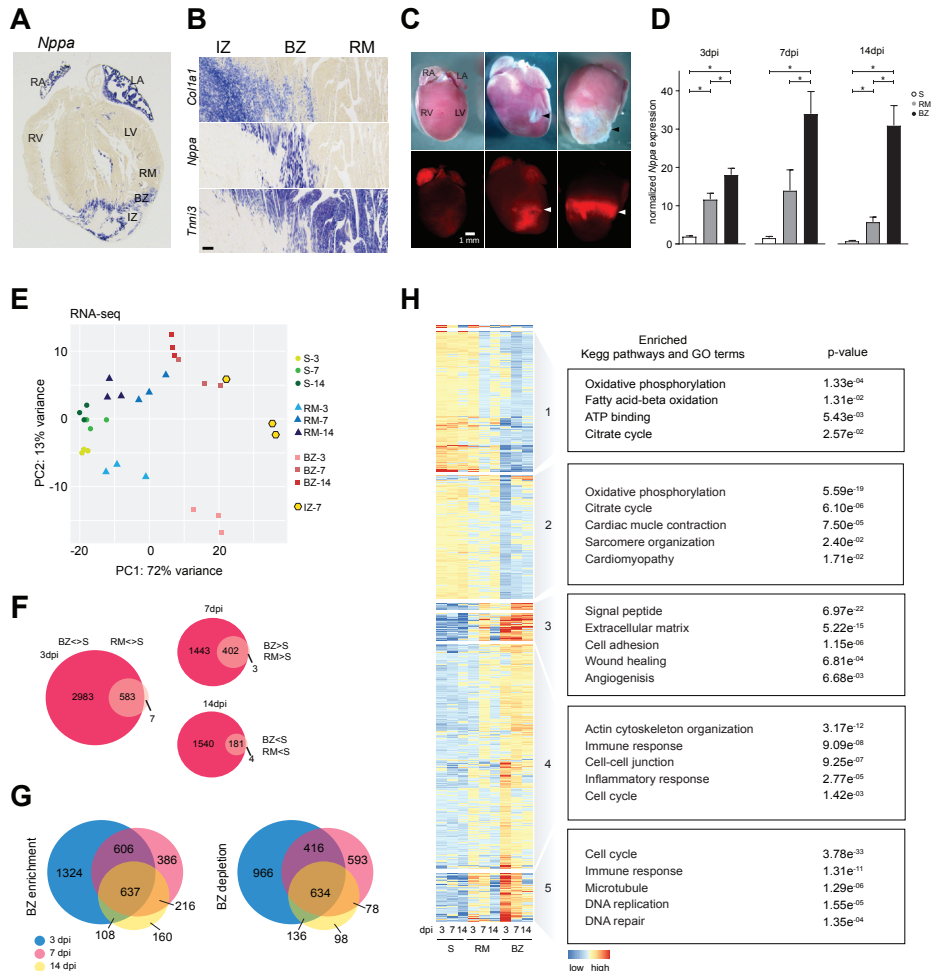


FIGURE 1. RNA-sequencing identifies the border zone based on a distinct expression profile on microdissected LV tissue.

(A) *In situ* hybridization analysis showing the expression pattern of *Nppa* in the 7 dpi heart. (B) Spatial expression patterns and corresponding *in situ* hybridization of three reference genes *Col1a1*, *Nppa*, and *Tnni3* at 7 dpi. *Nppa* expression highlights the BZ. (C) Light (upper row) and fluorescent microscopic pictures (lower row) of hearts of 7 dpi BAC-Nppb::Katushka mice, revealing the relatively sharply defined BZ (white arrowheads) around both a small and large infarct area (black arrowheads). (D) Following microdissection of the BZ and RM, *Nppa* expression was assessed by qPCR and compared to control sham hearts. Values are means \pm SEM; * $p < 0.05$. (E) Principal component analysis (PCA) clustered the microdissected LV tissue by zone and time post-injury. Samples from different zones and time-points are designated by colors. (F) Comparison of differentially expressed genes of BZ ($n=3$) and RM ($n=3$) to sham ($n=3$) at 7 dpi showed that majority of differentially expressed genes originate from the BZ. (G) The set of differentially expressed genes of BZ tissue was cross-referenced with data obtained from infarcted LV tissue to highlight those differentially expressed genes that potentially play a part in the cardiomyocyte response to injury. (H) Functional annotation heatmap of sham, RM, and BZ at different time-points ($n=3$ per time-point per tissue) based on differentially expressed genes sham vs BZ. RA = right atrium; LA = left atrium; RV = right ventricle; LV = left ventricle; RM = remote zone; BZ = border zone; IZ = infarct zone.

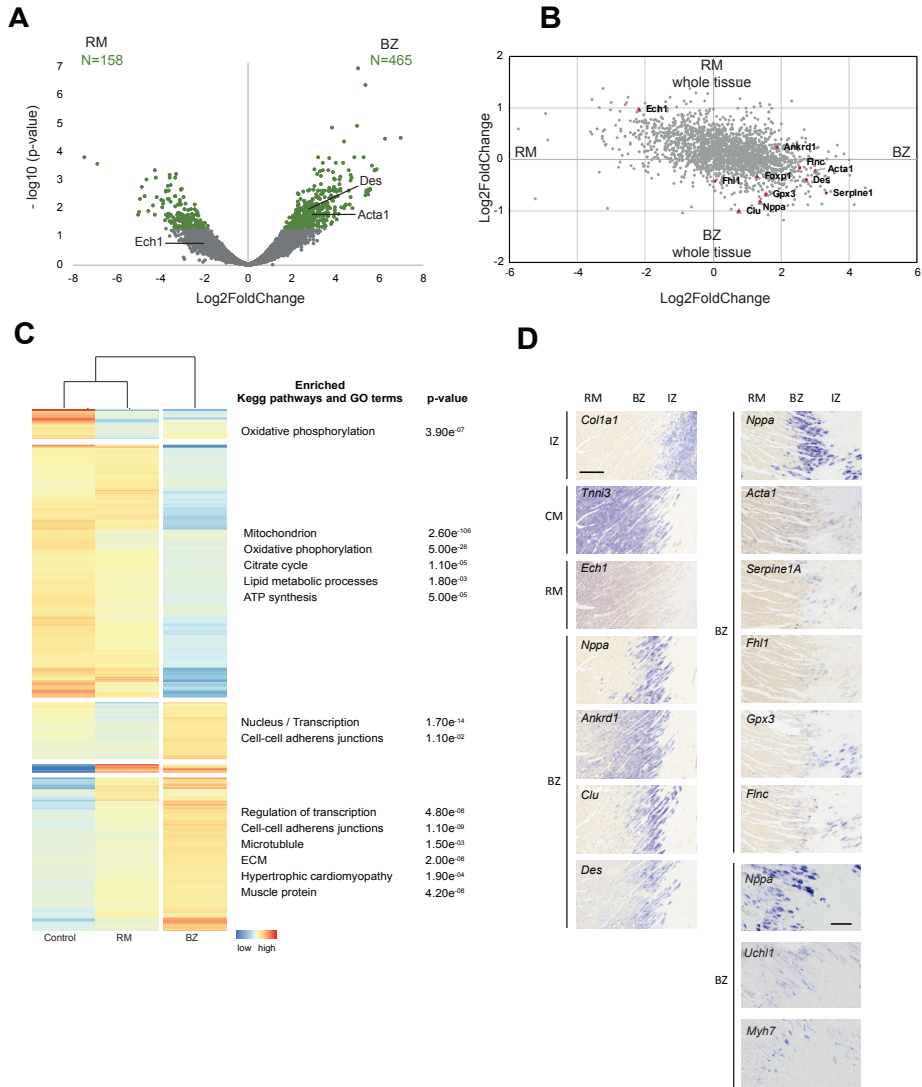


FIGURE 2. Gene expression in border zone cardiomyocytes. (A) Volcano plot showing cardiomyocyte nuclear transcripts differentially expressed between remote myocardium (RM; n=2) and border zone (BZ; n=3) tissues. Green dots indicate significantly differentially expressed genes (p-adjusted for multiple testing: FDR < 0.05). (B) Scatter plot of differentially expressed genes (Log2FoldChange) between the RM and BZ samples. (C) Unsupervised functional annotation heatmap of control²⁹, RM and BZ samples. Gene ontology analysis was performed on each cluster. (D) *In situ* hybridization shows the three reference genes *Col1a1* for the infarct zone (IZ), *Tnni3* for cardiomyocytes and *Ech1* for remote myocardium (RM). *Nppa* marks the border zone (BZ). New markers of the BZ resemble the expression pattern of *Nppa*. Scale bar indicates 0.5 mm and 0.1 mm (right, lower panel).

BZ CMs partially revert to a neonatal CM state

To gain insight into the state of differentiation of the BZ and RM, we compared our tissue and PCM1+ CM RNA-seq data sets with those from isolated neonatal and adult CMs.²⁹ The BZ profiles clustered with those of neonatal CMs (Supplemental Figure 4A). The RM and sham profiles clustered with those of adult CMs, indicating that RM does not dedifferentiate significantly after injury, in keeping with previous observations.³⁰ Scatter plot and GoTerm analysis (Supplemental Figure 4B) revealed that genes expressed at lower levels in neonatal as well as BZ CMs are involved in oxidation-reduction processes and lipid metabolism. Genes expressed at higher levels in neonatal CMs and BZ CMs control transcription and cell-cell adherent junctions. However, many genes expressed at higher levels in neonatal CMs were not upregulated in BZ CMs, including genes involved in cell cycle regulation. Taken together, BZ CMs partially revert to the immature state of neonatal CMs.

Identification of the BZ in human infarcted hearts

Next, we addressed whether a conserved transcriptional BZ could be identified in the ischemic human heart. Histological analysis of human cardiac tissue samples from individuals that suffered from MI (n=3) identified areas of coagulation necrosis of CMs, compatible with MI of 1-3 days post coronary artery occlusion, and collagen rich areas, compatible with MI scars of ≥ 2 months old (Figure 3A). The infarcted areas of selected samples were located in the sub-endocardial region of the left ventricle or intraventricular septum. These locations were confirmed by immunostaining against C4d, an excreted complement factor that is specific to necrotic CMs³¹ (Figure 3B). Most of the surviving myocardium was found in the compact myocardium, away from the infarcted area, or in oxygenated peri-vascular and sub-endocardial regions (Figure 3A, orange). Areas of surviving myocardium towards the epicardial layer were considered to be RM.

A number of genes with region-specific expression in the murine heart were selected for spatial expression analysis. Most tested BZ-induced genes (e.g. *NPPA*, *NPPB*, *ANKRD1*, *DES*, *UCHL1*, *JUN*, *MYH7*, *FOXP1*) showed similar expression patterns in the infarcted human hearts, with consistent but low expression in-between the IZ and the RM (Figure 3C, arrows) and around blood vessels with presumed residual blood flow (Figure 3C, stars). Interestingly, strongest expression of the examined genes was observed in the *NPPA*-positive BZ CMs located in-between the IZ and the endocardium (Figure 3C, D and Supplemental Figure 5A). This strong sub-endocardial expression was observed in all three ischemic heart samples that were investigated (Supplemental Figure 5B-D). The size of the sub-endocardial BZ was consistently around 0.4 mm, similar to the BZ size in murine hearts. The RM-specific, sarcomeric genes *ECH1* and *TCAP*, showed strong expression in the RM and weak expression in the *NPPA*-positive sub-endocardial BZ region (Figure 3D and Supplemental Figure 5A).

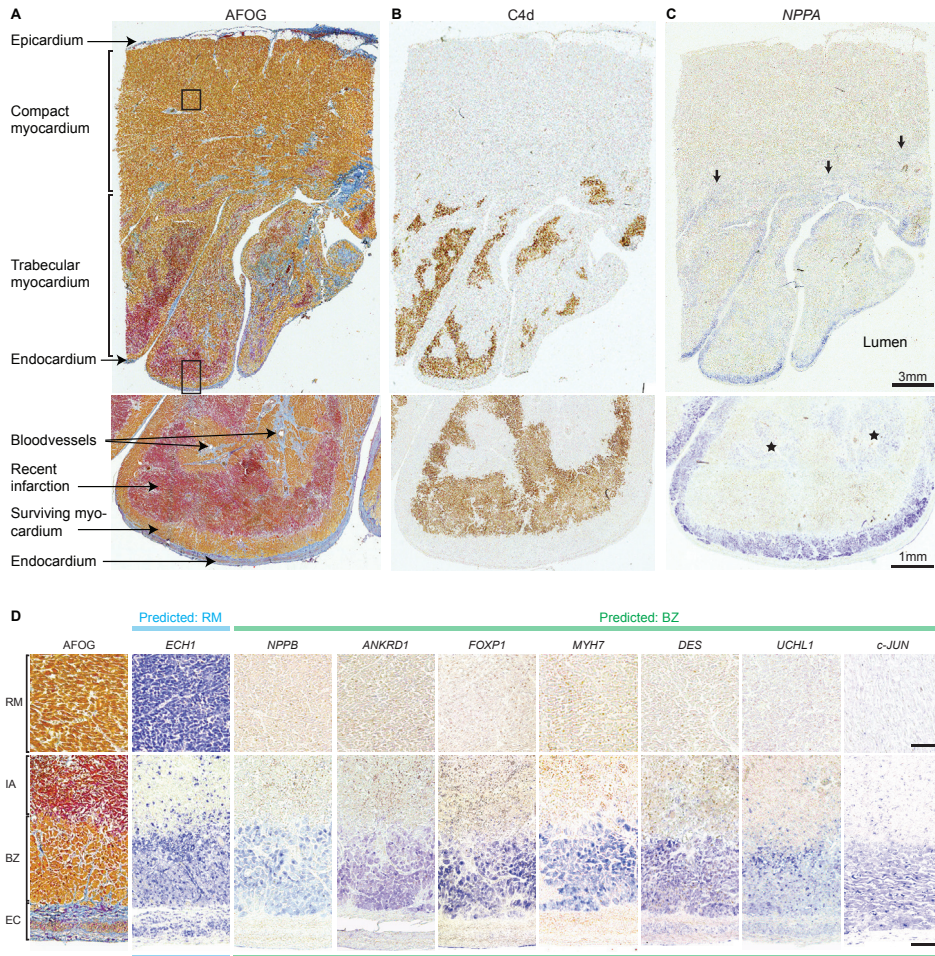


FIGURE 3. Human ischemic hearts show most pronounced expression of border zone markers in the sub-endocardium. (A) Acid fuchsin orange G (AFOG) staining on human heart tissue showing a with a large myocardial infarction. AFOG marks cytoplasm (orange), elastic fibrin (red) and collagen fibrils (blue). Elastic fibrin is indicative of coagulation necrosis, thus revealing a non-transmural recent infarction (red). In addition, collagen depositions suggest previous cardiac insults (blue). Black boxes indicate zoom locations for figure (D). (B) Anti-C4d antibody staining on a consecutive section marking necrotic cardiomyocytes overlying with the fibrin rich region. (C) *In situ* hybridization against *NPPA* on a consecutive section. *NPPA* expression was observed in regions adjacent to the fibrin, including light staining in regions in the compact muscle layer (marked by arrows) and around blood vessels (marked by stars). Most pronounced staining is found at the surviving cells of the sub-endocardium. (D) Zoom of the remote myocardium (RM) and the sub-endocardial region, including the injury area (IA), border zone (BZ) and endocardium (EC). *In situ* hybridization on consecutive sections confirmed expression of *ECH1* in RM. Predicted border zone genes showed specific expression in sub-endocardial myocardium. Scale bars represent 100 μ m.

The histological analysis identified regions that experienced a recent MI (1-3 days old, C4d and fibrin-positive) and regions with older fibrotic scars (collagen positive, C4d negative). A consistently higher expression of BZ genes was observed in CMs in close proximity to recent infarcted areas (fibrin positive) compared to their expression levels in CMs close to older collagen rich scars within the same heart (Supplemental Figure 6), indicating that expression of BZ genes in human MI hearts is temporally regulated. We conclude that in the ischemic injured human heart, a distinct BZ is formed that is most pronounced at the sub-endocardial location, comprised of CMs with high expression of BZ markers involved in processes such as the stress response (*JUN*, *JUNB*, *ANKRD1*), development and proliferation (*NPPA*, *NPPB*, *FOXP1*) and muscle structure (*MYH7*, *DES*), and reduced expression of metabolic and sarcomeric genes (*ECH1*, *TCAP*). Based on the similar presence of these marker genes in the injured murine heart, we conclude that these injury responsive processes are evolutionarily conserved.

***Nppb* is required during recovery from myocardial infarction**

To gain insight into the role of the BZ-induced transcriptional program, we investigated the role of the conserved BZ gene *Nppb* after MI. We generated two independent *Nppb* knockout mouse lines using CRISPR/Cas9 genome editing technology (Figure 4A and Supplemental Figure 7). To assess to what extent our *Nppb* knockout model is affected we performed RNA-sequencing of adult left ventricles of wildtype (n=4) and *Nppb*^{-/-} mice (n=4). Consistent with previous findings,³² *Nppa* was significantly upregulated (Figure 4B). Surprisingly, only 27 additional genes were mildly differentially expressed in *Nppb*^{-/-} mice (Figure 4C). We could not identify any fibrosis markers among the differentially expressed genes in *Nppb*^{-/-} mice, did not observe fibrotic lesions (Supplemental Figure 8C, D) and did not observe differences in left ventricular systolic and diastolic function between genotypes (Figure 4D, E and Supplemental Figure 8E-L).

To assess the function of *Nppb* after injury, we subjected *Nppb*^{-/-} mice and wildtype littermates to MI surgeries. *Nppb*^{-/-} mice of both independent transgenic lines died more frequently shortly after MI due to acute heart failure (Figure 4F and Supplemental Figure 7A). *Nppb*^{-/-} mice that did not die of rupture presented shortness of breath, excess fluid in chest cavity and fluid leakage from the nose, blood coagulation in the left atrium (Figure 4H) and white spots were found locally on the lungs (Figure 4I), in line with the occurrence of acute heart failure. These heart failure symptoms were not observed in wildtype mice after MI. No differences between genotypes were observed in relative heart weight, left ventricular function, or left atrial dimensions at 1 dpi between the two genotypes (Figure 4D, E and Supplemental Figure 8B, E-J). Left ventricular diastolic parameters at 3 dpi showed a significant decrease in left ventricular internal diameter (LVID) and left ventricular volume in *Nppb*^{-/-} mice in diastole compared to wildtype (Supplemental Figure 8K, L).



Both before and after MI, we did not find differences between genotypes in ventricular expression levels of myocardial hypertrophy markers (*Myh7* and *Atp2a2* (SERCA2A)) or fibrosis markers (*Col1a1* and *Pstn*) (Figure 4J). A more detailed description of the data is provided in the Supplemental Material. Together, these findings suggest that *Nppb*^{-/-} mice do not show a baseline phenotype but die 1-3 days after MI due to acute heart failure, indicating the requirement of induced *Nppb* expression to survive acute cardiac injury. This illustrates the importance of BZ-induced gene program after MI.

Dynamic epigenetic landscape in the border zone cardiomyocytes

Chromatin accessibility patterns reveal positions in the genome of actively engaged regulatory DNA elements, *i.e.* promoters, enhancers, repressors and insulators. We assessed how open chromatin states differ across homeostatic (sham) and 4, 7 and 14 dpi BZ CMs *in vivo* using ATAC-seq,³³ a technique sufficiently sensitive to detect these states in the limited number (50,000) of CM nuclei that were isolated from the BZ (Figure 5A). Analysis of the distribution of accessible sites revealed that the majority mapped to intra- and intergenic regions and on average 15,000 to promoters (Figure 5B). In sham-operated mice, promoter accessibility at three different time points overlapped for 86% (Figure 5C), indicating that the experiments performed on these tissues were reproducible and peak calling consistent between samples. Inspection of loci likely to be accessible in CMs confirmed accessible promoters originating from CMs (Figure 5D, E).

To determine the correlation between promoter accessibility and gene expression, we integrated the ATAC-seq data with BZ whole-tissue RNA-seq data. Because of the observed correlation between accessibility of promoters and expression levels of their respective genes (Figure 5F), we analysed the dynamic temporal changes in promoter accessibility 4, 7 and 14 dpi. A large number of promoters gained or lost accessibility after injury (Figure 5G), which correlated well with the induction (*e.g.* *Nppa*, *Nppb*) and reduction (*e.g.* *Ryr2*, *Pln*), respectively, of gene expression in the BZ (Supplemental Figure 9). In contrast, promoters of cell cycle genes and of Hippo-, NRG-, BMP-, and Wnt-signalling, implicated in CM renewal and regeneration, did not show consistent changes in accessibility. Cluster analysis of differentially accessible promoters between the BZ and sham CMs indicated at least 5 temporal patterns of changed accessibility (Figure 5H). A large number of promoters of cardiac lineage-specific genes involved in contraction, sarcoplasmic reticulum, ion handling, calcium signalling became less accessible in the BZ CMs. Promoters of genes involved in angiogenesis and hypoxia response showed an early response but normalized thereafter, whereas other promoters for genes involved in the immune response, wound healing and extracellular matrix became accessible (Figure 5H).

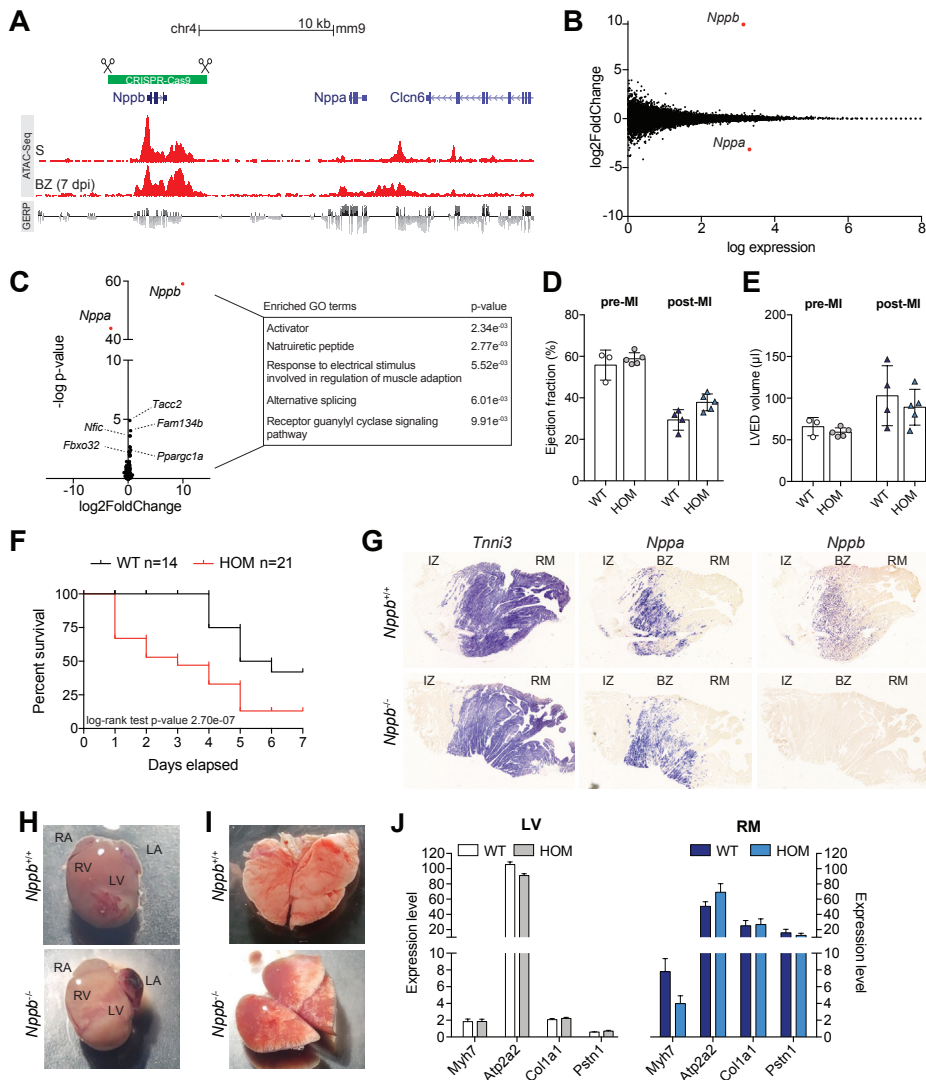


FIGURE 4. *Nppb* is required during recovery of myocardial infarction. (A) Using CRISPR/Cas9 genome editing technology *Nppb* was targeted. (B) MA plot showing approximately 15,000 transcripts detected in wildtype (WT) LV (n=4) and *Nppb*^{-/-} (HOM) LV (n=4). *Nppa* is significantly upregulated in HOM LV. (C) Volcano plot showing significantly differentially expressed genes in HOM LV (p-adjusted for multiple testing: FDR<0.05). Included gene ontology analysis of several genes shown in the volcano plot (D, E) Echocardiographic parameters showing ventricular function: ejection fraction (EF) and left ventricular end diastolic volume (LVED) pre- (WT n=3; HOM n=5) and post-MI (WT n=4; HOM n=5) at 7 dpi. (F) Kaplan-Meier survival curve of HOM mice (n=21) and wildtype littermates (n=14) showed significant difference in survival (log-rank test p=2.70e-07). (G) *In situ* hybridization analysis showing the expression pattern of *Tnni3*, *Nppa* and *Nppb* in HOM mouse and wildtype at 7 dpi. (H, I) Whole heart and lung of a HOM mouse presenting acute heart failure and a wildtype. (J) Following microdissection of RM (WT n=6; HOM n=6), expression of hypertrophy markers (*Myh7* and *Atp2a2* (SERCA2A)) and fibrosis markers (*Col1a1* and *Pstn1*) were assessed by qPCR and compared to left ventricular tissue (WT n=6; HOM n=6). Values are means \pm SEM. RA = right atrium; LA = left atrium; RV = right ventricle; LV = left ventricle; RM = remote zone BZ = border zone; IZ = Infarct zone.

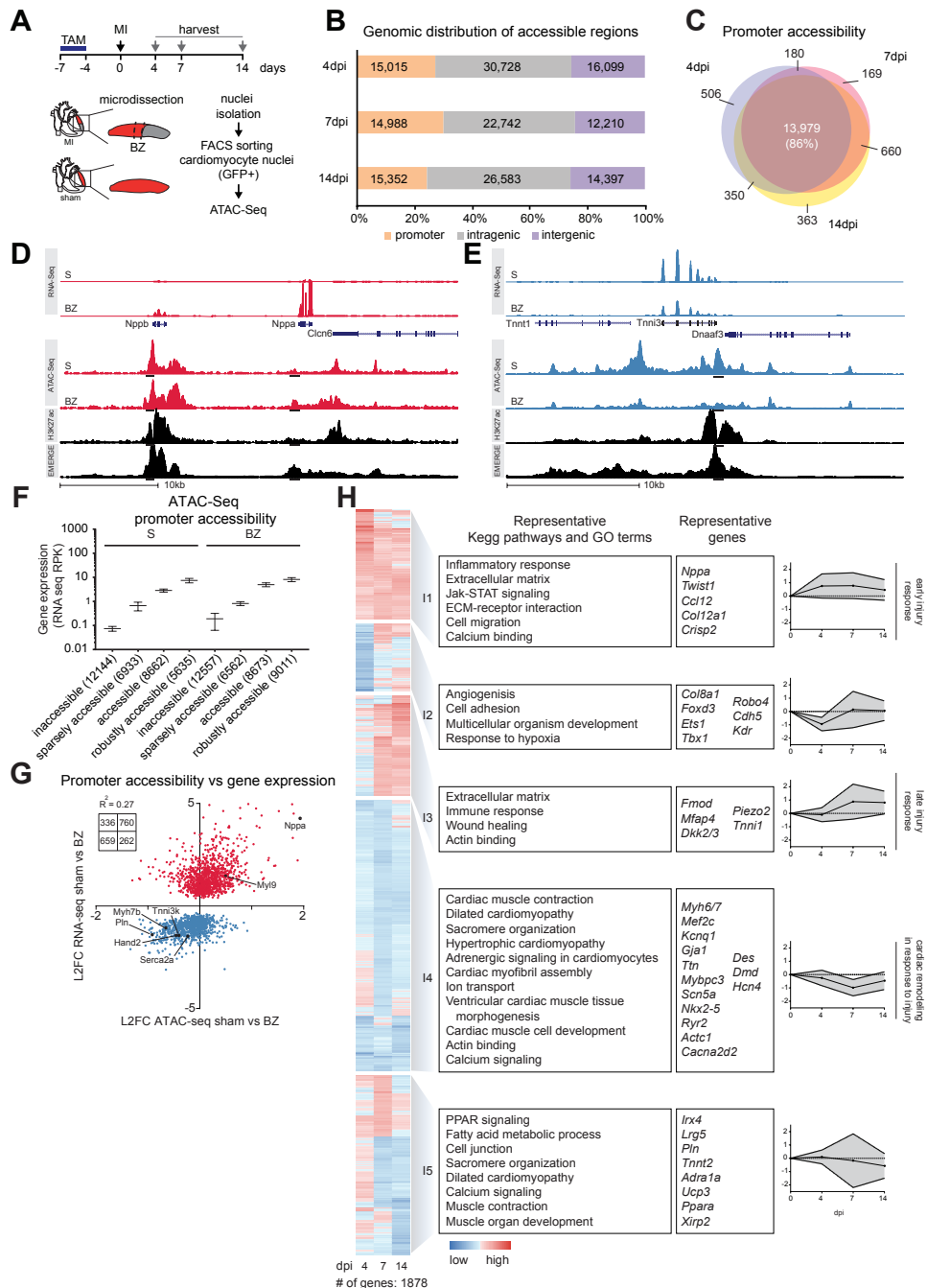


FIGURE 5. Epigenetic profiling of BZ cardiomyocyte response to injury. (A) Schematic of GFP+ nuclei sorting for ATAC-sequencing. (B) Analysis of the distribution of accessible sites intra-, intergenic regions, and promoters at different time-points. (C) Overlapping promoter accessibility at three time-points in sham operated mice (86%) indicated that performed experiments were reproducible. (D,

E) Representative loci containing accessible promoters originating from cardiomyocytes. **F**) Dotplot plotting average gene expression levels (RNA-seq RPK) as a function of promoter accessibility (as determined by ATAC-seq). **G**) Scatterplot showing the relation between BZ differential expression (RNA-seq) and BZ differential accessibility of promoters (ATAC-seq). All significantly DE genes (p -value adjusted for multiple testing: $FDR < 0.05$) between sham and BZ at 7 dpi (RNA-seq) were included. Correlation coefficient and number of genes per quadrant are given. **H**) Functional annotation heatmap showing dynamics of chromatin accessibility of promoters between sham and BZ ($n=3$ per tissue per time-point).

In addition to promoter accessibility studies, we investigated accessibility patterns of putative regulatory elements (e.g. enhancers). Although the majority of signals remained stable between sham and BZ CMs, we identified thousands of sites that either gain or lose accessibility, indicative of profound changes in gene regulation (Figure 6B). Unchanging accessible sites were enriched for CM-specific H3K27ac signatures, indicating that these represent regulatory elements active in both sham and BZ CMs (Figure 6C). Sites displaying decreasing accessibility were enriched for H3K27ac marks, suggesting that regulatory elements active under homeostatic conditions lose activity after injury. In contrast, emerging sites and sites with increasing accessibility were much less frequently marked by H3K27ac, suggesting that these regulatory elements are not typically active in CMs during normal homeostasis (Figure 6C).

To determine which transcription factors may interact with the accessibility-enriched or -depleted sites at the three time points after MI, we used HOMER to identify enriched sequence motifs potentially recognized by specific transcriptional regulators (Figure 6D, E). Both disappearing sites and sites with decreasing accessibility were highly enriched for motifs recognized by members of the Mef2 transcription factor family, and to a lesser extent by members of the T-box, Meis and Smad (TGFbeta/BMP-signalling) transcription factor families. Members of each of these families are involved in cardiogenesis and CM lineage-specific gene regulation.³⁴ In contrast, both sites with increasing and emerging accessibility were strikingly enriched for motifs recognized by Jun and Fos family members (Figure 6D, E).²⁵ In addition, Runx, Erg, Smad, E-box (MyoD), and TEAD recognition sites were enriched.

To gain insight into the temporal pattern of accessibility, we identified 933 chromatin sites differentially accessible at at least one time point (Figure 6F and Supplemental Figure 10). We observed that depleted sites, enriched in recognition sites for Mef2 family members, are less accessible during the onset of pathology, whereas at a later stage (14 dpi) partially restored their accessibility. In contrast, sites in clusters 5 and 6, highly enriched in AP-1 recognition sites (Jun/Fos), became more accessible after MI and sustained accessibility until at least 14 dpi.



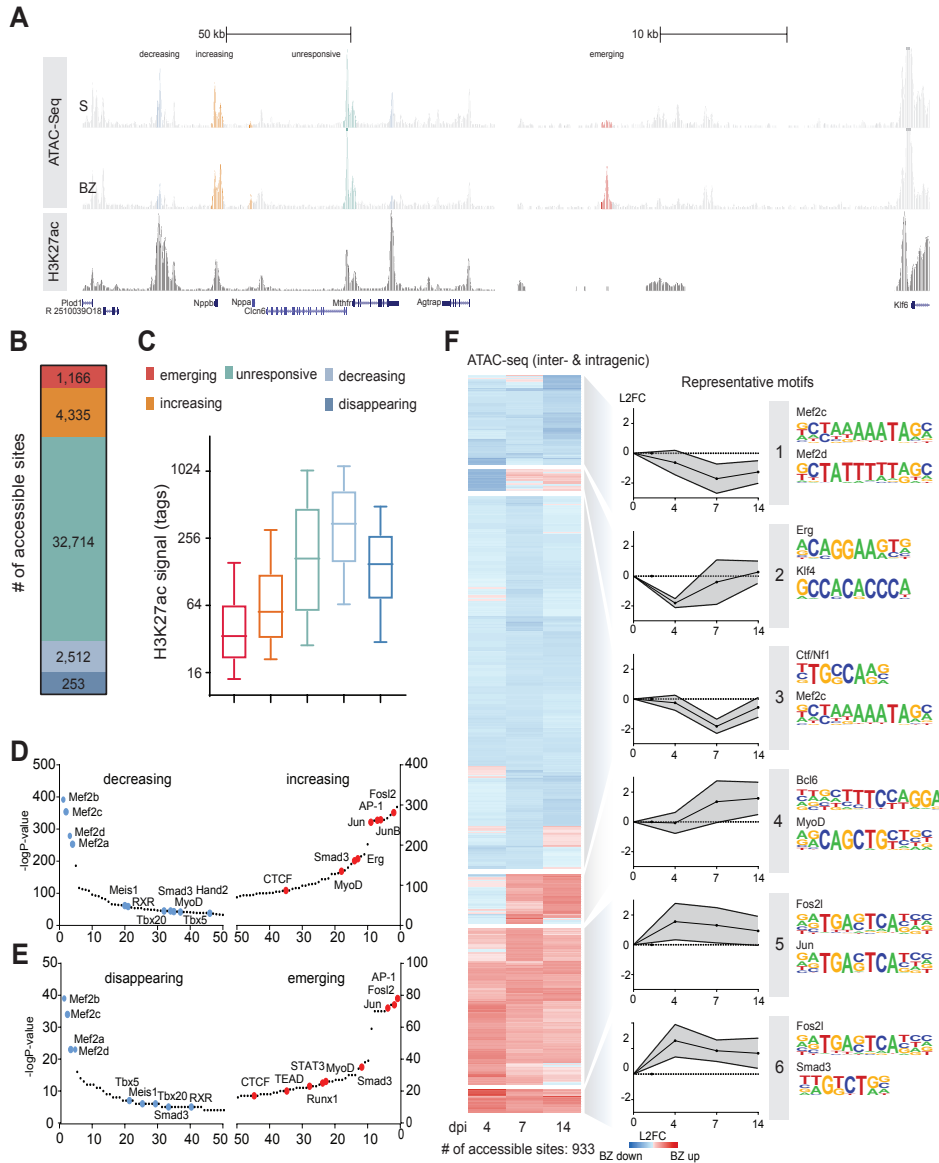


FIGURE 6. Identification of enriched motifs in BZ cardiomyocytes. (A) Representative inter- and intragenic accessibility patterns, reflecting changes in activity of enhancers and other types of regulatory elements in the BZ. (B) Distribution of distal accessibility regions across the five classes of dynamic peaks. (C) Box plots showing the intensity of ACM H3K27ac signal (total tags) per dynamic peak class. Enriched transcription factor binding motifs in decreasing and increasing (D) and disappearing and emerging (E) ATAC-seq peaks, as determined by HOMER, were ranked based on their p-value. Motifs involved in maintaining the CM lineage homeostasis such as Mef2c, were no longer accessible, whereas AP-1 binding sites gained accessibility. (F) Hierarchical clustering heatmap of distal accessible regions detectable at all time points (n=3 per tissue per time-point) and differentially affected at at least 1 time point. The highest enriched motifs per cluster (as calculated by HOMER) are given.

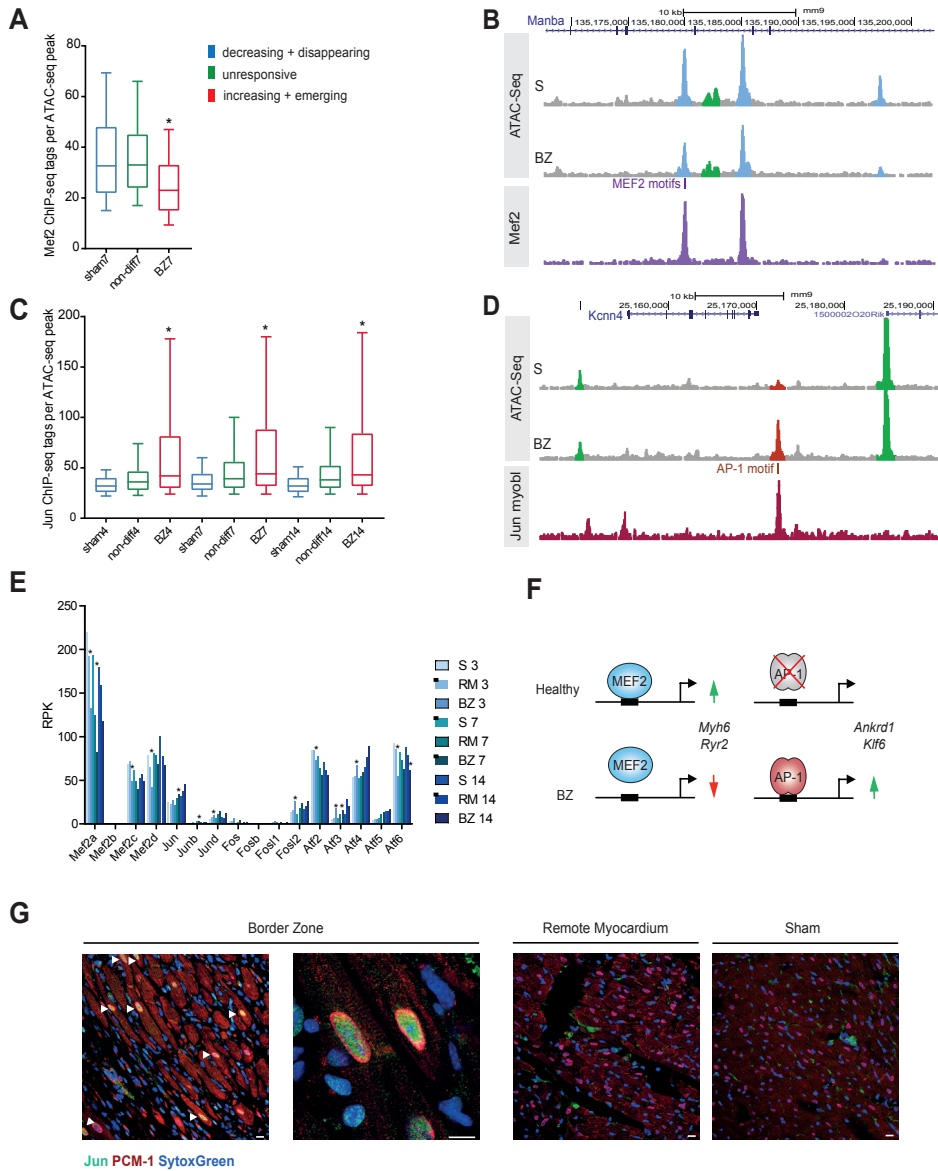


FIGURE 7. BZ cardiomyocytes are enriched for AP-1 binding motifs. (A) Box plots showing the intensity of MEF2 ChIP-seq signal (total tags) per dynamic peak class at 7 dpi. (B) Example UCSC browser view of BZ decreasing accessibility regions that overlap with MEF2 ChIP-seq peaks. A MEF2 consensus motif was found and noted for one of the peaks. (C) Box plots showing the intensity of Jun ChIP-seq signal (total tags) per dynamic peak class across all measured time points. (D) Example UCSC browser view of a BZ emerging accessibility region that overlaps with a Jun ChIP-seq peak, containing a consensus AP-1 motif. (E) Average RPK values obtained from whole tissue RNA-seq (n=3 per tissue per time-point) for the members of the AP-1 family of transcription factors and the Mef2 family of transcription factors (F) Cardiac lineage specific transcription binding sites, such as Mef2, whereas accessibility of non-CM lineage typical promoters /genes and enhancers with binding motifs for AP-1 and other stress responsive transcription factors increases. (G) Immunohistochemical

staining of pericentriolar material 1 (PCM-1), c-Jun and Sytox Green of BZ, RM and sham at 7 dpi. Arrow-heads indicate c-Jun positive cardiomyocyte nuclei. Scale bar: 10 μm . BZ = Border zone, RM = Remote Myocardium, S = Sham, dpi = days post infarction, RPK = read per kilobase. * $p < 0.05$ in a one-way ANOVA.

To test whether the motif enrichment results correspond to increased binding, we cross-referenced our different ATAC-seq signal classes (increased, maintained, decreased) with available adult cardiac MEF2³⁵ and myoblast c-Jun³⁶ ChIP-seq data. We plotted heart MEF2 ChIP-seq tag abundance per ATAC-seq peak group (Figure 7A, B), which shows that regions that become accessible in the BZ have markedly less MEF2 binding. Reduced MEF2 binding could not be attributed to lower expression of *Mef2a*, the main postnatal cardiac isoform,³⁷ *Mef2c* or *Mef2d*, as BZ CMs readily expressed these genes (Figure 7E and Supplemental Figure 11E and Supplemental Table 3). Likewise, we plotted c-Jun (AP-1 component) ChIP-seq tag abundance (Figure 7C), and find that the BZ-enriched peaks show stronger c-Jun binding activity at all measured timepoints (Figure 7C, D). The expression of AP-1 component genes *Jun*, *Junb*, *Jund*, *Fosl1* and *Fosl2* was increased in BZ CM nuclei compared to RM nuclei (Figure 7E and Supplemental Figure 11E and Supplemental Table 3, 4). Furthermore, we detected c-Jun in BZ CM nuclei at 7 and at 14 dpi, but not in CM of RM or of sham operated mice (Figure 7G and Supplemental Figure 12), and we validated the dependency of several of the stress-response enhancer fragments to c-Jun, (Supplemental Figure 11B-D). These data corroborate the motif enrichment findings, and indicate that the CM specific BZ response is, in part, driven by activated c-Jun.

Taken together, these data suggest that the CM lineage specific program is downregulated after injury in BZ CMs, involving reduced MEF2 interaction with target regulatory sequences, whereas a stress program is induced by, amongst others, induced c-Jun (AP-1) activity in the BZ CM nuclei (Figure 7F).

DISCUSSION

In this study we identified the BZ of the ischemically injured ventricular wall as a transcriptionally discrete compartment distinct from the RM. The observed expression patterns of many novel BZ markers including *Gpx3*, *Clu* and *Ankrd1* closely matched those of *Nppa*, indicating a generalized transcriptional BZ compartment forms around the infarct in the mouse heart. In the BZ and to a much lesser extent in the RM, we observed a striking and immediate downregulation of genes implicated in cardiac muscle contraction, oxidative phosphorylation, mitochondrial activity and fatty acid beta oxidation, all of which are specifically highly active in the mature CM lineage. This genome wide-assessment is in agreement with previous studies in which CMs close to the infarct were found to activate

Nppa (ANF), *Acta2* (aSMA), and *Runx1*, amongst others, and to show accumulation of lipid droplets, perinuclear sarcomere depletion and glycogen accumulation.^{4,5,13} These changes, however, may also result from stress mechanisms instead of dedifferentiation in the strict developmental sense. For example, the induction of *Nppa*, *Nppb* and presumably other genes in adult cardiac stress, often referred to as the activation of the “fetal gene program” is achieved through adult stress regulatory DNA sequences that are different from those that activate *Nppa* and *Nppb* during development.³⁸

Adult post MI CMs were reported to not revert back to the neonatal stage.³⁰ We note, however, that in these studies CMs were isolated from whole heart, which mainly comprises RM CMs, as the BZ is but a small fraction of the total cell population. Both our ATAC-seq data and the PCM-1+ CM nuclear expression profiling data revealed a striking absence of induction of cell cycle and glycolysis genes (Figure 5 and Supplemental Figure 9), which were expected to be induced if BZ CMs would revert to the neonatal stage. Indeed, CM cell cycle activity in the BZ after MI is negligible¹⁵. Furthermore, promoters of genes for signaling pathway components associated with CM proliferation and cardiac regeneration¹⁴⁻¹⁸ were not induced in BZ CMs. Thus, the BZ CMs downregulate mature CM lineage-specific genes but fail to induce neonatal programs for proliferation and metabolic switching to glycolysis. Interestingly, transgenic mice in which the CM cell cycle is stimulated show CM proliferation after MI preferentially in the BZ,¹⁵⁻¹⁸ suggesting that the dedifferentiated (or stressed) state the BZ CMs acquire after MI is involved but not sufficient for CM renewal after injury.

B-type natriuretic peptide (BNP), encoded by *NPPB*, is a widely used biomarker for diagnosis and prognosis in patients with acute or chronic heart failure.³⁹ While *Nppb*^{-/-} mice do not show elevated blood pressure or hypertrophy, they were reported to develop cardiac fibrosis from 15 weeks of age onwards, which was exaggerated in response to pressure overload.^{32,40} Infusion of BNP in mice lead to arrhythmia and calcium handling alterations in the heart.⁴¹ In contrast, local BNP treatment by viral delivery to the heart restored calcium homeostasis in CMs and restored contractility.⁴² However, in our mutants we did not observe changed expression of any of the genes implicated in these processes both before and after MI, indicating they are not predisposed to develop heart failure or fibrosis in response to MI. Further analysis will be required to gain insight into the underlying mechanism and possibly secondary effects such as pulmonary vascular remodeling.⁴³ The acute development of heart failure and death of *Nppb*^{-/-} mice after MI illustrates the importance of a proper injury response by the BZ after MI. We expect many other vital processes to occur in this region and the RNA-seq and ATAC-seq data presented here might form the starting point for their discovery. Furthermore, it may be interesting to assess the relation between BNP levels and vulnerability to develop complications after MI.

ATAC-seq analysis of CM nuclei revealed that sites losing accessibility after MI were marked

by CM-specific acetylated H3K27, a marker for active transcription regulatory sequences (*i.e.* enhancers), and were enriched in motifs for binding of MEF2, though to a lesser extent, TBX and MEIS families of transcription factors. The Mef2 family of transcription factors plays an important role during cardiac development and cardiac hypertrophy.^{44, 45} *Mef2a* maintains CM differentiation and mitochondrial activity.³⁷ The reduced accessibility of MEF2-enriched elements in BZ CMs indicates the Mef2-driven program is downregulated, which is in line with the observed reduction of mature state and mitochondrial activity of the BZ CMs. In heart failure-induced enhancers (H3K27ac signals), the MEF2 motif is enriched,⁴⁶ compatible with the activation of Mef2 function in hypertrophy.^{44, 45} This suggests that BZ CMs respond opposite to stress in heart failure and after MI, and indicate CM lineage-specific enhancers are being inactivated after MI.

Sites that gained accessibility, in contrast, were much less frequently marked by CM-specific H3K27ac, suggesting they were activated *de novo* in response to MI. These sites were highly enriched in motifs for members of the Jun and Fos families of transcription factors.²⁵ *Jun* and *Fosl2* were found to be required for heart development.^{26, 27} A recent study found that in skin wound repair, cells lose homeostatic lineage-specific properties when injury-induced stress-responsive enhancers are activated by factors such as AP-1 that override homeostatic regulatory elements governing lineage specificity.⁴⁷ Our data indicate such a mechanism occurs in BZ CMs as well. We observe a massive reduction of accessibility of CM lineage-specific promoters/genes and enhancers with CM lineage-specific transcription factor binding motifs, whereas accessibility of non-CM lineage typical promoters/genes and enhancers with binding motifs for AP-1, TEAD and other stress-responsive transcription factors increased (Figure 6D-F). The MEF2 and AP-1 motif enrichment results were supported by overlap analysis with available ChIP-seq data and the selective BZ CM nuclear localization of c-Jun (Figure 7).

When the cell cycle is stimulated through cardiac overexpression of for example cyclin D2, Tbx20 or YAP, CM cycling is observed predominantly in the BZ, suggesting that the phenotype of the BZ CMs is favorable for the stimulation of proliferation.^{15, 17, 18} In mice, direct or indirect activation of nuclear YAP leads to proliferation of both healthy and post-injury CMs.^{16, 46} YAP interacts with TEAD, a DNA-binding transcription factor, to regulate downstream gene expression.⁴⁸ ChIP-seq and ATAC-seq data revealed that YAP-TEAD binding sites are enriched for AP-1 binding sites.^{46, 49, 50} In breast cancer cells, YAP-TEAD was found to associate with AP-1/JUN/FOS at enhancers controlling proliferation.⁵⁰ We speculate that the emergence of AP-1 motif enhancers in BZ CMs associated with activation of a stress-responsive gene program creates a favorable state poised for proliferation to occur when YAP-TEAD signaling is activated experimentally in post-injury CMs (Supplemental Figure 13).

For future targeted therapy it is relevant to identify and characterize the BZ CMs in the ischemic human heart. In this study, we show that the BZ is transcriptionally conserved between mouse and human and identified novel BZ marker genes. CMs adjacent to both the IZ and endocardium showed strongest expression of these BZ markers. Likely, these cells survive the MI by oxygen and nutrients supplied directly from the ventricular lumen. This region of activated myocardium is important since the CMs in this rim might be most responsive to proliferative stimuli like YAP-TEAD. Furthermore, our data suggests that this responsiveness might be restricted to a temporal window, since the expression of marker genes subsides with the maturation of the scar. For therapeutic purposes, techniques could be developed to target this sub-endocardial rim of surviving and activated CMs with stimuli to promote regeneration of the human heart.

METHODS

An expanded methods section is available in the Supplemental Material. The data, analytic methods, and study materials will be made available by the authors to other researchers for purposes of reproducing the results or replicating the procedure.

Mice

Animal care and experiments conform to the Directive 2010/63/EU of the European Parliament. All animal work was approved by the Animal Experimental Committee of the Academic Medical Center, Amsterdam, and was carried out in compliance with the Dutch government guidelines.

BAC-Nppb-Katushka,¹⁹ *Myh6-MerCreMer*²⁰ and *nTnG* (JAX stock #023035) mice were bred on the FVB/N background. Tamoxifen (20 mg/kg) was administered i.p. one week prior to t=0 and repeated the two following days. Myocardial infarction was performed. Two independent *Nppb*-deficient mouse lines were generated by CRISPR/Cas9-mediated genome editing in FVB oocytes.

Human material

Paraffin embedded infarcted human heart tissue from 3 individuals that had died due to myocardial infarction were retrieved from the pathology archive of the University Medical Center Utrecht. Material was handled in a coded manner that met the criteria of the Code of Conduct used in the Netherlands for the responsible use of human tissue in medical research (www.federa.org/codes-conduct). Collection of the archive material was approved by the local biobank review committee (protocol 15–252).

Statistical analysis

Differential expression analysis was performed using the DESeq2 package.²¹ P-values were corrected for multiple testing using the false discovery rate (FDR) method of Benjamini-Hochberg ($p < 0.05$).

To compare the survival distributions between *Nppb*^{-/-} mice and wildtype littermates after MI we used a log-rank test ($p < 0.05$).

Motifs detected with HOMER were considered enriched when $p < 1^{-10}$ was reached, as recommended by the authors (<http://homer.ucsd.edu/homer/>).²²

To determine whether ATAC-seq peak categories were differentially bound by TFs, we counted the number of ChIP-seq tags present per peak. To test for differences between groups a one-way ANOVA was performed, using a multi comparison procedure post hoc Games-Howell test ($p < 0.05$). We performed a log-transformation on the ChIP-seq count data when the counts were not normally distributed.

Data Availability

All RNA-seq and ATAC-seq data have been deposited at the Gene Expression Omnibus under the accession number (GSE110209); as well as PCM-1 (GSE128034) and *Nppb*^{-/-} (GSE128196) RNA-seq data. An Excel file has been made available in the Supplemental Material that contains tables with candidate BZ genes using various criteria.

Acknowledgements

We thank Corrie de Gier-de Vries for help with the *in situ* hybridizations.

Sources of Funding

This study was supported by Netherlands Heart Foundation COBRA3 and Cardiovasculair Onderzoek Nederland HUSTCARE to VMC and JB, an European Research Area Network-Cardiovascular Diseases CARDIOPRO grant to JB, and a Leducq Foundation grant (14CVD01) to VMC.

Conflicts of Interests Disclosures

None.

REFERENCES

1. Bergmann O, Zdunek S, Felker A, Salehpour M, Alkass K, Bernard S, Sjostrom SL, Szewczykowska M, Jackowska T, Dos Remedios C, Malm T, Andra M, Jashari R, Nyengaard JR, Possnert G, Jovinge S, Druid H and Frisen J. Dynamics of Cell Generation and Turnover in the Human Heart. *Cell*. 2015;161:1566-1575.
2. Factor SM, Sonnenblick EH and Kirk ES. The histologic border zone of acute myocardial infarction--islands or peninsulas? *Am J Pathol*. 1978;92:111-124.
3. Driesen RB, Verheyen FK, Dijkstra P, Thone F, Cleutjens JP, Lenders MH, Ramaekers FC and Borgers M. Structural remodelling of cardiomyocytes in the border zone of infarcted rabbit heart. *Mol Cell Biochem*. 2007;302:225-232.
4. Sharov VG, Sabbah HN, Ali AS, Shimoyama H, Lesch M and Goldstein S. Abnormalities of cardiocytes in regions bordering fibrous scars of dogs with heart failure. *Int J Cardiol*. 1997;60:273-279.
5. Dispersyn GD, Mesotten L, Meuris B, Maes A, Mortelmans L, Flameng W, Ramaekers F and Borgers M. Dissociation of cardiomyocyte apoptosis and dedifferentiation in infarct border zones. *Eur Heart J*. 2002;23:849-857.
6. Ounzain S, Micheletti R, Beckmann T, Schroen B, Alexanian M, Pezzuto I, Crippa S, Nemir M, Sarre A, Johnson R, Dauvillier J, Burdet F, Ibberson M, Guigo R, Xenarios I, Heymans S and Pedrazzini T. Genome-wide profiling of the cardiac transcriptome after myocardial infarction identifies novel heart-specific long non-coding RNAs. *Eur Heart J*. 2015;36:353-368a.
7. Kaikkonen MU, Halonen P, Liu OH, Turunen TA, Pajula J, Moreau P, Selvarajan I, Tuomainen T, Aavik E, Tavi P and Yla-Herttuala S. Genome-Wide Dynamics of Nascent Noncoding RNA Transcription in Porcine Heart After Myocardial Infarction. *Circulation Cardiovascular genetics*. 2017;10:1-11.
8. Lacraz GPA, Junker JP, Gladka MM, Molenaar B, Scholman KT, Vigil-Garcia M, Versteeg D, de Ruiter H, Vermunt MW, Creighton MP, Huibers MMH, de Jonge N, van Oudenaarden A and van Rooij E. Tomo-Seq Identifies SOX9 as a Key Regulator of Cardiac Fibrosis During Ischemic Injury. *Circulation*. 2017;136:1396-1409.
9. Gladka MM, Molenaar B, de Ruiter H, van der Elst S, Tsui H, Versteeg D, Lacraz GPA, Huibers MMH, van Oudenaarden A and van Rooij E. Single-Cell Sequencing of the Healthy and Diseased Heart Reveals Ckap4 as a New Modulator of Fibroblasts Activation. *Circulation*. 2018:166-180.
10. Jackson BM, Gorman JH, Moainie SL, Guy TS, Narula N, Narula J, John-Sutton MG, Edmunds LH, Jr. and Gorman RC. Extension of borderzone myocardium in postinfarction dilated cardiomyopathy. *Journal of the American College of Cardiology*. 2002;40:1160-1167; discussion 1168-1171.
11. de Bakker JM, van Capelle FJ, Janse MJ, Wilde AA, Coronel R, Becker AE, Dingemans KP, van Hemel NM and Hauer RN. Reentry as a cause of ventricular tachycardia in patients with chronic ischemic heart disease: electrophysiologic and anatomic correlation. *Circulation*. 1988;77:589-606.
12. Francis Stuart SD, De Jesus NM, Lindsey ML and Ripplinger CM. The crossroads of inflammation, fibrosis, and arrhythmia following myocardial infarction. *J Mol Cell Cardiol*. 2016;91:114-122.
13. Ursell PC, Gardner PI, Albala A, Fenoglio JJ, Jr. and Wit AL. Structural and electrophysiological changes in the epicardial border zone of canine myocardial infarcts during infarct healing. *Circ Res*. 1985;56:436-451.
14. Wu CC, Kruse F, Vasudevarao MD, Junker JP, Zebrowski DC, Fischer K, Noel ES, Grun D, Berezikov E, Engel FB, van Oudenaarden A, Weidinger G and Bakkens J. Spatially Resolved Genome-wide Transcriptional Profiling Identifies BMP Signaling as Essential Regulator of Zebrafish Cardiomyocyte Regeneration. *Dev Cell*. 2016;36:36-49.
15. Pasumarthi KB, Nakajima H, Nakajima HO, Soonpaa MH and Field LJ. Targeted expression of cyclin D2 results in cardiomyocyte DNA synthesis and infarct regression in transgenic mice. *Circ Res*. 2005;96:110-118.
16. Leach JP, Heallen T, Zhang M, Rahmani M, Morikawa Y, Hill MC, Segura A, Willerson JT and Martin JF. Hippo pathway deficiency reverses systolic heart failure after infarction. *Nature*. 2017;550:260-264.
17. Xiang FL, Guo M and Yutzey KE. Overexpression of Tbx20 in Adult Cardiomyocytes Promotes Proliferation and Improves Cardiac Function After Myocardial Infarction. *Circulation*. 2016;133:1081-1092.
18. Lin Z, von Gise A, Zhou P, Gu F, Ma Q, Jiang J, Yau AL, Buck JN, Gouin KA, van Gorp PR, Zhou B, Chen J, Seidman JG, Wang DZ and Pu WT.

- Cardiac-specific YAP activation improves cardiac function and survival in an experimental murine MI model. *Circ Res*. 2014;115:354-363.
19. Sergeeva IA, Hooijkaas IB, van der Made I, Jong WM, Creemers EE and Christoffels VM. A transgenic mouse model for the simultaneous monitoring of ANF and BNP gene activity during heart development and disease. *Cardiovasc Res*. 2014;78-86.
 20. Sohal DS, Nghiem M, Crackower MA, Witt SA, Kimball TR, Tymitz KM, Penninger JM and Molkenin JD. Temporally regulated and tissue-specific gene manipulations in the adult and embryonic heart using a tamoxifen-inducible Cre protein. *Circ Res*. 2001;89:20-25.
 21. Love MI, Huber W and Anders S. Moderated estimation of fold change and dispersion for RNA-seq data with DESeq2. *Genome biology*. 2014;15:550.
 22. Heinz S, Benner C, Spann N, Bertolino E, Lin YC, Laslo P, Cheng JX, Murre C, Singh H and Glass CK. Simple combinations of lineage-determining transcription factors prime cis-regulatory elements required for macrophage and B cell identities. *Mol Cell*. 2010;38:576-589.
 23. Frangogiannis NG. The inflammatory response in myocardial injury, repair, and remodelling. *Nat Rev Cardiol*. 2014;11:255-265.
 24. Fu X, Khalil H, Kanisicak O, Boyer JG, Vagnozzi RJ, Maliken BD, Sargent MA, Prasad V, Valiente-Alandi I, Blaxall BC and Molkenin JD. Specialized fibroblast differentiated states underlie scar formation in the infarcted mouse heart. *J Clin Invest*. 2018;128:2127-2143.
 25. Hess J, Angel P and Schorpp-Kistner M. AP-1 subunits: quarrel and harmony among siblings. *J Cell Sci*. 2004;117:5965-5973.
 26. Eferl R, Sibilia M, Hilberg F, Fuchsbichler A, Kufferath I, Guertl B, Zenz R, Wagner EF and Zatloukal K. Functions of c-Jun in liver and heart development. *J Cell Biol*. 1999;145:1049-1061.
 27. Jahangiri L, Sharpe M, Novikov N, Gonzalez-Rosa JM, Borikova A, Nevis K, Paffett-Lugassy N, Zhao L, Adams M, Guner-Ataman B, Burns CE and Burns CG. The AP-1 transcription factor component Fos12 potentiates the rate of myocardial differentiation from the zebrafish second heart field. *Development*. 2016;143:113-122.
 28. Pinto AR, Illyikh A, Ivey MJ, Kuwabara JT, D'Antoni ML, Debuque R, Chandran A, Wang L, Arora K, Rosenthal NA and Tallquist MD. Revisiting Cardiac Cellular Composition. *Circ Res*. 2016;118:400-409.
 29. Preissl S, Schwaderer M, Raulf A, Hesse M, Gruning BA, Kobele C, Backofen R, Fleischmann BK, Hein L and Gilsbach R. Deciphering the Epigenetic Code of Cardiac Myocyte Transcription. *Circ Res*. 2015;117:413-423.
 30. Quaife-Ryan GA, Sim CB, Ziemann M, Kaspi A, Rafahi H, Ramialison M, El-Osta A, Hudson JE and Porrello ER. Multicellular Transcriptional Analysis of Mammalian Heart Regeneration. *Circulation*. 2017;136:1123-1139.
 31. Jenkins CP, Cardona DM, Bowers JN, Oliari BR, Allan RW and Normann SJ. The utility of C4d, C9, and troponin T immunohistochemistry in acute myocardial infarction. *Arch Pathol Lab Med*. 2010;134:256-263.
 32. Tamura N, Ogawa Y, Chusho H, Nakamura K, Nakao K, Suda M, Kasahara M, Hashimoto R, Katsuura G, Mukoyama M, Itoh H, Saito Y, Tanaka I, Otani H and Katsuki M. Cardiac fibrosis in mice lacking brain natriuretic peptide. *Proc Natl Acad Sci U S A*. 2000;97:4239-4244.
 33. Buenrostro JD, Giresi PG, Zaba LC, Chang HY and Greenleaf WJ. Transposition of native chromatin for fast and sensitive epigenomic profiling of open chromatin, DNA-binding proteins and nucleosome position. *Nature methods*. 2013;10:1213-1218.
 34. Liu Q, Jiang C, Xu J, Zhao MT, Van Bortle K, Cheng X, Wang G, Chang HY, Wu JC and Snyder MP. Genome-Wide Temporal Profiling of Transcriptome and Open Chromatin of Early Cardiomyocyte Differentiation Derived From hiPSCs and hESCs. *Circ Res*. 2017;121:376-391.
 35. Guo A, Wang Y, Chen B, Wang Y, Yuan J, Zhang L, Hall D, Wu J, Shi Y, Zhu Q, Chen C, Thiel WH, Zhan X, Weiss RM, Zhan F, Musselman CA, Pufall M, Zhu W, Au KF, Hong J, Anderson ME, Grueter CE and Song LS. E-C coupling structural protein junctophilin-2 encodes a stress-adaptive transcription regulator. *Science*. 2018;362:1-9.
 36. Umansky KB, Feldmesser E and Groner Y. Genomic-wide transcriptional profiling in primary myoblasts reveals Runx1-regulated genes in muscle regeneration. *Genom Data*. 2015;6:120-122.
 37. Naya FJ, Black BL, Wu H, Bassel-Duby R, Richardson JA, Hill JA and Olson EN. Mitochondrial deficiency and cardiac sudden death in mice lacking the MEF2A transcription factor. *Nat Med*. 2002;8:1303-1309.
 38. Sergeeva IA, Hooijkaas IB, Ruijter JM, van der Made I, de Groot NE, van de Werken HJ, Creemers EE and Christoffels VM. Identification of a regulatory domain controlling the Nppa-Nppb gene cluster during heart development and stress. *Development*. 2016;143(12):2135-2146.
 39. Ponikowski P, Voors AA, Anker SD, Bueno H,

- Cleland JGF, Coats AJS, Falk V, Gonzalez-Juanatey JR, Harjola VP, Jankowska EA, Jessup M, Linde C, Nihoyannopoulos P, Parissis JT, Pieske B, Riley JP, Rosano GMC, Ruilope LM, Ruschitzka F, Rutten FH, van der Meer P and Group ESCSD. 2016 ESC Guidelines for the diagnosis and treatment of acute and chronic heart failure: The Task Force for the diagnosis and treatment of acute and chronic heart failure of the European Society of Cardiology (ESC) Developed with the special contribution of the Heart Failure Association (HFA) of the ESC. *Eur Heart J*. 2016;37:2129-2200.
40. Holditch SJ, Schreiber CA, Nini R, Tonne JM, Peng KW, Geurts A, Jacob HJ, Burnett JC, Cataliotti A and Ikeda Y. B-Type Natriuretic Peptide Deletion Leads to Progressive Hypertension, Associated Organ Damage, and Reduced Survival: Novel Model for Human Hypertension. *Hypertension*. 2015;66:199-210.
 41. Thireau J, Karam S, Fauconnier J, Roberge S, Cassan C, Cazorla O, Aïmond F, Lacampagne A, Babuty D and Richard S. Functional evidence for an active role of B-type natriuretic peptide in cardiac remodelling and pro-arrhythmogenicity. *Cardiovasc Res*. 2012;95:59-68.
 42. Moilanen AM, Rysa J, Mustonen E, Serpi R, Aro J, Tokola H, Leskinen H, Manninen A, Levijoki J, Vuolteenaho O and Ruskoaho H. Intramyocardial BNP gene delivery improves cardiac function through distinct context-dependent mechanisms. *Circ Heart Fail*. 2011;4:483-495.
 43. Casserly B and Klinger JR. Brain natriuretic peptide in pulmonary arterial hypertension: biomarker and potential therapeutic agent. *Drug Des Devel Ther*. 2009;3:269-287.
 44. Desjardins CA and Naya FJ. The Function of the MEF2 Family of Transcription Factors in Cardiac Development, Cardiogenomics, and Direct Reprogramming. *J Cardiovasc Dev Dis*. 2016;3:1-19.
 45. Wei J, Joshi S, Speransky S, Crowley C, Jayathilaka N, Lei X, Wu Y, Gai D, Jain S, Hoosien M, Gao Y, Chen L and Bishopric NH. Reversal of pathological cardiac hypertrophy via the MEF2-coregulator interface. *JCI Insight*. 2017;2:1-16.
 46. Monroe TO, Hill MC, Morikawa Y, Leach JP, Heallen T, Cao S, Krijger PHL, de Laat W, Wehrens XHT, Rodney GG and Martin JF. YAP Partially Reprograms Chromatin Accessibility to Directly Induce Adult Cardiogenesis In Vivo. *Dev Cell*. 2019;48(6):765-779.
 47. Ge Y, Gomez NC, Adam RC, Nikolova M, Yang H, Verma A, Lu CP, Polak L, Yuan S, Elemento O and Fuchs E. Stem Cell Lineage Infidelity Drives Wound Repair and Cancer. *Cell*. 2017;169:636-650 e614.
 48. Piccolo S, Dupont S and Cordenonsi M. The biology of YAP/TAZ: hippo signaling and beyond. *Physiol Rev*. 2014;94:1287-1312.
 49. Stein C, Bardet AF, Roma G, Bergling S, Clay I, Ruchti A, Agarinis C, Schmelzle T, Bouwmeester T, Schubeler D and Bauer A. YAP1 Exerts Its Transcriptional Control via TEAD-Mediated Activation of Enhancers. *PLoS Genet*. 2015;11:e1005465.
 50. Zanconato F, Forcato M, Battilana G, Azzolin L, Quaranta E, Bodega B, Rosato A, Bicciato S, Cordenonsi M and Piccolo S. Genome-wide association between YAP/TAZ/TEAD and AP-1 at enhancers drives oncogenic growth. *Nat Cell Biol*. 2015;17:1218-1227.

SUPPLEMENTARY INFORMATION

EXTENDED RESULTS

Function of BZ marker genes

Clu is thought to play a protective role by acting as an antioxidant during oxidative stress.¹ Similar to *Nppa*, in the postnatal heart *Clu* is expressed in the atria and re-activated upon myocardial stress. It was shown to inhibit cell apoptosis by acting on the NF- κ B signaling pathway and Bax/Bcl-xL expression.² In a rat model of myocardial infarction, *Clu*, as an inflammatory modulator, could reduce infarct size and improve survival, while increasing macrophage infiltration at the infarcted area.³ Recently, plasma CLU levels have been associated with left ventricular remodeling after MI.⁴

Gpx3 encodes a member of the glutathione peroxidase family, which catalyze the reduction of organic hydroperoxides and hydrogen peroxide by glutathione, and thereby protect cells against oxidative damage. Although reduced *Gpx3* activity has been associated with increased risk of cardiovascular events^{5, 6}, still little is known about its role in cardiovascular disease.

Ankrd1 encodes cardiac ankyrin repeat protein (CARP).⁷⁻⁹ Ventricular *Ankrd1* upregulation was observed in models of pressure overload or clinical heart failure due to dilated and arrhythmogenic RV cardiomyopathy.¹⁰⁻¹² Moreover, mutations in *Ankrd1* were found to be associated with dilated and hypertrophic cardiomyopathy.^{13, 14} Functionally, myocardial *Ankrd1* acts as an anti-apoptotic survival factor after ischemia-reperfusion injury and hypoxia.^{15, 16}

Foxp1 is a member of the forkhead box family of transcription factors that is required for heart development in mouse and human. It coordinates the balance of CM proliferation and differentiation during development and postnatally represses hypertrophy-associated gene expression.¹⁷⁻¹⁹

***Nppb* is required during recovery from myocardial infarction**

NPPB is induced in the BZ from fish^{20, 21} to human (our study) and serves as a paradigm for cardiac injury responsive gene expression. Previous reports have revealed that loss of *Nppb* leads to increased age-related progression of fibrosis under both baseline and pathological conditions.²² Furthermore, it has been demonstrated in animal studies that exogenous administration of BNP exerts an anti-fibrotic effect by limiting the infarct size after MI, which is regulated by endogenous NOS/NO component and opening of KATP channels^{23, 24}. RNA-seq analysis detected transcripts of approximately 15,000 genes in the left ventricle of *Nppb*^{-/-} mice under baseline conditions. However, we could not identify any fibrosis markers among the differentially expressed genes in *Nppb*^{-/-} mice, and GO term annotation analysis

did not reveal pathological processes of fibrosis (Figure 4C). We stained microdissected left ventricular tissue of 12 wks and 20 wks old *Nppb*^{-/-} mice with Picosirius Red, and did not observe fibrotic lesions (Supplemental Figure 7C, D in the Supplemental Material).

Of the 21 *Nppb*^{-/-} mice subjected to MI surgeries with an infarct size $\geq 30\%$, 9 mice (42%) died between 1-3 days after MI. During the course of 7 days, additional *Nppb*^{-/-} mice died (n=13), only 2 of which had infarct rupture (n=2) (Figure 7A and Supplemental Figure 8B in the Supplemental Material). In contrast, wildtype littermates with infarct size of 40-50% (n=5) survived 7 days post-MI or died as a result of infarct rupture (n=7) or discomfort (n=1) (Figure 4F and Supplemental Figure 7A in the Supplemental Material). Note, the FVB genetic background used has an infarct rupture frequency of approximately 1 in 3.²⁵

Using *in situ* hybridization, we validated the absence of *Nppb* expression and induction of *Nppa* in the BZ of wildtype and *Nppb*^{-/-} mice (Figure 4G and Supplemental Figure 8F in the Supplemental Material). We assessed the transcript levels of myocardial hypertrophy markers (*Myh7* and *Atp2a2* (SERCA2A)), a two fibrosis markers (*Col1a1* and *Pstn*) in healthy myocardium and (WT n=6; HOM n=6) and 7 dpi RM (WT n=6; HOM n=6). Neither the healthy hearts nor the RM after MI showed any differences in expression of the indicated marker genes between *Nppb*^{-/-} and wildtypes (Figure 4J).

SUPPLEMENTAL METHODS

Animals

Animal care and experiments conform to the Directive 2010/63/EU of the European Parliament. All animal work was approved by the Animal Experimental Committee of the Academic Medical Center, Amsterdam, and was carried out in compliance with the Dutch government guidelines. Myh6-MerCreMer²⁶, nTnG (JAX stock #023035) and Gt(ROSA)26Sortm5(CAG-Sun1/sfGFP)Nat/J (JAX stock #021039) mice were bred on the FVB/N background. Tamoxifen (20 mg/kg) was administrated i.p. one week prior to t=0 and repeated the two following days.

Myocardial infarction

Mice were analgesized subcutaneously with buprenorfine (0.075 mg/kg). Anesthesia was induced with 4% Isoflurane in 1L/min O₂. Mice were shaved, intubated and locally analgesized subcutaneously with Lidocaine (2 mg/kg) and Bupivacaine (3 mg/kg) at the site of incision. Mice were placed on a heating mat to maintain body temperature. Anesthesia was maintained via ventilation by a Minivent Mouse Ventilator (Hugo Sachs Electronic, Harvard Apparatus) with 2% Isoflurane in 1L/min O₂. Left thoracotomy was performed at the fourth intercostal space. Infarction was created by permanent ligation of the left anterior descending coronary artery (LAD) by surpassing a BV130-5 6.5mm taper point needle with a 8-0 Nylon wire (Ethilon, Ethicon, Johnson&Johnson) under the LAD, tied with a triple knot.

The thoracotomy and skin were closed with a C-1 12mm cutting needle with a 6-0 silicone coated braided silk wire (SOF SILK, Covidien). Analgesia was maintained up till 2 days after MI using buprenorphine (0.075 mg/kg) or Meloxicam (0.02 mg/kg).

Echocardiographic measurements in mice

Mice were anesthetized using isoflurane inhalation (4% induction, 1-1.5% in 700 ml O₂/minute for maintenance) and echocardiographic measurements were recorded as previously described.²⁷

Histological analysis

Microdissected left ventricle were fixed overnight in 4% paraformaldehyde, transferred to 70% ethanol, dehydrated, and embedded using standard techniques. Sections of 7 µm were stained with Picosirius Red for fibrosis.

In situ hybridization was performed as described previously.²⁸ Briefly, hearts or microdissected tissue were fixed in 4% formaldehyde, embedded in paraplast and sectioned at 10 µm. The cDNA probes were designed against mouse tissue were *Nppa*, *Nppb*, *Col1a2*, *Ech1*, *Ankrd1*, *Clu*, *Des*, *Acta1*, *Serpine1A*, *Fhl1*, *Gpx3*, *Fln* and *Tnni3*. For human tissue, cDNA probes used were *AFOG*, *Cd4*, *NPPA*, *NPPB*, *ECH1*, *ANKRD1*, *FOXP1*, *MYH7*, *DES*, *UCHL1*, *TMSB4X*, *CCR9*, *SERPINE1*, *JUNB* and *TCAP*. Images were acquired with Leica DM3000 microscope.

Immunohistochemistry

Immunohistochemistry was performed as described previously.²⁹ Briefly, sections of 7 µm were deparaffinized and dehydrated by a series of ethanol. For antigen retrieval, sections were boiled in unmasking solution (H3300, Vector) and blocked in 4% BSA. Sections were incubated with rabbit anti-PCM-1 (1:400, Atlas Antibodies, HPA023370), mouse anti-Jun (1:400, BD Bioscience, 610327), rabbit anti-Dystrophin (1:200, Abcam, ab15277). SytoxGreen (1:40,000, Thermo Fischer Scientific, S7020) was used as a nuclear stain. Fluorescence was visualized with the Leica TCS SP8 confocal microscope and the LasX software (Leica microsystems).

CRISPR/Cas9 genome editing

Three single guide RNAs (sgRNAs) (sgRNA 1: GGGTGATCTGCCATGTAGTC; sgRNA 2: GGGGCTTATGGCGTGACTCA; sgRNA 3: GGGAATGCCTCAGCTACTGT) were designed using the online tool ZIFIT Targeter^{30, 31} to target the *Nppb* gene. The sgRNAs (DR274) and Cas9 (MLM3613)³² were *in vitro* transcribed according to manufacturer's instructions (ThermoFisher Scientific). The sgRNAs (10 ng/µl per sgRNA) and Cas9 mRNA (25 ng/µl) were micro-injected into the cytoplasm of one-cell embryo's for generation of founder mouse lines on FVB/N background. Myocardial infarction was performed as described previously.³³

RNA isolation and quantitative real-time PCR (qPCR)

Total RNA was extracted from the border zone, remote zone, and the left ventricle of sham-operated mice at 3, 7, and 14 dpi and from the remote zone at 7 dpi and the left ventricle of *Nppb*-deficient mice using RNeasy according to manufacturer's instructions (Sigma-Aldrich). Prior to cDNA synthesis, total RNA samples were treated with RNase-free DNase I according to manufacturer's instructions (Invitrogen). The cDNA synthesis was carried out on 500 ng DNase-treated RNA using oligo-dT following the Superscript II system protocol (Invitrogen). Expression levels were assayed by quantitative real-time PCR using the LightCycler 480 system. Relative start concentrations were calculated as previously described.³⁴ Values were normalized to the geometric mean of *Hprt* and *Eef1e1* expression levels.

Isolation of nuclei from cardiomyocytes

Nuclear isolation was performed as described previously.³⁵ Briefly, all steps were carried out on ice. Snap frozen samples from the border zone and remote myocardium were blended and homogenized in 3ml lysis buffer (10 mM Tris-HCL (pH8.0), 5 mM CaCl₂, 2 mM EDTA, 0.5 mM EGTA, 1 mM DTT, 3 mM MgAc) using the Ultra-Turrax homogenizer (IKA). The suspension was dounced 10 times with a large pestle and 10 times with a tight pestle (Wheaton) in lysis buffer added with 0.4% Triton-X. The solution was filtered through 100 µm and 30 µm filters (Sysmex) and subsequently centrifuged for 5 min at 1000 g at 4°C. The nuclear pellet was resuspended in 500 µl staining buffer (PBS (pH 8.0) with 5% BSA and 0.2% Igepal CA-630). Cardiomyocyte nuclei were incubated with rabbit-anti PCM-1 antibody (Atlas antibodies, 1:1000, HPA023370) and a secondary antibody Alexa-647 (1:500, Invitrogen) for 1h. DAPI (1:1000, Sigma-Aldrich, D9542) was used as a nuclear stain. Sorting was performed on the BD Influx cell sorter (BD Bioscience). RNA was isolated using the RNeasy plus micro Kit (Qiagen).

RNA sequencing

For RNA isolated from cardiac nuclei, 500 pg was used for library generation with the Ovation RNA-seq v2 kit (NuGEN) kit. Libraries were prepared with the UltraLow V2 (NuGEN) kit and sequenced on the HiSeq4000 system (Illumina) with 50 bp single-end reads.

For RNA-seq libraries from whole tissue, 40 ng DNase-treated total RNA was amplified and converted to cDNA using the Ovation RNA-seq v2 kit (NuGEN). Amplified cDNA was sheared to an average fragment length of 200-400 bp and used with the SOLiD system (Life Technologies) to generate index-tagged sequencing libraries. Library quality and size distribution were determined with TapeStation (Agilent Technologies). Pooled libraries sequenced on a HiSeq 2500 system (Illumina) with 125 bp single-end reads. Data was cross-referenced to available PCM1-sorted RNA-seq data.³⁵

Nppb^{-/-} left ventricle RNA-seq library was prepared with the Truseq Stranded Total RNA Library Preparation Kit (Illumina, Part# 15031048 Rev. E). Total RNA (1 µg) was purified and

sheared into small fragments followed by cDNA synthesis and ligation of the adapter. The quality and size distribution of the cDNA library templates were validated with Agilent DNA 1000 on 2100 Bioanalyzer (Agilent Technologies). cDNA samples were pooled per lane of single-end 50 bp sequencing on an Illumina HiSeq 2500 system (Illumina).

Differential expression analysis

Reads were mapped to mm10 build of the mouse transcriptome using STAR.³⁶ Differential expression analysis was performed using the DESeq2 package based on a model using the negative binomial distribution.³⁷ Unsupervised hierarchical clustering was performed on genes differentially expressed between BZ and sham using the R package pheatmap, version 1.0.8. (<http://cran.r-project.org/web/packages/pheatmap/index.html>).

Besides DAVID³⁸, ClueGO³⁹ was used to find overrepresented gene ontology (GO) terms and Kegg pathways in the categories 'biological process' and 'molecular function'. P-values were corrected for multiple testing using the false discovery rate (FDR) method of Benjamini-Hochberg. We have used 0.05 as FDR control level. Significantly enriched terms were functionally grouped and visualized. The highest significant term of the group was displayed as leading term.

Differentially expressed genes were also cross-referenced with a list of published transcription factors.⁴⁰

ATAC sequencing

Nuclei isolation was performed on BZ tissue and the left ventricle of Tamoxifen-treated, sham-operated Myh6-MerCreMer (JAX stock #005657);nTnG (JAX stock #023035) mice at 7 and 14 dpi or PCM-1 (SIGMA stock #HPA023370) mice 4 dpi. Subsequently, isolated nuclei were sorted on a SH800 flow cytometer (Sony). Samples were gated in such a way that debris, nuclei clumps, and nuclei with no cardiomyocyte origin were excluded. A total of 50.000 nuclei per sample was collected and successively washed with PBS and used as input for ATAC-seq. Prior to sequencing, a quality check was performed to assure cardiomyocyte-specific open chromatin. Illumina sequencing libraries were generated and sequenced using the NextSeq platform.

Differential accessibility analysis

Reads were mapped to mm9 build of the mouse genome using BWA⁴¹; the default settings were used. The numbers of aligned reads from each sample are shown in Suppl. data files, Table 3. The BEDTools suite⁴² was used to distribute the genome wide signal into bins of 500bp. For promoter accessibility analysis the ATAC-seq signal was distributed into promoter bins defined as 1500bp upstream and 500bp of the canonical TSS (BioMart, mm9 build). To allow for differential peak calling between datasets, quantile normalization was

applied using the deepTools2 suite⁴³. Unsupervised hierarchical clustering was performed using the R package pheatmap, version 1.0.8. (<http://cran.r-project.org/web/packages/pheatmap/index.html>) on promoters and putative enhancers determined to be differentially accessible between BZ and sham. Motif enrichment analysis was performed on the 200bp summits of clustered putative enhancers using HOMER (<http://homer.ucsd.edu/homer/>).⁴⁴

Overlap with H3K27ac, MEF2 and c-Jun ChIP-seq

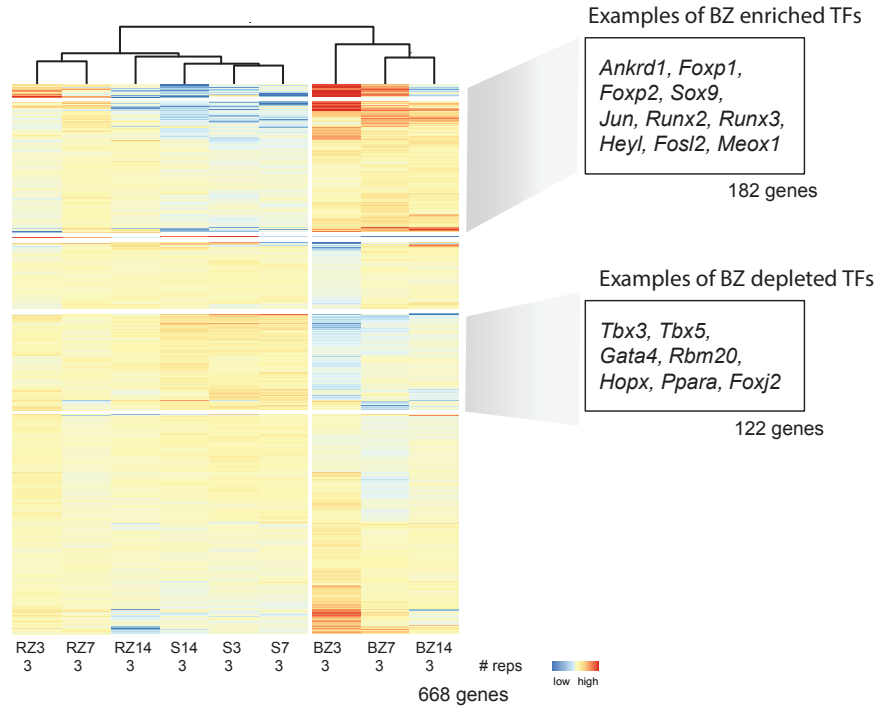
ATAC-seq peaks were cross-referenced with ChIP-seq data from PCM1-sorted H3K27ac³⁵, MEF2 from whole heart tissue⁴⁵ and c-Jun from myoblasts (GSE56077).⁴⁶ Raw ChIP-seq reads were extracted from the Sequence Read Archives (GSM851290) and mapped to the mouse genome (mm9) using BWA.⁴¹ Peaks were called and subsequently overlapped with different categories of ATAC-seq peaks using the BEDTools suite.⁴²

Luciferase assays

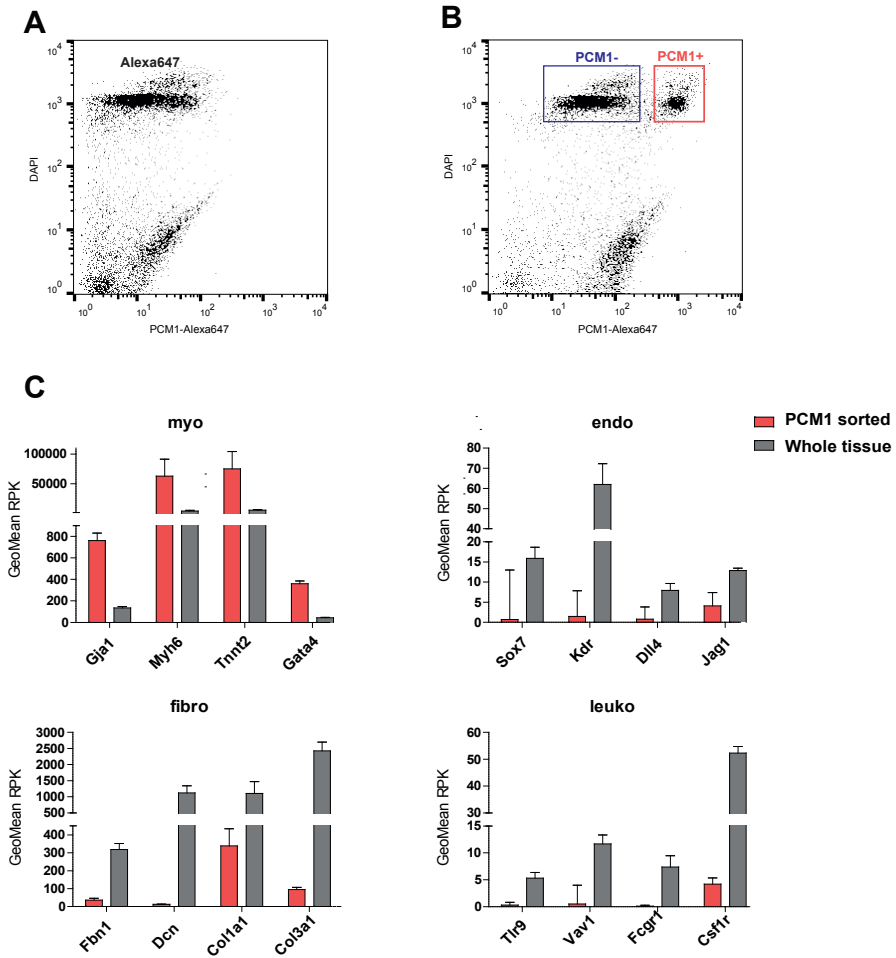
Putative regulatory elements cloned into pGL2-basic upstream of a minimal SV40 promoter. This vector, without cloned element, also served as control. Transfections were performed in duplicate to COS7 cells using polyethyleneimine (Brunswick). Standard 24 well scale transfections used 1 ug of reporter plasmid cotransfected with 6 ng pHRG-TK Renilla for normalization. Luminescence was measured using a Promega Explorer luminometer. Mutations in regulatory elements were made using the Quickchange mutagenesis kit (Agilent), after which mutated regulatory elements were digested recloned to the pGL2-SV40 min reporter vector.



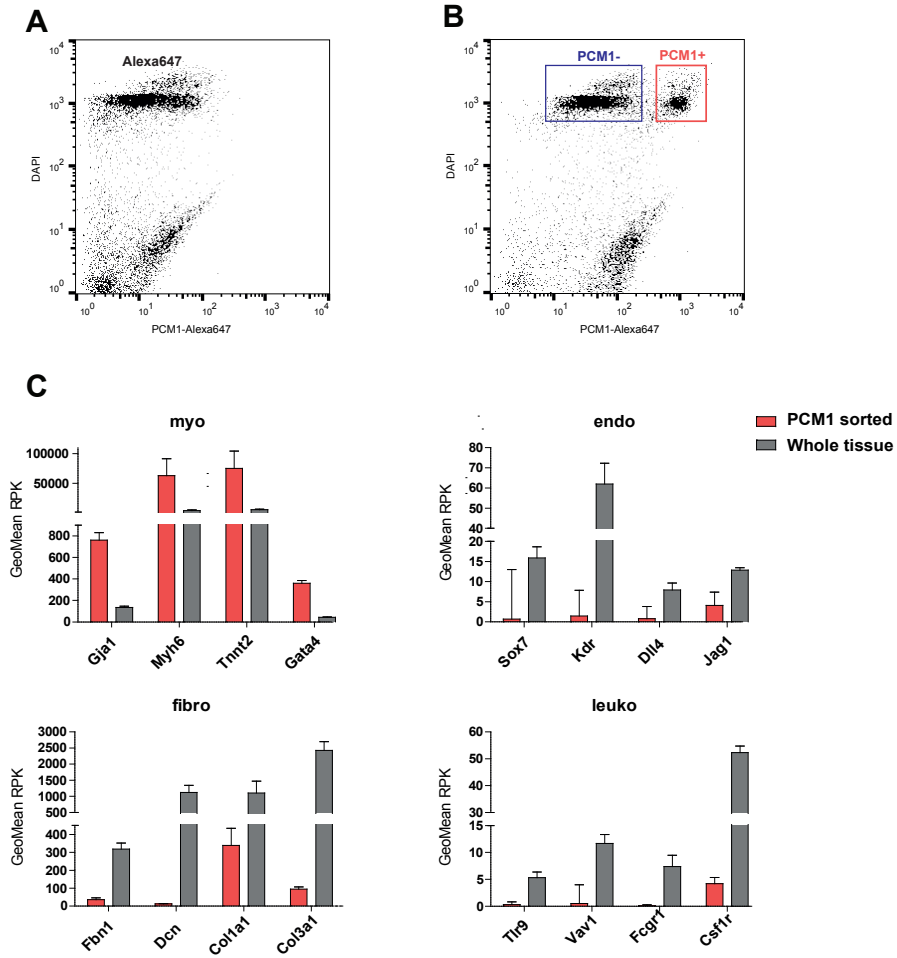
SUPPLEMENTAL FIGURES



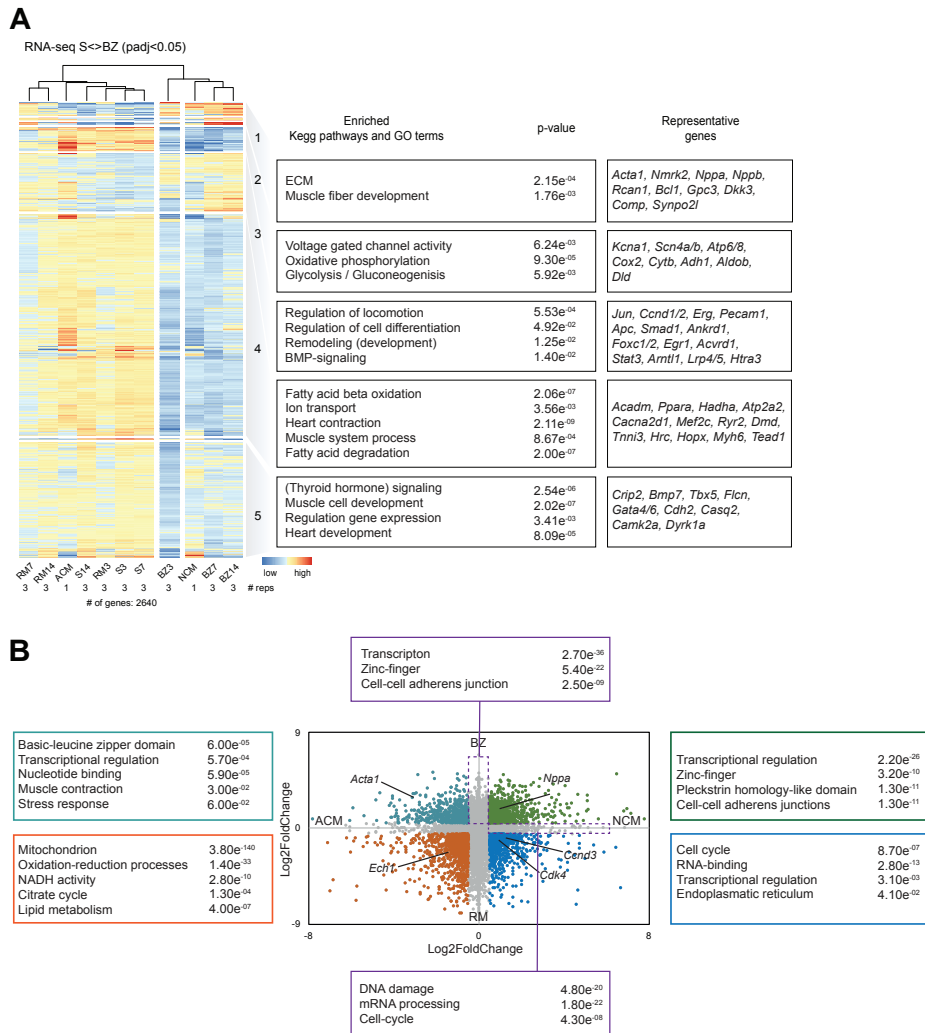
SUPPLEMENTAL FIGURE 1. Venn diagrams: overlapping border zone (BZ) & remote myocardium (RM) differential gene expression versus sham (RNA-seq).



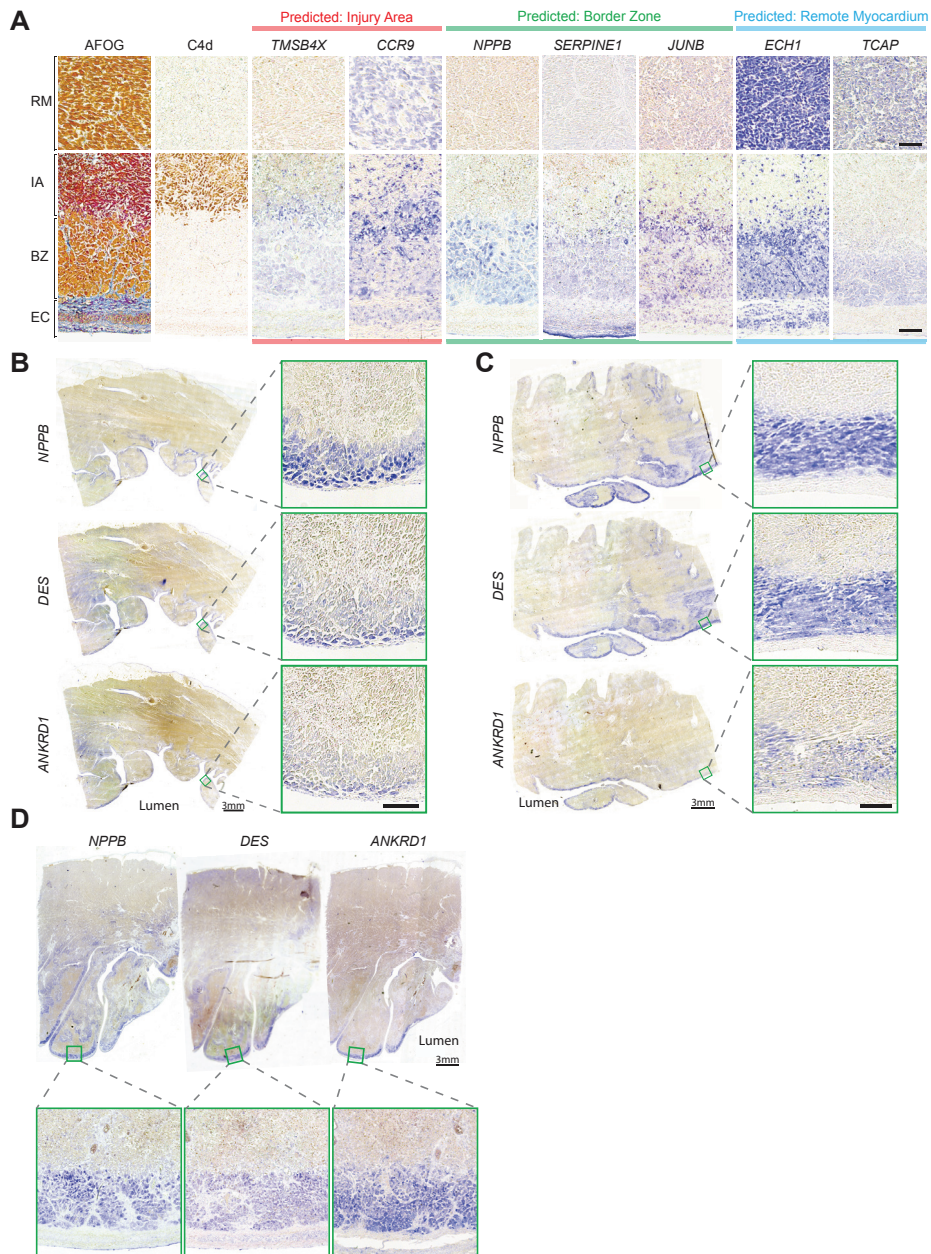
SUPPLEMENTAL FIGURE 2. Hierarchical clustering heatmaps of all border zone (BZ) differentially expressed transcription factors.



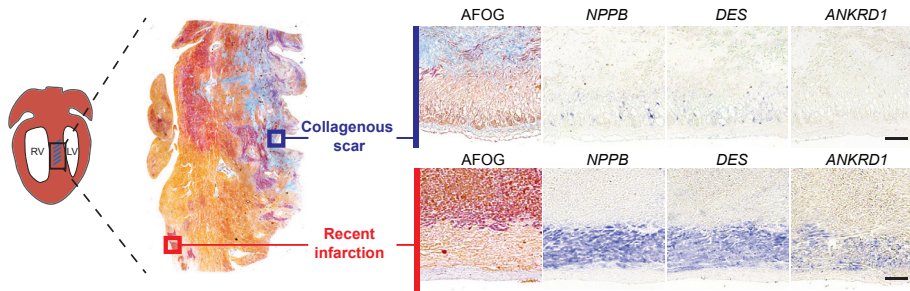
SUPPLEMENTAL FIGURE 3. Flow cytometry analysis of cardiomyocyte nuclei by pericentriolar material 1 (PCM-1) staining validation of enrichment for cardiomyocytes. **(A)** Flow cytometry dot plot showing nuclei isolated from border zone tissue stained with DAPI and a secondary AB (Alexa647). **(B)** Cardiomyocyte nuclei were identified by staining with anti-PCM-1 antibody bound by the secondary antibody Alexa-647. **C.** GeoMean RPK values for selected genes expressed by cardiomyocytes (myo), fibroblasts (fibro), leukocytes (leuko) and endothelial cells (endo) shows enrichment of the PCM-1 sorted RNAseq dataset for cardiomyocytes when compared to RNAseq data obtained from whole tissue.



SUPPLEMENTAL FIGURE 4. Cardiomyocytes originating from the BZ partially revert to an immature state. **(A)** Unsupervised functional annotation heatmap of sham, RM, and BZ at different time points based on differentially expressed genes sham vs BZ compared to RNA-seq data from isolated neonatal cardiomyocytes (NCM) and adult CMs (ACM). Samples from RMs and sham cluster with ACM, whereas BZ 7 and 14 dpi clustered with NCMs. Only genes expressed at sufficient levels (RPK >240 in NCM or ACM) and at lower levels than in infarct zone samples were included. **(B)** Scatter plot of cardiomyocytes specific differentially expressed genes (Log₂FoldChange) between RM and BZ and ACM and NCM. Gene ontology analysis was performed on each quadrant.

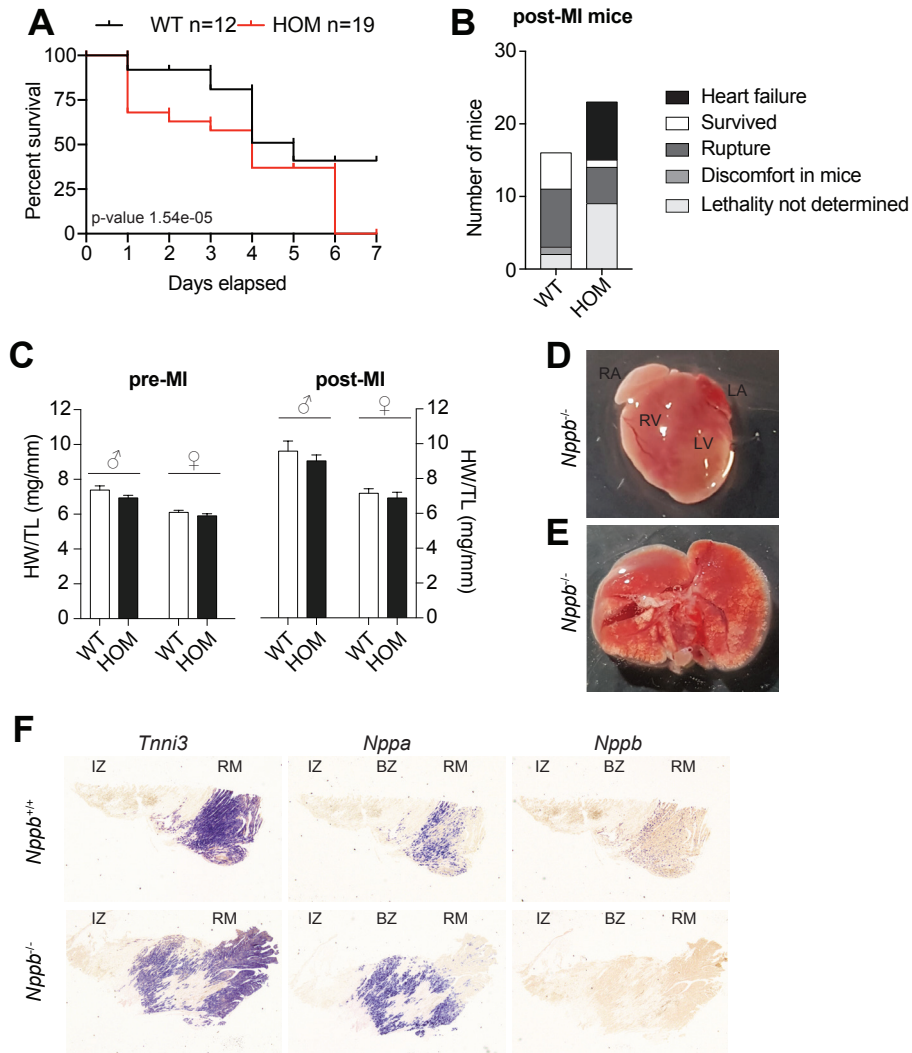


SUPPLEMENTAL FIGURE 5. Identified zone-specific marker genes for the ischemic human heart. **(A)** *In situ* hybridization of predicted marker genes on ischemic human heart tissues. Scale bars represent 100 μ m **(B-D)** *In situ* hybridization on left ventricular trans-mural samples **(B, D)** and intraventricular septum **(C)** of three different individuals. *NPPB*, *DES* and *ANKRD1* were expressed in a sub-endocardial region in all 3 samples. The tissue sample in **(D)** was from the same individual as the samples shown in **(A)**. Scale bars represent 200 μ m unless indicated otherwise.

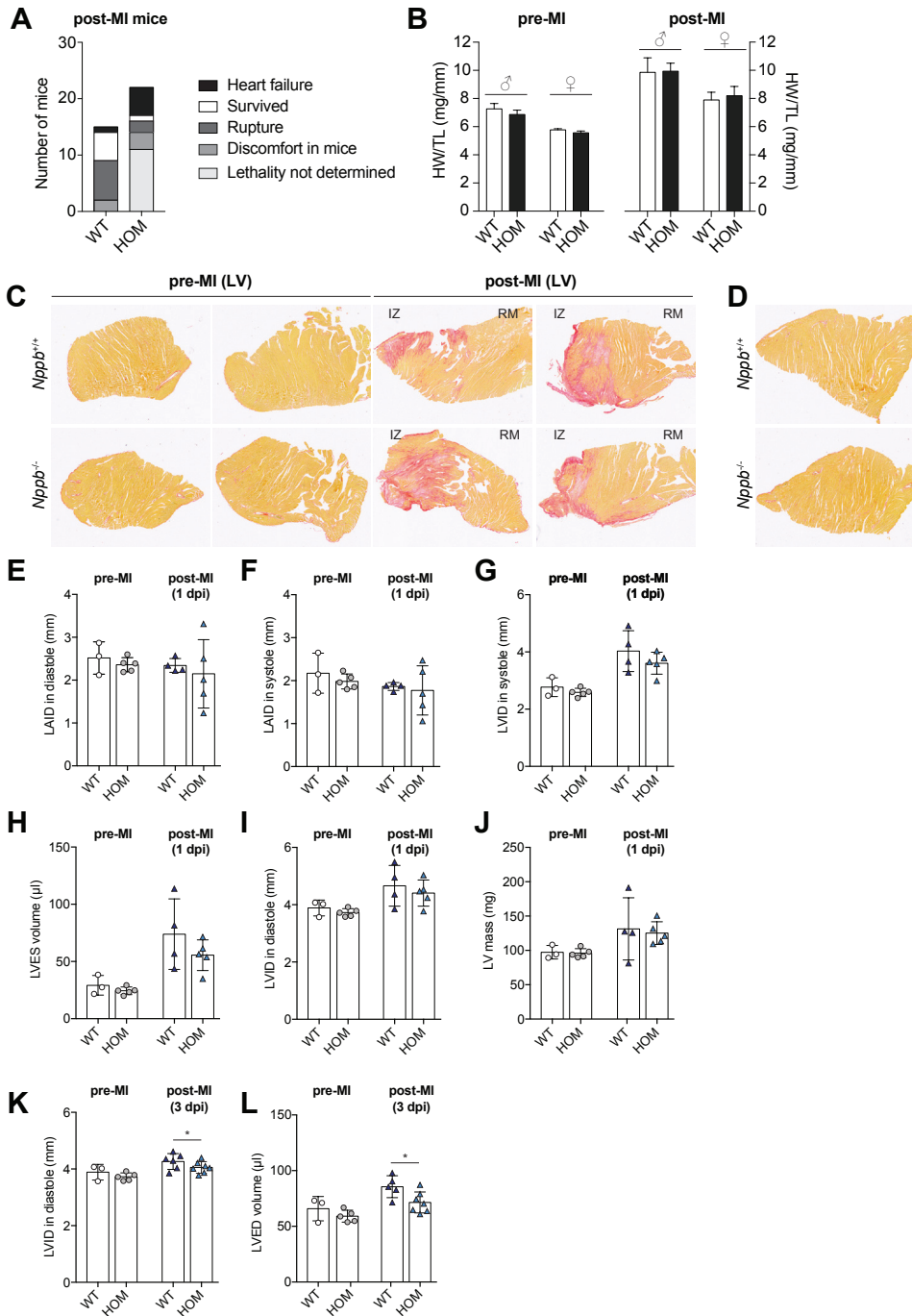


SUPPLEMENTAL FIGURE 6. Expression of border zone markers is temporally restricted. Human interventricular septum was analysed in AFOG, marking cytoplasm (orange), elastic fibrin (red) and collagen fibrils (blue), identifying recent infarcts (red) and matured scars (blue). *In situ* hybridization for BZ marker genes was performed on consecutive sections, showing strong signal adjacent to recent infarcts but not matured scars. Scale bars represent 200 μm.



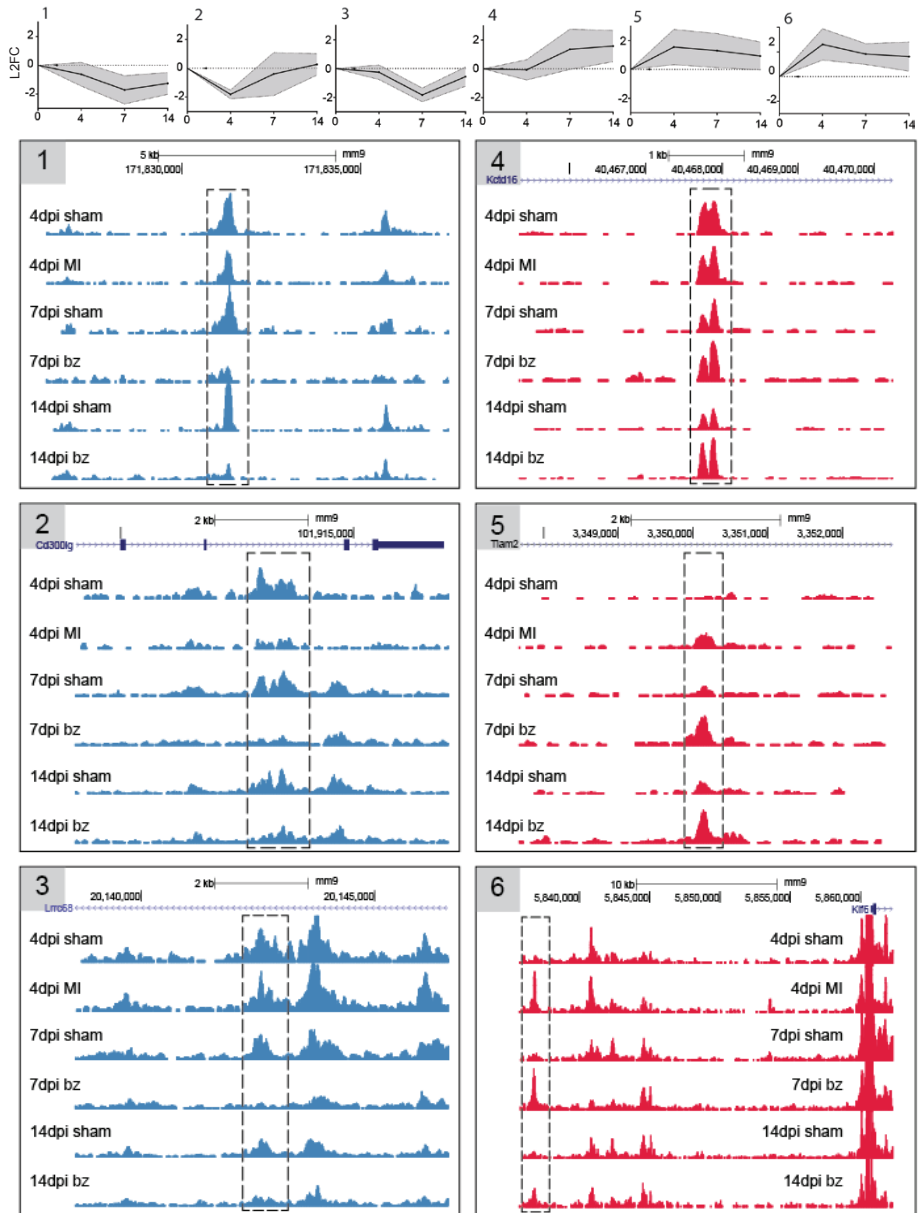


SUPPLEMENTAL FIGURE 7. Analysis of second independent *Nppb* knockout mouse line. **(A)** Kaplan-Meier curve of *Nppb*^{-/-} mice (n=19) and wildtype littermates (n=12) showed significant difference in survival ($p=1.54e-05$). **(B)** The causes of death in the post-MI *Nppb*^{-/-} mice and wildtype littermates. **(C)** Heart weight-to-tibia length ratio of male and female *Nppb*^{-/-} mice and wildtype pre- (males, WT n=6; HOM n=4 and females, WT n=5; HOM n=4) and post-MI, 7 dpi (males, WT n=8; HOM n=15 and females, WT n=5; HOM n=2). **(D, E)** Whole heart and lungs of a *Nppb*^{-/-} mouse presenting acute heart failure. **(F)** *In situ* hybridization analysis showing the expression pattern of *Tnni3*, *Nppa* and *Nppb* in *Nppb*^{-/-} mouse and wildtype at 3 dpi. RA = right atrium; LA = left atrium; RV = right ventricle; LV = left ventricle; RM = remote zone; BZ = border zone; IZ = infarct zone.

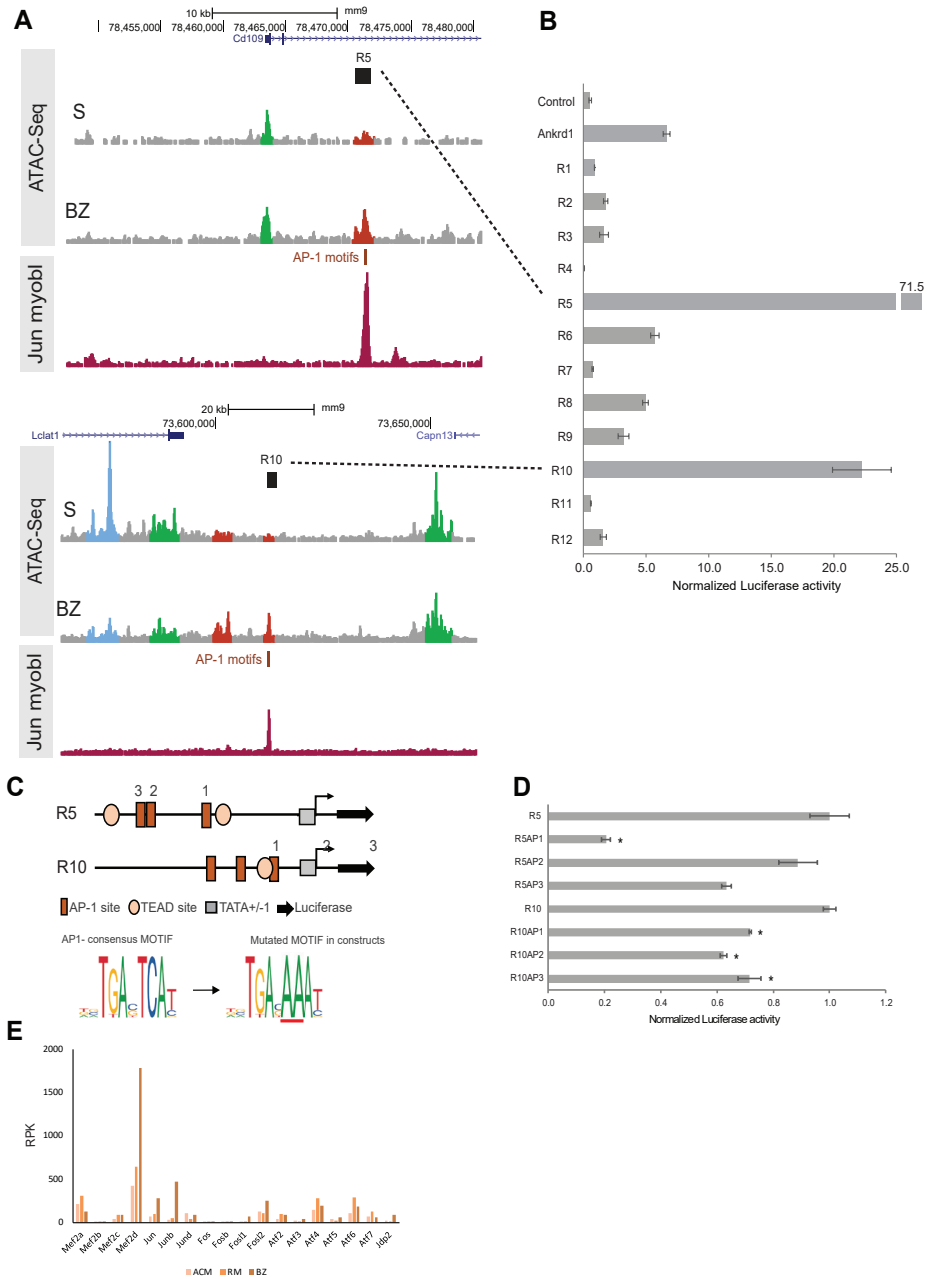


SUPPLEMENTAL FIGURE 8. Histological and echocardiographic analysis of primary *Nppb* knock mouse line. **(A)** The causes of death in the post-MI *Nppb*^{-/-} mice and wildtype littermates. **(B)** Heart weight-to-tibia length ratio of male and female *Nppb*^{-/-} mice and wildtype pre- and post-MI. **(C)** Picosirius Red staining of microdissected left ventricle of *Nppb*^{-/-} hearts, 12 wks pre- (males, WT n=4; HOM n=5

and females, WT n=4; HOM n=8) and post-MI, 7 dpi (males, WT n=3; HOM n=8 and females, WT n=6; HOM n=8). **(D)** Picosirius Red staining of microdissected left ventricle of *Nppb^{-/-}* hearts, 20 wks under baseline conditions. Echocardiographic parameters showing left atrial and ventricular function pre- and post-MI (1 dpi): **(E)** LA internal diameter in diastole. **(F)** LA internal diameter in systole. **(G)** LV internal diameter in systole. **(H)** left ventricular endsystolic volume. **(I)** LV internal diameter in diastole. **(J)** LV mass. Echocardiographic parameters showing **(K)** LV internal diameter in diastole (* p=0.02) and **(L)** LV enddiastolic volume (* p=0.02) pre- (WT n=3; HOM n=5) and post-MI, 3 dpi (WT n=4; HOM n=5). LV = left ventricle, LA = left atrium.

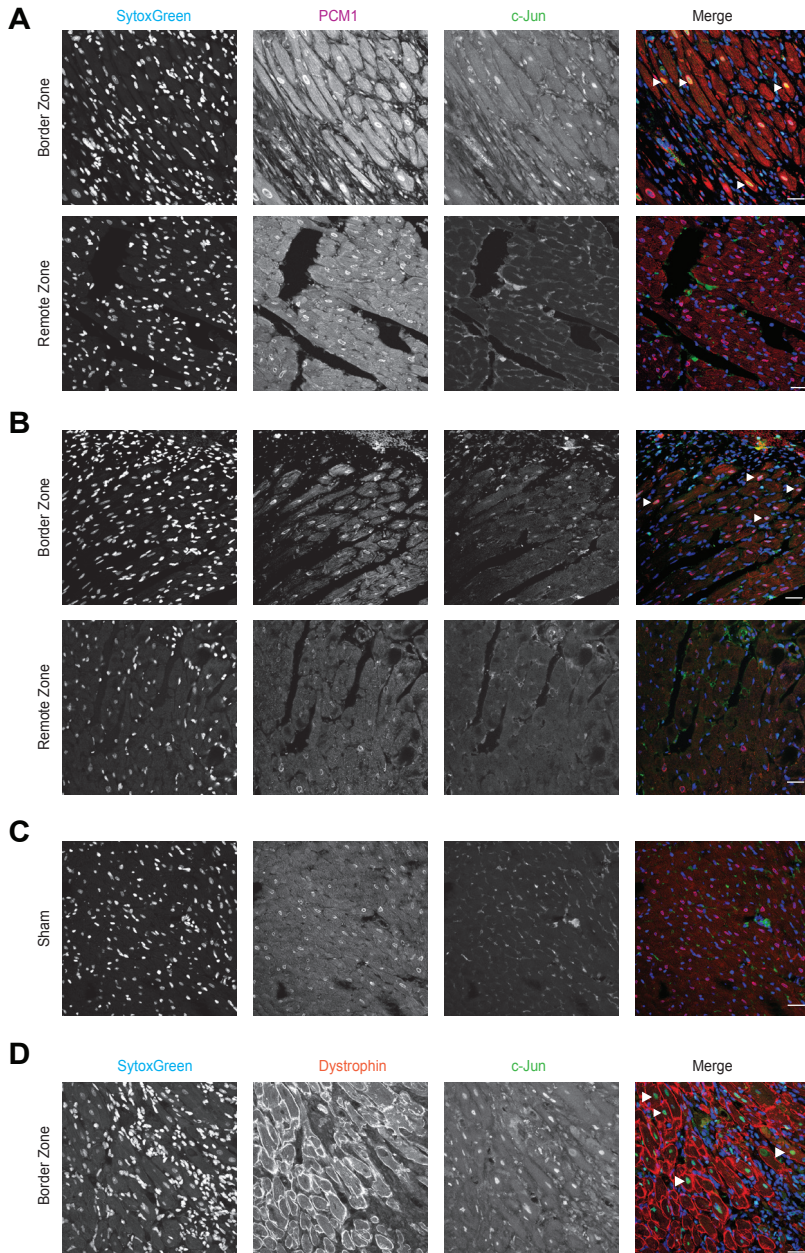


SUPPLEMENTAL FIGURE 10. UCSC browser views of representative examples of each of the six different temporal accessibility profiles of distal elements (ATAC-seq).



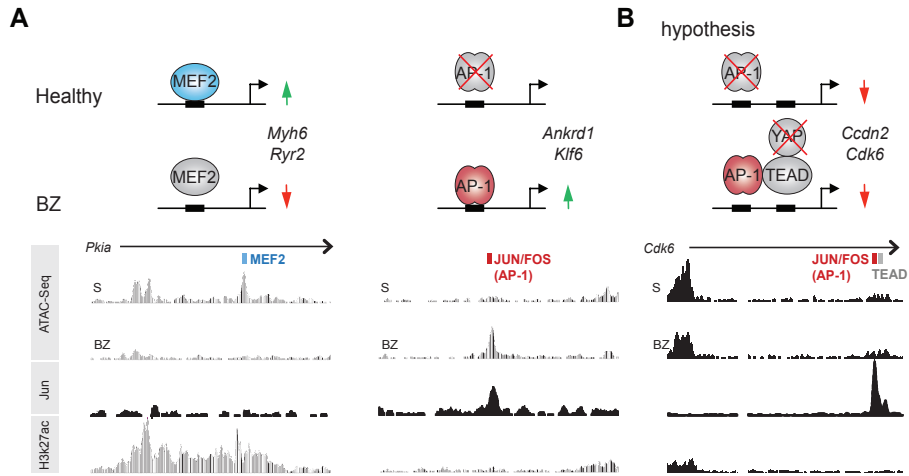
SUPPLEMENTAL FIGURE 11. *In vitro* reporter analysis of putative regulatory regions. **(A)** UCSC browser views of 2 example regions selected on basis of ATAC-seq and ChIP-seq (c-Jun in myoblasts and H3K27ac mouse heart) analysis. Regions chosen for PCR and subsequent cloning to the luciferase reporter vector are marked by dotted lines and correspond to the regions names in; **(B)** Shows the normalized luciferase activities of the selected putative regulatory regions. Regions 5 and 10, showing the highest fold activations compared to the control vector were selected for AP-1 mutational analysis; **(C)** Relative positions of high scoring predicted AP-1 sites (JASPAR⁴⁷) and TEAD sites are marked for constructs R5 and R10 respectively. The conserved TC of each of the predicted consensus was mutated to AA. **(D)** Shows the effect on fold activation of mutating the AP1 consensus in the luciferase

reporter assay. Asterisk denotes $p < 0.05$ in a student T-test relative to the wild type allele. **(E)** RPKs showing the average expression of Mef2 and AP-1 transcription factors in cardiomyocyte nuclei of adult cardiomyocytes (ACM), border zone (BZ) and remote myocardium (RM).



SUPPLEMENTAL FIGURE 12. Co-localization of c-Jun with border zone (BZ) cardiomyocytes. **(A)** Sham mice do not show c-Jun staining within the cardiomyocytes stained with dystrophin. **(B)** c-Jun co-localizes with BZ cardiomyocytes stained with dystrophin at 14 dpi. **(C)** c-Jun co-localizes

with cardiomyocytes nuclei stained with PCM-1 at 14 dpi. **(D)** c-Jun in BZ cardiomyocytes stained with dystrophin. Scale bars indicates 10 μm . Arrowheads indicate examples of c-Jun positive cardiomyocytes.



SUPPLEMENTAL FIGURE 13. A model for the role of AP-1 motif binding in governing cardiomyocyte lineage specificity. Binding of AP-1 motifs overrides homeostatic regulatory elements governing cardiomyocyte lineage specificity. **(A)** Cardiac injury results in the reduction of accessibility of CM-lineage-specific transcription binding sites, such as Mef2, whereas accessibility of non-CM lineage typical promoters/genes and enhancers with binding motifs for AP-1 and other stress-responsive transcription factors increases. **(B)** In absence of YAP, the BZ cardiomyocytes increasing AP-1 accessibility does not activate cell cycle genes, but creates a favorable dedifferentiated state poised for proliferation to occur.

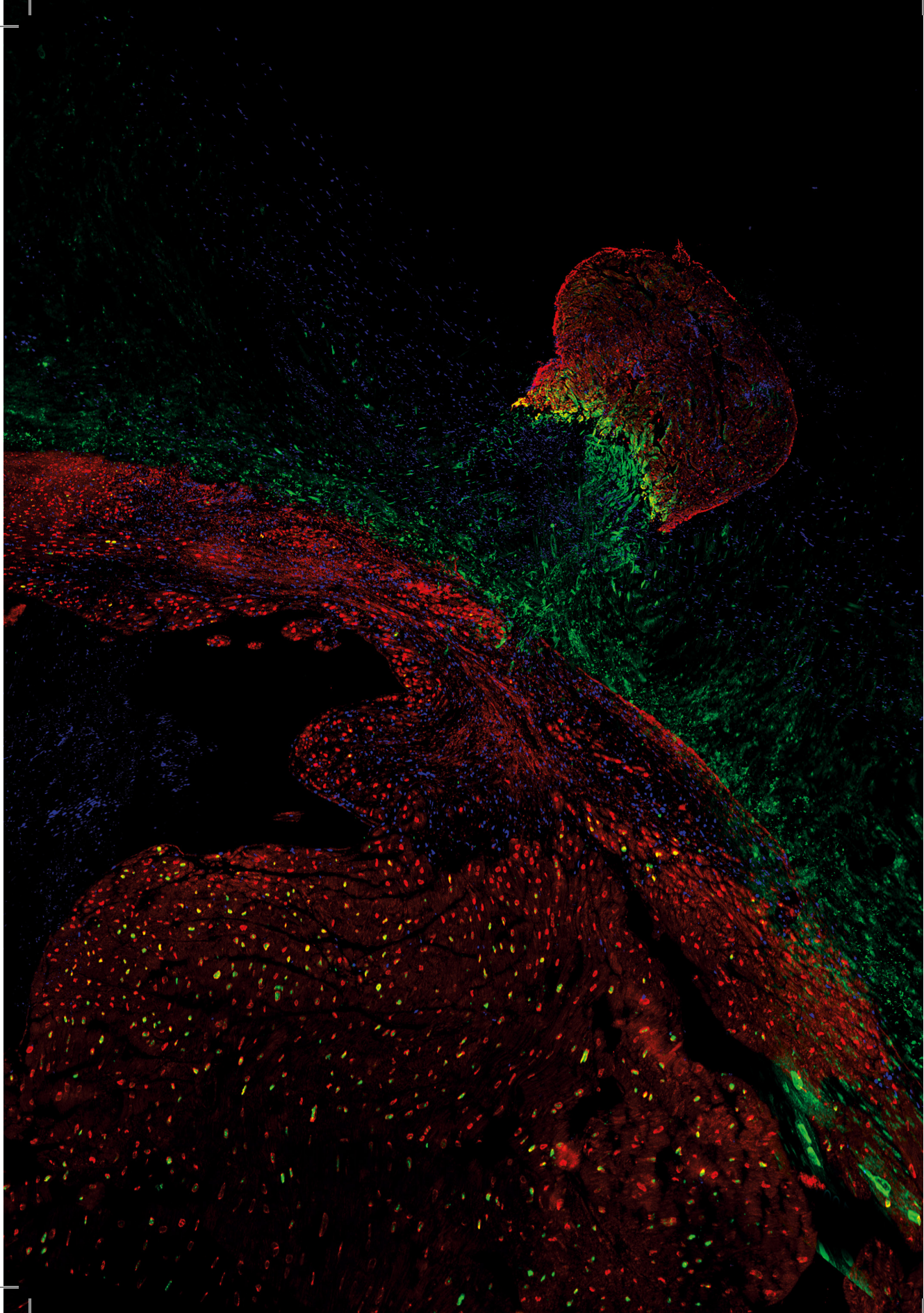
SUPPLEMENTAL REFERENCES

1. Ma H, Wang L, Yin C, Liu J and Qian L. In vivo cardiac reprogramming using an optimal single polycistronic construct. *Cardiovasc Res.* 2015;108:217-219.
2. Liu G, Zhang H, Hao F, Hao J, Pan L, Zhao Q and Wo J. Clusterin Reduces Cold Ischemia-Reperfusion Injury in Heart Transplantation Through Regulation of NF- κ B Signaling and Bax/Bcl-xL Expression. *Cell Physiol Biochem.* 2018;45:1003-1012.
3. Van Dijk A, Vermond RA, Krijnen PA, Juffermans LJ, Hahn NE, Makker SP, Aarden LA, Hack E, Spreeuwenberg M, van Rossum BC, Meischl C, Paulus WJ, Van Milligen FJ and Niessen HW. Intravenous clusterin administration reduces myocardial infarct size in rats. *Eur J Clin Invest.* 2010;40:893-902.
4. Turkieh A, Fertin M, Bouvet M, Mulder P, Drobecq H, Lemesle G, Lamblin N, de Groote P, Porouchani S, Chwastyniak M, Beseme O, Amouyel P, Mouquet F, Balligand JL, Richard V, Bauters C and Pinet F. Expression and Implication of Clusterin in Left Ventricular Remodeling After Myocardial Infarction. *Circ Heart Fail.* 2018;11:e004838.
5. Pastori D, Pignatelli P, Farcomeni A, Menichelli D, Nocella C, Carnevale R and Violi F. Aging-Related Decline of Glutathione Peroxidase 3 and Risk of Cardiovascular Events in Patients With Atrial Fibrillation. *J Am Heart Assoc.* 2016;5.
6. Buijsse B, Lee DH, Steffen L, Erickson RR, Luepker RV, Jacobs DR, Jr. and Holtzman JL. Low serum glutathione peroxidase activity is associated with increased cardiovascular mortality in individuals with low HDLc's. *PLoS One.* 2012;7:e38901.
7. Piccolo S, Dupont S and Cordenonsi M. The biology of YAP/TAZ: hippo signaling and beyond. *Physiol Rev.* 2014;94:1287-1312.
8. Zanconato F, Forcato M, Battilana G, Azzolin L, Quaranta E, Bodega B, Rosato A, Bicciato S, Cordenonsi M and Piccolo S. Genome-wide association between YAP/TAZ/TEAD and AP-1 at enhancers drives oncogenic growth. *Nat Cell Biol.* 2015;17:1218-1227.
9. Monroe TO, Hill MC, Morikawa Y, Leach JP, Heallen T, Cao S, Krijger PHL, de Laat W, Wehrens XHT, Rodney GG and Martin JF. YAP Partially Reprograms Chromatin Accessibility to Directly Induce Adult Cardiogenesis In Vivo. *Dev Cell.* 2019;48(6):765-779.
10. Aihara Y, Kurabayashi M, Saito Y, Ohyama Y, Tanaka T, Takeda S, Tomaru K, Sekiguchi K, Arai M, Nakamura T and Nagai R. Cardiac ankyrin repeat protein is a novel marker of cardiac hypertrophy: role of M-CAT element within the promoter. *Hypertension.* 2000;36:48-53.
11. Nagueh SF, Shah G, Wu Y, Torre-Amione G, King NM, Lahmers S, Witt CC, Becker K, Labeit S and Granzier HL. Altered titin expression, myocardial stiffness, and left ventricular function in patients with dilated cardiomyopathy. *Circulation.* 2004;110:155-162.
12. Wei YJ, Cui CJ, Huang YX, Zhang XL, Zhang H and Hu SS. Upregulated expression of cardiac ankyrin repeat protein in human failing hearts due to arrhythmic right ventricular cardiomyopathy. *European journal of heart failure.* 2009;11:559-566.
13. Moulik M, Vatta M, Witt SH, Arola AM, Murphy RT, McKenna WJ, Boriek AM, Oka K, Labeit S, Bowles NE, Arimura T, Kimura A and Towbin JA. ANKRD1, the gene encoding cardiac ankyrin repeat protein, is a novel dilated cardiomyopathy gene. *Journal of the American College of Cardiology.* 2009;54:325-333.
14. Arimura T, Bos JM, Sato A, Kubo T, Okamoto H, Nishi H, Harada H, Koga Y, Moulik M, Doi YL, Towbin JA, Ackerman MJ and Kimura A. Cardiac ankyrin repeat protein gene (ANKRD1) mutations in hypertrophic cardiomyopathy. *Journal of the American College of Cardiology.* 2009;54:334-342.
15. Lee MJ, Kwak YK, You KR, Lee BH and Kim DG. Involvement of GADD153 and cardiac ankyrin repeat protein in cardiac ischemia-reperfusion injury. *Exp Mol Med.* 2009;41:243-252.
16. Han XJ, Chae JK, Lee MJ, You KR, Lee BH and Kim DG. Involvement of GADD153 and cardiac ankyrin repeat protein in hypoxia-induced apoptosis of H9c2 cells. *J Biol Chem.* 2005;280:23122-23129.
17. Zhang Y, Li S, Yuan L, Tian Y, Weidenfeld J, Yang J, Liu F, Chokas AL and Morrissey EE. Foxp1 coordinates cardiomyocyte proliferation through both cell-autonomous and nonautonomous mechanisms. *Genes Dev.* 2010;24:1746-1757.
18. Bai S and Kerppola TK. Opposing roles of FoxP1 and Nfat3 in transcriptional control of cardiomyocyte hypertrophy. *Mol Cell Biol.* 2011;31:3068-3080.
19. Chang SW, Mislankar M, Misra C, Huang N, Dajusta DG, Harrison SM, McBride KL, Baker LA and Garg V. Genetic abnormalities in FOXP1 are associated with congenital heart defects. *Human mutation.* 2013;34:1226-1230.
20. Wu CC, Kruse F, Vasudevarao MD, Junker JP, Zebrowski DC, Fischer K, Noel ES, Grun D, Berezikov E, Engel FB, van Oudenaarden A,

- Weidinger G and Bakkers J. Spatially Resolved Genome-wide Transcriptional Profiling Identifies BMP Signaling as Essential Regulator of Zebrafish Cardiomyocyte Regeneration. *Dev Cell*. 2016;36:36-49.
21. Gupta V, Gemberling M, Karra R, Rosenfeld GE, Evans T and Poss KD. An injury-responsive gata4 program shapes the zebrafish cardiac ventricle. *Current biology : CB*. 2013;23:1221-1227.
 22. Tamura N, Ogawa Y, Chusho H, Nakamura K, Nakao K, Suda M, Kasahara M, Hashimoto R, Katsuura G, Mukoyama M, Itoh H, Saito Y, Tanaka I, Otani H and Katsuki M. Cardiac fibrosis in mice lacking brain natriuretic peptide. *Proc Natl Acad Sci U S A*. 2000;97:4239-4244.
 23. D'Souza SP, Yellon DM, Martin C, Schulz R, Heusch G, Onody A, Ferdinandy P and Baxter GF. B-type natriuretic peptide limits infarct size in rat isolated hearts via KATP channel opening. *Am J Physiol Heart Circ Physiol*. 2003;284:H1592-1600.
 24. Burley DS and Baxter GF. B-type natriuretic peptide at early reperfusion limits infarct size in the rat isolated heart. *Basic research in cardiology*. 2007;102:529-541.
 25. van den Borne SW, van de Schans VA, Strzelecka AE, Vervoort-Peters HT, Lijnen PM, Cleutjens JP, Smits JF, Daemen MJ, Janssen BJ and Blankesteijn WM. Mouse strain determines the outcome of wound healing after myocardial infarction. *Cardiovasc Res*. 2009;84:273-282.
 26. Sohal DS, Nghiem M, Crackower MA, Witt SA, Kimball TR, Tymitz KM, Penninger JM and Molkentin JD. Temporally regulated and tissue-specific gene manipulations in the adult and embryonic heart using a tamoxifen-inducible Cre protein. *CircRes*. 2001;89:20-25.
 27. Ram R, Mickelsen DM, Theodoropoulos C and Blaxall BC. New approaches in small animal echocardiography: imaging the sounds of silence. *Am J Physiol Heart Circ Physiol*. 2011;301:H1765-1780.
 28. Moorman AFM, Houweling AC, de Boer PAJ and Christoffels VM. Sensitive nonradioactive detection of mRNA in tissue sections: novel application of the whole-mount in situ hybridization protocol. *JHistochemCytochem*. 2001;49:1-8.
 29. Snarr BS, O'Neal JL, Chintalapudi MR, Wirrig EE, Phelps AL, Kubalak SW and Wessels A. Isl1 Expression at the Venous Pole Identifies a Novel Role for the Second Heart Field in Cardiac Development. *CircRes*. 2007;101:971-974.
 30. Sander JD, Maeder ML, Reyon D, Voytas DF, Joung JK and Dobbs D. ZiFIT (Zinc Finger Targeter): an updated zinc finger engineering tool. *Nucleic Acids Res*. 2010;38:W462-468.
 31. Sander JD, Zaback P, Joung JK, Voytas DF and Dobbs D. Zinc Finger Targeter (ZiFIT): an engineered zinc finger/target site design tool. *Nucleic Acids Res*. 2007;35:W599-605.
 32. Hwang WY, Fu Y, Reyon D, Maeder ML, Tsai SQ, Sander JD, Peterson RT, Yeh JR and Joung JK. Efficient genome editing in zebrafish using a CRISPR-Cas system. *Nat Biotechnol*. 2013;31:227-229.
 33. Sergeeva IA, Hooijkaas IB, van der Made I, Jong WM, Creemers EE and Christoffels VM. A transgenic mouse model for the simultaneous monitoring of ANF and BNP gene activity during heart development and disease. *CardiovascRes*. 2014;78-86.
 34. Ruijter JM, Ramakers C, Hoogaars WM, Karlen Y, Bakker O, van den Hoff MJ and Moorman AF. Amplification efficiency: linking baseline and bias in the analysis of quantitative PCR data. *Nucleic Acids Res*. 2009;37:e45.
 35. Gilsbach R, Preissl S, Gruning BA, Schnick T, Burger L, Benes V, Wurch A, Bonisch U, Gunther S, Backofen R, Fleischmann BK, Schubeler D and Hein L. Dynamic DNA methylation orchestrates cardiomyocyte development, maturation and disease. *Nature communications*. 2014;5:5288.
 36. Dobin A, Davis CA, Schlesinger F, Drenkow J, Zaleski C, Jha S, Batut P, Chaisson M and Gingeras TR. STAR: ultrafast universal RNA-seq aligner. *Bioinformatics*. 2013;29:15-21.
 37. Love MI, Huber W and Anders S. Moderated estimation of fold change and dispersion for RNA-seq data with DESeq2. *Genome biology*. 2014;15:550.
 38. Huang dW, Sherman BT and Lempicki RA. Systematic and integrative analysis of large gene lists using DAVID bioinformatics resources. *NatProtoc*. 2009;4:44-57.
 39. Bindea G, Mlecnik B, Hackl H, Charoentong P, Tosolini M, Kirilovsky A, Fridman WH, Pages F, Trajanoski Z and Galon J. ClueGO: a Cytoscape plug-in to decipher functionally grouped gene ontology and pathway annotation networks. *Bioinformatics*. 2009;25:1091-1093.
 40. Lambert SA, Jolma A, Campitelli LF, Das PK, Yin Y, Albu M, Chen X, Taipale J, Hughes TR and Weirauch MT. The Human Transcription Factors. *Cell*. 2018;172:650-665.
 41. Li H and Durbin R. Fast and accurate short read alignment with Burrows-Wheeler transform. *Bioinformatics*. 2009;25:1754-1760.
 42. Quinlan AR and Hall IM. BEDTools: a flexible suite of utilities for comparing genomic features. *Bioinformatics*. 2010;26:841-842.

43. Ramirez F, Ryan DP, Gruning B, Bhardwaj V, Kilpert F, Richter AS, Heyne S, Dundar F and Manke T. deepTools2: a next generation web server for deep-sequencing data analysis. *Nucleic Acids Res.* 2016;44:W160-165.
44. Heinz S, Benner C, Spann N, Bertolino E, Lin YC, Laslo P, Cheng JX, Murre C, Singh H and Glass CK. Simple combinations of lineage-determining transcription factors prime cis-regulatory elements required for macrophage and B cell identities. *Mol Cell.* 2010;38:576-589.
45. Guo A, Wang Y, Chen B, Wang Y, Yuan J, Zhang L, Hall D, Wu J, Shi Y, Zhu Q, Chen C, Thiel WH, Zhan X, Weiss RM, Zhan F, Musselman CA, Pufall M, Zhu W, Au KF, Hong J, Anderson ME, Grueter CE and Song LS. E-C coupling structural protein junctophilin-2 encodes a stress-adaptive transcription regulator. *Science.* 2018;362:1-9.
46. Umansky KB, Feldmesser E and Groner Y. Genomic-wide transcriptional profiling in primary myoblasts reveals Runx1-regulated genes in muscle regeneration. *Genom Data.* 2015;6:120-122.
47. Khan A, Fornes O, Stigliani A, Gheorghe M, Castro-Mondragon JA, van der Lee R, Bessy A, Cheneby J, Kulkarni SR, Tan G, Baranasic D, Arenillas DJ, Sandelin A, Vandepoele K, Lenhard B, Ballester B, Wasserman WW, Parcy F and Mathelier A. JASPAR 2018: update of the open-access database of transcription factor binding profiles and its web framework. *Nucleic Acids Res.* 2018;46:D260-D266.





CHAPTER IV

Interspecies comparison reveals Hmga1 as a driver of cardiac regeneration

Dennis E.M. de Bakker¹, Phong D Nguyen¹, Hessel Honkoop¹, Daniel Colquhoun², Marta Vigil-Garcia¹, Danielle Versteeg¹, Lieneke Kooijman¹, Rob Janssen³, Ingeborg Hooijkaas³, Marie Gunthel³, Vincent M. Christoffels³, Jan Kaslin², Eva van Rooij¹, Jeroen Bakkens^{1,4,*}

¹Hubrecht Institute-KNAW and University Medical Center Utrecht, Utrecht, Netherlands

²Monash University, Australian Regenerative Medicine Institute, Clayton, Australia

³Departments of Medical Biology, Amsterdam Cardiovascular Sciences, Academic Medical Center, Amsterdam, The Netherlands

⁴Department of Pediatric Cardiology, Division of Pediatrics, University Medical Center Utrecht, Utrecht, Netherlands.

* Corresponding author

Manuscript and patent in preparation

ABSTRACT

Myocardial infarction causes a massive loss of cardiomyocytes, leading to the formation of a fibrotic scar resulting in impaired cardiac function. Due to the inability of the mammalian heart to regenerate the lost cardiomyocytes, ischemic injury is considered a chronic affliction. In contrast to mammals, zebrafish can regenerate the lost cardiomyocytes by inducing cell cycle re-entry of cardiomyocytes at the injury border zone. The molecular mechanisms underlying the difference in regenerative capacity between species have yet to be resolved. To address this, we employed spatial resolved transcriptomics on injured mouse and zebrafish hearts to allow transcriptomic comparison between the mouse and zebrafish border zone. Through this comparison, we identified many genes and processes overlapping and diverging between the two species. Through functional validation of one of the identified candidate genes (*hmga1a*), we provide a proof-of-principle that this dataset can be used to identify novel drivers of cardiac regeneration. Indeed, we show that in zebrafish *hmga1a* is required for cardiomyocyte proliferation and heart regeneration through loss-of-function analysis combined with single-cell RNA sequencing. By combining RNA- and ATAC-sequencing, we found that inducing ectopic *hmga1a* expression leads to reorganization of chromatin accessibility and the induction of a transcriptional program facilitating ECM remodelling, metabolic reprogramming and cell division. Importantly, we show that overexpression of *hmga1a* is sufficient to induce cardiomyocyte proliferation in uninjured zebrafish hearts. Furthermore, viral overexpression of Hmga1 in injured mouse hearts induces cardiomyocyte cell cycle re-entry of border zone cardiomyocytes and promotes functional recovery. We conclude that differences in chromatin accessibility and transcriptional regulation mediated by Hmga1 in cardiomyocytes can help explain differences in regenerative capacity between zebrafish and mouse hearts. Furthermore, we reveal Hmga1 as a novel driver of cardiac regeneration.

INTRODUCTION

Cardiovascular disease remains the biggest cause of death in the western world, including the consequences of myocardial infarction (WHO, 2019). Patients suffering from a myocardial infarction often survive the initial injury but permanently lose millions of heart muscle cells. Although the heart is able to efficiently repair the injury by formation of a permanent scar, almost no new cardiomyocytes are being regenerated (Kretzschmar et al., 2018). Due to the inability of the heart to replace the lost cardiomyocytes, ischemic heart injury is considered a chronic affliction. Since hearts with ischemic injuries will ultimately develop heart failure, the field is in desperate need of treatments focussing on regenerating the lost myocardium. Interestingly, some species have a robust endogenous capacity to regenerate the heart, including the zebrafish (Poss et al., 2002). In zebrafish the surviving cardiomyocytes (CMs) adjacent to the injury area, also known as the border zone (BZ), de-differentiate towards an embryo-like state and proliferate to replace the lost cardiomyocytes (Honkoop et al., 2019; Jopling et al., 2010; Kikuchi et al., 2010; Wu et al., 2015). In addition, BZ CMs undergo robust changes in their chromatin organization which underlies their regenerative response (Beisaw et al., 2020).

This raises the question why zebrafish BZ CMs are re-entering the cell cycle while mammalian BZ CMs do not. A potential answer could be formed when looking at the intrinsic properties of cardiomyocyte nuclei. While mammalian CMs are mainly polyploid (human) or multinuclear (mice), zebrafish CMs are mononuclear and diploid, which has been shown to be detrimental for efficient proliferation and zebrafish heart regeneration (González-Rosa et al., 2018; Patterson et al., 2017; Windmueller et al., 2020).

Regardless of these restrictions, a low level of endogenous CM turnover was observed in the adult human heart (Bergmann et al., 2009). In addition, the neonatal mouse heart has been shown to contain the capacity to induce CM proliferation and heart regeneration in a small time-window after birth (Porrello et al., 2011). Together, these observations suggest the mammalian heart could retain a latent capacity to regenerate.

Indeed, studies in mice have shown that inhibition of the HIPPO signaling pathway can unlock the regenerative capacity of the mammalian heart (Heallen et al., 2013; Leach et al., 2017a). In addition, overexpression of the constitutively active *ErbB2* receptor induces efficient cardiomyocyte proliferation in mice, allowing for the near complete regeneration of injured hearts (D'Uva et al., 2015).

These studies, among others, report that BZ cardiomyocytes are most prone to proliferate upon stimulation (D'Uva et al., 2015; Leach et al., 2017b; Lin et al., 2014; Pasumarthi et al., 2005; Xiang et al., 2016). Although mammalian BZ CMs do not initiate proliferation

endogenously like zebrafish BZ CMs, they do undergo drastic changes in terms of their transcriptome and chromosomal organization (K. van Duijvenboden et al., 2019), which might potentiate their susceptibility to mitogenic stimuli.

Regardless, we are still far from fully understanding the striking difference in regenerative capacity between zebrafish and mammalian hearts. Therefore, studying the molecular differences in the BZ between these species may lead to the identification of factors with the potential to stimulate mammalian heart regeneration.

Here, we identify the architectural transcription factor High mobility group A1 (Hmga1) by its specific mRNA expression in the BZ of the injured zebrafish heart and near absence from the injured mouse heart. While the role of Hmga1 in cancer progression and embryonic development has been extensively studied, its function during regeneration remains largely unknown. Here, we reveal that *hmga1a* is indispensable for injury- and NRG1 induced cardiomyocyte proliferation and zebrafish heart regeneration. Furthermore, we demonstrate that overexpression of *hmga1a* induces a broad BZ-like program including the stress response, ECM production, metabolic reprogramming and changes in chromatin accessibility, which is sufficient to stimulate CM proliferation even in absence of injury. Importantly, we provide evidence suggesting that Hmga1 overexpression can have similar effects in mammalian hearts, inducing cell cycle re-entry by BZ CMs and stimulating functional recovery post myocardial infarction.

RESULTS

Comparison of transcriptional border zone profiles reveals species specific gene expression. We previously used spatially resolved transcriptomics (TOMO-seq) to determine gene expression in the zebrafish BZ at 3, 7 and 14 days post injury (dpi) (Junker et al., 2014; Wu et al., 2015). To allow comparison between the zebrafish and mouse BZ, we performed similar TOMO-seq experiments on injured mouse hearts. Mice were subjected to myocardial infarction (MI) through permanent occlusion of the left-anterior descending coronary artery. Spatial patterns of *Nppb/Katushka* in the *BAC-Nppb-Katushka* mice allowed for the localization of the BZ (Sergeeva et al., 2014) and the BZ with the surrounding injury area and remote myocardium were isolated at 3, 7 and 14 days post-MI (Fig.1A). Next, the isolated tissue was cryosectioned from injury area to remote area and each section was subjected to RNA-sequencing (RNA-seq). Pearson's correlation analysis across all genes for each pairwise combination of sections revealed clusters of genes with expression in distinct areas (Fig.1B). Based on these gene clusters as well as marker gene expression, we identified the locations of the injury area (cluster 1, *Rhoc*, *Fstl1*, *Tmsb4x*), border zone (Cluster 2, *Nppa*, *Des*, *Ankrd1*) and remote myocardium (cluster 3, *Tnnt2*, *Tnni3*, *Ech1*) within the TOMO-seq

datasets (Lacruz et al., 2017; Karel Van Duijvenboden et al., 2019), which was validated through *in situ* hybridization (Fig.1C).

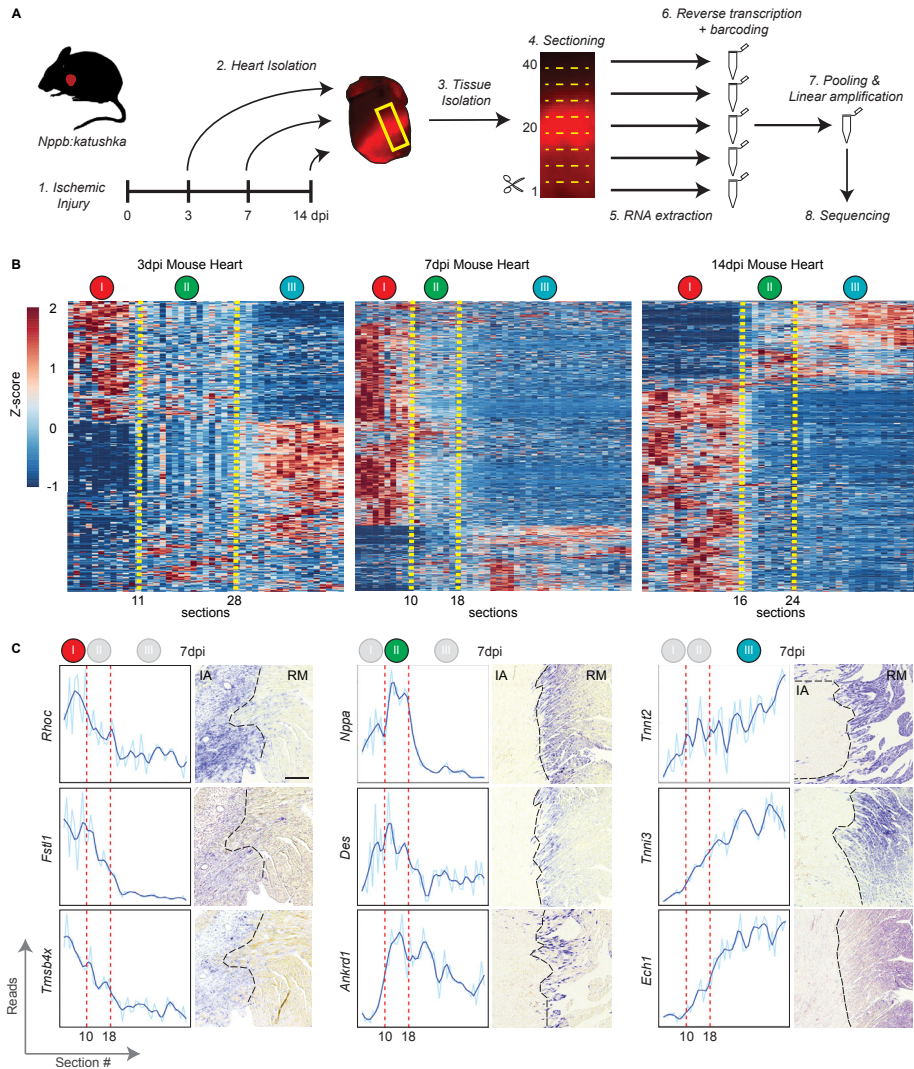


FIGURE 1. Tomo-seq reveals transcriptionally distinct regions in the injured mouse heart. (A) Schematic overview of the workflow. **(B)** Hierarchical clustering for genes with a clear expression peak (Z score > 1 in > 4 consecutive sections). Genes are on the y-axis and section numbers on the x-axis. Each section represents 100µm of tissue. Roman numerals indicate consecutive sections with distinct gene profiles, separated by yellow dotted lines. **(C)** Tomo-seq plots and *in situ* hybridization on sections from injured hearts for representative genes for each zone. Both plots and tissue was obtained from 7dpi samples. Red dotted lines indicate zone borders, black dotted lines in images indicate the border of the injured area. Scale bar represents 200µm.

Next, we identified all genes that are differentially expressed in the mouse BZ compared to the injury and remote areas using the EdgeR algorithm (Fig.S1A,B). A similar analysis was performed on a previously generated TOMO-sequencing datasets of the injured zebrafish heart (Fig.S1C,D) (Wu et al., 2015). The differentially expressed genes in the mouse and zebrafish BZ from different timepoints (3, 7 and 14dpi) were pooled to mitigate any temporal differences between both species. In order to compare expression of mouse and zebrafish genes, we first identified all differentially expressed BZ genes with an annotated homologue in the mouse and zebrafish genomes resulting in 11779 homologues gene-pairs. Next, we plotted for all these gene-pairs their Log Fold Change (LogFC) (BZ versus the rest of the tissue) in a scatter plot (Fig.2A,B) and selected all genes with a P-value below 0.05 and a LogFC above 0.5 or below -0.5. This revealed 331 gene-pairs with enhanced expression in the BZ in both species and 326 gene-pairs with reduced expression in the BZ of both species, respectively. Gene ontology analysis of the 331 upregulated genes revealed that these are enriched for genes with a function in extracellular matrix, calcium binding and regulation of apoptosis, while the 326 downregulated gene-pairs have functions in mitochondria such as oxidative phosphorylation and aerobic respiration (Fig. 2C,D). Together, these results indicate that both zebrafish and mouse BZ cells are responding to the injury through downregulation of their oxygen dependent metabolism and is consistent with previous studies, showing that both zebrafish and mouse BZ CMs downregulate genes with a role in oxidative phosphorylation (Honkoop et al., 2019; K. van Duijvenboden et al., 2019; Wu et al., 2015).

More interesting are the observed differences between the zebrafish and mouse border zone, as they may shed light on the limited regenerative capacity of the injured mammalian heart (Fig.2E,F). We identified 366 gene-pairs that are upregulated in the mouse BZ, but not in the zebrafish BZ. These gene-pairs have functions in wound healing, extracellular matrix organization and TGF β signaling, together suggesting profound differences in the pro-fibrotic response between the zebrafish and mouse BZ (Ikeuchi et al., 2004; Okada et al., 2005).

Vice versa, we identified 371 gene-pairs that are upregulated in the zebrafish BZ, but not in the mouse BZ. For some of these genes we confirmed the BZ-enriched expression in zebrafish through *in situ* hybridization and the lack of BZ enrichment in the mouse BZ using quantitative PCR analysis (Fig.S2A,B). The 371 gene-pairs specific for the zebrafish BZ have functions in processes such as actin filament binding and myosin complex, which may relate to a remodelling of the contractile apparatus. In addition, gene ontologies such as response to insulin stimulus are consistent with important roles for insulin signaling and metabolic reprogramming in the regulation of CM proliferation during zebrafish heart regeneration (Fukuda et al., 2020; Honkoop et al., 2019; Y. Huang et al., 2013).

In summary, we used TOMO-seq to resolve the transcriptome of the BZ of the injured adult mouse heart and compared this with the BZ of the regenerating zebrafish heart. The comparison of the BZ transcriptomes revealed processes that are shared such as reduced mitochondrial oxidative phosphorylation and processes that are species-specific such as an altered fibrotic response in mouse BZ and insulin signaling in the zebrafish BZ. Together, these results may lead to the identification of processes and pathways that promote heart regeneration.

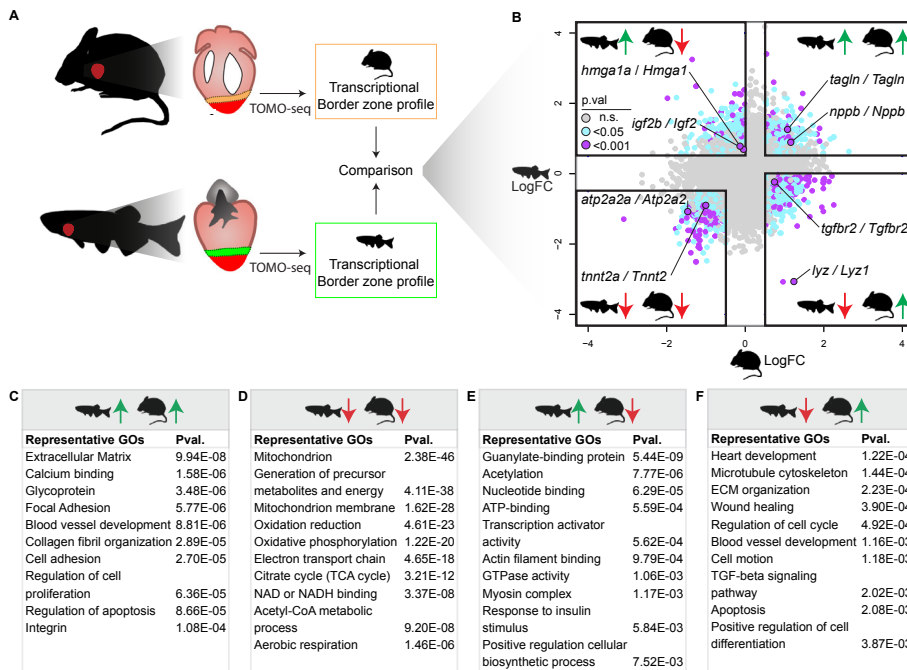


FIGURE 2. Transcriptional comparison between the zebrafish and mouse border zone identifies overlapping and divergent gene expression. (A) Schematic overview of the workflow. (B) Scatterplot analysis comparing border zone expression as LogFC for homologous gene-pairs. (C-F) Representative gene ontologies for each of the four quadrants of the scatterplot. Gene-pairs were selected based on the following criteria; (C) Zebrafish: $\logFC > 0.5$, $Pval < 0.05$; Mouse: $\logFC > 0.5$, $Pval < 0.05$. (D) Zebrafish: $\logFC < -0.5$, $Pval < 0.05$; Mouse: $\logFC < -0.5$, $Pval < 0.05$. (E) Zebrafish: $\logFC > 0.5$, $Pval < 0.05$; Mouse: $\logFC < 0$. (F) Zebrafish: $\logFC < 0$; Mouse: $\logFC > 0.5$, $Pval < 0.05$.

Hmga1a is required for zebrafish heart regeneration

Next, we aimed to identify a novel driver of cardiac regeneration. We selected *hmga1a* from the list of zebrafish-specific BZ genes, as it encodes an architectural protein that binds to and relaxes chromatin to induce and maintain cellular pluripotency and self-renewal (Battista et

al., 2003; Kishi et al., 2012; Shah et al., 2012; Xian et al., 2017). Considering these reported functions, we hypothesized that *hmga1a* could play a regulatory role during zebrafish heart regeneration. To confirm the TOMO-seq results, we established the spatial and temporal dynamics of *hmga1a/Hmga1* expression in injured zebrafish and mouse hearts by *in situ* hybridization (Fig.3A,B). In both uninjured and 1dpi zebrafish hearts, *hmga1a* expression was undetectable. At 3dpi *hmga1a* expression was weak but consistent in the BZ, which further increased at 7dpi with robust *hmga1a* expression in BZ CMs (arrows). In contrast, the zebrafish paralogue *hmga1b* did not show any expression in BZ CMs (Fig.S3D). In addition, *in situ* hybridization for *Hmga1* on sections of injured mouse hearts revealed no signal above background (Fig.3B) and qPCR on BZ and RM tissues validated that *Hmga1* is not induced in the BZ of the mouse heart (Fig.S2B). Next, we wondered whether *Hmga1* expression correlates with the regenerative window of the neonatal mouse heart. Indeed, we did observe mosaic *Hmga1* expression throughout the uninjured neonatal P1 heart (Fig.3B). Importantly, qPCR analysis demonstrated that *Hmga1* expression levels decline rapidly in the first week after birth, coinciding with the loss of regenerative capacity of the mouse heart (Fig.3C) (Porrello et al., 2011). From these results we conclude that *hmga1a/Hmga1* expression spatially and temporally overlaps with the regenerative capacity of the injured zebrafish and neonatal mouse heart.

To investigate whether *Hmga1* is essential for zebrafish heart regeneration, we generated a loss-of-function mutant line by targeting the start of first exon of *hmga1a* using a TALEN-based strategy. The resulting 8bp deletion directly after the start-codon causes a frame-shift and introduction of a pre-mature stop codon, resulting in a truncated *Hmga1a* protein (7aa instead of 101aa, Fig.S3A,B). Homozygous *hmga1a* mutant embryos developed normally and could be grown to adulthood to study the potential role for *Hmga1* during heart regeneration. Importantly, expression of *hmga1a* was strongly reduced in injured hearts of *hmga1a*^{-/-} fish compared to their wild-type siblings, likely due to non-sense mediated mRNA decay, consistent with a loss of *Hmga1a* function (Fig.S3C). Upregulation of *hmga1b* was not observed in the *hmga1a*^{-/-} hearts, suggesting *hmga1b* is not compensating for the loss of *hmga1a* (Fig.S3D).

Next, we assessed whether the *hmga1a*^{-/-} fish have a heart regeneration defect by visualizing fibrosis with AFOG in injured hearts 30 days post cryoinjury. Indeed, scar size at 30dpi was significantly increased in *hmga1a*^{-/-} hearts compared to their siblings, indicating impaired regeneration (Fig.4A,B). These findings indicate that *hmga1a* is required for zebrafish heart regeneration.

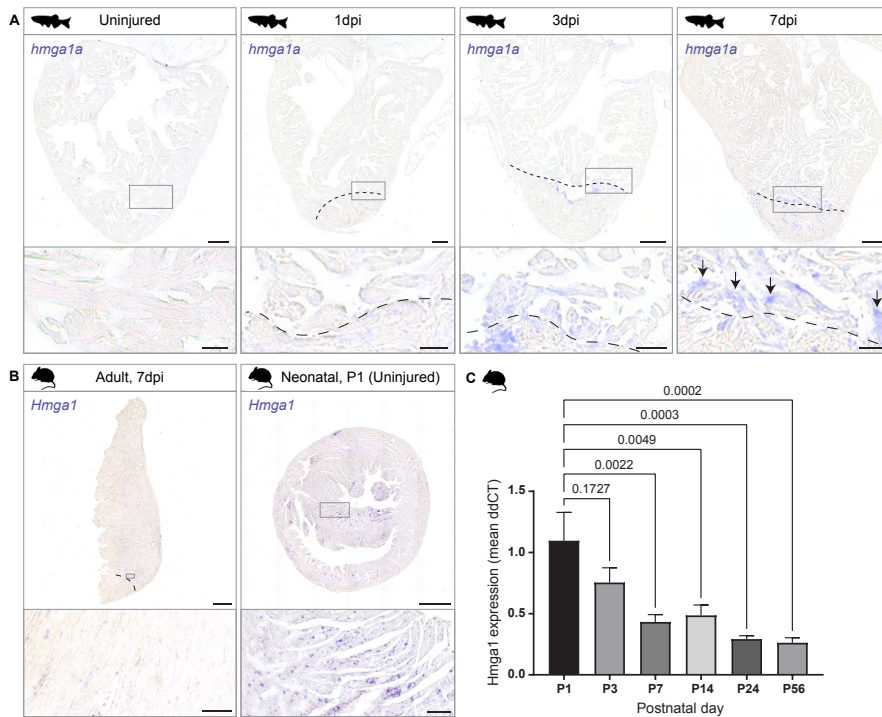


FIGURE 3. *hmga1a* expression is correlated with regenerative potential. (A) Representative images for *in situ* hybridization against *hmga1a* in uninjured or injured zebrafish hearts at different time points. At least 3 hearts were stained per time point. Expression in border zone cardiomyocytes starts at 1 dpi and is strong at 3 and 7dpi (arrows). Scale bars represent 100 μ m in the overview and 25 μ m in the zoom-ins. Dashed line indicates border with the injured region (B) *In situ* hybridization against *Hmga1* in left ventricular tissue of injured adult mouse hearts and in uninjured neonatal hearts (P1). No specific signal was observed in adult mouse heart while strong signal was observed in the neonatal heart. Scale bars represent 0.5mm in the overview and 50 μ m in the zoom-ins. (C) qPCR analysis was done on cDNA libraries from whole mouse hearts at different postnatal time points. 5 biological replicates were used per time-point. One-way ANOVA analysis indicates a significant difference in *Hmga1* expression between different timepoints (p .val = 0.0002). Dunnett's multiple comparison test was used to identify which specific columns significantly differ from the P1 timepoints. Error bars indicate standard variation.

Hmga1a is required for cardiomyocyte proliferation

To gain insight into the function of *hmga1a* during heart regeneration we aimed to identify which processes occurring in BZ CMs dependent on *hmga1a*. To accomplish this, we crossed the *hmga1a*^{-/-} mutants with the previously published *nppa:mCitrine* reporter line which marks BZ CMs (Honkoop et al., 2019) (Fig.4C). This allowed us to sort out BZ CMs (mCitrine high) of 7dpi *hmga1a*^{-/-} and sibling hearts using FACsorting (Fig.S4A). Next, we submitted the isolated cells to single-cell RNA-sequencing using the SORT-seq (Sorting and Robot-assisted Transcriptome SEQuencing) platform (Fig.4D) (Muraro et al., 2016). We analysed 1311 cells with over 600 reads per cell using the Race-ID3 algorithm resulted in the identification of 6 cell clusters grouped based on their transcriptomic features (Fig.4E, Fig.

S4B-D). All analysed cells contain reads of the cardiomyocyte marker *myl7*, validating that we specifically sorted out CMs. In addition, all clusters with the exception of cluster 5 show expression of BZ markers *nppa* and *desma*, indicating that these cells represent BZ CMs. Cluster 5 cells instead express a high level of mitochondrial mRNAs like *NC_002333.17* suggesting a more remote origin (Fig.S5A,B).

To investigate where the *hmga1a*^{-/-} cells are represented in the t-SNE map, we plotted the genotype specific contribution (Fig.4F). Quantification of the genotype contribution per cluster (Fig.4G,H) indicates that while most clusters are slightly enriched for *hmga1a*^{-/-} cells, clusters 1 and 6 are almost exclusively formed by wild-type CMs. We validated this by *in situ* hybridization for the cluster 6-enriched genes *fth1a*, *uba52* and *gamt* (Fig.S6A) and indeed observed reduced expression of these genes in the BZ CMs of *hmga1a*^{-/-} hearts. To address transcriptional differences between cell clusters we performed gene ontology analysis on cluster-enriched genes (Fig.S6B). Importantly, cluster 1 and 6 specific genes are enriched in genes with a role in cell cycle regulation, suggesting that CM proliferation is affected in *hmga1a*^{-/-} hearts.

To gain insight into the processes regulated by Hmga1a we performed unsupervised pseudo-time ordering of the single cells (Fig.4I). Next, gene expression profiles were unbiasedly grouped together in self organizing modules (SOMs) of similarly expressed genes, resulting in 8 transcriptionally distinct modules (Fig.4I,J). Module 1 represents genes with high expression at the start of the pseudo-time line with a role in the respiratory chain, indicating that this represents the most differentiated CM state. Importantly, module 5 contains *hmga1a* as well as genes with a role in cell cycle control (e.g. *pcna* and *cdc14*), consistent with a close temporal correlation between Hmga1a expression and CM proliferation. Next, we wondered how *hmga1a*^{-/-} cells are distributed across the pseudo time line. To this end, we plotted the relative genotype contribution across 100 bins constituting the pseudo time (Fig.4K). Interestingly, we observe a trend in which there is a gradual loss of *hmga1a*^{-/-} cell contribution as pseudo time progresses. Strikingly, after module 5, the number of *hmga1a*^{-/-} cells contributing to the pseudo-timeline drops from constituting ~50% (during module 5) to ~28% (modules 6-8). Directly preceding the drop in mutant cell contribution, a peak in mutant cell contribution is observed at the edge of module 5 (grey dotted line, Fig.4I,K). These data suggest that *hmga1a*^{-/-} BZ CMs fail to progress in pseudo time, but instead are arrested at earlier stages. Indeed, *in situ* hybridization for *hk1* (module 6 marker) and *ak1* (module 7 marker) revealed reduced expression in *hmga1a*^{-/-} hearts at 7dpi (Fig.4L,M). The co-expression of *hmga1a* with cell cycle regulators and reduced expression of *hk1*, encoding the rate-limiting glycolysis enzyme hexokinase, in *hmga1a*^{-/-} hearts further suggested that Hmga1a is specifically required for cell cycle induction and/or progression. To validate this, we assessed BZ CM proliferation through immunohistochemistry with PCNA and indeed observed a significant decrease in PCNA⁺ CMs in *hmga1a*^{-/-} hearts compared to their siblings (Fig.5A-C).

Taken together, these data indicate that *hmg1a* promotes CM proliferation in the BZ, while it appears dispensable for the early injury response of BZ CMs.

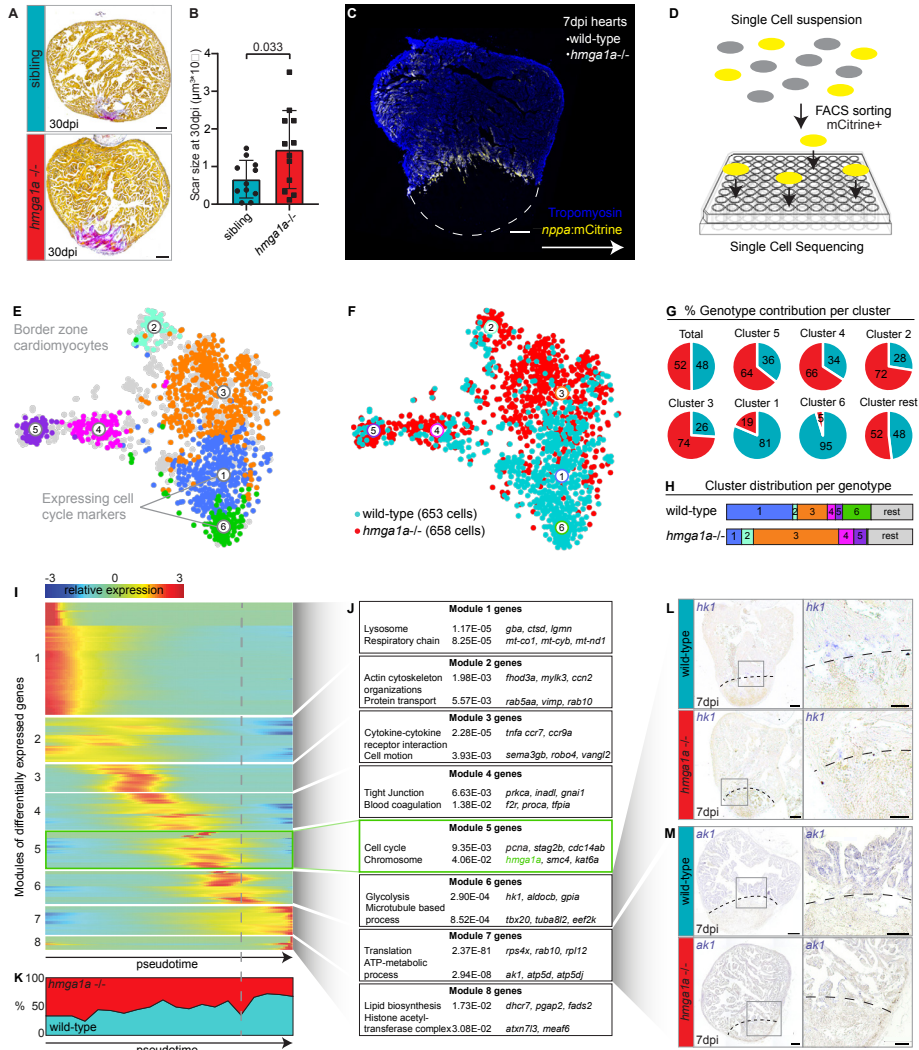


FIGURE 4. Hmga1a is required for zebrafish heart regeneration and allows border zone cardiomyocytes to assume specific cellular states. (A) AFOG staining of *hmg1a*^{-/-} and sibling hearts at 30dpi. Orange = cytoplasm, blue = collagen, red = fibrin. Scale bars represent 100µm. (B) Quantification of scar sizes. (C,D) Workflow for the scRNAseq. Nppa:mCitrine⁺ cardiomyocytes were isolation from wild-type and *hmg1a*^{-/-} hearts at 7dpi and sorted on 384-wells plates followed by scRNAseq. (E) tSNE-plot of the data showing 6 transcriptionally distinct cardiomyocyte cell clusters. (F) tSNE-map showing the contribution of wild-type cells (cyan) and *hmg1a*^{-/-} cells (red). (G) Pie charts showing percentages of wild-type and *hmg1a*^{-/-} cells per cluster. (H) Stacked bar graph showing relative cell contribution to major clusters in either wild-type or *hmg1a*^{-/-} hearts. (I) Heat map from pseudo time analysis. One-dimensional SOM of z-score transformed expression profiles along the differentiation

trajectory incurred by StemID analysis. Y-axis represents the eight modules with differentially expressed genes. X-axis represents the pseudo time in which the cells were ordered. **(J)** Gene ontologies derived from all genes expressed in the module with p-values and some representative genes listed. **(K)** Distribution of genotype contribution across pseudotime. **(L,M)** Representative images from *in situ* hybridization for *hk1* **(L)**, a gene from module 6, and *ak1* **(M)**, a gene from module 7, on cryoinjured (7dpi) wild type and *hmga1a*^{-/-} mutant heart sections. At least 3 hearts were analysed per time point. Dotted lines indicate the injury area. Scale bars represent 100µm in the overview and 50µm in the zoom-ins.

Hmga1a acts downstream of Nrg1 signaling

The growth factor Nrg1, which is produced and secreted by epicardial derived cells in response to heart injury, induces CM proliferation (Gemberling et al., 2015b). As we observed that efficient BZ CM proliferation requires Hmga1a, we addressed whether Nrg1 induces *hmga1a* expression and whether Hmga1a is also required for Nrg1-induced CM proliferation. Therefore, we injected fish intraperitoneal with human recombinant NRG1, once a day for three consecutive days (Fig.5D). Similar as reported for a genetic *nrg1* overexpression model (Gemberling et al., 2015a), increased cardiomyocyte proliferation was observed upon NRG1-injection, which was most pronounced in the outermost myocardial layers of the heart (Fig.5E). Furthermore, ectopic NRG1 induced *hmga1a* expression throughout the entire heart, including the outermost myocardial layers (Fig.5F). To investigate whether NRG1-induced CM proliferation is dependent on *hmga1a*, we injected NRG1 in *hmga1a*^{-/-} fish. Importantly, while NRG1 induced CM proliferation in wild-type siblings, ectopic NRG1 failed to induce CM proliferation in *hmga1a*^{-/-} hearts (Fig.5G). Together, these results indicate that *hmga1* acts downstream of Nrg1 signaling to induce CM proliferation.

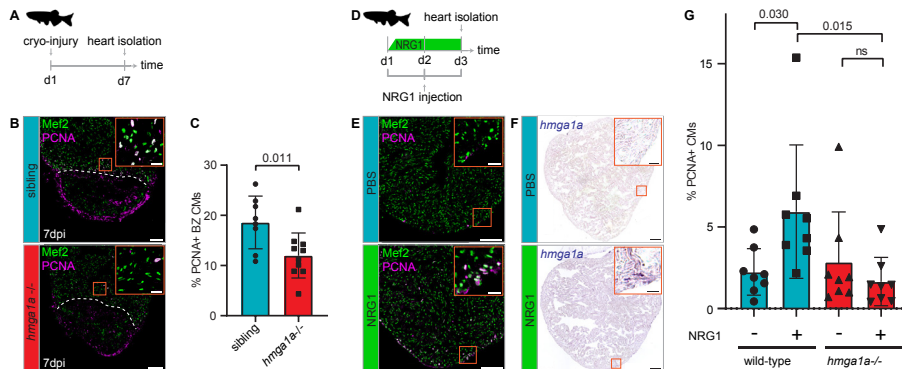


FIGURE 5. Impaired injury- and NRG1-induced cardiomyocyte proliferation in *hmga1a*^{-/-}. **(A)** Workflow of cryo-injury and heart isolation used in **(B,C)**. **(B)** Antibody staining against Mef2 (cardiomyocyte nuclei) and PCNA (nuclei of proliferating cells). Dotted lines indicate the injury area. Overview scale bars represents 100µm, zoom-in scale bars represents 20µm. **(C)** Quantification of proliferating border zone cardiomyocytes. **(D)** Workflow of intraperitoneal NRG1 injections and heart isolation used in **(E-G)**. **(E)** Antibody staining against Mef2 and PCNA to identify proliferating zebrafish cardiomyocytes in PBS or NRG1 injected hearts. **(F)** *In situ* hybridization against *hmga1a* in hearts of PBS or NRG1 injected zebrafish. At least 3 hearts were analysed for each condition. **(E,F)** Overview scale bars represents 100µm, zoom-in scale bars represents 20µm. **(G)** Quantification of proliferating cardiomyocytes in PBS or NRG1 injected zebrafish hearts, either in *hmga1a*^{-/-} or wild-type sibling hearts.

Hmga1a alters chromatin accessibility and induces an injury-related gene program

Hmga1 is an architectural chromatin protein that preferentially binds to AT-rich domains and competes for DNA binding with Histone H1, as shown through *in vitro* experimentation (Catez et al., 2004). Upon chromatin binding, Hmga1 facilitates binding of chromatin remodelling complexes and transcription factors to induce gene transcription (Catez et al., 2004; Ozturk et al., 2014; Reeves, 2001). To reveal whether *hmga1a* overexpression in zebrafish CMs leads to changes in chromatin accessibility and gene expression we generated a *Tg(ubi:Loxp-stop-Loxp-hmga1a-eGFP)* line. To achieve Hmga1a overexpression in CMs, we crossed this line with *Tg(myf7:CreERT2)* and subjected the fish to tamoxifen treatment. Next, we isolated nuclei from *hmga1a* overexpression and Cre-only control hearts 14 days post recombination and FACsorted CM nuclei using the CM nuclear reporter line *Tg(myf7:DsRed-nls)* (Fig.6A). Then, CM nuclei were subjected to an assay for transposase-accessible chromatin using sequencing (ATAC-seq) (Buenrostro et al., 2013), resulting in 311,968,790 sequencing reads that were mapped to the zebrafish genome (GRCz10). Genomic regions were mapped using Bowtie2 and accessible regions were identified using MACS2 peak calling. In total, we identified 35,014 accessible regions in the *hmga1a* overexpression dataset and 37,718 accessible regions in the control dataset (q-value > 0.05, calculated with Benjamini-Hochberg procedure). Most accessible regions are in inter- and intragenic regions, while a smaller fraction was found in promotor regions (Fig.6B). A large proportion of these accessible promotor regions (n=1,308) are shared between the control and *hmga1a* overexpression datasets (Fig.6C). We identified 12,906 emerging and 15,855 disappearing accessible chromatin regions upon *hmga1a* overexpression, while 22,430 chromatin regions remained stably accessible (Fig.6D). As these results support a role for Hmga1a in changing chromatin accessibility we next wanted to know whether these regions are correlated with specific transcription factors that may bind to these regions. Therefore, we identified enriched transcription factor binding motifs within the emerging and disappearing peaks, using the web based MEME suite tool Analysis of Motif Enrichment (AME v5.3.0) (Bailey et al., 2009; McLeay & Bailey, 2010). Strikingly, both emerging and disappearing peaks showed strong enrichment in binding motifs for the transcription factors NF-YA, FOXK1 and FOXK2, indicating that Hmga1a overexpression modulates their respective binding sites (Fig.6E).

To investigate the correlation between promotor accessibility and transcription we also performed RNA-seq on *hmga1a* overexpressing- and control-hearts and integrated these data with the ATAC-seq data. We found that promotor accessibility and transcription are well correlated for both control and *hmga1a* overexpression datasets, as a significantly higher RNA-expression was observed for genes with accessible promotor regions (Fig.6F). In *hmga1a* overexpression hearts 1,647 genes are upregulated (p.value < 0.05, LogFC > 0.5), including genes with a role in *DNA replication*, corroborating a role for Hmga1a in cell proliferation (Fig.6G,H). Surprisingly, the natriuretic peptide genes are also induced by *hmga1a* overexpression. This is striking as it indicates induction of an injury responsive

program, while the hearts used for the analysis had not been injured. This is consistent with the downregulation of many genes with functions in mitochondrial oxidative phosphorylation. As these adaptations are highly reminiscent of the processes occurring in the zebrafish BZ after injury, we compared *hmga1a* overexpression transcriptomes with the BZ transcriptomes (Fig.6I). Strikingly, we observed a significant overlap for *hmga1a*-induced genes and genes upregulated in the injury BZ (11.5% overlap, $p = 6.6e-5$) as well as for *hmga1a*-repressed genes and genes downregulated in the injury BZ (18.2% overlap, $p = 4.0e-11$). In summary, these results demonstrate that ectopic *hmga1a* expression in CMs of uninjured hearts leads to profound changes in chromatin accessibility and the subsequent induction of a partial BZ-like transcriptional program.

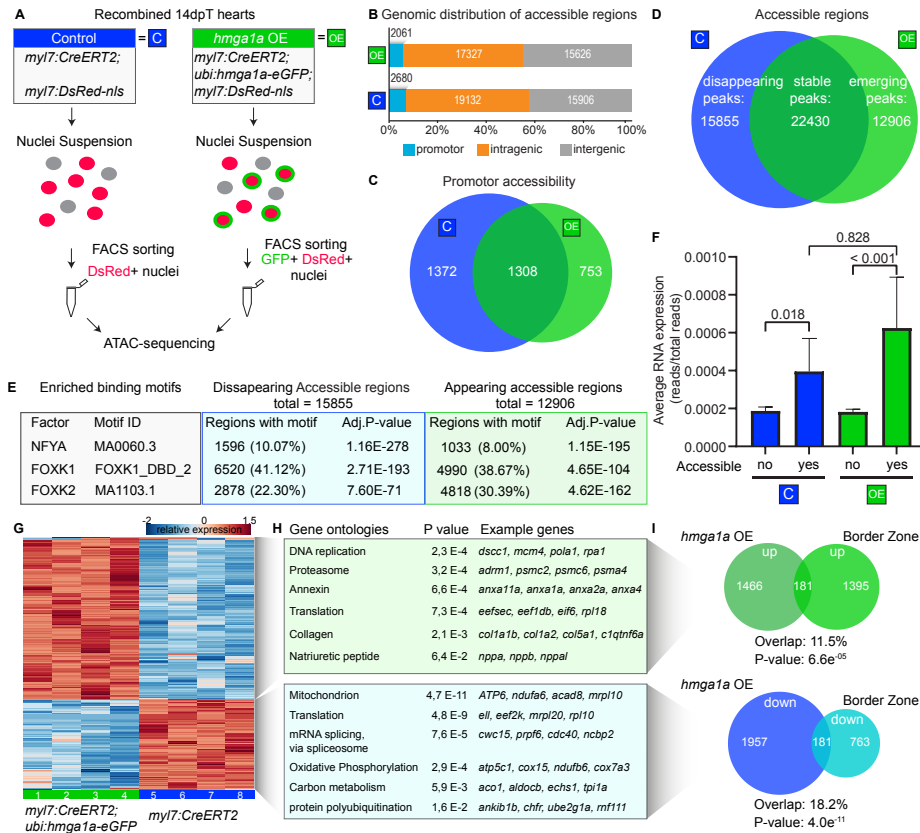


FIGURE 6. Hmga1a-eGFP overexpression induces changes in chromatin organization and gene expression. (A) Workflow of ATAC-sequencing (Assay for Transposase-Accessible Chromatin using sequencing) used to produce the data described in (B-F). (B) Distribution of the location of accessible regions, which were identified using MACS2 peak calling. (C) Venn-diagram showing the overlap between the accessible promotor regions obtained from control (*myl7:CreERT2*) and Hmga1a-eGFP overexpressing (*myl7:CreERT2*; *ubi:hmga1a-eGFP*) cardiomyocyte nuclei. (D) Venn-diagram showing the overlap between the accessible promotor regions identified in control or Hmga1a-eGFP

overexpressing cardiomyocyte nuclei. **(E)** Enriched binding motifs were identified in disappearing and emerging accessible regions using the Analysis of Motif Enrichment (AME) webtool available as part of the MEME-suite (v5.3.0), indicating that both emerging and disappearing accessible regions share enrichment in binding motifs from transcription factors NFYA, FOXK1 and FOXK2. **(F)** Average RNA-expression of genes with or without accessible promoters, obtained through RNA-sequencing on whole zebrafish hearts. **(G)** Heatmap representing RNA-sequencing data obtained from whole-hearts of control (*myl7:CreERT2*) and Hmga1a-eGFP overexpressing (*cmic2:CreERT2; ubi:hmg1a-eGFP*) zebrafish. **(H)** Gene ontology analysis on genes differentially expressed ($P\text{-val} < 0.05$, $\text{LogFC} > 0.5$) between control and Hmga1a-GFP overexpressing hearts with p-values and representative genes listed. **(I)** Venn-diagrams indicating the overlap between gene expression upon Hmga1a-eGFP overexpression ($P\text{-val} < 0.05$, $\text{LogFC} > 0.5$ (top) or $\text{LogFC} < -0.5$ (bottom) and gene expression in the zebrafish border zone ($P\text{-val} < 0.05$, $\text{LogFC} > 0.5$ (top) or $\text{LogFC} < -0.5$ (bottom) identified through tomo-sequencing. P-values were calculated using the R-function phyper and indicates the chance of finding such an overlap by chance.

Hmga1a overexpression is sufficient to drive proliferation in zebrafish cardiomyocytes

Next, we wondered whether overexpression of Hmga1a can induce cardiomyocyte proliferation and lead to changes in heart morphology. First, we addressed whether overexpression of *hmg1a* is sufficient to drive proliferation in zebrafish CMs. To analyse the effect of *hmg1a* overexpression we treated 4- to 6-month old *Tg(ubi:Loxp-stop-Loxp-hmg1a-eGFP, myl7:CreERT2)* and *Tg(myl7:CreERT2)* control fish with tamoxifen and extracted hearts 14 days post induction, followed by quantification of CM proliferation by PCNA expression (Fig. 7A,B). This revealed a significant increase in PCNA+ CMs throughout the heart from ~7% in controls to ~18% in *hmg1a* overexpressing hearts (Fig.7C). Next, we determined long-term effects of *hmg1a* overexpression and analysed hearts 1 year post induction (Fig.7D). We observed a significant increase in myocardial surface area (Fig.7E,F), which coincided with a slight, but non-significant, increase in total surface area (including cardiac lumen) of the heart (Fig.7G). This increase in myocardial surface area is mainly due to an expansion of the trabecular region at the expense of the cardiac lumen (Fig.7H). Furthermore, the increase in trabecular tissue is likely due to the modest but significant increase in CM proliferation (Fig.7I), but not due an increase in CM size (Fig.7J). Together, these results show that Hmga1a-eGFP overexpression induces CM proliferation, which has profound effects on heart morphology.

Hmga1 induces mammalian cardiomyocyte cell cycle re-entry and functional recovery after myocardial infarction

Our previous results demonstrate that in zebrafish, Hmga1a is required for efficient heart regeneration and that Hmga1a overexpression is sufficient to induced CM proliferation. Unlike in zebrafish, murine *Hmga1* expression is not induced by a cardiac injury, which may be explained by the absence of an Nrg1-induced activation of ErbB2 signaling (D'Uva et al., 2015). Therefore, we first wanted to investigate whether activation of ErbB2 signaling in murine cardiomyocytes induces Hmga1 expression. Indeed, in mouse hearts expressing the constitutively active (ca) ERBB2 receptor, we observed enhanced nuclear Hmga1 protein accumulation (Fig.8A,B).

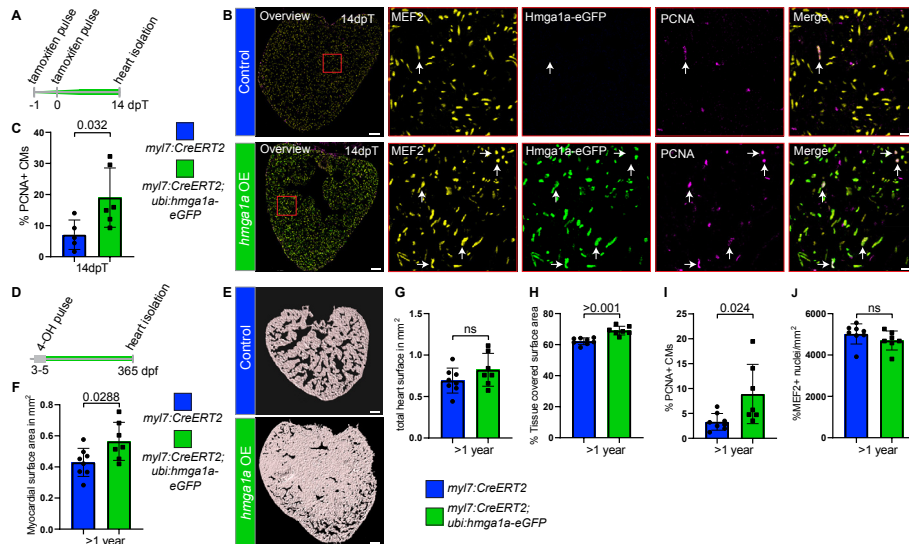


FIGURE 7. *hmg1a* overexpression is sufficient to induce proliferation in zebrafish cardiomyocytes. (A) Workflow of tamoxifen treatment to induce recombination and heart extraction for analysis used in (B-C). (B) Antibody staining against Mef2 and PCNA to identify proliferating cardiomyocytes, as well as against GFP to validate successful recombination, for control (*myl7:CreERT2*) and Hmga1a-eGFP overexpressing (*myl7:CreERT2; ubi:hmg1a-eGFP*) hearts. Overview scale bars represent 100 μ m, zoom-in scale bars represent 20 μ m. (C) Quantification of proliferating cardiomyocytes in control and Hmga1a-eGFP overexpressing hearts. Each dot represents the average of three analysed sections of single heart. (D) Workflow of tamoxifen treatment to induce recombination and heart extraction for analysis used in (E-J). (E) Surface rendering of autofluorescence of heart sections using Imaris software. Grey indicates myocardial surface. Scale bars represents 100 μ m. (F-J) Quantification of differences between control and Hmga1a-eGFP overexpressing hearts, including (F) myocardium covered surface area, (G) total heart surface (myocardium + lumen), (H) the percentage of total heart surface covered with myocardium, (I) percentage of proliferating CMs and (J) the density of cardiomyocyte nuclei.

To address whether Hmga1 is able to stimulate proliferation in mammalian CMs, we induced ectopic Hmga1 expression in primary isolated neonatal rat cardiomyocytes (NRCMs) (Fig.8C). CMs were isolated from P1 neonatal rats and incubated for 2 days before virus treatment. Hmga1-eGFP overexpressing virus (*EF1a:Hmga1-eGFP*) or GFP only control virus (*EF1a:eGFP*) was administered in the medium, as well as EdU to track newly synthesized DNA. After another 2 days of incubation, cells were fixed and analyzed for proliferation markers. Interestingly, a significant increase in EdU and Ki67 was observed in the Hmga1-eGFP transfected CMs compared to the eGFP only transfected CMs (Fig.8D,E). In addition, a positive trend was found for an increase in mitosis marker pH3 in the Hmga1-eGFP transfected cells (*p.val.* = 0.064) (Fig.8F). Taken together, these results indicate that Hmga1 overexpression in mammalian CMs can increase their proliferative capacity.

Next we wanted to address whether ectopic *Hmga1* expression in adult mouse hearts induces CM cell cycle re-entry *in vivo*. To induce *Hmga1* expression, we employed adeno-associated virus 9 (AAV9), which preferentially targets CMs (Bish et al., 2008), carrying a *CMV:HA-Hmga1* cassette. Upon MI, hearts were injected twice with 15ul virus (1×10^{11} virus particles / mouse) in regions bordering the area at risk of ischemic injury. In addition, to assess CM cell cycle activity mice were injected with EdU bidaily for two weeks post MI (Fig.8G).

At 14 days post MI and virus injection, hearts were isolated, sectioned and stained for EdU (indicating newly synthesized DNA), PCM-1 (marking CM nuclei) and the HA-tag (marking cells with HA-*Hmga1* overexpression) (Fig.8H). Importantly, while EdU incorporation in CMs located in the remote area was not affected by HA-*Hmga1* expression, EdU incorporation in CMs located at the BZ was increased 5-fold in CMs expressing HA-*Hmga1* (from 0.2% to 1.2%) (Fig.8I).

Next, we wondered whether overexpression of HA-*Hmga1* can lead to a functional improvements post MI. Therefore, virus treated mice were subjected to echocardiography at 42dpi, after which the hearts were isolated and sectioned for histological analysis (Fig.8J). Immunohistochemistry against HA-tag was performed to assess the transfection efficiency in the border zone. As the transfection efficiency showed high variability between hearts, correlation analysis between transfection efficiency and heart functionality was performed. In addition, inefficiently transfected hearts (average of <30 transfected BZ cells) were excluded when comparing between AAV9(empty) and AAV9(*CMV:HA-Hmga1*) treated hearts.

Significant correlations were found between transfection efficiency and ejection fraction as well as fractional shortening, where hearts with a higher number of transfected BZ cells showed improved functionality (Fig.8K,M). Direct comparison between AAV9(empty) and effectively transfected AAV9(*CMV:HA-Hmga1*) treated hearts indicates a significant increase in ejection fraction ($p.val = 0.015$) (Fig.8L), as well as a positive trend in fractional shortening ($p.val. = 0.084$) (Fig.8N).

Together, these results indicate that ectopic *Hmga1* expression in injured mammalian hearts promotes cardiomyocyte cell cycle re-entry and stimulates functional recovery post myocardial infarction.

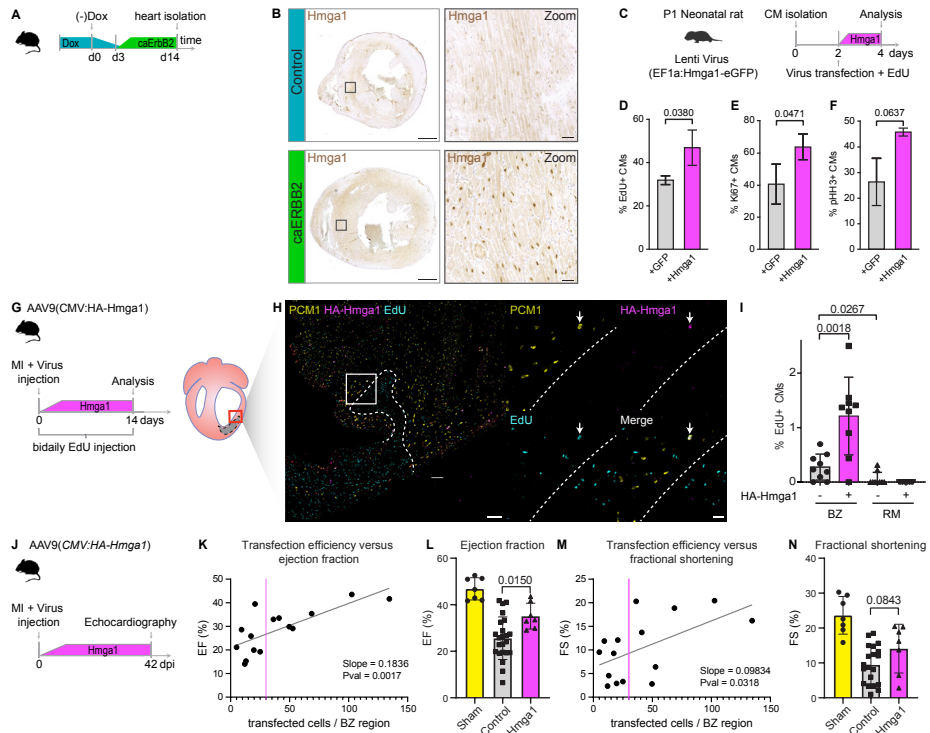


FIGURE 8. Hmga1 overexpression stimulates cell-cycle re-entry of mammalian cardiomyocytes and promotes functional recovery post-MI. (A) Workflow of caErbB2 overexpression in adult mouse hearts used in **(B)**. **(B)** Immunohistochemistry for Hmga1 on sections of control and caErbB2 OE mouse hearts. In control hearts, Hmga1 shows low nuclear expression in a mosaic manner. Hearts overexpressing the caErbB2 receptor for 14 days show robust homogenous expression of nuclear Hmga1 throughout the heart. Scale bars represent 1mm in the overview and 50µm in the zoom-ins. $n = 3$ for both conditions. **(C)** Workflow of Hmga1-eGFP overexpression in neonatal rat cardiomyocytes used in **(D-F)**. **(D-F)** Quantification of indicated cell-cycle markers on eGFP only or Hmga1-eGFP transfected cardiomyocytes. For Edu, Ki67 and pHH3 quantification, 3 biological replicates were quantified per condition, except for the pHH3 Hmga1-eGFP condition for which only 2 technical replicates were available. **(E)** Workflow of myocardial infarction (MI), intracardiac injection of AAV9(CMV:HA-Hmga1) or control AAV9 virus and bidaily intraperitoneal injection of EdU. **(F)** Antibody staining against PCM-1 (marking CM nuclei), HA (marking transfected cells expressing HA-Hmga1) and EdU (indicating newly synthesized DNA). Dotted line indicates the start of the injury area. Scale bars represent 100µm in the overview and 20µm in the zoom-in. **(G)** Quantification of Edu+ cells within the border zone (BZ) or remote myocardium (RM) of hearts transfected with HA-Hmga1. At least 3 heart sections were quantified per heart. **(H)** Workflow of myocardial infarction (MI), intracardiac injection of AAV9(CMV:HA-Hmga1) or control AAV9 virus and consequent analysis. Echocardiography data was obtained followed by heart extraction and immunohistochemical analysis for HA-Hmga1 transfection. **(I, K)** The ejection fraction **(I)** or fractional shortening **(K)** was plotted against the average amount of transfected cells found in the BZ (defined as no further than 200µm from the injury area). At least 3 heart sections were quantified per heart. Magenta line indicates the transfection efficiency cut-off used in **(J, L)**. **(J, L)** Quantification of the ejection fraction **(J)** or fractional shortening **(L)** of sham operated hearts, or MI hearts that were injected with either control or CMV:HA-Hmga1 virus. Hearts with <30 transfected BZ cells were excluded from the analysis.

DISCUSSION

Here, we aimed to identify molecular mechanisms underlying the difference in regenerative capacity between species. To achieve this, we performed a screen to identify transcriptional differences between the border zone of the regenerating zebrafish heart and the non-regenerating mouse heart. This resulted in an extensive list of various genes and processes overlapping and diverging between the two species. Through functional validation of one of the identified candidate genes (*hmga1a*), we provide a proof-of-principle that this dataset can be used to identify novel drivers of cardiac regenerative capacity.

Hmga1a is an architectural chromatin protein which can bind DNA through three AT-hook binding motifs. It competes with Histone H1 for DNA binding, thereby counteracting the inhibitory effects of H1 on transcription (Catez et al., 2004). As Hmga1 is a small protein (107 amino acids in humans), it can freely move through the nuclear membrane. Its localization to the nucleus is therefore not dependent on active transport, but on binding affinity to the DNA which is regulated through phosphorylation (Zhang & Wang, 2007). Besides phosphorylation, HMGA1 is also subjected to acetylation and methylation (reviewed in (Zhang & Wang, 2008)). In addition, Hmga1 has been shown to act both up-and down-stream of the insulin signaling pathway (Chiefari et al., 2012, 2018).

Using a combination of RNA- and ATAC-sequencing, we identify that *hmga1a* overexpression leads to the induction of a broad BZ-like program, including a stress response, ECM production and metabolic adaptation. In addition, *hmga1a* overexpression led to robust changes in chromatin organization, in particular at regions rich in binding motifs for transcription factor NF-YA. This is in line with previous work showing that Hmga1 can bind a highly conserved DBD element of NF-YA with one of its AT-hook motifs, thereby stabilising the interaction between the NFY-complex and promotor regions containing a CCAAT box (e.g. the murine $\alpha 2(I)$ collagen promoter) (Currie, 1997). Interestingly, NF-YA has recently been shown to induce cardiomyocyte proliferation in neonatal mice (Cui et al., 2020). Together, these data suggest that Hmga1 might act together with NF-YA to stimulate CM proliferation.

In addition, *hmga1a* overexpression led to changes in chromatin organization specifically at sites with FOXK1 and FOXK2 binding motifs. FOXK1 and FOXK2 are known regulators of aerobic glycolysis (Sukonina et al., 2019), which they accomplish by inducing glycolytic enzymes (i.e. HK1, PFK1, LDH) while inhibiting pyruvate oxidation (through PDK1 and PDK4). Interestingly, the induction of glycolysis has been shown detrimental to cardiomyocyte proliferation (Honkoop et al., 2019). Therefore, we hypothesize that Hmga1 might help establish the right metabolic conditions for CM proliferation to occur by reorganizing the accessibility of FOXK1 and FOXK2 binding sites. This is in line with the lack of *hk1* expression in *hmga1a*^{-/-} hearts, as well as the strong reduction of oxidative phosphorylation associated

gene expression upon *hmga1a* overexpression. The reduction in oxidative phosphorylation upon *hmga1a* expression is in line with previous reports indicating that Hmga1 can directly influence mitochondrial function and maintenance (Dement et al., 2007). In contrast, the pseudo time analysis suggests that reduced oxidative phosphorylation still occurs in BZ CMs of injured *hmga1a*^{-/-} hearts, suggesting that *hmga1a* might be sufficient, but not required to reduce oxidative phosphorylation in zebrafish CMs. It should be noted that *hmga1a* overexpression reorganises the locations at which these transcription factors will bind, rather than making more regions accessible for binding. We therefore propose a model in which Hmga1 directs other transcription factors (i.e. NFYA, FOXK1, FOXK2) to activate a pro-regenerative program. This model is supported by the observation that *hmga1a* overexpression leads to broad transcriptional changes, indicated by the RNA- and ATAC-sequencing data. Taken together, we conclude that differences in chromatin accessibility and transcriptional regulation mediated by Hmga1 in cardiomyocytes can help explain differences in regenerative capacity between zebrafish and mouse hearts.

Activation of Nrg1/ErbB2 signaling induces CM proliferation in the zebrafish and murine heart (D'Uva et al., 2015; Gemberling et al., 2015a). Here, we show that in zebrafish Hmga1 is required downstream of the Nrg1-induced CM proliferation. Long-term overexpression of *nrg1* in the zebrafish heart induces hyperplastic heart growth resulting in cardiomegaly and enhanced internal fibrosis (Gemberling et al., 2015a). While our results demonstrate that overexpression of *hmga1a* also induces hyperplastic heart growth and increases pro-fibrotic gene expression, long-term *hmga1a* expression does not lead to cardiomegaly. Instead, we observed an expansion of myocardial tissue at the expense of luminal volume. The difference in growth dynamics might be due to the location of the induced CM expression. Overexpression of *nrg1* induces CM proliferation primarily in the cortical (outer) myocardial layer, allowing outward heart growth. Overexpression of *hmga1a*, however, induces CM proliferation throughout the heart and not specifically at the outermost layers, which might limit the outward growth potential.

Overexpression of Hmga1 in injured mouse hearts resulted in a small but significant increase in EdU-positive CMs *in vivo*. Whether the small increase in cell cycle re-entry of BZ CMs (1.2%) directly led to the increase in functional improvement, or whether Hmga1 induces other effects beneficial to functional recovery post MI, remains to be elucidated. However, previous studies have shown that relatively little BZ CM proliferation can result in near complete heart regeneration (D'Uva et al., 2015).

The potential pro-proliferative effect of Hmga1 in murine hearts is limited to BZ CMs, which is in good accordance with previous studies showing that BZ CMs are most likely to respond to mitogenic signals (Leach et al., 2017b; Lin et al., 2014; Pasumarthi et al., 2005; Xiang et al., 2016). The niche-dependent pro-proliferative effect of Hmga1 could therefore form

a distinct advantage in a clinical setting, where Hmga1-induced proliferation would cease once the BZ-niche has resolved, preventing hyperplastic overgrowth. Indeed, the BZ-niche naturally resolves with time in infarcted human hearts (K. van Duijvenboden et al., 2019). Taken together, we have shown that Hmga1 is a driver of cardiac regeneration and forms a promising new substrate for the stimulation of heart regeneration in mammals.

METHODS

Animal experiments

All procedures involving animals were approved by the local animal experiments committees and performed in compliance with animal welfare laws, guidelines, and policies, according to national and European law.

Zebrafish and mouse lines

The following zebrafish lines were used: TL, *TgBAC(nppa:mCitrine)* (Honkoop et al., 2019), *Tg(myl7:CreER)pd10* (Kikuchi et al., 2010), *Tg(myl7:DsRed2-NLS)* (Mably et al., 2003). The *hmg1a*^{-/-} was produced using a TALEN based strategy, targeting the region adjacent to the transcription start site, leading to a frameshift and an early stop codon (Fig.S3A). The *tg(ubi:Loxp-stop-Loxp-hmg1a-eGFP)* was produced using gBlocks and Gibson Assembly, using the pDESTp3A destination vector (Kwan et al., 2007) and the p5E ubi promoter (Mosimann et al., 2011). The following mouse lines were used: C57BL/6J males (Charles River), *tg(Nppb:katushka)* (Sergeeva et al., 2014).

Cryoinjuries in zebrafish

To induce cardiac injury in zebrafish, cryo-injuries were performed on fish of ~4 to 18 months of age. The cryoinjuries were performed as described in (Schnabel et al., 2011), with the exception of the use of a copper filament (0.3mm) cooled in liquid nitrogen instead of dry ice. Animals were excluded from the study in case of signs of aberrant behavior/sickness/infection, according to animal guidelines.

Myocardial infarction in mice

Cardiac ischemic injuries were accomplished by permanent occlusion of the left anterior descending artery (LAD), previously described in (Sergeeva et al., 2014), using adult male mice between 7-12 weeks of age.

Transthoracic echocardiography

Transthoracic echocardiography was performed to address heart function. In brief, mice were anesthetized with a mixture of ketamine and xylazine by IP injection, and hair was shaved from the thorax. A tracheal tube two-dimensional transthoracic echocardiography

on sedated, adult mice (2% isoflurane) using a Visual Sonic Ultrasound system with a 30 MHz transducer (VisualSonics Inc., Toronto, Canada). The heart was imaged in a parasternal longaxis as well as short-axis view at the level of the papillary muscles, to record Mmode measurements, determine heart rate, wall thickness, and end-diastolic and end-systolic dimensions. Fractional shortening (defined as the end-diastolic dimension minus the end-systolic dimension normalized for the end-diastolic dimension) as well as ejection fraction (defined as the stroke volume normalized for the end-diastolic volume), were used as an index of cardiac contractile function.

Virus-mediated overexpression of *Hmga1* in neonatal rat cardiomyocytes

Cardiomyocytes of 1-day-old neonatal rat hearts were isolated by enzymatic dissociation with trypsin (Thermo Fisher Scientific, #15400054) and cultured as described in (Gladka et al., 2021). Overexpression of *Hmga1* was accomplished through lenti-virus mediated delivery of *pHAGE2-EF1a:Hmga1-T2A-GFP* construct.

Virus injections in mice

To induce *Hmga1* expression, we employed AAV9 virus which preferentially targets CMs, carrying a *CMV:HA-Hmga1* cassette. Upon myocardial infarction, hearts were injected twice with 15 μ l virus (1×10^{11} virus particles / mouse) in regions bordering the area at risk of ischemic injury.

EdU injections in mice

To assess cell cycle re-entry at 14 days post MI, adult mice received bi-daily intraperitoneal injections starting at day 2 (resulting in 6 EdU injections in total, per mice). EdU concentrations were determined based on the individual weight of each mouse (50 μ g/g).

***In Situ* Hybridization**

Paraffin sections: After o/n fixation in 4% PFA, hearts were washed in PBS twice, dehydrated in EtOH, and embedded in paraffin. Serial sections were made at 10 μ m thickness. In situ hybridization was performed on paraffin-sections as previously described (Moorman et al., 2001) except that the hybridization buffer used did not contain heparin and yeast total RNA. Cryosections: Sections were obtained as described earlier. In situ hybridization was performed as for paraffin, however sections were prefixed for 10 min in 4% PFA + 0.25% glutaraldehyde before Proteinase K treatment. Moreover, slides were fixed for 1 hr in 4% PFA directly after staining.

qPCR

Total RNA was isolated from heart ventricles using TRIzol reagent reagent (Life Technologies, Carlsbad, CA, USA) according to the manufacturer's instructions. Total RNA (1 μ g) was reverse transcribed using iScript cDNA Synthesis Kit (Bio-Rad, Hercules, CA, USA). Real-

time PCR was performed using iQ SYBRgreen kit and CFX96 real-time PCR detection system (BioRAD). Data was normalized using housekeeping genes *Gapdh* (Fig.3C) or *Hprt* and *Eefe1e* (Fig.S2).

(Immuno)histochemistry

Adult zebrafish ventricles were isolated and fixed in 4% PFA (4°C O/N on shaker). The next day, the hearts were washed 3x 10 minutes in 4% sucrose phosphate buffer, after which they were incubated at RT for at least 5h in 30% sucrose phosphate buffer until the hearts floated. Then, they were embedded in cryo-medium (OCT). Cryo-sectioning of the hearts was performed at 10µm thickness. Primary antibodies used include anti-PCNA (Dako #M0879, 1:800), anti-GFP (aves #GFP-1010, 1:1000), and anti-Mef2c (Santa Cruz #SC313, Biorbyt #orb256682 both 1:1000). Antigen retrieval was performed by heating slides containing heart sections at 85°C in 10 mM sodium citrate buffer (pH 6) for 15 min. On mouse paraffin sections: After o/n fixation in 4% PFA, hearts were washed in PBS twice, dehydrated in EtOH and Xylene and embedded in paraffin. Serial sections were made at 6µm. Antigen retrieval was performed by heating slides containing heart sections under pressure at 120°C in 10 mM sodium citrate buffer (pH 6) for 1 hour. Primary antibodies used were anti-HMGA1 (Santa Cruz #sc393213), anti-HA (Abcam #ab9111) and anti-PCM (Sigma #HPA023370). EdU was visualized with the Click-iT EdU Cell Proliferation Imaging Kit, Alexa Fluor 647, ThermoFisher, #C10340, according to the instructions. For both mouse and zebrafish tissue, Secondary antibodies include Anti-chicken Alexa488 (Thermofisher, #A21133, 1:500), anti-rabbit Alexa555 (Thermofisher, #A21127, 1:500), anti-mouse Cy5 (Jackson ImmunoR, #118090, 1:500) used at a dilution of 1:500. DAB staining was performed using the DAB Substrate Kit (SK-4100) (Vector laboratories). Nuclei were shown by DAPI (4',6-diamidino-2-phenylindole) staining. Images of immunofluorescence stainings are single optical planes acquired with a Leica Sp8 microscope.

Quantification and statistics

All data was quantified in a double-blinded fashion. Unless stated otherwise, statistical testing was performed by unpaired T-tests. Histological quantifications of border-zone specific populations was performed on cardiomyocytes situated within 150µm from the wound border on 3 sections per heart, of at least 3 hearts. qPCR results comparing *Hmga1* expression throughout postnatal development (Fig.3C) was statistically tested using one-way ANOVA and Dunnett's multiple comparison test. qPCR results comparing target gene expression at different time-points was statistically tested using two-way ANOVA.

Zebrafish Intraperitoneal injections of NRG1

Intraperitoneal injections of human recombinant NRG1 (peprotech: recombinant human heregulin-b1, catalog#:100-03) were performed as described by Kinkel et al. (Kinkel et al., 2010). Fish were sedated using MS222 (0.032% wt/vol). Injections were performed using a

Hamilton syringe (Gauge 30), cleaned before use by washing in 70% ethanol followed by 2 washes in PBS. Injection volumes were adjusted on the weight of the fish (30ul/g) and a single injection contained 60 ug/kg of human recombinant NRG1 (diluted in PBS/BSA 0.1%).

Tomo-Sequencing

Under a fluorescent stereoscope, injured mouse hearts were isolated and cut open longitudinally and tissue was selected based on the katushka signal. Tissue was isolated from the injured hearts (n=3) containing part of the injury, katushka signal and part of the remote myocardium respectively. Tomo-seq was conducted as previously described (Junker et al., 2014) whereby the tissue was embedded in Jung tissue freezing medium (Leica), sectioned at 20um from the injured area to the remote myocardium, of which every fifth section was collected into a single tube. RNA was extracted from each tube using Trizol (Ambion) after adding a defined amount of spike-in RNA to correct for technical variations during the downstream processing. RNA-seq was performed as previously described (Junker et al., 2014) including the reverse transcription using primers containing a tube-specific barcode. The barcoding of the cDNA allowed for the pooling of material, since the barcode could later be used to determine the positional origin of the labeled transcript. The pooling of cDNA was followed by linear amplification and sequencing.

Single cell RNA sequencing

Tg(nppa:mCitrine) positive cells showing high mCitrine expression were isolated from cyoinjured zebrafish hearts (7 days post injury). From 12 hmga1a^{-/-} mutant hearts, 768 cells were isolated. From 12 hmga1a^{+/+} wild-type hearts, 768 cells were isolated. Single-cell sequencing libraries were prepared using SORT-seq (Muraro et al., 2016). Live cells were sorted into 384-well plates with Vapor-Lock oil containing a droplet with barcoded primers, spike-in RNA and dNTPs, followed by heat-induced cell lysis and cDNA syntheses using a robotic liquid handler. Primers consisted of a 24 bp polyT stretch, a 4 bp random molecular barcode (UMI), a cell-specific 8 bp barcode, the 5' Illumina TruSeq small RNA kit adapter and a T7 promoter. After cell-lysis for 5 min at 65°C, RT and second strand mixes were distributed with the Nanodrop II liquid handling platform (Inovadyne). After pooling all cells in one library, the aqueous phase was separated from the oil phase, followed by IVT transcription. The CEL-Seq2 protocol was used for library prep (Hashimshony et al., 2016). Illumina sequencing libraries were prepared with the TruSeq small RNA primers (Illumina) and paired-end sequenced at 75 bp read length on the Illumina NextSeq platform.

ATAC- and RNA-sequencing

Nuclei isolation was performed on whole zebrafish hearts 14 days post tamoxifen treatment. Fish either contained 3 transgenes allowing cardiomyocyte specific overexpression of hmga1a-eGFP tg(ubi:Loxp-stop-Loxp-hmga1a-eGFP); Tg(myI7:DsRed2-NLS); Tg(myI7:CreER)pd10 or formed the control fish containing only two transgenes

(Tg(my17:DsRed2-NLS); Tg(my17:CreER)pd10). A total of 50,000 DsRed positive control nuclei were sorted as well as 45,000 DsRed/GFP+ hmga1a nuclei, both originating from 20 hearts each. DNA was isolated, treated with transposase TDE1 (Nextera Tn5 Transposase from Nextera kit; Illumina, cat. no. FC-121-1030) as described previously in (Buenrostro et al., 2015). Illumina sequencing libraries were generated and sequenced using the NextSeq platform. Bulk RNA-sequencing was performed on whole zebrafish ventricles 14 days post tamoxifen treatment. Fish either contained 2 transgenes allowing cardiomyocyte specific overexpression of hmga1a-eGFP tg(ubi:Loxp-stop-Loxp-hmga1a-eGFP); Tg(my17:CreER)pd10 or formed the control fish containing only one transgenes (Tg(my17:CreER)pd10). Each biological replicate (5 overexpressing and 5 control conditions) were produced out of 3 pooled hearts each. RNA was isolated using Trizol (Ambion). Library preparation was performed following the CEL-Seq1 protocol described in (Junker et al., 2014). Again, Illumina sequencing libraries were generated and sequenced using the NextSeq platform.

Bioinformatical analysis: Tomo-sequencing data

Mapping was performed against the zebrafish reference assembly version 9 (Zv9) and the mouse reference assembly version 9 (mm9). The Tomo-Sequencing analysis was done based on the log₂-transformed fold-change (zlf_c) of the Z score (number of standard deviations above the mean) of all genes. Bioinformatic analyses were largely performed with R software using custom-written code (R Core Team, 2013). Hierarchical cluster analysis on the entire dataset (after Z score transformation) was performed on all genes with a peak in >4 consecutive sections (Z score > 1). Based on hierarchial clustering analysis, together with maker gene expression (BZ markers *Nppa*, *Nppb*, *Des*), we defined the locations of the injury area (IA), border zone (BZ) and remote myocardium (RM) within our datasets. To transcriptionally compare the zebrafish and mouse border zone, we first pooled all injury area, border zone and remote zone regions from the different timepoints into one species specific dataset per species, resulting in 14 (IA), 43 (BZ) and 43 (RM) sections in the zebrafish dataset and 14 (IA), 65 (BZ) and 54 (RM) sections in the mouse dataset. Gene ontology analysis was performed on these combined lists using the R package edgeR (Robinson et al., 2009). These gene lists were subjected to GO analysis using the online tool DAVID (D. W. Huang et al., 2009). The transcriptional comparison between the zebrafish and mouse border zone was performed by scatterplotting annotated gene-pairs annotated in Ensembl(v89). Genes with no annotated homolog were excluded from analysis. Genes with multiple annotated homologs were plotted as separate gene pairs.

Next, gene pairs were selected using the following tresholds; Upregulated in both the mouse and zebrafish BZ: Zebrafish log₂FC > 0.5, P.val < 0.05 ; Mouse: log₂FC > 0.5, P.val < 0.05. Downregulated in both the mouse and zebrafish BZ: Zebrafish: log₂FC < -0.5, P.val < 0.05 ; Mouse: log₂FC < -0.5, P.val < 0.05. Upregulated in the zebrafish BZ, but not the mouse BZ: Zebrafish: log₂FC > 0.5, P.val < 0.05 ; Mouse: log₂FC < 0. Upregulated in the mouse BZ, but

not the zebrafish BZ: Zebrafish: $\log_{FC} < 0$; Mouse: $\log_{FC} > 0.5$, $P_{val} < 0.05$. Furthermore, after determining the zebrafish and mouse specific gene-pairs, gene-pairs were removed of which at least one paralogous gene showed expression outside of the selection thresholds, accounting for redundant functions between paralogous genes. These gene-pairs were subjected to GO analysis using their mouse name in the online tool DAVID (D. W. Huang et al., 2009). All datasets can be accessed via the tomo-seq web site (<http://mouse.genomes.nl/tomoseq/2018>). Username: tomodata ; Password: mouseheart18).

Bioinformatical analysis: Single-cell RNA sequencing data

In total, eight 384-well plates were sequenced, containing one cell per well. Four plates were obtained per genotype (*hmga1a*^{-/-} or wild-type). Sequencing one of the wild-type containing plates failed, hence no data was obtained. Mapping was performed against the zebrafish reference assembly version 9 (Zv9). Based on the distribution of the log₁₀ total reads plotted against the frequency, we introduced a cutoff at minimally 600 reads per cell before further analysis, reducing the amount of analysed cells to 653 wild-type and 658 *hmga1a*^{-/-} cells (1311 cells in total). Batch-effects were analyzed and showed a good overlap in the scRNAseq data from the plates containing cells from the same genotype. Next, the single cell RNA sequencing data was analyzed using an updated version (RaceID2) of the previously published RaceID algorithm (Grün et al., 2015), resulting in the characterization of 6 main cell clusters with transcriptionally distinct characteristics. To identify modules of co-expressed genes along a specific differentiation trajectory (defined as a succession of significant links between clusters as identified by StemID, as previously published (Grün et al., 2016) all cells assigned to these links were assembled in pseudo-temporal order based on their projection coordinate. Next, all genes that are not present with at least two transcripts in at least a single cell are discarded from the sub-sequent analysis. Next, a local regression of the z-transformed expression profile for each gene is computed along the differentiation trajectory. These pseudo-temporal gene expression profiles are topologically ordered by computing a one-dimensional self-organizing map (SOM) with 1000 nodes. Due to the large number of nodes relative to the number of clustered profiles, similar profiles are assigned to the same node. Only nodes with more than three assigned profiles are retained for visualization of co-expressed gene modules. Neighboring nodes with average profiles exhibiting a Pearson's correlation coefficient >0.9 are merged to common gene expression modules. These modules are depicted in the final pseudo-temporal map. Analyses were performed as previously published (Grün et al., 2016).

Bioinformatical analysis: ATAC- and RNA-sequencing data

Both ATAC- and RNA-seq data was mapped against the zebrafish reference assembly version 10 (DanRer10). The ATAC-sequencing data were uploaded to the Galaxy web platform, and we used the public server at usegalaxy.org to analyze the data (Afgan et al., 2016). Mapping of the ATAC-sequencing data was done with Bowtie2. Peaks were

called using MACS2 peak calling, using a minimum q-value of 0.05 (minimum FDR) cutoff to call significant regions. Q-values were calculated from p-values using Benjamini-Hochberg procedure (--qvalue). The genomic distribution of accessible regions was defined using annotations of Ensembl BioMart, DanRer10 build. For promoter accessibility analysis the ATAC-seq signal was distributed into promoter bins defined as 1500bp upstream and 500bp of the canonical TSS (BioMart, DanRer10 build). Motif enrichment analysis was performed using the web based MEME suite tool Analysis of Motif Enrichment (AME v5.3.0) ((Bailey et al., 2009; McLeay & Bailey, 2010). The RNA-sequencing data contained a total of 27996054 reads over 10 conditions (5 times overexpression and 5 control conditions, produced out of 3 pooled hearts per conditions). Due to low read-count ($<1 \times 10^6$ reads), one overexpression and one control conditions were excluded from analysis, resulting in a dataset of 8 biological replicates with a total read count of 26646640 reads. Total read normalization was performed, as well as normalization against spiked-in control RNA to account for technical variation in RNA-isolation between the different conditions. Differentially expressed genes were obtained from the RNA-sequencing data using the R package edgeR (Robinson et al., 2009). These gene lists were subjected to GO analysis using the online tool DAVID (D. W. Huang et al., 2009).

REFERENCES

- Afgan, E., Baker, D., van den Beek, M., Blankenberg, D., Bouvier, D., Čech, M., Chilton, J., Clements, D., Coraor, N., Eberhard, C., Grüning, B., Guerler, A., Hillman-Jackson, J., Von Kuster, G., Rasche, E., Soranzo, N., Turaga, N., Taylor, J., Nekrutenko, A., & Goecks, J. (2016). The Galaxy platform for accessible, reproducible and collaborative biomedical analyses: 2016 update. *Nucleic Acids Research*, *44*(W1), W3–W10. <https://doi.org/10.1093/nar/gkw343>
- Bailey, T. L., Boden, M., Buske, F. A., Frith, M., Grant, C. E., Clementi, L., Ren, J., Li, W. W., & Noble, W. S. (2009). MEME Suite: Tools for motif discovery and searching. *Nucleic Acids Research*. <https://doi.org/10.1093/nar/gkp335>
- Battista, S., Pentimalli, F., Baldassarre, G., Fedele, M., Fidanza, V., Croce, C. M., & Fusco, A. (2003). Loss of Hmga1 gene function affects embryonic stem cell lympho-hematopoietic differentiation. *The FASEB Journal: Official Publication of the Federation of American Societies for Experimental Biology*. <https://doi.org/10.1096/fj.02-0977je>
- Beisaw, A., Kuenne, C., Guenther, S., Dallmann, J., Wu, C. C., Bentsen, M., Looso, M., & Stainier, D. Y. R. (2020). AP-1 Contributes to Chromatin Accessibility to Promote Sarcomere Disassembly and Cardiomyocyte Protrusion during Zebrafish Heart Regeneration. *Circulation Research*. <https://doi.org/10.1161/CIRCRESAHA.119.316167>
- Bergmann, O., Bhardwaj, R. D., Bernard, S., Zdunek, S., Barnabé-Heide, F., Walsh, S., Zupicich, J., Alkass, K., Buchholz, B. A., Druid, H., Jovinge, S., & Frisén, J. (2009). Evidence for cardiomyocyte renewal in humans. *Science*. <https://doi.org/10.1126/science.1164680>
- Bish, L. T., Morine, K., Sleeper, M. M., Sanmiguel, J., Wu, D., Gao, G., Wilson, J. M., & Sweeney, H. L. (2008). Adeno-associated virus (AAV) serotype 9 provides global cardiac gene transfer superior to AAV1, AAV6, AAV7, and AAV8 in the mouse and rat. *Human Gene Therapy*. <https://doi.org/10.1089/hum.2008.123>
- Buenrostro, J. D., Giresi, P. G., Zaba, L. C., Chang, H. Y., & Greenleaf, W. J. (2013). Transposition of native chromatin for fast and sensitive epigenomic profiling of open chromatin, DNA-binding proteins and nucleosome position. *Nature Methods*, *10*(12), 1213–1218. <https://doi.org/10.1038/nmeth.2688>
- Catez, F., Yang, H., Tracey, K. J., Reeves, R., Misteli, T., & Bustin, M. (2004). Network of Dynamic Interactions between Histone H1 and High-Mobility-Group Proteins in Chromatin. *Molecular and Cellular Biology*. <https://doi.org/10.1128/mcb.24.10.4321-4328.2004>
- Chablais, F., & Jaźwińska, A. (2012). The regenerative capacity of the zebrafish heart is dependent on TGFβ signaling. *Development*, *139*(11), 1921–1930. <https://doi.org/10.1242/dev.078543>
- Chiefari, E., Foti, D. P., Sgarra, R., Pegoraro, S., Arcidiacono, B., Brunetti, F. S., Greco, M., Manfioletti, G., & Brunetti, A. (2018). Transcriptional regulation of glucose metabolism: The emerging role of the HMGA1 chromatin factor. *Frontiers in Endocrinology*, *9*(JUL), 1–14. <https://doi.org/10.3389/fendo.2018.00357>
- Chiefari, E., Nevolo, M. T., Arcidiacono, B., Maurizio, E., Nocera, A., Iritano, S., Sgarra, R., Possidente, K., Palmieri, C., Paonessa, F., Brunetti, G., Manfioletti, G., Foti, D., & Brunetti, A. (2012). HMGA1 is a novel downstream nuclear target of the insulin receptor signaling pathway. *Scientific Reports*, *2*, 1–10. <https://doi.org/10.1038/srep00251>
- Cui, M., Wang, Z., Chen, K., Shah, A. M., Tan, W., Duan, L., Sanchez-Ortiz, E., Li, H., Xu, L., Liu, N., Bassel-Duby, R., & Olson, E. N. (2020). Dynamic Transcriptional Responses to Injury of Regenerative and Non-regenerative Cardiomyocytes Revealed by Single-Nucleus RNA Sequencing. *Developmental Cell*. <https://doi.org/10.1016/j.devcel.2020.02.019>
- Currie, R. A. (1997). Functional interaction between the DNA binding subunit trimerization domain of NF-Y and the high mobility group protein HMG-I(Y). *Journal of Biological Chemistry*. <https://doi.org/10.1074/jbc.272.49.30880>
- D'Uva, G., Aharonov, A., Lauriola, M., Kain, D., Yahalom-Ronen, Y., Carvalho, S., Weisinger, K., Bassat, E., Rajchman, D., Yifa, O., Lysenko, M., Konfino, T., Hegesh, J., Brenner, O., Neeman, M., Yarden, Y., Leor, J., Sarig, R., Harvey, R. P., & Tzahor, E. (2015). ERBB2 triggers mammalian heart regeneration by promoting cardiomyocyte dedifferentiation and proliferation. *Nature Cell Biology*, *17*(5). <https://doi.org/10.1038/ncb3149>
- Dement, G. A., Maloney, S. C., & Reeves, R. (2007). Nuclear HMGA1 nonhistone chromatin proteins directly influence mitochondrial transcription, maintenance, and function. *Experimental Cell Research*, *313*(1), 77–87. <https://doi.org/10.1016/j.yexcr.2006.09.014>
- Fukuda, R., Marín-Juez, R., El-Sammak, H., Beisaw, A., Ramadass, R., Kuenne, C., Guenther, S., Konzer, A., Bhagwat, A. M., Graumann, J., & Stainier, D. Y. (2020). Stimulation of glycolysis

- promotes cardiomyocyte proliferation after injury in adult zebrafish. *EMBO Reports*. <https://doi.org/10.15252/embr.201949752>
- Gemberling, M., Karra, R., Dickson, A. L., & Poss, K. D. (2015a). Nrg1 is an injury-induced cardiomyocyte mitogen for the endogenous heart regeneration program in zebrafish. *ELife*, 2015(4), 1–17. <https://doi.org/10.7554/eLife.05871>
- Gemberling, M., Karra, R., Dickson, A. L., & Poss, K. D. (2015b). Nrg1 is an injury-induced cardiomyocyte mitogen for the endogenous heart regeneration program in zebrafish. *ELife*, 4, 1–17. <https://doi.org/10.7554/eLife.05871>
- Gladka, M. M., Kohela, A., Molenaar, B., Versteeg, D., Kooijman, L., Monshouwer-Kloots, J., Kremer, V., Vos, H. R., Huibers, M. M. H., Haigh, J. J., Huylebroeck, D., Boon, R. A., Giacca, M., & van Rooij, E. (2021). Cardiomyocytes stimulate angiogenesis after ischemic injury in a ZEB2-dependent manner. *Nature Communications*, 12(1). <https://doi.org/10.1038/s41467-020-20361-3>
- González-Rosa, J. M., Sharpe, M., Field, D., Soonpaa, M. H., Field, L. J., Burns, C. E., & Burns, C. G. (2018). Myocardial Polyploidization Creates a Barrier to Heart Regeneration in Zebrafish. *Developmental Cell*, 44(4), 433–446.e7. <https://doi.org/10.1016/j.devcel.2018.01.021>
- Grün, D., Lyubimova, A., Kester, L., Wiebrands, K., Basak, O., Sasaki, N., Clevers, H., & van Oudenaarden, A. (2015). Single-cell messenger RNA sequencing reveals rare intestinal cell types. *Nature*, 525(7568), 251–255. <https://doi.org/10.1038/nature14966>
- Grün, D., Muraro, M. J., Boisset, J. C., Wiebrands, K., Lyubimova, A., Dharmadhikari, G., van den Born, M., van Es, J., Jansen, E., Clevers, H., de Koning, E. J. P., & van Oudenaarden, A. (2016). De Novo Prediction of Stem Cell Identity using Single-Cell Transcriptome Data. *Cell Stem Cell*, 19(2), 266–277. <https://doi.org/10.1016/j.stem.2016.05.010>
- Heallen, T., Morikawa, Y., Leach, J., Tao, G., Willerson, J. T., Johnson, R. L., & Martin, J. F. (2013). Hippo signaling impedes adult heart regeneration. *Development*, 140(23), 4683–4690. <https://doi.org/10.1242/dev.102798>
- Honkoop, H., de Bakker, D. E. M., Aharonov, A., Kruse, F., Shakked, A., Nguyen, P. D., de Heus, C., Garric, L., J Muraro, M., Shoffner, A., Tessadori, F., Peterson, J. C., Noort, W., Bertozzi, A., Weidinger, G., Posthuma, G., Grün, D., van der Laarse, W. J., Klumperman, J., ... Bakkers, J. (2019). Single-cell analysis uncovers that metabolic reprogramming by ErbB2 signaling is essential for cardiomyocyte proliferation in the regenerating heart. *ELife*, 8, 1–27. <https://doi.org/10.7554/eLife.50163>
- Huang, D. W., Lempicki, R. a, & Sherman, B. T. (2009). Systematic and integrative analysis of large gene lists using DAVID bioinformatics resources. *Nature Protocols*, 4(1), 44–57. <https://doi.org/10.1038/nprot.2008.211>
- Huang, Y., Harrison, M. R., Osorio, A., Kim, J., Baugh, A., Duan, C., Suvoc, H. M., & Lien, C.-L. (2013). Igf Signaling is Required for Cardiomyocyte Proliferation during Zebrafish Heart Development and Regeneration. *PLoS One*, 8(6), e67266. <https://doi.org/10.1371/journal.pone.0067266>
- Ikeuchi, M., Tsutsui, H., Shiomi, T., Matsusaka, H., Matsushima, S., Wen, J., Kubota, T., & Takeshita, A. (2004). Inhibition of TGF- β signaling exacerbates early cardiac dysfunction but prevents late remodeling after infarction. *Cardiovascular Research*. <https://doi.org/10.1016/j.cardiores.2004.07.017>
- Jopling, C., Sleep, E., Raya, M., Martí, M., Raya, A., & Belmonte, J. C. I. (2010). Zebrafish heart regeneration occurs by cardiomyocyte dedifferentiation and proliferation. *Nature*, 464(7288), 606–609. <https://doi.org/10.1038/nature08899>
- Junker, J. P., No??l, E. S., Guryev, V., Peterson, K. A., Shah, G., Huisken, J., McMahon, A. P., Berezikov, E., Bakkers, J., & Van Oudenaarden, A. (2014). Genome-wide RNA Tomography in the Zebrafish Embryo. *Cell*, 159(3), 662–675. <https://doi.org/10.1016/j.cell.2014.09.038>
- Kikuchi, K., Holdway, J. E., Werdich, A. A., Anderson, R. M., Fang, Y., Egnaczyk, G. F., Evans, T., Macrae, C. A., Stainier, D. Y. R., & Poss, K. D. (2010). Primary contribution to zebrafish heart regeneration by gata4(+) cardiomyocytes. *Nature*, 464(7288), 601–605. <https://doi.org/10.1038/nature08804>
- Kishi, Y., Fujii, Y., Hirabayashi, Y., & Gotoh, Y. (2012). HMGA regulates the global chromatin state and neurogenic potential in neocortical precursor cells. *Nature Neuroscience*. <https://doi.org/10.1038/nn.3165>
- Kretschmar, K., Post, Y., Bannier-Hélaouët, M., Mattiotti, A., Drost, J., Basak, O., Li, V. S. W., van den Born, M., Gunst, Q. D., Versteeg, D., Kooijman, L., van der Elst, S., van Es, J. H., van Rooij, E., van den Hoff, M. J. B., & Clevers, H. (2018). Profiling proliferative cells and their progeny in damaged murine hearts. *Proceedings of the National Academy of Sciences of the United States of America*. <https://doi.org/10.1073/pnas.1805829115>
- Lacruz, G. P. A., Junker, J. P., Gladka, M. M., Molenaar, B., Scholman, K. T., Vigil-Garcia, M., Versteeg,

- D., de Ruiter, H., Vermunt, M. W., Creighton, M. P., Huibers, M. M. H., de Jonge, N., van Oudenaarden, A., & van Rooij, E. (2017). Tomo-seq Identifies SOX9 as a Key Regulator of Cardiac Fibrosis During Ischemic Injury. *Circulation*. <https://doi.org/10.1161/CIRCULATIONAHA.117.027832>
- Leach, J. P., Heallen, T., Zhang, M., Rahmani, M., Morikawa, Y., Hill, M. C., Segura, A., Willerson, J. T., & Martin, J. F. (2017a). Hippo pathway deficiency reverses systolic heart failure after infarction. *Nature*. <https://doi.org/10.1038/nature24045>
- Leach, J. P., Heallen, T., Zhang, M., Rahmani, M., Morikawa, Y., Hill, M. C., Segura, A., Willerson, J. T., & Martin, J. F. (2017b). Hippo pathway deficiency reverses systolic heart failure after infarction. *Nature*, 550(7675), 260–264. <https://doi.org/10.1038/nature24045>
- Lin, Z., Von Gise, A., Zhou, P., Gu, F., Ma, Q., Jiang, J., Yau, A. L., Buck, J. N., Gouin, K. A., Van Gorp, P. R. R., Zhou, B., Chen, J., Seidman, J. G., Wang, D. Z., & Pu, W. T. (2014). Cardiac-specific YAP activation improves cardiac function and survival in an experimental murine MI model. *Circulation Research*, 115(3), 354–363. <https://doi.org/10.1161/CIRCRESAHA.115.303632>
- McLeay, R. C., & Bailey, T. L. (2010). Motif Enrichment Analysis: A unified framework and an evaluation on ChIP data. *BMC Bioinformatics*. <https://doi.org/10.1186/1471-2105-11-165>
- Muraro, M. J., Dharmadhikari, G., Grün, D., Groen, N., Dielen, T., Jansen, E., van Gorp, L., Engelse, M. A., Carlotti, F., de Koning, E. J. P., & van Oudenaarden, A. (2016). A Single-Cell Transcriptome Atlas of the Human Pancreas. *Cell Systems*, 3(4), 385–394.e3. <https://doi.org/10.1016/j.cels.2016.09.002>
- Okada, H., Takemura, G., Kosai, K. I., Li, Y., Takahashi, T., Esaki, M., Yuge, K., Miyata, S., Maruyama, R., Mikami, A., Minatoguchi, S., Fujiwara, T., & Fujiwara, H. (2005). Postinfarction gene therapy against transforming growth factor- β signal modulates infarct tissue dynamics and attenuates left ventricular remodeling and heart failure. *Circulation*. <https://doi.org/10.1161/01.CIR.0000165066.71481.8E>
- Ozturk, N., Singh, I., Mehta, A., Braun, T., & Barreto, G. (2014). HMGA proteins as modulators of chromatin structure during transcriptional activation. In *Frontiers in Cell and Developmental Biology*. <https://doi.org/10.3389/fcell.2014.00005>
- Pasumarthi, K. B. S., Nakajima, H., Nakajima, H. O., Soonpaa, M. H., & Field, L. J. (2005). Targeted expression of cyclin D2 results in cardiomyocyte DNA synthesis and infarct regression in transgenic mice. *Circulation Research*, 96(1), 110–118. <https://doi.org/10.1161/01.RES.0000152326.91223.4F>
- Patterson, M., Barske, L., Van Handel, B., Rau, C. D., Gan, P., Sharma, A., Parikh, S., Denholtz, M., Huang, Y., Yamaguchi, Y., Shen, H., Allayee, H., Crump, J. G., Force, T. I., Lien, C. L., Makita, T., Lusic, A. J., Kumar, S. R., & Sucov, H. M. (2017). Frequency of mononuclear diploid cardiomyocytes underlies natural variation in heart regeneration. *Nature Genetics*. <https://doi.org/10.1038/ng.3929>
- Porrello, E. R., Mahmoud, A. I., Simpson, E., Hill, J. A., Richardson, J. A., Olson, E. N., & Sadek, H. A. (2011). Transient regenerative potential of the neonatal mouse heart. *Science*. <https://doi.org/10.1126/science.1200708>
- Poss, K. D., Wilson, L. G., & Keating, M. T. (2002). Heart regeneration in zebrafish. *Science (New York, N.Y.)*, 298(5601), 2188–2190. <https://doi.org/10.1126/science.1077857>
- Reeves, R. (2001). Molecular biology of HMGA proteins: hubs of nuclear function. *Gene*, 277(1–2), 63–81. [https://doi.org/10.1016/s0378-1119\(01\)00689-8](https://doi.org/10.1016/s0378-1119(01)00689-8)
- Robinson, M. D., McCarthy, D. J., & Smyth, G. K. (2009). edgeR: A Bioconductor package for differential expression analysis of digital gene expression data. *Bioinformatics*, 26(1), 139–140. <https://doi.org/10.1093/bioinformatics/btp616>
- Sergeeva, I. A., Hooijkaas, I. B., Van Der Made, I., Jong, W. M. C., Creemers, E. E., & Christoffels, V. M. (2014). A transgenic mouse model for the simultaneous monitoring of ANF and BNP gene activity during heart development and disease. *Cardiovascular Research*, 101(1), 78–86. <https://doi.org/10.1093/cvr/cvt228>
- Shah, S. N., Kerr, C., Cope, L., Zambidis, E., Liu, C., Hillion, J., Belton, A., Huso, D. L., & Resar, L. M. S. (2012). HMGA1 Reprograms Somatic Cells into Pluripotent Stem Cells by Inducing Stem Cell Transcriptional Networks. *PLoS ONE*. <https://doi.org/10.1371/journal.pone.0048533>
- Sukonina, V., Ma, H., Zhang, W., Bartesaghi, S., Subhash, S., Heglind, M., Foyn, H., Betz, M. J., Nilsson, D., Lidell, M. E., Naumann, J., Hauf-Brusberg, S., Palmgren, H., Mondal, T., Beg, M., Jedrychowski, M. P., Taskén, K., Pfeifer, A., Peng, X. R., ... Enerbäck, S. (2019). FOXK1 and FOXK2 regulate aerobic glycolysis. *Nature*. <https://doi.org/10.1038/s41586-019-0900-5>
- van Duijvenboden, K., de Bakker, D. E. M., Man, J. C. K., Janssen, R., Günthel, M., Hill, M. C., Hooijkaas, I. B., van der Made, I., van der Kraak, P. H., Vink, A., Creemers, E. E., Martin, J. F., Barnett, P., Bakkers, J., & Christoffels, V. M. (2019). Conserved NPPB+ Border Zone Switches From MEF2- to AP-1-Driven Gene Program. *Circulation*, 140(10). <https://doi.org/10.1161/CIRCULATIONAHA.118.038944>

- Van Duijvenboden, Karel, De Bakker, D. E. M., Man, J. C. K., Janssen, R., Günthel, M., Hill, M. C., Hooijkaas, I. B., Van Der Made, I., Van Der Kraak, P. H., Vink, A., Creemers, E. E., Martin, J. F., Barnett, P., Bakkers, J., & Christoffels, V. M. (2019). Conserved NPPB + Border Zone Switches from MEF2- to AP-1-Driven Gene Program. *Circulation*, *140*(10), 864–879. <https://doi.org/10.1161/CIRCULATIONAHA.118.038944>
- WHO. (2019). *Health topics | Cardiovascular diseases*. Cardiovascular Diseases.
- Windmueller, R., Leach, J. P., Babu, A., Zhou, S., Morley, M. P., Wakabayashi, A., Petrenko, N. B., Viatour, P., & Morrissey, E. E. (2020). Direct Comparison of Mononucleated and Binucleated Cardiomyocytes Reveals Molecular Mechanisms Underlying Distinct Proliferative Competencies. *Cell Reports*. <https://doi.org/10.1016/j.celrep.2020.02.034>
- Wu, C. C., Kruse, F., Vasudevarao, M. D., Junker, J. P., Zebrowski, D. C., Fischer, K., Noël, E. S., Grün, D., Berezikov, E., Engel, F. B., van Oudenaarden, A., Weidinger, G., & Bakkers, J. (2015). Spatially Resolved Genome-wide Transcriptional Profiling Identifies BMP Signaling as Essential Regulator of Zebrafish Cardiomyocyte Regeneration. *Developmental Cell*, 36–49. <https://doi.org/10.1016/j.devcel.2015.12.010>
- Xian, L., Georgess, D., Huso, T., Cope, L., Belton, A., Chang, Y. T., Kuang, W., Gu, Q., Zhang, X., Senger, S., Fasano, A., Huso, D. L., Ewald, A. J., & Resar, L. M. S. (2017). HMGA1 amplifies Wnt signalling and expands the intestinal stem cell compartment and Paneth cell niche. *Nature Communications*. <https://doi.org/10.1038/ncomms15008>
- Xiang, F. L., Guo, M., & Yutzey, K. E. (2016). Overexpression of Tbx20 in adult cardiomyocytes promotes proliferation and improves cardiac function after myocardial infarction. *Circulation*, *133*(11), 1081–1092. <https://doi.org/10.1161/CIRCULATIONAHA.115.019357>
- Zhang, Q., & Wang, Y. (2007). Homeodomain-interacting protein kinase-2 (HIPK2) phosphorylates HMGA1a at Ser-35, Thr-52, and Thr-77 and modulates its DNA binding affinity. *Journal of Proteome Research*. <https://doi.org/10.1021/pr700571d>
- Zhang, Q., & Wang, Y. (2008). High mobility group proteins and their post-translational modifications. In *Biochimica et Biophysica Acta - Proteins and Proteomics*. <https://doi.org/10.1016/j.bbapap.2008.04.028>

SUPPLEMENTARY INFORMATION

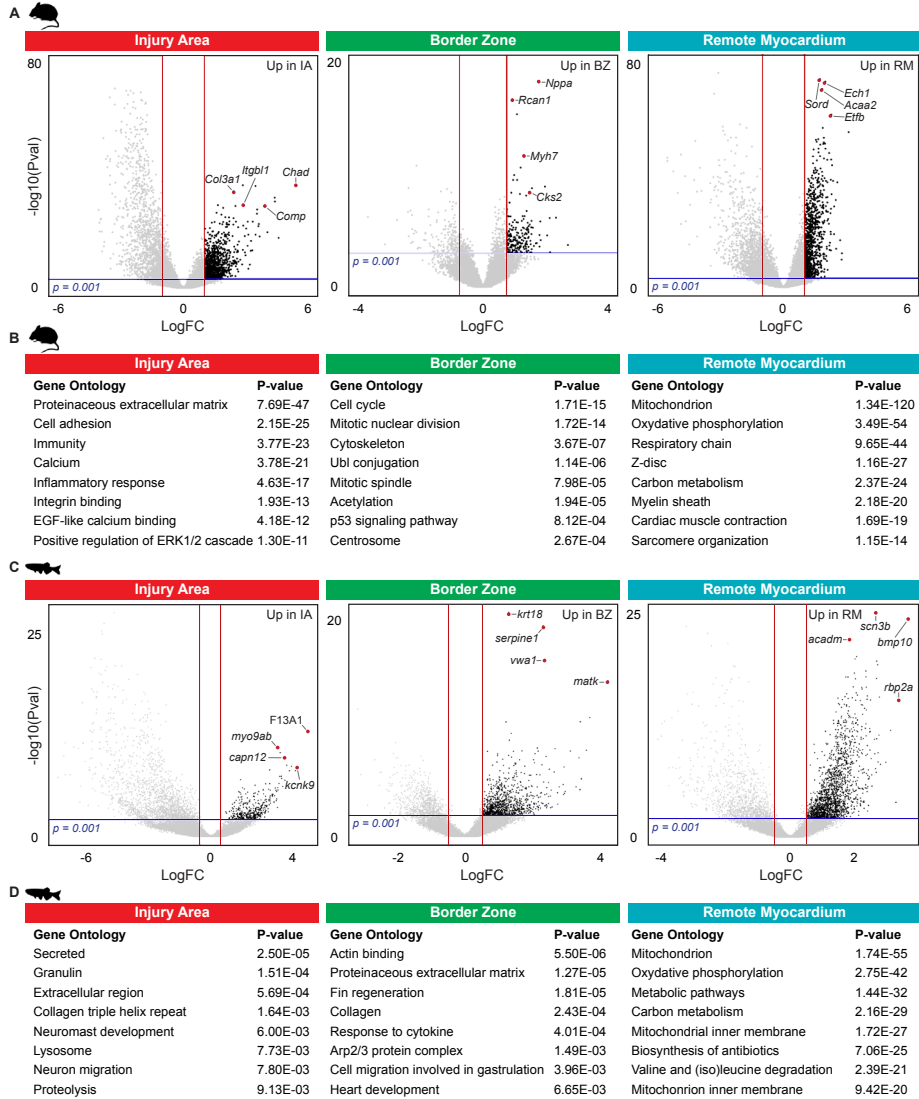


FIGURE S1. Spatial analysis reveals zone specific processes. (A,C) Vulcano plots highlighting genes differentially expressed in the injury area (left), border zone (middle) and remote myocardium (right) of the injured **(A)** mouse or **(B)** zebrafish heart. Red dots indicate representative genes per zone. Red line indicates threshold log₂ fold change and blue line indicates threshold of p-value. **(B,D)** Gene ontology analysis for differentially expressed, upregulated genes from each zone of the injured **(B)** mouse or **(D)** zebrafish heart. For the spatial analysis, datasets from individual timepoints (3, 7 and 14dpi) were merged.

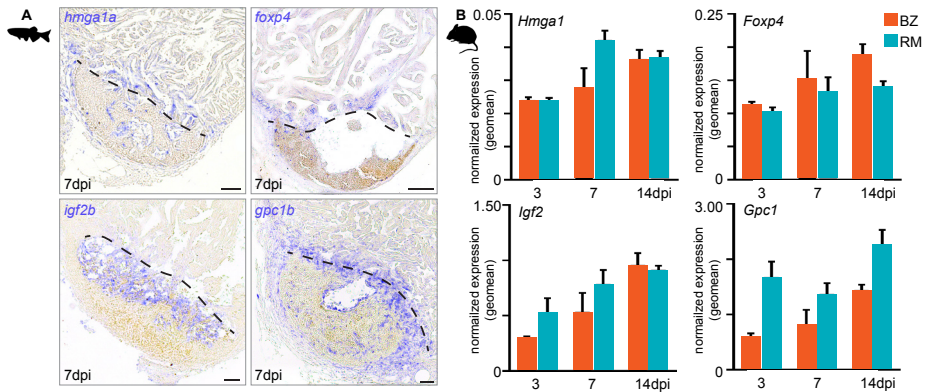


FIGURE S2. Species specific BZ gene expression identified. (A) In situ hybridization against four candidate genes. All hearts are 7 days post cryoinjury. Dotted line indicates begin of injury area. Scale bars represent 50 μ m. (B) Candidate genes were analysed with quantitative PCR on cDNA libraries obtained from isolated border zone (BZ) and remote myocardial (RM) tissue of injured mouse hearts 3, 7 or 14 days post myocardial infarction (induced by LAD occlusion). No differences between the BZ and RM was observed for *Hmga1* ($P = 0.263$), *Foxp4* ($P = 0.134$) and *Igf2* ($P = 0.143$). For *Gpc1*, a significant difference was observed where significantly higher expression is found in the RM compared to the BZ ($P < 0.001$). P-values were obtained using two-way ANOVA testing. No significant interaction of zone and dpi were observed for any of the presented genes.

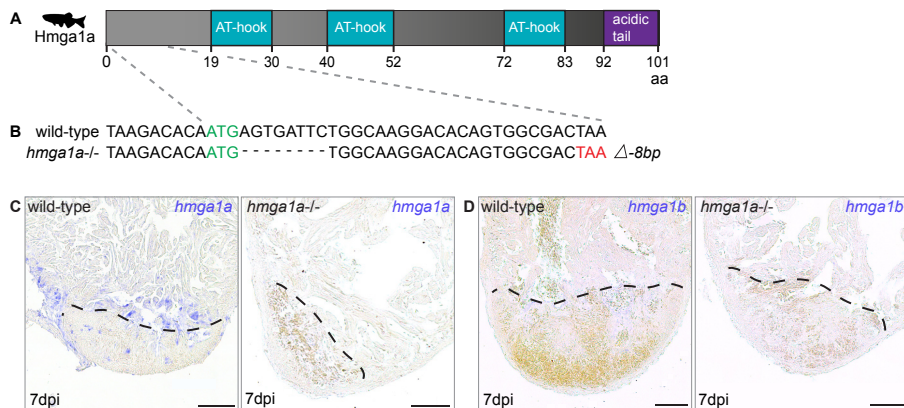


FIGURE S3. 8bp deletion causes frameshift in *hmga1a* coding region, leading to a strong reduction of *hmga1a* mRNA expression in the injury border zone. (A) *Hmga1a* protein structure, including 3 AT-hook DNA binding domains and an C-terminal acidic tail. (B) TALEN-based -8bp deletion behind the start codon (green) causing a frameshift leading to an early stop codon (red). (C, D) *In situ* hybridization against (C) *hmga1a* or (D) *hmga1b* in wild-type or *hmga1a*^{-/-} hearts. n=3 for each condition. Dotted line indicates the injury area. Scale bars represent 100 μ m.

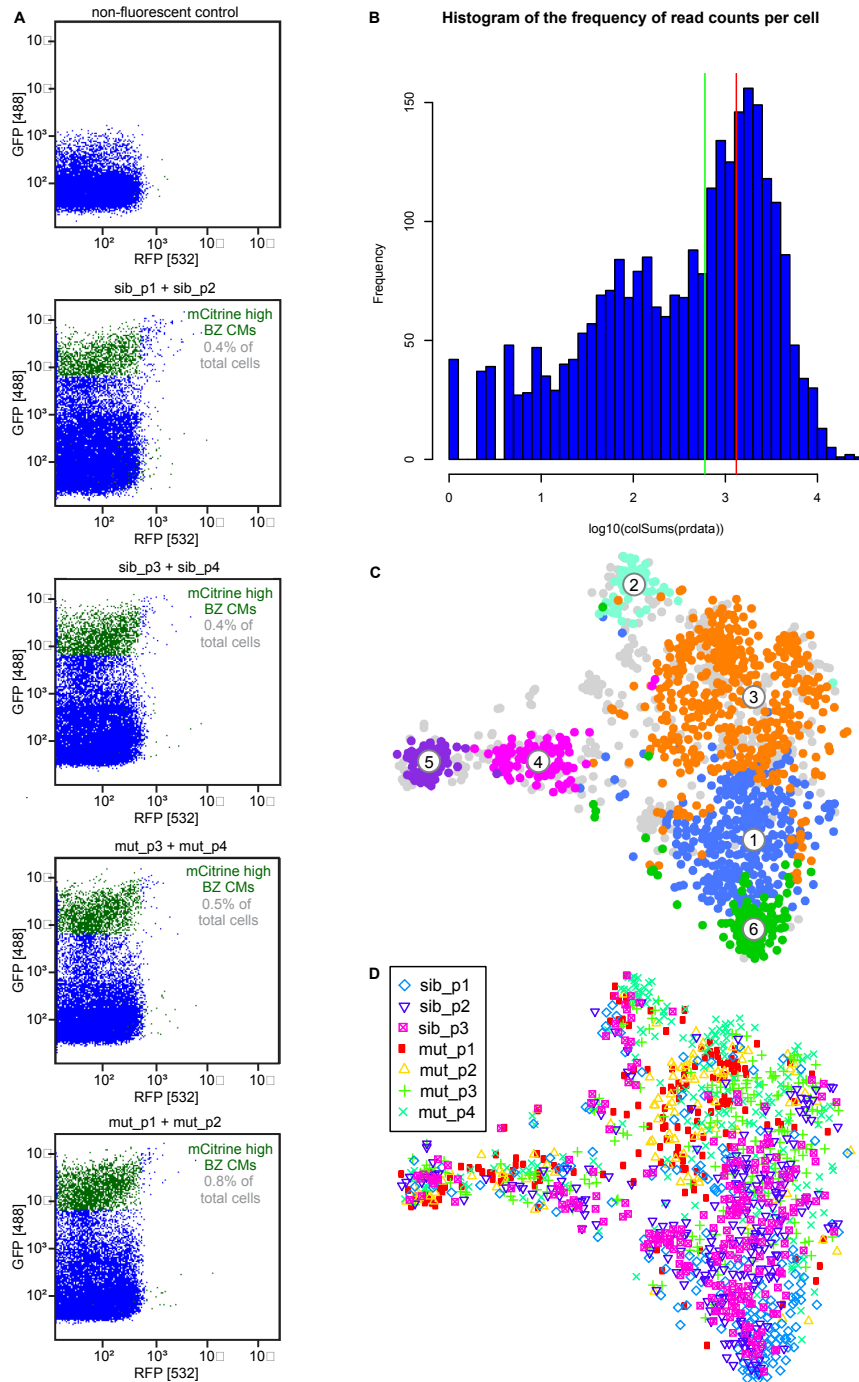


FIGURE S4. Fluorescence-activated cell sorting of mCitrine high border zone cardiomyocytes from injured *hmg1a*^{-/-} and wild-type hearts. (A) 5 tubes were processed containing single-cell suspensions obtained from 6 pooled injured hearts, 7 days post injury. These contained non-fluorescent control hearts, wild-type sibling hearts and *hmg1a*^{-/-} hearts. Two 384-well plates were sorted per tube

and processed for single-cell sequencing. BZ = border zone, CM = cardiomyocytes. **(B)** Histogram of the frequency of read counts per cell. Green line indicates the read based cut-off (at least 600 reads per cell) for the downstream analysis. The red line indicates the 1000 reads per cell threshold. **(C)** tSNE-plotting of the data results in 6 transcriptionally distinct cardiomyocyte cell clusters. **(D)** tSNE-map showing the contribution of cells from the individually sequenced plates.

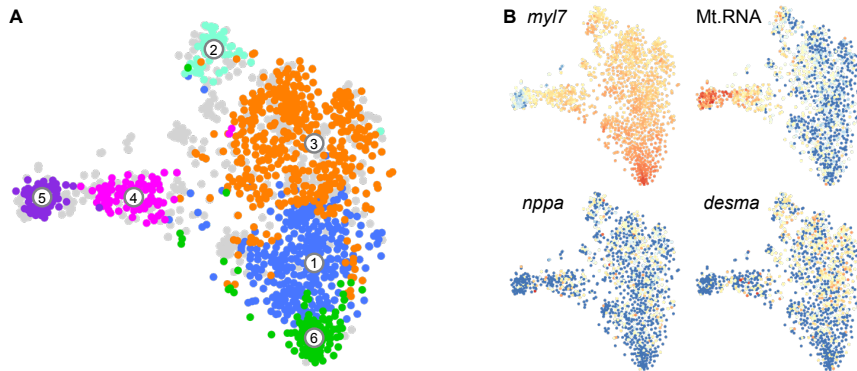


FIGURE S5. Marker gene expression. **(A)** tSNE-plotting of the data results in 6 transcriptionally distinct clusters. **(B)** tSNE maps visualizing log₂-transformed read-counts for *myl7* (cardiomyocytes), *NC_002333.17* (mitochondrial transcribed RNA) and *nppa* and *desma* (border zone markers).

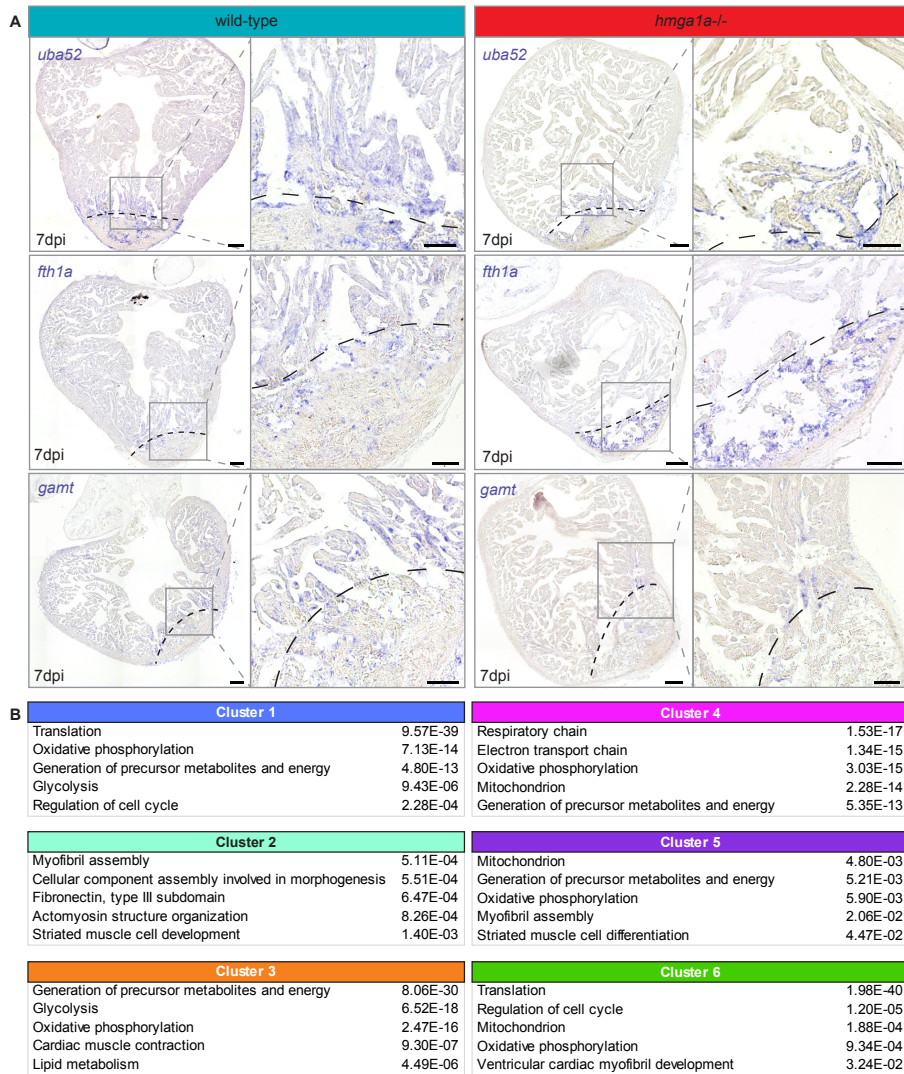
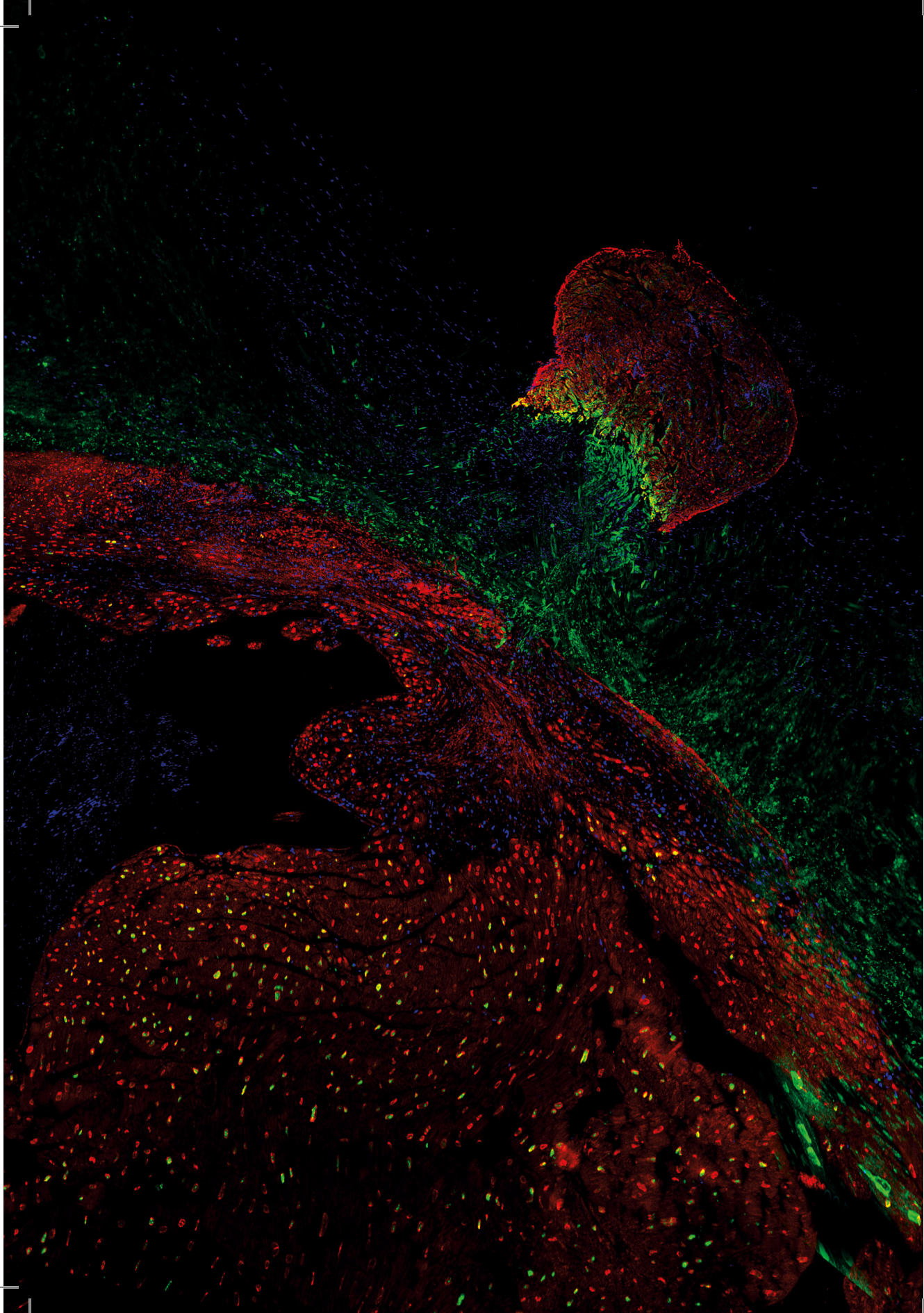


FIGURE S6. Single cell sequencing reveals *hmga1a* is required for the formation of specific sub-populations of border zone cardiomyocytes. (A) Gene ontologies representing genes showing cluster specific expression. **(B)** *In situ* hybridization against markers for t-SNE cluster 6, including *uba52*, *fth1a* and *gamt*. Dotted lines indicate the injury area. Scale bars represent 100µm in the overview and 50µm in the zoom-ins.



CHAPTER V

Prrx1b restricts fibrosis and promotes Nrg1-dependent cardiomyocyte proliferation during zebrafish heart regeneration

Dennis E.M. de Bakker^{1,#}, Mara Bouwman^{1,#}, Esther Dronkers², Filipa C. Simões³, Paul R. Riley³, Marie-José Goumans², Anke M. Smits², Jeroen Bakkens^{1,4,*}

¹Hubrecht Institute and University Medical Center Utrecht, Utrecht, The Netherlands

²Department of Cell and Chemical Biology, Leiden University Medical Centre, Leiden, the Netherlands

³Department of Physiology, Anatomy and Genetics, University of Oxford, Oxford, United Kingdom

⁴Department of Pediatric Cardiology, University Medical Centre Utrecht, Utrecht, The Netherlands

Contributed equally

* Corresponding author

Published in *Development* (2021)

ABSTRACT

Fibroblasts are activated to repair the heart following injury. Fibroblast activation in the mammalian heart leads to a permanent fibrotic scar that impairs cardiac function. In other organisms, like zebrafish, cardiac injury is followed by transient fibrosis and scar-free regeneration. The mechanisms that drive scarring versus scar-free regeneration are not well understood. Here we show that the homeo-box containing transcription factor Prrx1b is required for scar-free regeneration of the zebrafish heart as the loss of Prrx1b results in excessive fibrosis and impaired cardiomyocyte proliferation. Through lineage tracing and single-cell RNA-sequencing we find that Prrx1b is activated in epicardial-derived cells (EPDCs) where it restricts TGF- β ligand expression and collagen production. Furthermore, through combined *in vitro* experiments in human fetal EPDCs and *in vivo* rescue experiments in zebrafish, we conclude that Prrx1 stimulates Nrg1 expression and promotes cardiomyocyte proliferation. Collectively, these results indicate that Prrx1 is a key transcription factor that balances fibrosis and regeneration in the injured zebrafish heart.

Key words

Prrx1, Nrg1, zebrafish, heart regeneration, EPDC, fibroblast

Summary statement

In this study we find that the epicardial expressed Prrx1 ensures the balance between the fibrotic response and myocardial regeneration post injury in zebrafish.

INTRODUCTION

Regenerative capacity of damaged organs and body parts differs widely within the animal kingdom, which is particularly true for the heart (Nguyen et al., 2021; Poss, 2010). Indeed, while zebrafish display robust regeneration after heart injury, the wound response in mammalian hearts does not include replenishment of the lost myocardium. Instead, the affected myocardium is permanently lost and replaced by a fibrotic scar, which does not contribute to cardiac contraction resulting in reduced cardiac output.

The fibrotic scar is formed by cardiac fibroblasts that become activated to produce large amounts of extracellular matrix (ECM) components, like collagens. Cardiac fibroblasts mainly originate from the embryonic epicardium, which consists of a heterogeneous population of epithelial cells that cover the heart (Acharya et al., 2012; Cao et al., 2016; Gittenberger-de Groot et al., 1998; Hortells et al., 2020; Travers et al., 2016; Weinberger et al., 2020). During embryonic heart development a subset of epicardial cells undergoes an epithelial-to-mesenchymal transition (EMT) and migrates into the cardiac wall to give rise to a variety of cell types, which are commonly referred to as epicardial derived cells (EPDCs) and include predominantly cardiac fibroblasts and vascular support cells (Cao & Poss, 2018).

In contrast to mammals, adult zebrafish can fully regenerate their heart after resection or cryoinjury of 20-30% of the ventricle (Chablais et al., 2011; González-Rosa et al., 2011; Poss et al., 2002; Schnabel et al., 2011), which is due to the reactivation of proliferation in border zone cardiomyocytes (Jopling et al., 2010; Kikuchi et al., 2010; Wu et al., 2015). One of the first responses upon injury is the activation of a developmental gene expression program in the epicardium, at 1-2 days after the injury (Lepilina et al., 2006). This response becomes confined to the injury area as the epicardium is regenerated, which completely surrounds the injury area between 3 and 7 days post injury (dpi) (Kikuchi et al., 2011; Lepilina et al., 2006). The epicardium is essential for the regeneration process as ablating *tcf21*-expressing epicardial cells from the injured zebrafish heart impairs cardiomyocyte proliferation and regeneration (Wang et al., 2015). Similar to the results in the mammalian heart, lineage tracing of *wt1b* and *tcf21* expressing cells in zebrafish revealed that the embryonic epicardium gives rise to EPDCs such as cardiac fibroblasts and vascular support cells (González-Rosa et al., 2012; Kikuchi et al., 2011; Sánchez-iranzo et al., 2018). Upon injury, EPDCs secrete signals guiding regeneration such as TGF- β ligands, platelet derived growth factor, cytokines like Cxcl12 and mitogenic factors such as Nrg1 (Chablais & Jazwinska, 2012; Gemberling et al., 2015; Itou et al., 2012; Kim et al., 2010). In addition, EPDCs also contribute to fibrosis by producing ECM components such as collagen (Sánchez-iranzo et al., 2018). Fibrosis in the zebrafish heart is transient and regresses as regeneration proceeds, which coincides with the inactivation of cardiac fibroblasts, ultimately resulting in a scar-free heart (Chablais et al., 2011; Sánchez-iranzo et al., 2018). While EPDCs play important roles during fibrosis and

pro-regenerative signaling, the molecular mechanism regulating these processes remains largely unknown.

The paired related homeobox 1 (Prrx1) gene encodes a transcription factor and its expression correlates with scar-free wound healing and limb regeneration (Satoh et al., 2010; Stelnicki et al., 1998; Yokoyama et al., 2011). While its function has been studied during embryonic development, its role during wound healing or regeneration remains largely unknown. Here we find that Prrx1b expression is induced in the epicardium and EPDCs during zebrafish heart regeneration and we show that Prrx1b is required for scar-free regeneration. By single cell RNA-sequencing of EPDCs we identified that loss of *prrx1b* results in an excess of pro-fibrotic fibroblasts and fibrosis. Furthermore, we find that Prrx1b is necessary for the induction of *nrg1* signaling, which we confirmed in an *in vitro* system of human fetal EPDCs. Altogether our data indicate that Prrx1b regulates zebrafish heart regeneration by maintaining the balance between the fibrotic and regenerative response after heart injury.

RESULTS

***prrx1b* is required for zebrafish cardiomyocyte proliferation and heart regeneration**

In order to address a potential role for Prrx1 in heart regeneration we utilized *prrx1a*^{-/-} and *prrx1b*^{-/-} adult fish, which harbour non-sense mutations upstream of the conserved DNA-binding domain (Barske et al., 2016). Both *prrx1a*^{-/-} and *prrx1b*^{-/-} display no developmental defects due to redundant gene functions and only *prrx1a*^{-/-};*prrx1b*^{-/-} embryos display craniofacial defects (Barske et al., 2016). We subjected adult *prrx1a*^{-/-} and *prrx1b*^{-/-} fish to cardiac cryoinjury and analysed scar sizes at 30dpi. While we observed comparable scar sizes in wild-type and *prrx1a*^{-/-} hearts, scar sizes were significantly larger in *prrx1b*^{-/-} hearts compared to their control siblings (Fig.1A,B, Fig.S1A). This difference in scar size was still apparent at 90dpi, when wild-type hearts had completely resolved their scars (12/12) while the majority of *prrx1b*^{-/-} hearts (4/7) had not (Fig.1C). Since myocardial regeneration is achieved through proliferation of the surviving cardiomyocytes at the injury border zone, we investigated cardiomyocyte proliferation in the *prrx1a*^{-/-} and *prrx1b*^{-/-} hearts. Indeed, *prrx1b*^{-/-} hearts showed a significant reduction in border zone cardiomyocyte proliferation at 7dpi while no significant differences were observed in *prrx1a*^{-/-} hearts (Fig.1D,E, Fig. S1B,C). From these results we conclude that *prrx1b*, but not *prrx1a*, is required for zebrafish cardiomyocyte proliferation and heart regeneration.

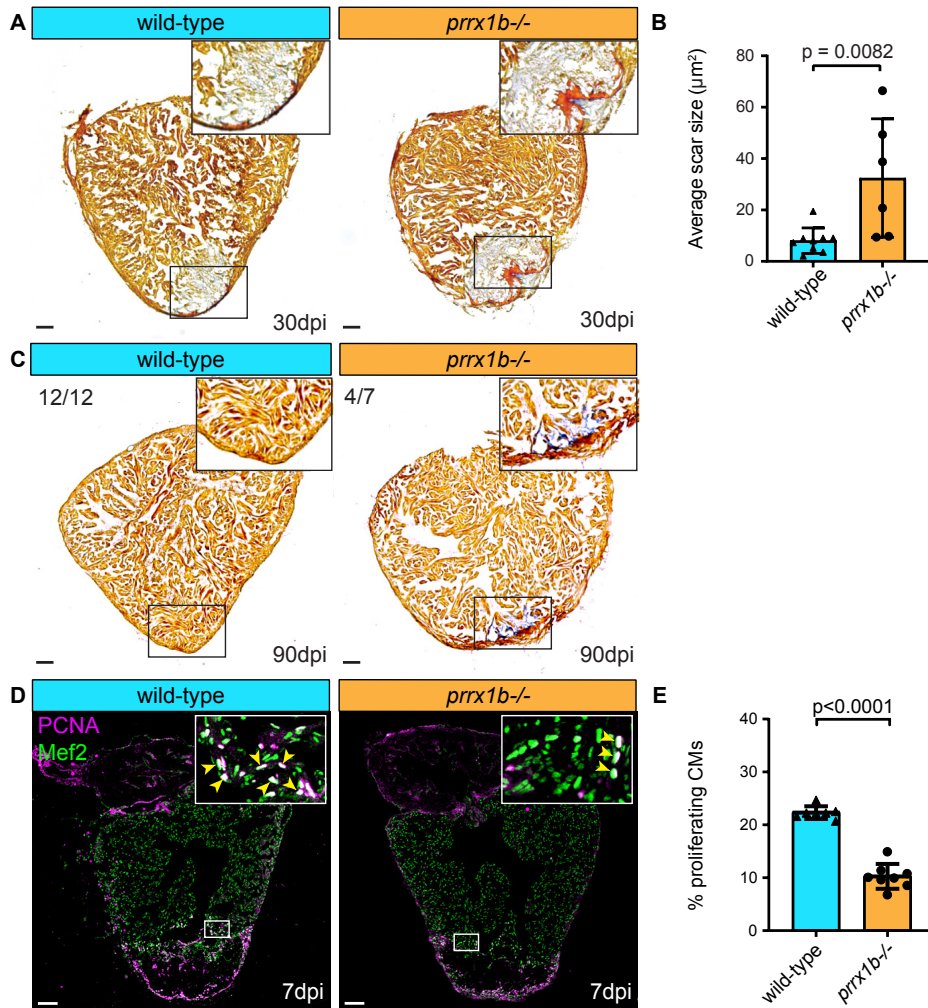


FIGURE 1. Heart regeneration and border zone cardiomyocyte proliferation is impaired in *prrx1b*^{-/-} zebrafish. (A) AFOG staining on 30dpi wild-type and *prrx1b*^{-/-} heart sections showing fibrin in red, collagen in light blue and remaining muscle tissue in orange. Scale bars represent 100μm. (B) Quantification of the remaining scar size at 30dpi between *prrx1b*^{-/-} hearts (n=6) and wild-type sibling hearts (n=9) (mean±s.d., *p*=0.0082, unpaired t-test). (C) AFOG staining on sections of 90dpi hearts. While scars were completely resolved in wild-type hearts (n=12), incomplete scar resolution was observed in *prrx1b*^{-/-} 4 out of 7 hearts. Scale bars represent 100μm. (D) Immunofluorescent staining on 7dpi wild-type and *prrx1b*^{-/-} heart sections using an anti-Mef2 antibody as a marker for cardiomyocyte nuclei, and an anti-PCNA antibody as a nuclear proliferation marker. Arrowheads in zoom-ins indicate proliferating cardiomyocytes. Scale bars represent 100μm in the overview images and 10μm in the zoom-ins. (E) Quantification of the percentage of (PCNA+) proliferating border zone cardiomyocytes between *prrx1b*^{-/-} hearts (n=8) and their wild-type siblings (n=7) (mean±s.d., *p*<0.0001, unpaired t-test).

Prrx1 is expressed in epicardial and epicardial-derived cells

To address how *Prrx1b* could function during zebrafish heart regeneration we investigated the spatial distribution of *Prrx1b* expression. By mRNA *in situ* hybridization (ISH) we only observed a very weak signal for *prrx1b* on sections of 7dpi hearts with some signal in the (sub)epicardium close to the border zone and some signal in the injury area (Fig.S2A). As these weak signals were difficult to interpret we instead used an antibody raised against the N-terminus of the axolotl *Prrx1* protein that recognizes zebrafish *Prrx1* (Gerber et al., 2018; Ocaña et al., 2017). *Prrx1* protein was mainly detected in (sub) epicardial cells covering the injury area and some sparse cells within the injury (Fig.S2B). Importantly, we could validate that the *Prrx1* antibody recognizes the zebrafish *Prrx1b* protein as injured *prrx1b*^{-/-} hearts show a near lack of the signal (Fig.S2B,C). In addition, *Prrx1* protein was nearly undetectable in uninjured zebrafish hearts (Fig.S2D), together indicating that *Prrx1* protein expression is induced upon heart injury and at 7dpi localizes in cells covering- and within the injury area.

As this localization of *Prrx1* suggested a possible expression in EPDCs we used the *Tg(tcf21:CreERT2)* line, which marks a subset of EPDCs when crossed with the ubiquitous reporter *Tg(ubi:loxP-EGFP-loxP-mCherry)* and recombined during embryonic heart development (Kikuchi et al., 2011). Hearts from embryonic recombined *Tg(tcf21:CreERT2; ubi:loxP-EGFP-loxP-mCherry)* fish were cryo-injured, extracted at different time points and analysed for *Prrx1* and mCherry expression (Fig.2A-F). At 1dpi, we observed a strong expression of *Prrx1* in the entire intact epicardium (Fig.2B), coinciding with the previously reported ventricle-wide injury response of the epicardium (Lepilina et al., 2006). At 3dpi and 7dpi, we started to observe double labelled mCherry⁺ and *Prrx1*⁺ cells around and in the injury area while *Prrx1* expression became less dense in the remote ventricle (Fig.2C,D,H). Interestingly, from 1-7dpi we observed an accumulation of mCherry/*Prrx1*⁺ cells in the regions where the (sub) epicardium is close to the border between injured and uninjured myocardium (so-called border zone, BZ), which we refer to as the BZ epicardium (Fig.2B,C,D,H). At 14dpi, we observed the majority of *Prrx1* expression in and around the injury area (Fig.2E,H). At 30dpi, only a few mCherry/*Prrx1*⁺ cells were detected, of which the majority was located at the apex and inside the remaining injury area (Fig.2F,H). Importantly, while at all timepoints *Prrx1* was mostly found in mCherry⁺ cells, not all mCherry⁺ cells were *Prrx1* positive and vice versa, confirming the previously reported heterogeneity of the epicardium and EPDCs (González-Rosa et al., 2012). To address whether other epicardial subpopulations express *Prrx1*, we analysed *Prrx1* expression in *Tg(tbx18:myr-eGFP)* and *Tg(wt1b:H2B-Dendra2)* hearts. Indeed, we observed that *Prrx1* is co-expressed with *tbx18* and *wt1b*, (Fig.S3). Taken together, these results indicate that upon cardiac injury, *Prrx1* expression is induced in *tcf21*⁺, *tbx18*⁺ and *wt1*⁺ epicardial subpopulations. *Prrx1* expression starts in the epicardium covering the remote myocardium after which it becomes more restricted to the injury epicardium followed by expression in EPDCs localized in the injury area at later stages.

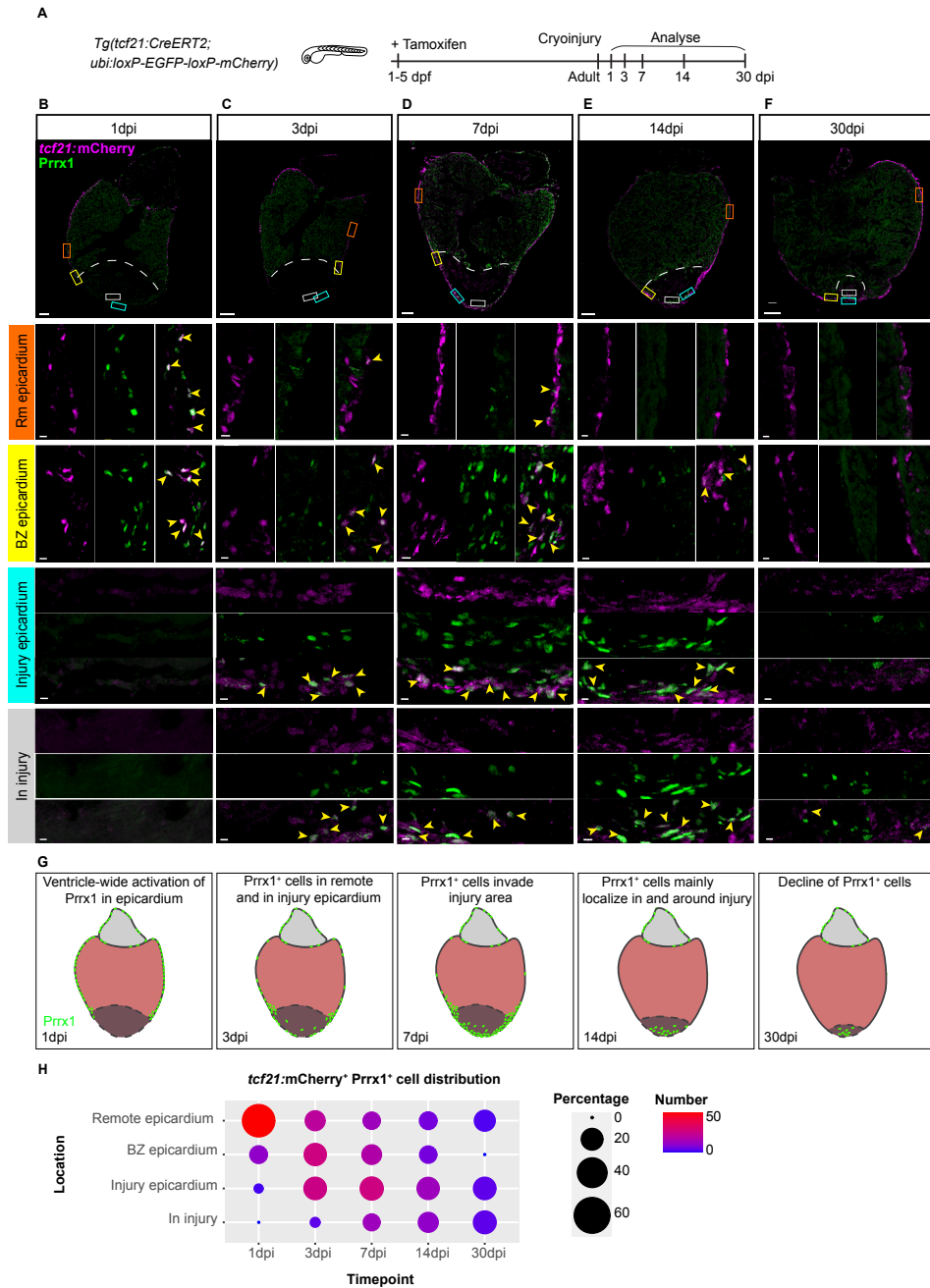


FIGURE 2. Prrx1 is expressed in the epicardium/EPDCs and follows epicardial dynamics post injury. (A) Cartoon illustrating experimental procedures. (B-F) Immunofluorescent staining on 1, 3, 7, 14 and 30dpi *tcf21:mCherry*⁺ wild-type heart sections staining Prrx1 (green) and mCherry (magenta). Arrowheads indicate *tcf21:mCherry*⁺/Prrx1⁺ cells. Scale bars represent 100µm in the overview images and 10µm in the zoom-ins. Rim epicardium = Remote epicardium, BZ epicardium = border zone epicardium. Hearts analysed per condition: 6. (G) Schematic representation of Prrx1 dynamics upon injury. Prrx1⁺ cells are in green. Dark color at the apex represents the injury area. (H) Quantification of the distribution of *tcf21:mCherry*⁺/Prrx1⁺ cells per timepoint. Size of the dots represents the percentage of *tcf21:mCherry*⁺/Prrx1⁺ cells and absolute count number is visualised by a color gradient.

Proliferation and invasion of epicardial cells is unaffected in *prrx1b*^{-/-} hearts

Since cardiac injury induces the proliferation of epicardial cells (Lepilina et al., 2006) and *Prrx1b* is expressed in this cell type we decided to investigate whether *prrx1b* plays a role in epicardial cell proliferation. To do so, we used the *Tg(tcf21:CreERT2; ubi:loxP-EGFP-loxP-mCherry)* line to identify epicardial cells in wild-type and *prrx1b*^{-/-} hearts and used PCNA expression to identify proliferating cells (Fig.S4A,B). We observed that the number of PCNA expressing epicardial cells was highest at 1 and 3 dpi, after which their number dropped to significantly lower amounts at 30dpi, which is in line with previous reports (Lepilina et al., 2006). We found no indication of an epicardial proliferation defect in *prrx1b*^{-/-} hearts, as no significant differences were observed in the number of PCNA expressing epicardial cells at any of the examined time points (Fig.S4B).

Furthermore, we wondered whether *prrx1b* could play a role during the invasion of EPDCs into the injury area. To quantify this, we determined the contribution of *tcf21:mCherry*⁺ surface area found within the injury area as part of the total *tcf21:mCherry*⁺ surface area found in and around the injury area (Fig.S4C). We used this percentage as a measure of invasion efficiency of the EPDCs. At all timepoints, except for 3dpi, there was no significant difference in the percentage of *mCherry*⁺ cells inside the injury between the wild-type and *prrx1b*^{-/-} hearts. At 3dpi, the percentage of *mCherry*⁺ cells invading the injury area is significantly lower in the *prrx1b*^{-/-} hearts, but this is mitigated from 7dpi onwards.

Taken together, we did not find evidence suggesting a profound role for *Prrx1* in epicardial proliferation or EMT. Although the incomplete labelling of *tcf21*⁺ cells resulted in substantial variation in the collected data, potentially masking a subtle difference between wild-type and *prrx1b*^{-/-} hearts, we conclude that *Prrx1* is largely dispensable for proliferation and invasion into the injury area of epicardial and epicardial derived cells.

Characterization of EPDCs in the regenerating heart by single cell sequencing

Next, we wanted to identify which processes are regulated by *Prrx1b* in EPDCs that could explain the impaired regenerative response observed in the *prrx1b*^{-/-} hearts. Given the epicardium and EPDCs are formed by heterogenous cell populations, we decided to take a single-cell RNA-sequencing (scRNAseq) approach to characterize these cells within the context of heart regeneration. First, we isolated ventricles from recombined *Tg(tcf21:CreERT2; ubi:loxP-EGFP-loxP-mCherry)* wild-type sibling or *prrx1b*^{-/-} fish at 7dpi and FACsorted the *mCherry*⁺ cells (Fig.S5A-C). Next, we performed scRNAseq using the SORT-seq (Sorting and Robot-assisted Transcriptome SEQuencing) platform on the isolated single cells (Muraro et al., 2016) (Fig.3A,B). We analysed over 1,400 cells with >1000 reads per cell using the Race-ID3 algorithm, which resulted in the identification of 10 cell clusters grouped based on their transcriptomic features (Fig.3C,D, *Online supplementary Table 1*).

To confirm that the sorting strategy worked we plotted the expression of epicardial markers *tcf21*, *tbx18*, *aldh1a2* and *wt1b* and observed that most cells express at least one of these albeit in different patterns (Fig.3E). These differences in *tcf21*, *tbx18*, *aldh1a2* and *wt1b* expression confirm the previously observed heterogeneity of epicardial cells and EPDCs (Cao et al., 2015; Weinberger et al., 2020). Unfortunately, *prrx1b* expression was too low to correlate it to any of the clusters (Fig. S6). To identify different cell types, we selected marker genes for known cell types and analysed their expression in the various clusters. The cells from clusters 4,7 and 10 express *tcf21* and *tbx18* but lack expression of *aldh1a2* and *wt1b*, suggesting that these represent epicardial cells covering the remote myocardium. Indeed, *in situ* hybridization (ISH) for additional genes with high expression in these clusters marks epicardial cells covering the uninjured part of the heart (Fig.3F). Vice versa, *wt1b* and *aldh1a2* are expressed in most of the remaining clusters, with highest expression in cluster 1. ISH for additional genes marking cluster 1 revealed that their expression was mostly located in the epicardial region covering the injury area but not the remote myocardium (Fig.3G).

Since the epicardium gives rise to fibroblasts and pericytes, we plotted known marker genes for these cell types. Pericytes express genes such as the potassium channel *kcnj8* and the Notch receptor *notch1b* (Guichet et al., 2015; Vanlandewijck et al., 2018). The expression of these genes is most abundant in cluster 6 and gene ontology analysis reveals cluster 6 has an enrichment in genes linked to smooth muscle contraction and cell junction organization. These findings suggest that cells in cluster 6 represent pericytes (Fig. 3H). Periostin (*postnb*) and fibronectin (*fn1a*) are expressed in fibroblasts and both genes showed highest expression in clusters 2,3 and 9 (Fig.3I). In addition, we observed that these clusters are enriched for various other genes reported to be expressed in fibroblasts in the context of tissue injury (e.g. *dkk3b*, *fstl1b*, *ptx3*) (*Online supplementary Table 2*), suggesting that these clusters are formed by injury-responsive cardiac fibroblasts (Sánchez-iranzo et al., 2018). Gene ontology analyses with genes enriched in clusters 2,3 and 9 indeed indicated processes such as extracellular matrix organization, dissolution of fibrin clot, collagen biosynthesis and modifying enzymes (*Online supplementary Table 3*).

From these results we conclude that the scRNAseq data represent different populations of epicardial and epicardial-derived cells from the regenerating heart. Based on our analysis we divided the cells into four general groups: remote epicardium (clusters 4, 7 and 10), injury epicardium (cluster 1), epicardial-derived fibroblasts (clusters 2, 3 and 9) and epicardial-derived pericytes (cluster 6).

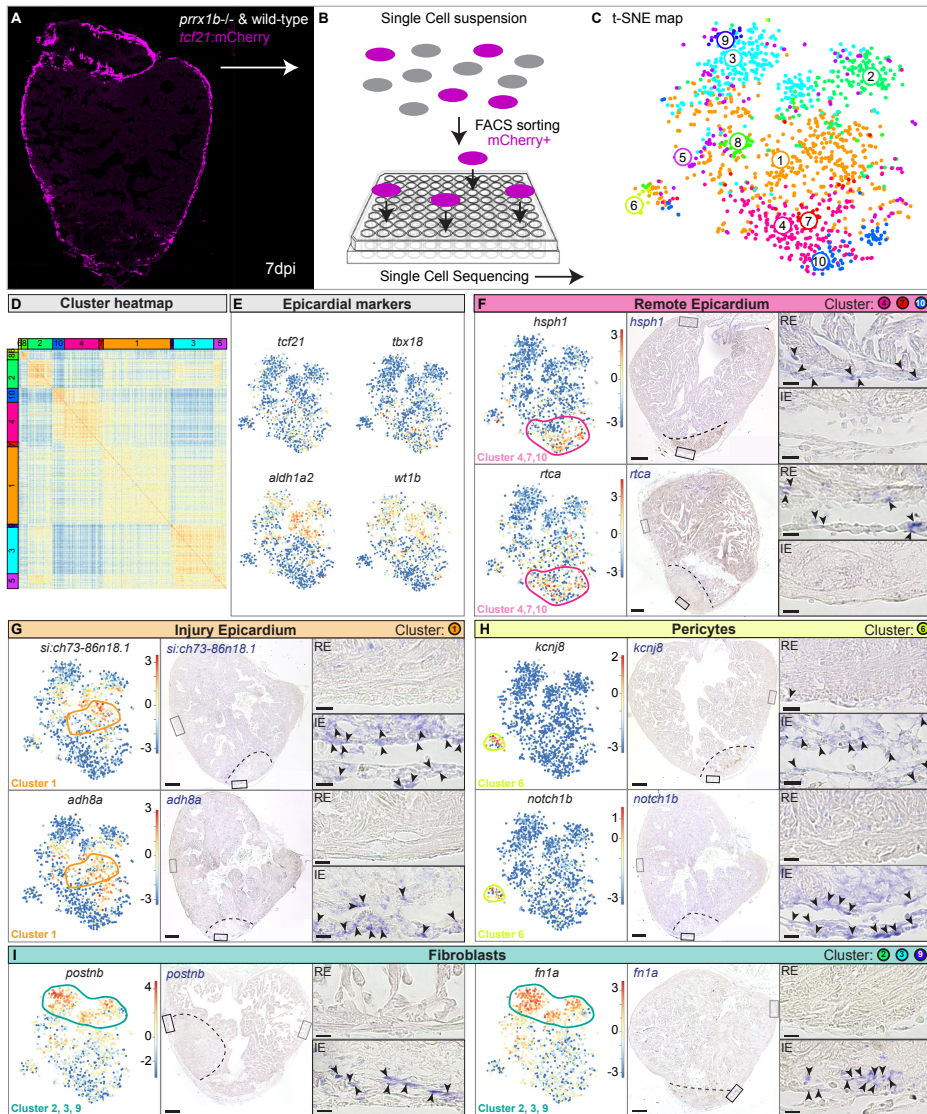


FIGURE 3. Single cell sequencing identifies epicardial derived cell populations in the injured zebrafish heart. (A) Workflow of the isolation and **(B)** sorting of *tcf21:mCherry*⁺ cells out of wildtype and *prrx1b*^{-/-} hearts at 7dpi. **(C)** tSNE-plotting of the data results in 10 transcriptionally distinct clusters, as also indicated by the heatmap **(D)**. **(E)** tSNE maps visualizing log₂-transformed read-counts for *tcf21*, *tbx18*, *aldh1a2* and *wt1b*. **(F-I)** Characterization of the different cell clusters. Left panels show tSNE maps visualizing log₂-transformed read-counts for genes with high expression in the indicated cluster. Middle panels display *in situ* hybridization for the cluster-enriched genes in wild-type hearts at 7 dpi. Dashed line indicates injury border and scale bars represent 100µm. Right panels display magnifications of the boxed regions in remote (RM) and injury area (IA) with arrowheads pointing to cells with high expression. Scale bars represent 10µm. Hearts analysed per condition: 3. Gene lists are provided in Online supplementary table 1.

Prrx1 restricts fibrosis

Next, we mapped the wild-type and *prrx1b*^{-/-} cells separately on the t-SNE map to reveal differences in contribution to the various cell clusters (Fig.4A,B). Interestingly, we found a clear difference in the contribution of wild-type and *prrx1b*^{-/-} cells to the fibroblast clusters 2 and 3. While cluster 2 consists of mostly wild-type cells (89%) and few *prrx1b*^{-/-} cells (11%), cluster 3 is enriched in *prrx1b*^{-/-} cells (71%) compared to wild-type cells (29%) (Fig.4B-D). While both cluster 2 and cluster 3 cells express markers for activated fibroblasts such as *postnb*, differential gene analysis between cluster 2 and 3 revealed that cluster 3 cells are enriched for genes involved in TGF- β signaling (*tgfb1a*, *tgfb2*, *tgfb3*, *P.val*: 7.1E-4), extracellular matrix proteins (*P.val*: 3.3E-4) and collagen fibril organization (*P.val*: 1.2E-4) (Fig. 4E). Instead, cluster 2 cells lack robust expression of fibrosis-related genes, therefore representing a more quiescent cell type that instead expresses genes linked to chordate embryonic development (*P.val*: 3.8E-10) and stress response (*P.val*: 7.9E-6). Together, the scRNAseq data suggests that injured *prrx1b*^{-/-} hearts contain more activated, pro-fibrotic fibroblasts. To validate these findings, we performed ISH for genes with high expression in cluster 2 or 3 cells. Indeed, we observed increased expression of *tgfb1a* and *col11a1b* in injured *prrx1b*^{-/-} hearts compared to their wild-type siblings (Fig.4F,G), while we identified a strong reduction in expression of cluster 2 marker *si:dkeyp-1h4.9* (Fig.S7). In addition, we performed Sirius Red staining to visualize collagen, which showed an excess of collagen fibres in the *prrx1b*^{-/-} hearts in and around the injury area (Fig.4H,I). From these results we conclude that in injured *prrx1b*^{-/-} hearts an excess of TGF- β ligand and ECM producing fibroblasts is formed, resulting in an enhanced fibrotic response to the injury.

NRG1 administration rescues the cardiomyocyte proliferation defect of *prrx1b*^{-/-} hearts

Fibroblasts are not only required for fibrosis in the injured zebrafish heart, they also exhibit pro-regenerative activity by stimulating cardiomyocyte proliferation (Sánchez-iranzo et al., 2018). Since EPDCs secrete Nrg1, a growth factor necessary to induce cardiomyocyte proliferation (Gemberling et al., 2015; Ieda et al., 2009; Wang et al., 2015), we hypothesized *nrg1* expression may be impaired in *prrx1b*^{-/-} hearts and responsible for the observed reduction in cardiomyocyte proliferation. Considering that *nrg1* expression was nearly absent in the scRNAseq data (<100 combined reads from 1438 cells), we investigated expression of *nrg1* through RNAscope ISH. We observed expression of *nrg1* in the epicardial and sub-epicardial region in wild-type hearts at 7dpi (Fig. 5A,B). The BZ epicardium regions show profound *nrg1* expression, which is in line with previously reported *nrg1* localization upon injury (Gemberling et al., 2015). Importantly, we observed co-expression of *nrg1* and Prrx1 in BZ epicardial cells at 7dpi (Fig.5A). Next, we wanted to investigate whether *nrg1* expression is impaired in *prrx1b*^{-/-} hearts. Corroborating our hypothesis, we found a significant reduction of *nrg1* expression in the BZ epicardium of injured *prrx1b*^{-/-} hearts compared to wild-type sibling hearts (Fig.5B,C). To address whether the impaired *nrg1*

expression in *prrx1b*^{-/-} hearts could explain the observed reduction in cardiomyocyte proliferation, we injected injured wild type and *prrx1b*^{-/-} fish daily with recombinant NRG1 protein or DMSO as a control from 3dpi to 7dpi and quantified cardiomyocyte proliferation in the border zone. Importantly, injecting *prrx1b*^{-/-} zebrafish with recombinant NRG1 protein indeed rescued cardiomyocyte proliferation in the border zone to wild-type levels (Fig.5D,E). Together, these results demonstrate that *nrg1* and *Prrx1* are co-expressed and that *Prrx1* promotes *nrg1* expression in EPDCs. Furthermore, the results suggest that the reduction in Nrg1 is responsible for the reduced cardiomyocyte proliferation observed in the border zones of *prrx1b* mutant hearts.

PRRX1 promotes NRG1 expression in human EPDCs

Next, we wanted to address whether *nrg1* expression in EPDCs is regulated by *Prrx1*. As the *prrx1b*^{-/-} fish lack *Prrx1* in all cells, we exploited a previously set-up *in vitro* model (Dronkers et al., 2018) in which human fetal epicardial cells can be cultured in an epithelial phenotype in the presence of the ALK4/5/7 kinase inhibitor SB431542. Removal of the inhibitor for at least 5 days results in the induction of EMT, which can be appreciated by the transition of cobblestone epithelial-like cells towards spindle-shaped mesenchymal cells and upregulation of mesenchymal genes *POSTN* and *FN1* (Fig.6A-C) (Moerkamp et al., 2016). Although some *PRRX1* expression was detected in cobblestone epithelial-like cells, its expression was increased 8-fold in spindle-shaped mesenchymal cells (Fig.6C). Importantly, *NRG1* expression followed the same pattern as *PRRX1* expression, as they were both increased in spindle-shaped cells. To determine whether *PRRX1* can regulate *NRG1* expression, spindle-shaped mesenchymal cells were subjected to *PRRX1* knock-down (KD) using siRNAs (Fig.6D). The effect of *PRRX1* KD was confirmed using western blot (Fig.6E). Indeed, *PRRX1* KD led to a significant decrease in *NRG1* mRNA, as well as a significant decrease of secreted NRG1-β1 protein (Fig.6F,G). From these results we conclude that in EPDCs after EMT induction, *PRRX1* and *NRG1* are co-expressed and that *PRRX1* is required for efficient *NRG1* expression.

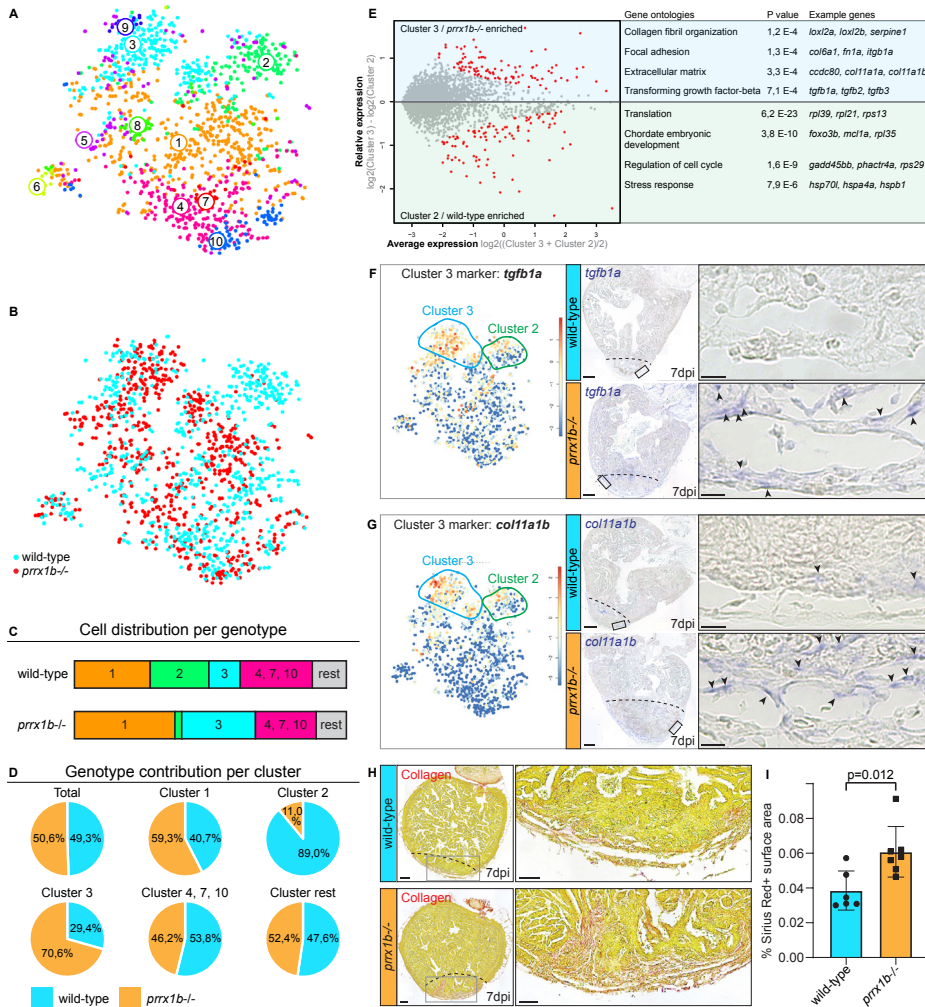


FIGURE 4. *prrx1b*^{-/-} hearts contain excessive amounts of pro-fibrotic fibroblasts. (A) tSNE-map of the single cell sequencing data, indicating 10 transcriptionally distinct cell populations. **(B)** tSNE-map showing the contribution of wild-type cells (cyan) and *prrx1b*^{-/-} cells (red). **(C)** Stacked bar graph showing relative cell contribution to major clusters in either wild-type or *prrx1b*^{-/-} hearts. **(D)** Pie charts showing contribution of wild-type and *prrx1b*^{-/-} cells per cluster. **(E)** Differential gene expression analysis using the DESeq algorithm between fibroblast clusters 2 and 3. Enriched genes were selected for either cluster 2 or 3 with a P-value cut-off of <0.05 (red). Gene ontology analysis was performed using the online tool DAVID. Gene and full Gene Ontology lists are provided in Online supplementary table 2 and 3. **(F-G)** Characterization of cluster 3. Left panels show tSNE maps visualizing log₂-transformed read-counts for genes with high expression in the indicated cluster. Middle panels display *in situ* hybridization for the cluster 3-enriched genes in wild-type and *prrx1b*^{-/-} hearts at 7 dpi. Dashed line indicates injury border and scale bars represent 100µm. Right panels display magnifications of the boxed regions in injury area with arrowheads pointing to cells with high expression. Scale bars represent 25µm. Hearts analysed per condition: 3 **(H)** Sirius red staining showing collagen in red on sections of wild-type and *prrx1b*^{-/-} hearts at 7 dpi. Middle and right panels show magnifications of boxed regions in sub epicardial layer and further inside the injury area. Scale bars represent either 100µm (overview) or 50µm (zoom-in). **(I)** Quantification of Sirius Red (collagen) staining in wild-type (n=6) and *prrx1b*^{-/-} (n=7) hearts showing significantly more fibrosis in *prrx1b*^{-/-} hearts inside and around the injury area (mean±s.d., p=0.012, unpaired t-test).

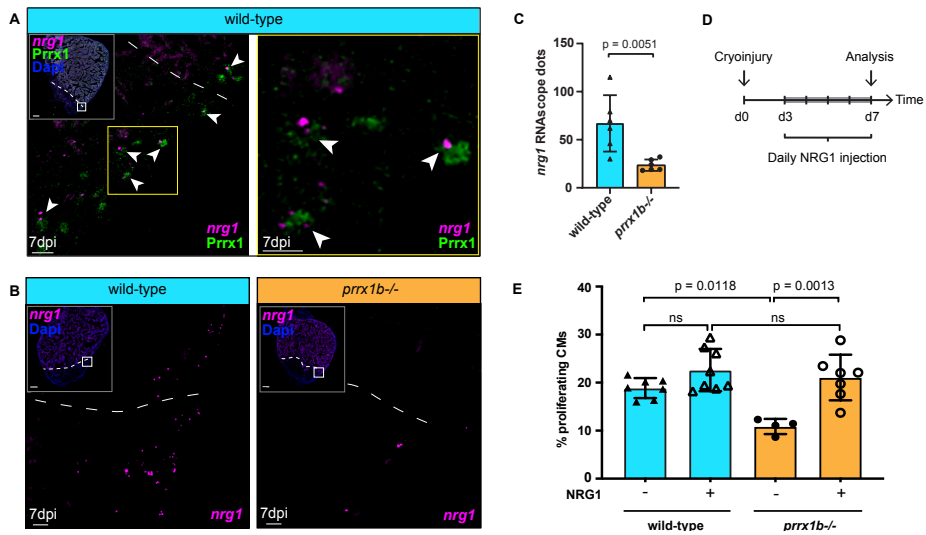


FIGURE 5. Prrx1b stimulates Nrg1 expression. (A) RNAscope *in situ* hybridization for *nrg1* co-detected with Prrx1 antibody on 7dpi wild-type hearts. Arrowheads indicate co-localization of *nrg1* and Prrx1. Dashed line marks edge of the border zone. Scale bars represent 100 μ m in the overview image and 10 μ m in the zoom-ins. Hearts analysed: 4. **(B)** RNAscope *in situ* hybridization for *nrg1* on 7dpi wild-type and *prrx1b*^{-/-} hearts. Dashed line marks edge of the border zone. Scale bars represent 100 μ m in the overview image and 10 μ m in the zoom-ins. **(C)** Quantification of *nrg1* RNAscope dots in the BZ epicardium in 7dpi wild-type (n=6) and *prrx1b*^{-/-} (n=5) hearts. BZ epicardium distinguished as 100 μ m wide, 100 μ m up and 100 μ m down from where the edge of intact myocardium meets the epicardium (mean \pm s.d., $p=0.0051$, unpaired t-test). **(D)** Schematic representation of the workflow used for NRG1 injection experiments in panel E. **(E)** Quantification of the percentage of (PCNA+) proliferation BZ cardiomyocytes (mean \pm s.d., wild-type -NRG1 n=7, wild-type +NRG1 n=8, *prrx1b*^{-/-} -NRG1 n=4, *prrx1b*^{-/-} +NRG1 n=7, wild-type -NRG1 vs *prrx1b*^{-/-} -NRG1 $p=0.0118$, *prrx1b*^{-/-} -NRG1 vs *prrx1b*^{-/-} +NRG1 $p=0.0013$, ns=not significant, one-way ANOVA followed by multiple comparisons analysis using Tukey's test).

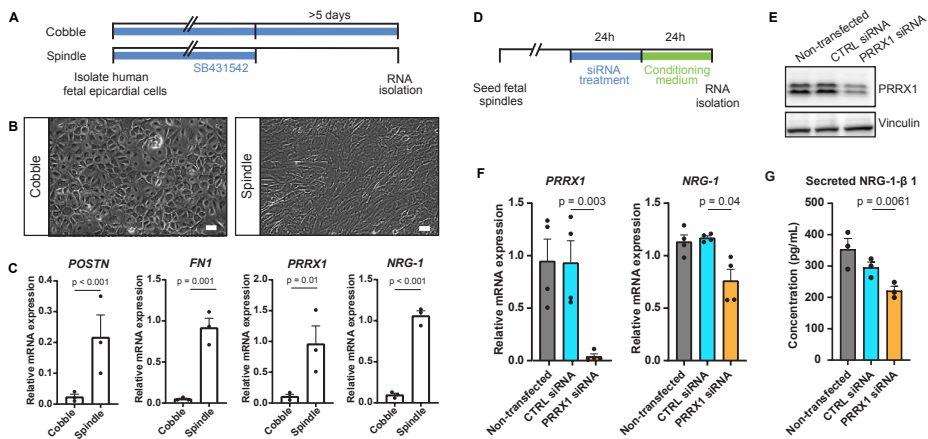


FIGURE 6. PRRX1 promotes NRG1 expression in human EPDCs. (A) Schematic representation of the workflow for panels B and C. After isolation, human fetal epicardial cells are cultured in the presence of ALK4/5/7 kinase inhibitor SB431542. Cells transform from cobble- to spindle-shape upon removal

of SB431542. **(B)** Representative brightfield pictures of cobble- and spindle-shaped human fetal epicardial cells. Scale bars represent 100 μm . **(C)** qPCR results for POSTN, FN1, PRRX1 and NRG1 in human fetal cobble (n=3) and spindle (n=3) epicardial cells (mean \pm s.d., POSTN p<0.001, FN1 p=0.001, PRRX1 p=0.01, NRG-1 p<0.001, unpaired t-tests). **(D)** Schematic representation of the workflow in panels E and F. **(E)** Western blot for PRRX1 in U87 cells. **(F)** qPCR results for PRRX1 and NRG1 in human fetal spindle epicardial cells after PRRX1 siRNA treatment (non-transfected cells n=4, CTRL siRNA n=4, PRRX1 siRNA n=4) (mean \pm s.d., PRRX1 CTRL siRNA vs PRRX1 siRNA p=0.003, NRG-1 CTRL siRNA vs PRRX1 siRNA p=0.04, unpaired t-tests) **(G)** ELISA results for secreted NRG1- β 1 in the conditioned cell culture medium of human fetal spindle epicardial cells between 24-48 hours after PRRX1 siRNA treatment (non-transfected cells n=3, CTRL siRNA n=3, PRRX1 siRNA n=3) (mean \pm s.d., CTRL siRNA vs PRRX1 siRNA p=0.0061, unpaired t-tests).

DISCUSSION

The results described here demonstrate that *prrx1b* is required for the scar-free regeneration of the injured zebrafish heart. The zebrafish genome contains a *prrx1a* and a *prrx1b* gene, which are likely the result of an ancient genome duplication that occurred in teleost (Howe et al., 2013). Our results demonstrate that while *prrx1b* is required for heart regeneration, *prrx1a* is dispensable which suggests these paralogs have non-redundant roles. This is different from their role during cartilage formation in the embryo where *prrx1a* and *prrx1b* are redundant (Barske et al., 2016).

Prrx1 expression is rapidly induced in the epicardium upon injury. This is reminiscent of the induction of other genes in the epicardium, such as *tbx18* and *raldh2*, and implies that Prrx1 induction is part of the early activation that occurs in the entire epicardium (Cao & Poss, 2018; Lepilina et al., 2006). Importantly, all three previously identified subpopulations (*tcf21+*, *tbx18+* and *wt1+*) of epicardial cells and EPDCs express Prrx1 (Cao et al., 2016; Weinberger et al., 2020).

It has been well established that EPDCs differentiate into various cell types (reviewed in Cao 2018). Retroviral labelling and Cre-mediated recombination studies in chick, mouse and zebrafish demonstrate that EPDCs differentiate into fibroblasts and vascular support cells (e.g. pericytes) (Acharya et al., 2012; Gittenberger-de Groot et al., 1998; González-Rosa et al., 2012; Kikuchi et al., 2011; Männer, 1999; Mikawa & Gourdie, 1996), which is in good agreement with our scRNAseq data. There are also numerous reported observations suggesting that EPDCs can differentiate into endothelial cells and cardiomyocytes (Cai et al., 2008; Guadix et al., 2006; Katz et al., 2012; Männer, 1999; Mikawa & Gourdie, 1996; Smart et al., 2011; Zangi et al., 2013), although some of these observations have been questioned by others (Christoffels et al., 2009; Rudat & Kispert, 2012). In our scRNAseq analysis of EPDCs recovered from the regenerating zebrafish heart we did not find a cell type representing endothelial cells or cardiomyocytes, which is in agreement with earlier observations that *tcf21*-derived EPDCs in the zebrafish do not contribute to either endothelial

or myocardial cell lineages (González-Rosa et al., 2012; Kikuchi et al., 2011).

Fibroblasts form one of the main contributors to ECM deposition in response to cardiac injury and are therefore an important cell type in maintaining the balance between the fibrotic and regenerative injury response (Chablais & Jazwinska, 2012; Gemberling et al., 2015; Sánchez-iranzo et al., 2018). In addition, subpopulations of cardiac fibroblasts can have distinct roles in cardiomyocyte maturation and innervation (Hortells et al., 2020). By scRNAseq analysis, we identified two distinct fibroblast cell states in the regenerating heart. The pro-fibrotic fibroblast cluster (cluster 3) expresses all three TGF- β ligands supporting earlier findings that these ligands are expressed in the injury area to activate a pro-fibrotic response (Chablais & Jazwinska, 2012). Pro-fibrotic fibroblasts express fibronectin-1 (*fn1a*) and various collagens (Sánchez-iranzo et al., 2018), which we found to be upregulated in the cluster 3 fibroblasts corroborating their pro-fibrotic nature. In *prrx1b*^{-/-} hearts these pro-fibrotic fibroblasts were more abundant which is consistent with the observed excess of collagen deposition. Whereas cardiac fibrosis is permanent in the injured mammalian heart, it is resolved in the zebrafish heart. The mechanism for this regression in the zebrafish heart is not well understood. It could be related to the observation that activated fibroblasts partially return to a quiescent state (Sánchez-iranzo et al., 2018). Our results showing that an increase in activated (pro-fibrotic) fibroblast cell numbers can lead to an excessive fibrotic response supports the theory that the de-activation of injury responsive pro-fibrotic fibroblasts is detrimental to successful scar regression.

Cluster 2 cells have only limited expression of pro-fibrotic genes and might therefore represent de-activated, quiescent fibroblasts. Many factors secreted by activated fibroblasts have been implicated to affect cardiac development and regeneration, suggesting that the pro-regenerative function of fibroblasts might be accomplished through their secretory role. In addition, experiments co-culturing fibroblasts with cardiomyocytes show that fibroblasts can induce cardiomyocyte proliferation (Ieda et al., 2009). Our results demonstrate Prrx1-dependent *nrg1* expression in EPDCs near the proliferating cardiomyocytes in the border zone. Nrg1 is a potent inducer of cardiomyocyte proliferation by activation of the ErbB2 signalling pathway (Bersell et al., 2009; D'Uva et al., 2015; Gemberling et al., 2015), which is consistent with our observation that the cardiomyocyte proliferation defect *prrx1b*^{-/-} hearts can be rescued by exogenous Nrg1. Both the *in vitro* experiments in human fetal EPDCs and the *in vivo* experiments in zebrafish demonstrate that *Nrg1* expression depends on Prrx1. Whether this is through binding of Prrx1 to regulatory sequences in the *Nrg1* locus or whether it is through a more indirect mechanism needs to be further investigated for example by chromatin immunoprecipitation (ChIP) experiments.

In conclusion, we have shown that during zebrafish heart regeneration Prrx1b expression in EPDCs restricts the amount of pro-fibrotic fibroblasts and stimulates cardiomyocyte

proliferation. In doing so, *Prrx1b* establishes a balance between fibrotic repair and the regeneration of lost myocardium during zebrafish heart regeneration.

METHODS

Animal experiments

Animal care and experiments conform to the Directive 2010/63/EU of the European Parliament. All animal work was approved by either the Animal Experimental Committee of the Instantie voor Dierenwelzijn Utrecht (IvD) and was performed in compliance with the Dutch government guidelines. Zebrafish were housed under standard conditions (Aleström et al., 2019).

Zebrafish lines

The following zebrafish lines were used: TL, *prrx1a*, *prrx1a^{el558}*, *prrx1b^{el491}* (Barske et al., 2016), Tg(*tcf21:CreERT2*)(Kikuchi et al., 2011); Tg(*ubi:loxP-EGFP-loxP-mCherry*)(Mosimann et al., 2011).

Cryoinjuries in zebrafish

To address experiments in a regeneration context, cardiac cryo-injuries were performed on TL and *prrx1b^{el491}* (with and without the Tg(*tcf21:CreERT2*; *ubi:loxP-EGFP-loxP-mCherry*)) fish of both sexes that were ~4 to 18 months of age. The cryoinjuries were performed as described in (Schnabel et al., 2011), with the exception of the use of a copper filament (0.3mm) cooled in liquid nitrogen instead of dry ice. Animals were excluded from the study in case of signs of aberrant behaviour/sickness/infection, according to animal guidelines.

Histology and enzyme histochemistry

Acid fuchsin orange G (AFOG) staining was performed on paraffin sections of zebrafish ventricles as previously described (Poss et al., 2002). Paraffin sections of 7, 30 and 90dpi hearts were prepared as described below (see Methods section: *In situ* hybridization). Sirius Red staining was performed on similar paraffin sections as previously described on http://www.ihcworld.com/_protocols/special_stains/sirius_red.htm, excluding the haematoxylin step.

Immunofluorescence

Adult zebrafish ventricles were isolated and fixed in 4% PFA (4°C O/N on shaker). The next day, the hearts were washed 3x 10 minutes in 4% sucrose phosphate buffer, after which they were incubated at RT for at least 5h in 30% sucrose phosphate buffer until the hearts sank. Then, they were embedded in cryo-medium (OCT). Cryo-sectioning of the hearts was performed at 10µm thickness. Primary antibodies used include anti-

PCNA (Dako#M0879, 1:800), anti-Mef2c (Santa Cruz #SC313, Biorbyt#orb256682 both 1:1000), Anti-tropomyosin (Sigma #122M4822, 1:400), Living Colors anti-DsRed (Clontech #632496, 1:100), anti-RFP (Novus Biologicals #42649), anti-Prrx1 (Gift from Tenaka lab, described in (Gerber et al. 2018; Oliveira et al. 2018), 1:200), mouse IgG2b anti-Dendra2 Origene #TA180094, clone OTI1G6 (for wt1b H2B dendra) (1:400), chicken polyclonal anti-GFP Abcam Cat# ab13970 (for tbx18 myr GFP) (1:200). Secondary antibodies include Anti-chicken Alexa488 (Thermofisher, #A21133, 1:500), anti-rabbit Alexa555 (Thermofisher, #A21127, 1:500), anti-mouse Cy5 (Jackson ImmunoR, #118090, 1:500), anti-mouse IgG2b Alexa647 (1:100). Nuclei were shown by DAPI (4',6-diamidino-2-phenylindole) or Hoechst staining. Images of immunofluorescence stainings are single optical planes acquired with a Leica Sp8 confocal microscope.

Quantitative analyses

All quantifications were performed blinded. Unless stated otherwise, three individual sections with the largest injuries per heart have been analysed including presented data obtained through *in situ* hybridization, immunohistochemistry and Sirius Red staining. Imaris x64 V3.2.1 software (Oxford Instruments) was used to analyse immunofluorescent images made with a Leica SP8 confocal microscope. Proliferation percentages of border zone cardiomyocytes were determined using the spots selection tool. A region of interest (200 μ m) consisting of the border zone was chosen and cardiomyocytes (Mef2) were selected by classifying them as 5 μ m diameter or bigger. Proliferating cardiomyocytes were selected by hand using the PCNA channel. To quantify the distribution of *tcf21*+ Prrx1+ cells over different locations and different timepoints, the spot selection tool in Imaris was used to select all Prrx1+ cells in the ventricle, after which a sub selection of all *tcf21*:mCherry+ Prrx1+ cells was made by hand. Distinguished regions were Remote epicardium, BZ epicardium (100 μ m up and 100 μ m down from the edge of intact myocardium), injury epicardium and in the injury. Double positive cells in each of these regions were counted and presented as a percentage of the total of double positive cells in the ventricle. To quantify the percentage of *tcf21*:mCherry+ cell invasion into the injury, the surface selection tool was used to mark the total *tcf21*:mCherry+ area in the ventricle. The measurement we used was the average value of the volume. Then, the total injury area plus 100 μ m border zone was chosen as a region of interest 'whole injury area'. Then, *tcf21*:mCherry+ surfaces within the injury were selected manually to create a subset of the whole injury area surface. Proliferation of *tcf21*:mCherry+ cells was measured as the amount of PCNA+ cells per μ m² of *tcf21*:mCherry+ tissue surface, since the cytoplasmic mCherry signal does not allow for the distinction between individual cells. *tcf21*: mCherry+ PCNA+ cells were counted manually. *Nrg1* RNAscope signal was quantified by using the spots selection tool in Imaris to count the absolute number of *nrg1* transcripts in the BZ epicardium regions. ImageJ software (NIH) was used to quantify the remaining scar size of 30 and 90dpi heart sections following AFOG staining. All heart sections of each heart were stained, imaged and quantified for scar tissue area using ImageJ. Sirius Red staining in wild-

type and *prrx1b*^{-/-} hearts was analysed using the image-J macros MRI fibrosis tool (http://dev.mri.cnrs.fr/projects/imagej-macros/wiki/Fibrosis_Tool).

Lineage tracing of zebrafish epicardial cells

To lineage trace epicardial and epicardial derived cells, we combined the Tg(*tcf21*:CreERT2) with the tg(*ubi*:loxP-EGFP-loxP-mCherry). Both wild-type and *prrx1b*^{-/-} embryos with a single copy of both transgenes Tg(*tcf21*:CreERT2; *ubi*:loxP-EGFP-loxP-mCherry) were incubated in 4-hydroxytamoxifen (4-OHT) as described in (Kikuchi et al., 2011; Mosimann et al., 2011) from 1 dpf until 5 dpf at a concentration of 5 μM. At 5 dpf, embryos were selected that were positive for epicardial mCherry signal and grown to adulthood.

Isolation of single cells from cryoinjured hearts

Cryoinjured hearts of either *prrx1b* wild-type siblings (n = 20) or *prrx1b* homozygous mutants (n = 20) previously recombined as embryo (Tg(*tcf21*:CreERT2; *ubi*:loxP-EGFP-loxP-mCherry) were extracted at seven dpi. Cells were dissociated according to (Tessadori et al., 2012). For cell sorting, viable cells were gated by negative DAPI staining and positive YFP-fluorescence. In brief, the FACS gating was adjusted to sort cells positive for mCherry (recombined epicardial derived cells) and negative for EGFP (unrecombined cells). In total 1536 cells (768 *prrx1b* wild-type sibling cells and 768 *prrx1b* homozygous mutant cells) were sorted into 384-well plates and processed for mRNA sequencing as described below.

Single-cell mRNA sequencing

Single-cell sequencing libraries were prepared using SORT-seq (Muraro et al., 2016). Live cells were sorted into 384-well plates with Vapor-Lock oil containing a droplet with barcoded primers, spike-in RNA and dNTPs, followed by heat-induced cell lysis and cDNA syntheses using a robotic liquid handler. Primers consisted of a 24 bp polyT stretch, a 4 bp random molecular barcode (UMI), a cell-specific 8 bp barcode, the 5' Illumina TruSeq small RNA kit adapter and a T7 promoter. After cell-lysis for 5 min at 65°C, RT and second strand mixes were distributed with the Nanodrop II liquid handling platform (Inovadyne). After pooling all cells in one library, the aqueous phase was separated from the oil phase, followed by IVT transcription. The CEL-Seq2 protocol was used for library prep (Hashimshony et al., 2016). Illumina sequencing libraries were prepared with the TruSeq small RNA primers (Illumina) and paired-end sequenced at 75 bp read length on the Illumina NextSeq platform. Mapping was performed against the zebrafish reference assembly version 9 (Zv9). The raw and processed single-cell RNA-sequencing data was uploaded on NCBI's GEO database under entry ID GSE153170 and can be accessed by entering the token spqzmckypnixpmd at <https://www.ncbi.nlm.nih.gov/geo/query/acc.cgi?acc=GSE153170>.

Bioinformatic analysis

To analyze the single-cell RNA-seq data, we used an updated version (RacelD3) of the

previously published RaceID algorithm (Grün et al., 2015). For the adult hearts we had a dataset consisting of two different libraries of 384 cells per genotype (*prrx1b* wild-type or homozygous mutants) each for a combined dataset of 768 cells, in which we detected a total of 20995 genes. We detected an average of 7022 reads per cell. Based on the distribution of the log₁₀ total reads plotted against the frequency, we introduced a cutoff at minimally 1000 reads per cell before further analysis. This reduced the number of cells used in the analysis to 711 wild-type and 727 mutant cells. The top 20 noisy genes were identified by the StemID algorithm, which we excluded from the downstream analysis to increase clustering robustness. Batch-effects were analyzed and showed no plate-specific clustering of certain clusters. The StemID algorithm were used as previously published (Grün et al., 2016). In short, StemID is an approach developed for inferring the existence of stem cell populations from single-cell transcriptomics data. StemID calculates all pairwise cell-to-cell distances (1 – Pearson correlation) and uses this to cluster similar cells into clusters that correspond to the cell types present in the tissue. The StemID algorithm calculates the number of links between clusters. This is based on the assumption that cell types with less links are more canalized while cell types with a higher number of links have a higher diversity of cell states. Besides the number of links, the StemID algorithm also calculates the change in transcriptome entropy. Differentiated cells usually express a small number of genes at high levels in order to perform cell specific functions, which is reflected by a low entropy. Stem cells and progenitor cells display a more diverse transcriptome reflected by high entropy (Banerji et al., 2013). By calculating the number of links of one cluster to other clusters and multiplying this with the change in entropy, it generates a StemID score, which is representative to ‘stemness’ of a cell population. Differential gene expression analysis was performed using the ‘diffexpnb’, which makes use of the DESeq algorithm. P-values were Benjamini-Hochberg corrected for false discovery rate to make the cutoff.

Statistical analysis of data

Statistical analyses were performed using the GraphPad Prism8 software. Unless stated otherwise, all statistical testing was performed by unpaired T-tests. Statistical testing for the NRG1 rescue experiment (Fig. 5E) was performed by One-Way ANOVA followed by multiple comparisons analysis using the Tukey’s test.

In situ hybridization

In situ hybridization was performed on paraffin sections. After o/n fixation in 4% PFA, hearts were washed in PBS twice, dehydrated in EtOH, and embedded in paraffin. Serial sections were made at 8µm thickness. *In situ* hybridization was performed as previously described (Moorman et al., 2001) except that the hybridization buffer used did not contain heparin and yeast total RNA. When *in situ* hybridization was done for multiple probes, INT-BCIP staining solution (red/brown staining) was used for the additional probe instead of NBT-BCIP (blue staining).

RNAscope

RNAscope *in situ* hybridization was performed on fixed frozen sections following the Advanced Cell Diagnostics company protocol for RNAscope® Multiplex Fluorescent Reagent Kit v2 with the following modification: target retrieval was not performed as this was not required for the *nrg1* probe. Probe used for *nrg1* detection is RNAscope® Probe-Dr-nrg1-CDS with Cat No. 414131. For co-detection with Prrx1 antibody, the RNA-Protein Co-detection Ancillary Kit was used following the Advanced Cell Diagnostics company protocol. Prrx1 antibody was used in a 1:200 dilution.

Intraperitoneal injections in zebrafish

Intraperitoneal injections of human recombinant NRG1 (peprotech: recombinant human heregulin-b1, catalog#:100-03) were performed as described by Kinkel et al. (Kinkel et al., 2010). Fish were sedated using MS222 (0.032% wt/vol). Injections were performed using a Hamilton syringe (Gauge 30), cleaned before use by washing in 70% ethanol followed by 2 washes in PBS. Injection volumes were adjusted on the weight of the fish (30ul/g) and a single injection contained 60 ug/kg (diluted in PBS/BSA 0.1%).

Human epicardial cell culture

Human fetal hearts of a gestational age between 12-18 weeks were collected anonymously and under informed consent from abortion material after elective abortion. Epicardial cells were isolated as described in (Dronkers et al., 2018). Cells were cultured in Dulbecco's modified Eagle's medium (DMEM low-glucose, Gibco) and Medium 199 (M199, Gibco) mixed in a 1:1 ratio, supplemented with 10% fetal bovine serum (heat inactivated for 25 minutes at 56 °C, Gibco), 100 U/mL penicillin (Roth), 100 mg/mL streptomycin (Roth), and 10 µM ALK4/5/7 kinase inhibitor SB431542 (Tocris) at 37 °C in 5% CO₂. EMT was induced by removal of SB431542 from the medium. This research was carried out according to the official guidelines of the Leiden University Medical Center and approved by the local Medical Ethics Committee. This research conforms to the Declaration of Helsinki. Cells are tested for contamination every 3 months.

Cell culture U87 cells

U87 cells were cultured in Dulbecco's modified Eagle's medium (DMEM high-glucose, Gibco), supplemented with 10% fetal bovine serum (Gibco), 100 U/mL penicillin (Roth) and 100 mg/mL streptomycin (Roth). Cells are tested for contamination every 3 months.

PRRX1 KD in human epicardial cells

Cells were treated with SMARTpool ON-TARGETplus PRRX1 or a non-targeting control siRNA according to the manufacturers' protocol in a concentration of 25 nM (Dharmacon). After 48 hours, cells were collected for qPCR or western blot. All experiments in human fetal epicardial cells were performed with three or four individual cell isolations.

qPCR

ReliaPrep™ RNA Miniprep Systems (Promega) was used to isolate mRNA, of which the concentration and purity were determined using NanoDrop 1000 Spectrophotometer (Thermo Fisher Scientific). cDNA synthesis was performed using the RevertAid H Minus First Strand cDNA Synthesis Kit (Thermo Fisher Scientific). Next, qPCR was performed using SYBR Green (Promega) and run on a C1000 Touch™ thermal cycler (Bio-Rad). All samples were run in triplicates, expression levels were corrected for primer efficiency and normalized for two reference genes (TBP and HPRT1).

Primer sequences

	Forward	Reverse
<i>POSTN</i>	GGA GGC AAA CAG CTC AGA GT	GGC TGA GGA AGG TGC TAA AG
<i>FN1</i>	CGTCATAGTGGAGGCACTGA	CAGACATTCGTTCCCACTCA
<i>PRRX1a</i>	CGCAGGAATGAGAGAGCCAT	AACATCTTGGGAGGGACGAG
<i>NRG-1</i>	CACATGATGCCGACCAAG	GGTGATCGCTGCCAAAATA
<i>TBP</i>	TGGAAAAGTTGTATTAACAGGTGCT	GCAAGGGTACATGAGAGCCA
<i>HPRT1</i>	CTCATGGACTGATTATGGACAGGAC	GCAGGTCAGCAAAGAACTTATAGCC

Western blot

Cells were lysed in radioimmunoprecipitation assay (RIPA) buffer containing protease and phosphatase inhibitors (complete protease inhibitor cocktail tablets, Roche Diagnostics). Protein concentration was determined using Pierce BCA Protein Assay Kit (ThermoFisher Scientific). For every sample, 50 ug of protein was loaded onto a 10% SDS-polyacrylamide gel. Subsequently, protein was transferred on Immobilon-P PVDF Membrane (Millipore). Blots were blocked in 5% bovine serum albumin (BSA) in Tris-Buffered Saline with 0.1% Tween 20 (TBST) for 1 hour and incubated overnight with primary antibody (anti-PRRX1, 1:500, Gift from Tenaka lab, described in (Gerber et al. 2018; Oliveira et al. 2018); anti-Vinculin, 1:5000, Sigma). Blots were incubated for 1 h with horse radish peroxidase (HRP) anti-rabbit secondary antibody (Abcam), which was detected by WesternBright Quantum (Advansta).

ELISA

Conditioned medium was collected for 24 hours after 24 hours of siRNA treatment, centrifuged and immediately frozen at -20°. Cell culture medium was taken along as a control sample. An NRG1-β1 ELISA assay was performed according to the protocol of the manufacturer (Human NRG1-β1 DuoSet ELISA, R&D systems). Absolute NRG1-β1 concentration was calculated based on the standard curve.

Acknowledgements

We would like to thank all members of the Bakkers lab for their input during this study, Jens Puschhof for technical help with the RNAscope analysis, Jeroen Korving for his help

with histology, and the Hubrecht Institute FACS facility and Single Cell Discoveries for their expertise with sorting and sequencing.

Competing interests

The authors have no competing interests.

Data availability

The raw and processed single-cell RNA-sequencing data was uploaded on NCBI's GEO database under entry ID GSE153170 and can be accessed by entering the token spqzmckypnixpmd at <https://www.ncbi.nlm.nih.gov/geo/query/acc.cgi?acc=GSE153170>.

Funding

D.E.M. de Bakker, M. Bouwman and J. Bakkens were funded by The Netherlands CardioVascular Research Initiative (CVON): the Dutch Heart Foundation, Dutch Federation of University Medical Centers, The Netherlands Organization for Health Research and Development, and the Royal Netherlands Academy of Sciences (CVON-Cobra3 and CVON-OUTREACH). A.M. Smits was funded by a Dekker fellowship of the Dutch Heart Foundation (2017T059). F. C. Simões and P. R. Riley were supported by a British Heart Foundation personal chair award CH/11/1/28798.

REFERENCES

- Acharya, A., Baek, S. T., Huang, G., Eskiocak, B., Goetsch, S., Sung, C. Y., Banfi, S., Sauer, M. F., Olsen, G. S., Duffield, J. S., Olson, E. N., & Tallquist, M. D. (2012). The bHLH transcription factor Tcf21 is required for lineage-specific EMT of cardiac fibroblast progenitors. *Development (Cambridge, England)*, 139(12), 2139–2149.
- Aleström, P., D'Angelo, L., Midtlyng, P. J., Schorderet, D. F., Schulte-Merker, S., Sohm, F., & Warner, S. (2019). Zebrafish: Housing and husbandry recommendations. *Laboratory Animals*. Volume: 54 issue: 3, page(s): 213-224
- Banerji, C. R. S., Miranda-Saavedra, D., Severini, S., Widschwendter, M., Enver, T., Zhou, J. X., & Teschendorff, A. E. (2013). Cellular network entropy as the energy potential in Waddington's differentiation landscape. *Scientific Reports*, 3, 3039
- Barske, L., Askary, A., Zuniga, E., Balczerski, B., Bump, P., Nichols, J. T., & Crump, J. G. (2016). Competition between Jagged-Notch and Endothelin1 Signaling Selectively Restricts Cartilage Formation in the Zebrafish Upper Face. *PLoS Genetics*, 12(4), e1005967.
- Bersell, K., Arab, S., Haring, B., & Kühn, B. (2009). Neuregulin1/ErbB4 Signaling Induces Cardiomyocyte Proliferation and Repair of Heart Injury. *Cell*. Volume 138, Issue 2, P257-270
- Cai, C. L., Martin, J. C., Sun, Y., Cui, L., Wang, L., Ouyang, K., Yang, L., Bu, L., Liang, X., Zhang, X., Stallcup, W. B., Denton, C. P., McCulloch, A., Chen, J., & Evans, S. M. (2008). A myocardial lineage derives from Tbx18 epicardial cells. *Nature*. 454, 104–108
- Cao, J., Navis, A., Cox, B. D., Dickson, A. L., Gemberling, M., Karra, R., Bagnat, M., & Poss, K. D. (2016). Single epicardial cell transcriptome sequencing identifies caveolin 1 as an essential factor in zebrafish heart regeneration. *Development (Cambridge)*, 143(2), 232–243.
- Cao, J., & Poss, K. D. (2018). The epicardium as a hub for heart regeneration. In *Nature Reviews Cardiology*. 15, pages631–647
- Chablais, F., & Jazwinska, A. (2012). The regenerative capacity of the zebrafish heart is dependent on TGFβ signaling. *Development (Cambridge, England)*, 139(11), 1921–1930.
- Chesterman, E.S., Gainey, G.D., Varn, A.C., Peterson, R.E., Jr and Kern, M.J. (2001). Investigation of *Prx1* protein expression provides evidence for conservation of cardiac-specific posttranscriptional regulation in vertebrates. *Developmental Dynamics*, 222: 459-470
- Chablais, F., Veit, J., Rainer, G., & Jaźwińska, A. (2011). The zebrafish heart regenerates after cryoinjury-induced myocardial infarction. *BMC Developmental Biology*, 11, 21.
- Christoffels, V. M., Grieskamp, T., Norden, J., Mommersteeg, M. T. M., Rudat, C., & Kispert, A. (2009). Tbx18 and the fate of epicardial progenitors. *Nature*. 458, pagesE8–E9
- D'Uva, G., Aharonov, A., Lauriola, M., Kain, D., Yahalom-Ronen, Y., Carvalho, S., Weisinger, K., Bassat, E., Rajchman, D., Yifa, O., Lysenko, M., Konfino, T., Hegesh, J., Brenner, O., Neeman, M., Yarden, Y., Leor, J., Sarig, R., Harvey, R. P., & Tzahor, E. (2015). ERBB2 triggers mammalian heart regeneration by promoting cardiomyocyte dedifferentiation and proliferation. *Nature Cell Biology*, 17, pages627–638.
- Dronkers, E., Moerkamp, A. T., van Herwaarden, T., Goumans, M. J., & Smits, A. M. (2018). The isolation and culture of primary epicardial cells derived from human adult and fetal heart specimens. *Journal of Visualized Experiments*. (134), e57370
- Gemberling, M., Karra, R., Dickson, A. L., & Poss, K. D. (2015). Nrg1 is an injury-induced cardiomyocyte mitogen for the endogenous heart regeneration program in zebrafish. *ELife*, 4, 1–17.
- Gerber, T., Murawala, P., Knapp, D., Masselink, W., Schuez, M., Hermann, S., Gac-Santel, M., Nowoshilow, S., Kageyama, J., Khattak, S., Currie, J. D., Camp, J. G., Tanaka, E. M., & Treutlein, B. (2018). Single-cell analysis uncovers convergence of cell identities during axolotl limb regeneration. *Science*, 362(6413).
- Gittenberger-de Groot, A. C., Vrancken Peeters, M. P., Mentink, M. M., Gourdie, R. G., & Poelmann, R. E. (1998). Epicardium-derived cells contribute a novel population to the myocardial wall and the atrioventricular cushions. *Circulation Research*, 82(10), 1043–1052.
- González-Rosa, J. M., Martín, V., Peralta, M., Torres, M., & Mercader, N. (2011). Extensive scar formation and regression during heart regeneration after cryoinjury in zebrafish. *Development (Cambridge, England)*, 138(9), 1663–1674.
- González-Rosa, J. M., Peralta, M., & Mercader, N. (2012). Pan-epicardial lineage tracing reveals that epicardium derived cells give rise to myofibroblasts and perivascular cells during zebrafish heart regeneration. *Developmental Biology*, 370(2), 173–186.

- Grün, D., Lyubimova, A., Kester, L., Wiebrands, K., Basak, O., Sasaki, N., Clevers, H., & van Oudenaarden, A. (2015). Single-cell messenger RNA sequencing reveals rare intestinal cell types. *Nature*, 525(7568), 251–255.
- Grün, D., Muraro, M. J., Boisset, J. C., Wiebrands, K., Lyubimova, A., Dharmadhikari, G., van den Born, M., van Es, J., Jansen, E., Clevers, H., de Koning, E. J. P., & van Oudenaarden, A. (2016). De Novo Prediction of Stem Cell Identity using Single-Cell Transcriptome Data. *Cell Stem Cell*, 19(2), 266–277.
- Guadix, J. A., Carmona, R., Muñoz-Chápuli, R., & Pérez-Pomares, J. M. (2006). In vivo and in vitro analysis of the vasculogenic potential of avian proepicardial and epicardial cells. *Developmental Dynamics*. Volume 235, Issue 4, Pages 1014-1026
- Guichet, P. O., Guelfi, S., Teigell, M., Hoppe, L., Bakalara, N., Bauchet, L., Duffau, H., Lamszus, K., Rothhut, B., & Hugnot, J. P. (2015). Notch1 stimulation induces a vascularization switch with pericyte-like cell differentiation of glioblastoma stem cells. *Stem Cells*. Volume 33, Issue 1, Pages 21-34
- Hashimshony, T., Senderovich, N., Avital, G., Klochender, A., de Leeuw, Y., Anavy, L., Gennert, D., Li, S., Livak, K. J., Rozenblatt-Rosen, O., Dor, Y., Regev, A., & Yanai, I. (2016). CEL-Seq2: Sensitive highly-multiplexed single-cell RNA-Seq. *Genome Biology*, 17(1).
- Hortells, L., Valiente-Alandi, Iñigo., Thomas, Z. M., Agnew, E. J., Schnell, D. J., York, A. J., Vagnozzi, R. J., Meyer, E. C., Molkentin, J. D., Yutzey, K. E. (2020). A specialized population of Periostin-expressing cardiac fibroblasts contributes to postnatal cardiomyocyte maturation and innervation. *PNAS*, 117(35):21469-21479.
- Howe, K., Clark, M. D., Torroja, C. F., Torrance, J., Berthelot, C., Muffato, M., Collins, J. E., Humphray, S., McLaren, K., Matthews, L., McLaren, S., Sealy, I., Caccamo, M., Churcher, C., Scott, C., Barrett, J. C., Koch, R., Rauch, G. J., White, S., ... Stemple, D. L. (2013). The zebrafish reference genome sequence and its relationship to the human genome. *Nature*. 496, pages 498–503
- Ieda, M., Tsuchihashi, T., Ivey, K. N., Ross, R. S., Hong, T. T., Shaw, R. M., & Srivastava, D. (2009). Cardiac Fibroblasts Regulate Myocardial Proliferation through $\beta 1$ Integrin Signaling. *Developmental Cell*, 16(2), 233–244.
- Itou, J., Oishi, I., Kawakami, H., Glass, T. J., Richter, J., Johnson, A., Lund, T. C., & Kawakami, Y. (2012). Migration of cardiomyocytes is essential for heart regeneration in zebrafish. In *Development* (Vol. 139, Issue 22, pp. 4133–4142).
- Jopling, C., Sleep, E., Raya, M., Martí, M., Raya, A., & Belmonte, J. C. I. (2010). Zebrafish heart regeneration occurs by cardiomyocyte dedifferentiation and proliferation. *Nature*, 464(7288), 606–609.
- Katz, T. C., Singh, M. K., Degenhardt, K., Rivera-Feliciano, J., Johnson, R. L., Epstein, J. A., & Tabin, C. J. (2012). Distinct Compartments of the Proepicardial Organ Give Rise to Coronary Vascular Endothelial Cells. *Developmental Cell*. VOLUME 22, ISSUE 3, P639-650
- Kikuchi, K., Gupta, V., Wang, J., Holdway, J. E., Wills, A. A., Fang, Y., & Poss, K. D. (2011). Tcf21+ epicardial cells adopt non-myocardial fates during zebrafish heart development and regeneration. *Development*, 138(14), 2895–2902.
- Kikuchi, K., Holdway, J. E., Werdich, A. A., Anderson, R. M., Fang, Y., Egnaczyk, G. F., Evans, T., Macrae, C. A., Stainier, D. Y. R., & Poss, K. D. (2010). Primary contribution to zebrafish heart regeneration by gata4(+) cardiomyocytes. *Nature*, 464(7288), 601–605.
- Kim, J., Wu, Q., Zhang, Y., Wiens, K. M., Huang, Y., Rubin, N., & Shimada, H. (2010). PDGF signaling is required for epicardial function and blood vessel formation in regenerating zebra fish hearts. 3–7. *PNAS* 107 (40) 17206-17210
- Kinkel, M. D., Eames, S. C., Philipson, L. H., & Prince, V. E. (2010). Intraperitoneal injection into adult zebrafish. *Journal of Visualized Experiments : JoVE*, 42, 3–6.
- Lepilina, A., Coon, A. N., Kikuchi, K., Holdway, J. E., Roberts, R. W., Burns, C. G., & Poss, K. D. (2006). A Dynamic Epicardial Injury Response Supports Progenitor Cell Activity during Zebrafish Heart Regeneration. *Cell*, 127(3), 607–619.
- Männer, J. (1999). Does the subepicardial mesenchyme contribute myocardioblasts to the myocardium of the chick embryo heart? A quail-chick chimera study tracing the fate of the epicardial primordium. *Anatomical Record*. Volume 255, Issue 2, Pages 212-226
- Mikawa, T., & Gourdie, R. G. (1996). Pericardial mesoderm generates a population of coronary smooth muscle cells migrating into the heart along with ingrowth of the epicardial organ. *Developmental Biology*. Volume 174, Issue 2, Pages 221-232
- Moerkamp, A. T., Lodder, K., Van Herwaarden, T., Dronkers, E., Dingenouts, C. K. E., Tengström, F. C., Van Brakel, T. J., Goumans, M. J., & Smits, A. M. (2016). Human fetal and adult epicardial-derived cells: A novel model to study their activation. *Stem Cell Research and Therapy*. 7, 174
- Mosimann, C., Kaufman, C. K., Li, P., Pugach, E. K., Tamplin, O. J., & Zon, L. I. (2011).

- Ubiquitous transgene expression and Cre-based recombination driven by the ubiquitin promoter in zebrafish. *Development (Cambridge, England)*, 138(1), 169–177.
- Muraro, M. J., Dharmadhikari, G., Grün, D., Groen, N., Dielen, T., Jansen, E., van Gorp, L., Engelse, M. A., Carlotti, F., de Koning, E. J. P., & van Oudenaarden, A. (2016). A Single-Cell Transcriptome Atlas of the Human Pancreas. *Cell Systems*, 3(4), 385–394.e3.
- Nguyen, P. D., de Bakker, D. E. M., & Bakkers, J. (2021). Cardiac regenerative capacity: an evolutionary afterthought?. *Cellular and molecular life sciences* : 10.1007/s00018-021-03831-9. Epub ahead of print.
- Ocaña, O. H., Coskun, H., Minguillón, C., Murawala, P., Tanaka, E. M., Galcerán, J., Muñoz-Chápuli, R., & Nieto, M. A. (2017). A right-handed signalling pathway drives heart looping in vertebrates. *Nature*, 549(7670), 86–90.
- Poss, K. D. (2010). Advances in understanding tissue regenerative capacity and mechanisms in animals. *Nature Reviews Genetics*, 11(10), 710–722.
- Poss, K. D., Wilson, L. G., & Keating, M. T. (2002). Heart regeneration in zebrafish. *Science (New York, N.Y.)*, 298(5601), 2188–2190.
- Rudat, C., & Kispert, A. (2012). Wt1 and epicardial fate mapping. *Circulation Research*, 111:165–169
- Héctor Sánchez-Iranzo, María Galardi-Castilla, Andrés Sanz-Morejón, Juan Manuel González-Rosa, Ricardo Costa, Alexander Ernst, Julio Sainz de Aja, Xavier Langa, Nadia Mercader (2018). *Transient fibrosis resolves via fibroblast inactivation in the regenerating zebrafish heart. PNAS* 115 (16) 4188–4193
- Satoh, A., Cummings, G. M. C., Bryant, S. V., & Gardiner, D. M. (2010). Neurotrophic regulation of fibroblast dedifferentiation during limb skeletal regeneration in the axolotl (*Ambystoma mexicanum*). *Developmental Biology*. Volume 337, Issue 2, Pages 444–457
- Schnabel, K., Wu, C. C., Kurth, T., & Weidinger, G. (2011). Regeneration of cryoinjury induced necrotic heart lesions in zebrafish is associated with epicardial activation and cardiomyocyte proliferation. *PLoS ONE*, 6(4): e18503
- Smart, N., Bollini, S., Dubé, K. N., Vieira, J. M., Zhou, B., Davidson, S., Yellon, D., Riegler, J., Price, A. N., Lythgoe, M. F., Pu, W. T., & Riley, P. R. (2011). De novo cardiomyocytes from within the activated adult heart after injury. *Nature*, 474, pages640–644
- Stelnicki, E. J., Arbeit, J., Cass, D. L., Saner, C., Harrison, M., & Largman, C. (1998). Modulation of the human homeobox genes PRX-2 and HOXB13 in scarless fetal wounds. *Journal of Investigative Dermatology*. vol.111, issue 1, p57-63
- Tessadori, F., van Weerd, J. H., Burkhard, S. B., Verkerk, A. O., de Pater, E., Boukens, B. J., Vink, A., Christoffels, V. M., & Bakkers, J. (2012). Identification and Functional Characterization of Cardiac Pacemaker Cells in Zebrafish. *PLoS ONE*, 7(10).
- Travers, J. G., Kamal, F. A., Robbins, J., Yutzey, K. E., & Blaxall, B. C. (2016). Cardiac Fibrosis: The Fibroblast Awakens. *Circulation Research*, 118(6), 1021–1040.
- Vanlandewijck, M., He, L., Mäe, M. A., Andrae, J., Ando, K., Del Gaudio, F., Nahar, K., Lebouvier, T., Laviña, B., Gouveia, L., Sun, Y., Raschperger, E., Räsänen, M., Zarb, Y., Mochizuki, N., Keller, A., Lendahl, U., & Betsholtz, C. (2018). A molecular atlas of cell types and zonation in the brain vasculature. *Nature*, 554(7693), 475–480.
- Wang, J., Cao, J., Dickson, A. L., & Poss, K. D. (2015). Epicardial regeneration is guided by cardiac outflow tract and Hedgehog signalling. *Nature*, 522, pages226–230
- Weinberger, M., Simões, F. C., Patient, R., Sauka-Spengler, T., & Riley, P. R. (2020). Functional Heterogeneity within the Developing Zebrafish Epicardium. *Developmental Cell*, 52(5), 574–590. e6.
- Wu, C. C., Kruse, F., Vasudevarao, M. D., Junker, J. P., Zebrowski, D. C., Fischer, K., Noël, E. S., Grün, D., Berezikov, E., Engel, F. B., van Oudenaarden, A., Weidinger, G., & Bakkers, J. (2015). Spatially Resolved Genome-wide Transcriptional Profiling Identifies BMP Signaling as Essential Regulator of Zebrafish Cardiomyocyte Regeneration. *Developmental Cell*, 36–49.
- Yokoyama, H., Maruoka, T., Aruga, A., Amano, T., Ohgo, S., Shiroishi, T., & Tamura, K. (2011). Prx-1 expression in xenopus laevis scarless skin-wound healing and its resemblance to epimorphic regeneration. *Journal of Investigative Dermatology*. vol.131, issue 12, p2477–2485
- Zangi, L., Lui, K. O., Von Gise, A., Ma, Q., Ebina, W., Ptaszek, L. M., Später, D., Xu, H., Tabebordbar, M., Gorbator, R., Sena, B., Nahrendorf, M., Briscoe, D. M., Li, R. A., Wagers, A. J., Rossi, D. J., Pu, W. T., & Chien, K. R. (2013). Modified mRNA directs the fate of heart progenitor cells and induces vascular regeneration after myocardial infarction. *Nature Biotechnology*, 31, pages898–907

SUPPLEMENTARY INFORMATION

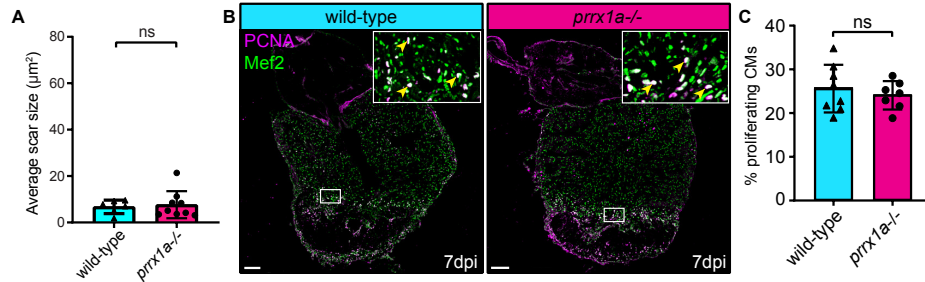


FIG. S1. *prrx1a* is dispensable for zebrafish border zone cardiomyocyte proliferation and heart regeneration. (A) Quantification of the remaining scar size at 30dpi shows no significant difference between *prrx1a*^{-/-} hearts (n=9) and wild-type siblings (n=6). (mean±s.d., ns= not significant, unpaired t-test). (B) Immunofluorescent staining on 7dpi wild-type and *prrx1a*^{-/-} heart sections using an anti-Mef2 antibody as a marker for cardiomyocyte nuclei, and an anti-PCNA antibody as a nuclear proliferation marker. Arrowheads in zoom-ins indicate proliferating cardiomyocytes. Scale bars represent 100μm in the overview images and 10μm in the zoom-ins. (C) Quantification of the percentage of (PCNA+) proliferating border zone cardiomyocytes shows no significant difference between *prrx1a*^{-/-} hearts (n=7) and their wild-type siblings (n=8). (mean±s.d., ns= not significant, unpaired t-test).

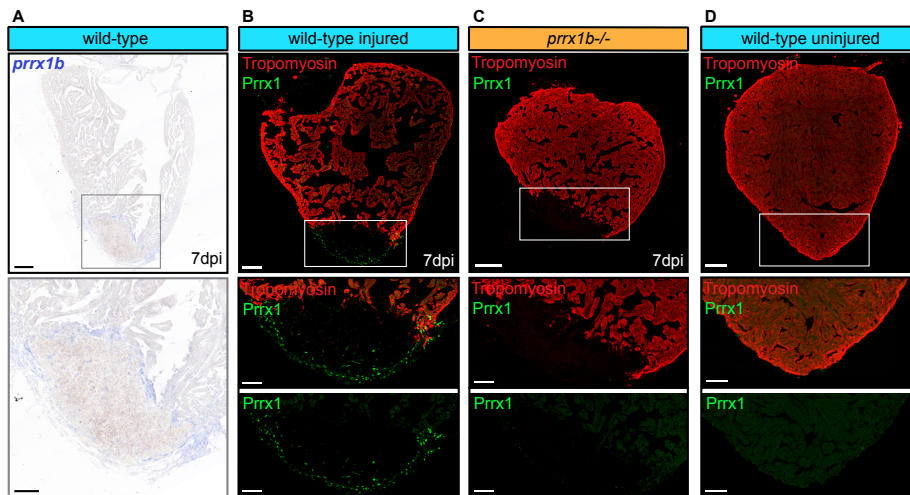


FIG. S2. Injured zebrafish hearts express Prrx1 in cells surrounding the injury area, which is severely reduced in the *prrx1b*^{-/-} hearts. (A) *in situ* hybridization for *prrx1b* on 7dpi wild-type hearts shows *prrx1b* mRNA surrounding and within the injury area. (B-D) Immunofluorescent staining of tropomyosin staining CM nuclei (red) and Prrx1 protein (green) in (B) injured wild-type hearts at 7dpi, (C) injured *prrx1b*^{-/-} hearts at 7 dpi and (D) uninjured wildtype hearts. Scale bars represent 100μm in the overview images and 50μm in the zoom-ins. Hearts analyzed per condition: 3.

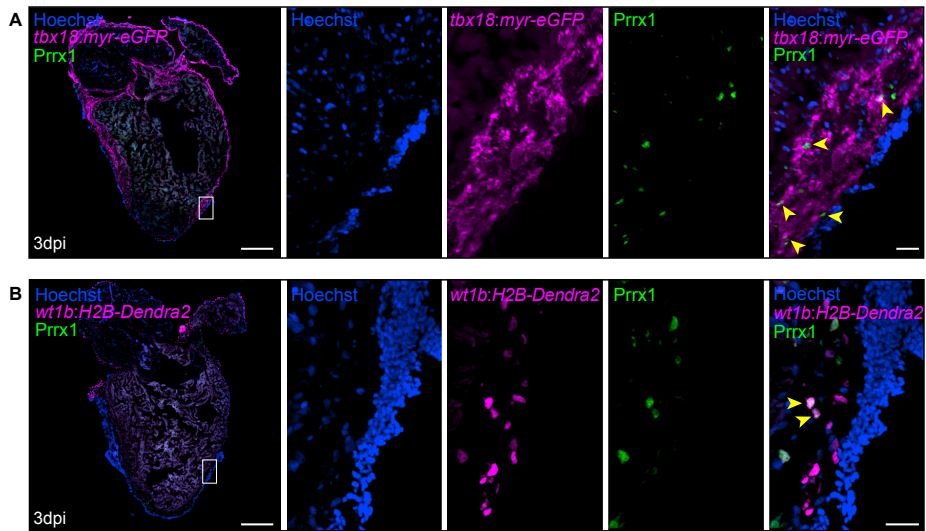


FIG. S3. Prrx1 is expressed in *tbx18+* and *wt1b+* epicardial cells. (A) Immunofluorescent staining on a 3dpi Tg(*tbx18:myr-eGFP*) heart, staining Hoechst, *tbx18:myr-eGFP* (membrane) and Prrx1 (nuclei). Arrowheads indicate double positive cells. **(B)** Immunofluorescent staining on a 3dpi Tg(*wt1b:H2B-Dendra2*) heart, staining Hoechst, *wt1b:H2B-Dendra2* (nuclei) and Prrx1 (nuclei). Arrowheads indicate double positive cells. Scale bars in the overview images represent 100um and in the zoom ins 20um.

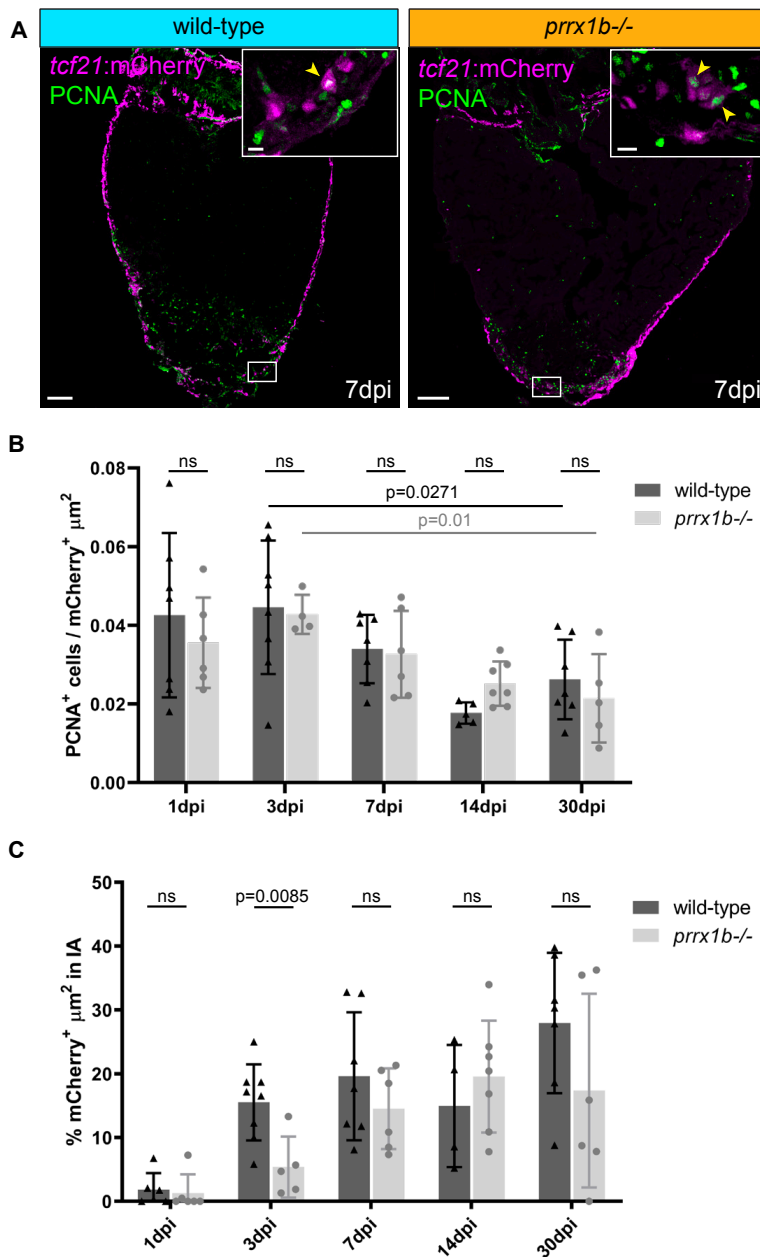


FIG. S4. Quantification of invasion and proliferation of *tcf21:mCherry*⁺ cells at 1, 3, 7, 14 and 30dpi in wild-type and *prrx1b*^{-/-} hearts. (A) Immunofluorescent staining showing PCNA (green) and *tcf21:mCherry* (magenta) in wild-type sibling and *prrx1b*^{-/-} hearts at 7dpi. Scalebar = 100µm, scale bar in zoom in = 10µm. **(B)** Proliferation of *tcf21:mCherry*⁺ cells quantified as amount of PCNA⁺ cells per total µm² of *tcf21:mCherry*⁺ tissue surface in the ventricle at 1, 3, 7, 14 and 30dpi. (mean±s.d., wild-type 3dpi vs wild-type 30dpi p=0.0271, *prrx1b*^{-/-} 3dpi vs *prrx1b*^{-/-} 30dpi p=0.01, ns= not significant, unpaired t-test). **(C)** Percentage of the total injury *tcf21:mCherry*⁺ µm² found inside the injury area at 1, 3, 7, 14 and 30dpi. (mean±s.d., wild-type 3dpi vs *prrx1b*^{-/-} 3dpi p=0.0085, ns=not significant, unpaired t-test). IA = injury area.

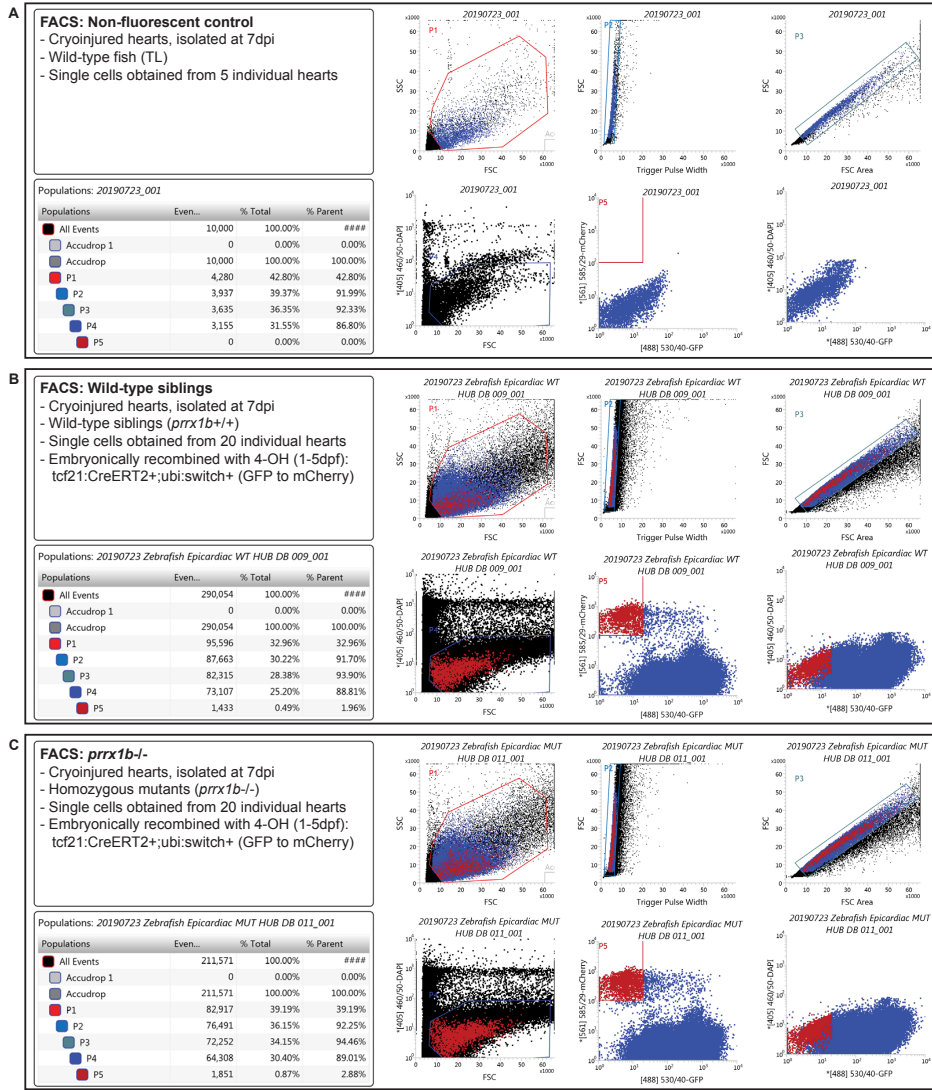


FIG. S5. Gating details for FACS. (A-C) Gates (P1-P5) used to sort out mCherry⁺/GFP⁻ cells used for single cell sequencing analysis.

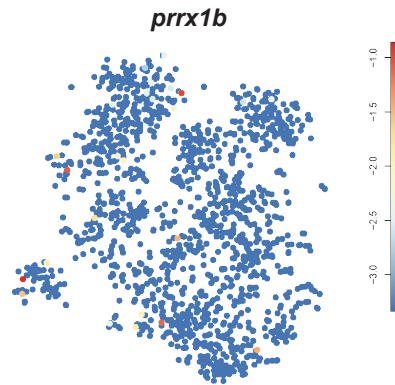


FIG. S6. *prrx1b* read counts. tSNE map visualizing log₂-transformed read-counts for *prrx1b* based on our scRNA sequencing of *tcf21:mCherry*⁺ cells.

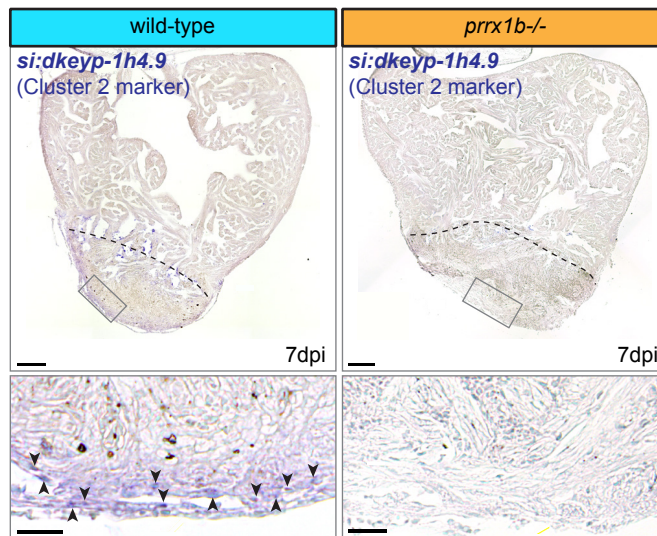
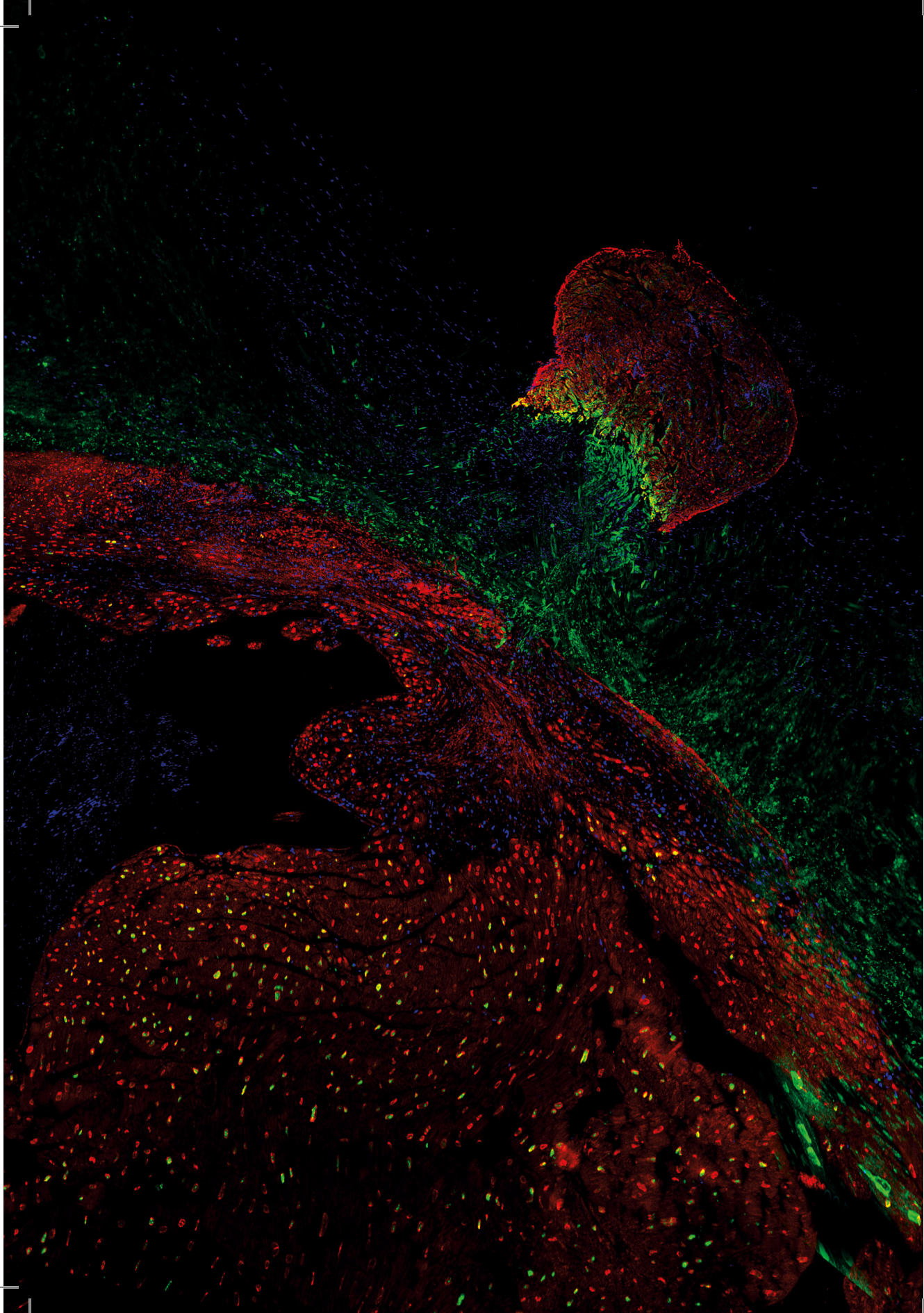


FIG. S7. *prrx1b*^{-/-} hearts show a strong reduction of *si:dkeyp-1h4.9* expression. (A,B) *In situ* hybridization for the cluster 2 gene *si:dkeyp-1h4.9* in either wild-type or *prrx1b*^{-/-} hearts at 7dpi. Arrowheads point to cells with high expression. Scale bars represent 100μm in the overview images and 25μm in the zoom-in. Hearts analysed per condition: 3



CHAPTER VI

Discussion

The border zone as cellular source for regenerated cardiomyocytes

In the past decades, several strategies have been explored that aim to replenish or regrow the cardiomyocytes lost due to ischemic heart injury. These strategies include (1) the stimulation of proliferation of resident stem/progenitor cells to produce new cardiomyocytes, (2) transplantation of stem/progenitor cells, (3) transplantation of induced pluripotent stem cell derived cardiomyocytes and (4) induction of proliferation in pre-existing, adult cardiomyocytes.

(1) To replace the lost myocardium, it was attempted to activate cardiomyocyte regeneration by stimulating proliferation of resident cardiac progenitor cells (i.e. stem cells). While many studies have reported stem cell marker expression in the mammalian heart (i.e. c-kit), it is now generally accepted that the adult heart is devoid of an endogenous cardiac stem cell population (Kretzschmar et al., 2018; Sultana et al., 2015; van Berlo et al., 2014). Consequently, the interest in this strategy has declined in recent years.

Cardiomyocyte regeneration*

The *in vivo* generation of new cardiomyocytes with the specific purpose to replace cardiomyocytes lost due to tissue injury.

Cardiomyocyte replenishment*

Transplantation of cardiomyocytes (or progenitors) into the heart which were produced *ex vivo*.

* as defined here

(2) In addition, it is explored whether the lost myocardium can be replenished through the transplantation of stem/progenitor cells. These include the use of bone marrow derived (c-kit⁺) mesenchymal cells. A big obstacle for this strategy is the low amount of cells retained in the heart, despite attempts to increase its efficiency (Hofmann et al., 2005; Hou et al., 2005; Wall et al., 2010). The low rate of retention and efficacy of the transplanted cells is likely due to the lack of a cellular niche supporting stem cell activity and thereby the maintenance of their pluripotent cell state. In addition, the degree of engraftment into the heart does not seem to reflect the degree of functional improvement, suggesting that the observed benefits are not due to a replenishment of cardiomyocytes (Loffredo et al., 2011). Despite the concerns about the efficacy of bone marrow-derived cell transplantation, clinical trials have been performed that show potential beneficial effects in patients suffering ischemic cardiomyopathy (Hare et al., 2012).

(3) Another, and perhaps more effective strategy to replenish lost cardiomyocytes, is through the direct transplantation of cardiomyocytes derived from induced pluripotent stem cells. Indeed, several recent studies indicate successful engraftment and potential beneficial effects, although long-term (>3 months) engraftment was not documented (Chong et al., 2014; Kawamura et al., 2016; Riegler et al., 2015; Shiba et al., 2012; Weinberger et al., 2016).

(4) Furthermore, recent studies have investigated whether stimulating proliferation of adult,

pre-existing cardiomyocytes can be used to regrow the lost myocardium following ischemic injury. Indeed, pre-clinical studies in mice indicate that modulating the Nrg1/ErbB2 and/or Hippo pathway is sufficient to induce cardiomyocyte proliferation and consequent heart regeneration in mice (D'Uva et al., 2015; Heallen et al., 2013). In addition, the downstream effects of ischemic injury (i.e. heart failure) could be reversed using this strategy (Aharonov et al., 2020; Leach et al., 2017).

In this thesis, pre-existing cardiomyocytes are targeted as the primary source for newly regenerated cardiomyocytes. In 2010, two back-to-back publications were the first to claim that the source of regenerated cardiomyocytes during endogenous zebrafish heart regeneration is formed by adult, pre-existing cardiomyocytes and not by a dedicated progenitor cell population (Jopling et al., 2010; Kikuchi et al., 2010). Using cellular lineage tracing, the authors showed that during zebrafish heart regeneration the new regenerate originates from *myl7* positive cells. Since *Myl7* is considered a marker for adult, differentiated cardiomyocytes, they concluded that the regenerated cardiomyocytes originate from adult, pre-existing cardiomyocytes and not from a dedicated stem cell population. More recent studies indicate that the regenerative capacity of the neonatal mouse heart also depends on pre-existing cardiomyocytes as a cellular source (Porrello et al., 2013). Hence, if we want to stimulate the endogenous regenerative capacity of the mammalian heart, focusing on adult pre-existing cardiomyocytes as cellular source might be the most effective strategy.

It should be noted, however, that adult, pre-existing cardiomyocytes are not a homogenous population. Indeed, single cell sequencing indicates that certain cardiomyocyte sub-populations of cardiomyocytes exist in the murine heart (Gladka et al., 2018). Besides differences on transcriptional level, cardiomyocytes of the mammalian heart can also differ in DNA-content. While most zebrafish cardiomyocytes are diploid and mononuclear (González-Rosa et al., 2018), the majority of mouse cardiomyocytes are multinuclear and the majority of human cardiomyocytes are polyploid (Brodsky et al., 1994; Li et al., 1996; Soonpaa et al., 1996). Both multi-nucleation and polyploidization are indicated to inhibit cellular proliferation (Patterson et al., 2017; Windmueller et al., 2020). Therefore, regenerative treatments have to either overcome these cell-intrinsic hurdles or instead focus exclusively on stimulating proliferation in mononuclear, diploid cardiomyocytes.

So far, we can postulate that adult, pre-existing cardiomyocytes with a mononuclear, diploid nucleus are the best source for newly formed cardiomyocytes. However, their localization should also be considered. Indeed, several studies have reported that the cardiomyocytes located at the injury border are more responsive to pro-mitogenic stimuli than more remotely localized cardiomyocytes. Work presented in this thesis (Chapter III) suggests that the susceptibility of border zone cardiomyocytes to mitogenic stimuli might be due to the partial dedifferentiation that occurs in border zone cardiomyocytes as they respond to ischemia

induced cellular stress. Considering that dedifferentiation is preceding cardiomyocyte proliferation in models of regeneration (D'Uva et al., 2015; Honkoop et al., 2019; Jopling et al., 2010), the partial dedifferentiation of border zone cardiomyocytes could prime them for pro-proliferative stimuli. Interestingly, a recent study suggests the existence of regeneration-specific enhancers that evolved from stress-responsive regulatory elements, illustrating the evolutionary relationship between the injury response and tissue regeneration (Wang et al., 2020). Indeed, the regenerative response of zebrafish border zone could be viewed as an adapted injury response, focused on not only limiting the effects of the injury but regenerating the lost tissue as well.

Elucidating the molecular mechanisms behind the striking difference in regenerative capacity between the zebrafish and mammalian heart

Now, I will explore the connection between the findings of the individual chapters, together forming a hypothetical model of a zebrafish-specific pathway that allows for heart regeneration (Fig.1). The inactivity of this pathway in mammalian hearts could help explain their limited regenerative capacity.

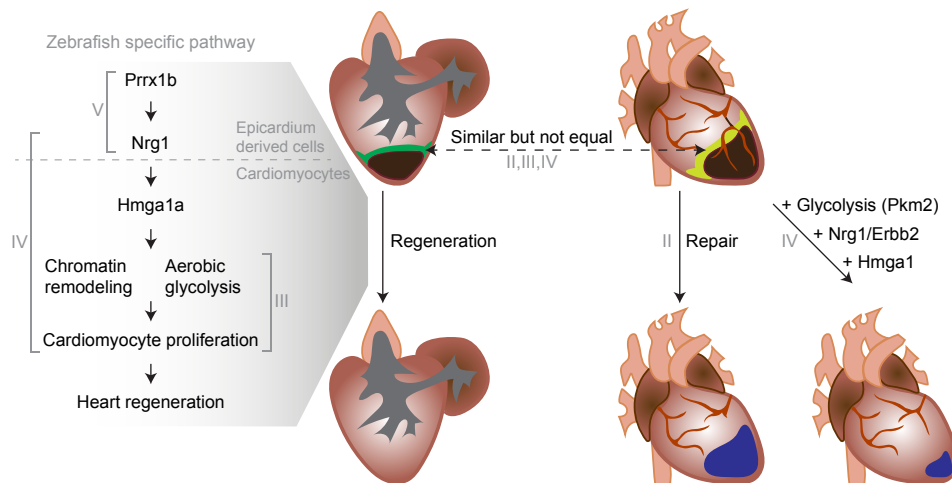


FIGURE 1. Overarching model of the work presented in this thesis. (Left) Zebrafish specific pathway leading to heart regeneration. (Right) Injured zebrafish and mammalian hearts form an injury border zone (green and light green) upon injury, which are similar but not equal. Border zone processes in the zebrafish heart allow it to regenerate. Border zone processes in the mammalian heart ensure immediate survival, but do not lead to regeneration. Instead, a permanent scar is formed (blue). Induction of factors that are endogenously employed during zebrafish heart regeneration (i.e. glycolysis, Nrg1 and potentially Hmga1) can induce tissue regeneration and functional improvement in injured mammalian hearts. Roman numbers (I to V) indicate the thesis chapters on which the specific steps are based.

The work presented in this thesis has focused on characterizing the zebrafish and mammalian border zone (Chapters II and III), making a direct transcriptomic comparison between the two (Chapter IV) and functional investigation of one of the identified differentially expressed genes, *hmga1a* (Chapter IV). In Chapter V, we have focused on the role of *prx1b* during zebrafish heart regeneration, which is expressed in epicardium derived cells. Therefore, Chapter V appears to hold little connection to the other chapters which focus on processes occurring in border zone cardiomyocytes. However, it should be noted that our interest in Prrx1b originated from the transcriptomic comparison between the zebrafish and mouse border zones. Indeed, unpublished data indicates that injured mouse and human ventricles shows a near lack of Prrx1/PRRX1 expression (Esther Dronkers, LUMC, data not shown). Besides their specific expression in the injured zebrafish heart, there is another interesting connection between *prx1b* and *hmga1a* – their genetic interaction with the mitogen Neuregulin 1 (Nrg1). We have shown that *prx1b* is required for Nrg1 production in epicardial derived cells and consequent border zone cardiomyocyte proliferation, placing Prrx1b upstream of Nrg1 signaling. In addition, we have shown that Nrg1 signaling induces *hmga1a* expression in cardiomyocytes which is required for the pro-proliferative effects of Nrg1. These results place *hmga1a* downstream of Nrg1 signaling. Considering these findings, one could hypothesize that *prx1b* and *hmga1a* act in the same Nrg1-dependent pathway, stimulating regeneration in the injured zebrafish heart.

In Chapter II, we have presented work indicating that induction of glycolysis is essential for cardiomyocyte proliferation during zebrafish heart regeneration. Furthermore, we have shown that Nrg1/ErbB2 signaling (where Nrg1 is the ligand and ErbB2 the receptor) induces glycolysis and that this metabolic adaptation is necessary for Nrg1/ErbB2 induced cardiomyocyte proliferation. Hence, both *hmga1a* and glycolysis are induced upon Nrg1/ErbB2 signaling. In addition, we have shown that both *hmga1a* and glycolysis are required for Nrg1-induced cardiomyocyte proliferation (Chapter II, V). Interestingly, overexpression of *hmga1a* in cardiomyocytes initiates metabolic reprogramming and *hmga1a*^{-/-} hearts fail to induce robust expression of the rate-limiting glycolysis enzyme hexokinase. Therefore, I hypothesize that glycolysis acts downstream of *hmga1a* to allow for cardiomyocyte proliferation and heart regeneration.

Important questions arise concerning this hypothetical model; Is the induction of glycolysis absent from the mammalian border zone? And could this help explain the limited regenerative capacity of the mammalian heart? Interestingly, inhibition of fatty acid utilization and stimulation of the oxidation of glycolytically derived pyruvate (through knock-out of PDK4) is sufficient to initiate cardiomyocyte proliferation in mammals (Cardoso et al., 2020). This finding suggests that adult mammalian cardiomyocytes retain proliferative capacity which can be accessed when the right metabolic conditions are met. Murine border zone cardiomyocytes do undergo metabolic adaptation in response to the ischemic injury, mainly

through the downregulation of fatty acid dependent metabolism (Chapter III, IV). However, no compelling evidence was found that suggests the induction of glycolysis in the murine border zone, as is the case in the zebrafish. Interestingly, overexpression of the glycolytic enzyme Pkm2 in murine border zone cardiomyocytes induces proliferation and heart regeneration (Magadam et al., 2020). In addition, Nrg1/ErbB2-induced cardiomyocyte proliferation and heart regeneration in the injured murine heart is also dependent on the ectopic induction of glycolysis (Chapter III). Together, these findings suggest that while mammalian border zone cardiomyocytes do undergo metabolic adaptations, glycolysis is not induced sufficiently to support the induction of cardiomyocyte proliferation. Therefore, similar to the induction of *prx1b* and *hmga1a* expression, the sufficient induction of glycolysis appears to be a trait specific to the zebrafish, but not the mammalian heart.

While the connection between *prx1b*, *nrg1*, *hmga1a* and glycolysis seems plausible, it should be noted that the presented model is merely hypothetical. Many important questions remain unanswered; Is *hmga1a* expression absent in *prx1b*^{-/-} hearts? Is the induction of glycolysis dependent on *hmga1a* and *prx1b*? Can we rescue the proliferation defect observed in the *hmga1a* and *prx1b* mutants by inducing glycolysis in border zone cardiomyocytes? These, together with many other questions need to be resolved if we want to fully understand the molecular reasons behind the striking difference in regenerative capacity between the zebrafish and mammalian heart. In addition, the factors and processes described in this thesis likely form only a small part of the complex regulatory system enabling the zebrafish heart to regenerate. Regardless, the work presented here contributes to the elucidation of a zebrafish-specific molecular pathway, which could be induced in injured mammalian hearts to stimulate regeneration. Indeed, in recent years several components of the pathway indicated in Figure 1 have been reported to stimulate heart regeneration in mammalian hearts, including Nrg1/ErbB2 signaling and glycolysis (Pkm2). In this thesis, we present data suggesting that Hmga1 could fulfill a similar function, providing another substrate that could be used to stimulate mammalian heart regeneration.

Stimulating heart regeneration in patients suffering ischemic heart injury

At the start of my PhD project in 2015, I wondered whether we would ever be able to initiate human heart regeneration. Now, six years later, I feel confident that I will be around to witness the implementation of the first pro-regenerative treatments for patients suffering heart disease (barring car accidents and coffee overdoses). I base this (perhaps naïve) prediction on the huge scientific leaps that have been made in the past decade, including the identification of the regenerative capacity of the neonatal mouse and potentially the human heart (Haubner et al., 2016; Porrello et al., 2011, 2013), as well as the low cardiomyocyte turnover in adult human hearts (Ali et al., 2014; Bergmann et al., 2009). Together, these findings suggest that cardiomyocytes of the adult mammalian heart might retain a latent proliferative capacity, which could be targeted to stimulate heart regeneration after ischemic

injury. Indeed, recent studies have indicated that modulating the Nrg1/ErbB2 and Hippo pathways can induce cardiomyocyte proliferation and consequent heart regeneration in murine hearts (D'Uva et al., 2015; Heallen et al., 2013). Excitingly, it appears that inducing cardiomyocyte proliferation by itself has the potential to induce regeneration in hearts suffering ischemic damage, including the regression of scar tissue. Furthermore, it has been shown that heart failure itself can be reversed by stimulating cardiomyocyte proliferation (Aharonov et al., 2020; Leach et al., 2017). Taken together, it appears we are closer than ever to develop a pro-regenerative treatment for patients suffering heart injuries.

However, substantial challenges remain to be overcome before successful pro-regenerative treatments can be developed. For instance, the induction of mitogenic factors could lead to uncontrolled cell division and cancer. Indeed, certain tumors are known to depend on glycolysis and both ErbB2 and Hmga1 are well-established oncogenes. Therefore, the spatially and temporally restricted administration of pro-mitogenic factors will be key to develop safe but potent pro-regenerative treatments. One way to accomplish temporally restricted mitogenic effects could be through the use of factors that are only active in the context of tissue injury (i.e. Hmga1 which appears to only act pro-mitotically in the injury border zone). In addition, we should be cautioned by the examples of other strategies explored to replenish the cardiomyocytes of the heart (i.e. transplantation of stem/progenitor cells) which showed promising results initially, but proved challenging to implement as a pro-regenerative treatment.

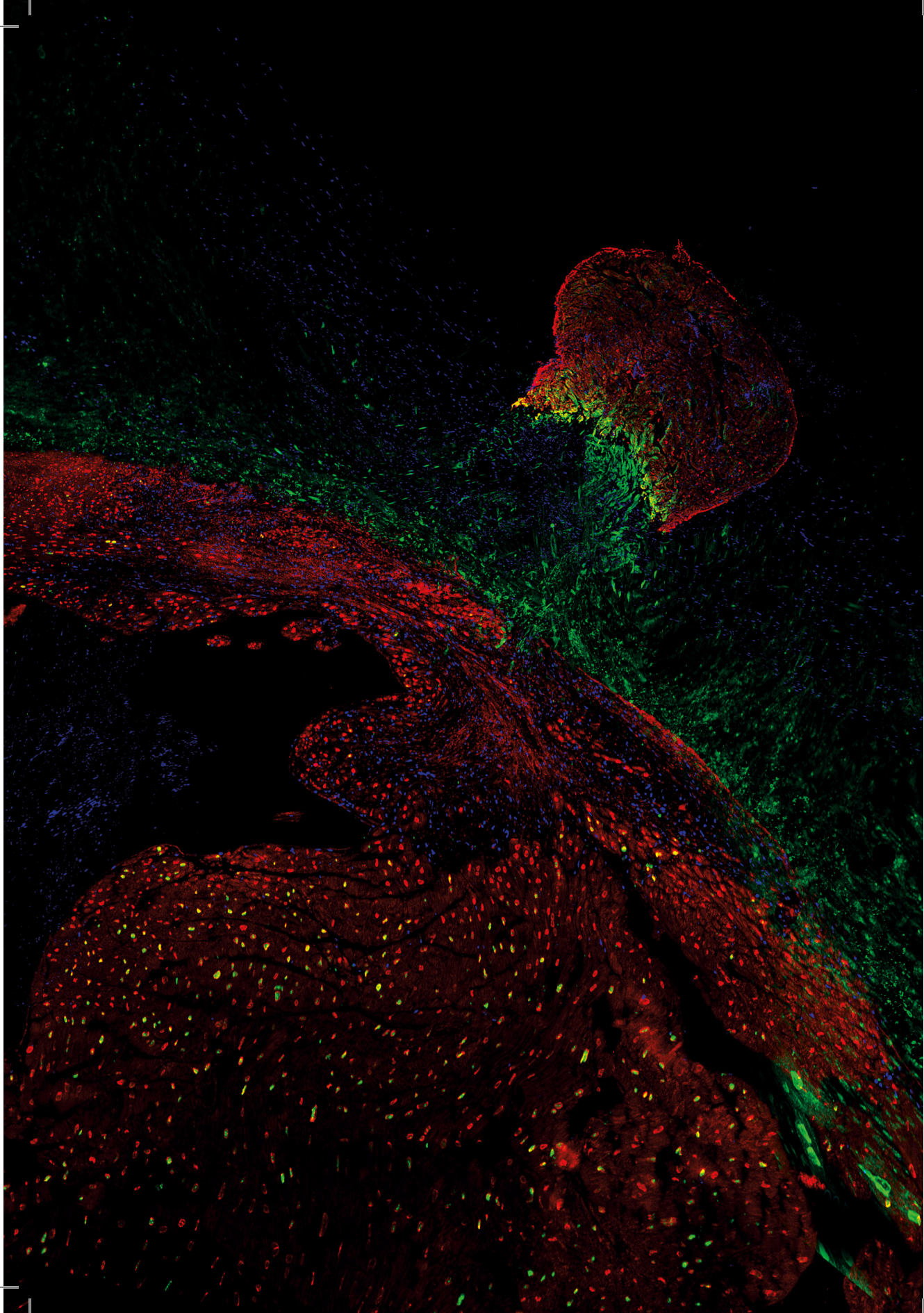
Despite these substantial hurdles, I feel confident that through the ongoing collaboration between fundamental and clinical researchers, pro-regenerative treatments for the heart are underway.

REFERENCES

- Aharonov, A., Shakked, A., Umansky, K. B., Savidor, A., Genzelinakh, A., Kain, D., Lendengolts, D., Revach, O.-Y., Morikawa, Y., Dong, J., Levin, Y., Geiger, B., Martin, J. F., & Tzahor, E. (2020). ERBB2 drives YAP activation and EMT-like processes during cardiac regeneration. *Nature Cell Biology*. <https://doi.org/10.1038/s41556-020-00588-4>
- Ali, S. R., Hippenmeyer, S., Saadat, L. V., Luo, L., Weissman, I. L., & Ardehali, R. (2014). Existing cardiomyocytes generate cardiomyocytes at a low rate after birth in mice. *Proceedings of the National Academy of Sciences of the United States of America*, 111(24), 8850–8855. <https://doi.org/10.1073/pnas.1408233111>
- Baehr, A., Umansky, K. B., Bassat, E., Jurisch, V., Klett, K., Bozoglu, T., Hornaschewitz, N., Solyanik, O., Kain, D., Ferraro, B., Cohen-Rabi, R., Krane, M., Cyran, C., Soehnlein, O., Laugwitz, K. L., Hinkel, R., Kupatt, C., & Tzahor, E. (2020). Agrin promotes coordinated therapeutic processes leading to improved cardiac repair in pigs. *Circulation*. <https://doi.org/10.1161/CIRCULATIONAHA.119.045116>
- Bergmann, O., Bhardwaj, R. D., Bernard, S., Zdunek, S., Barnabé-Heide, F., Walsh, S., Zupicich, J., Alkass, K., Buchholz, B. A., Druid, H., Jovinge, S., & Frisén, J. (2009). Evidence for cardiomyocyte renewal in humans. *Science*. <https://doi.org/10.1126/science.1164680>
- Brodsky, V. Y., Arefyeva, A. M., Gvasava, I. G., Sarkisov, D. S., & Panova, N. W. (1994). Polyploidy in cardiac myocytes of normal and hypertrophic human hearts; range of values. *Virchows Archiv*. <https://doi.org/10.1007/BF00190566>
- Cardoso, A. C., Lam, N. T., Savla, J. J., Nakada, Y., Pereira, A. H. M., Elnwasany, A., Menendez-Montes, I., Ensley, E. L., Bezan Petric, U., Sharma, G., Sherry, A. D., Malloy, C. R., Khemtong, C., Kinter, M. T., Tan, W. L. W., Anene-Nzeli, C. G., Foo, R. S. Y., Nguyen, N. U. N., Li, S., ... Sadek, H. A. (2020). Mitochondrial substrate utilization regulates cardiomyocyte cell-cycle progression. *Nature Metabolism*, 2(2), 167–178. <https://doi.org/10.1038/s42255-020-0169-x>
- Chong, J. J. H., Yang, X., Don, C. W., Minami, E., Liu, Y.-W., Weyers, J. J., Mahoney, W. M., Van Biber, B., Cook, S. M., Palpant, N. J., Gantz, J. A., Fugate, J. A., Muskheili, V., Gough, G. M., Vogel, K. W., Astley, C. A., Hotchkiss, C. E., Baldessari, A., Pabon, L., ... Murry, C. E. (2014). Human embryonic-stem-cell-derived cardiomyocytes regenerate non-human primate hearts. *Nature*, 510(7504), 273–277. <https://doi.org/10.1038/nature13233>
- D'Uva, G., Aharonov, A., Lauriola, M., Kain, D., Yahalom-Ronen, Y., Carvalho, S., Weisinger, K., Bassat, E., Rajchman, D., Yifa, O., Lysenko, M., Konfino, T., Hegesh, J., Brenner, O., Neeman, M., Yarden, Y., Leor, J., Sarig, R., Harvey, R. P., & Tzahor, E. (2015). ERBB2 triggers mammalian heart regeneration by promoting cardiomyocyte dedifferentiation and proliferation. *Nature Cell Biology*, 17(5). <https://doi.org/10.1038/ncb3149>
- Gladka, M. M., Molenaar, B., De Ruiter, H., Van Der Elst, S., Tsui, H., Versteeg, D., Lacraz, G. P. A., Huibers, M. M. H., Van Oudenaarden, A., & Van Rooij, E. (2018). Single-Cell Sequencing of the Healthy and Diseased Heart Reveals Cytoskeleton-Associated Protein 4 as a New Modulator of Fibroblasts Activation. *Circulation*. <https://doi.org/10.1161/CIRCULATIONAHA.117.030742>
- González-Rosa, J. M., Sharpe, M., Field, D., Soonpaa, M. H., Field, L. J., Burns, C. E., & Burns, C. G. (2018). Myocardial Polyploidization Creates a Barrier to Heart Regeneration in Zebrafish. *Developmental Cell*, 44(4), 433-446.e7. <https://doi.org/10.1016/j.devcel.2018.01.021>
- Hare, J. M., Fishman, J. E., Gerstenblith, G., DiFede Velazquez, D. L., Zambrano, J. P., Suncion, V. Y., Tracy, M., Ghersin, E., Johnston, P. V., Brinker, J. A., Breton, E., Davis-Sproul, J., Schulman, I. H., Byrnes, J., Mendizabal, A. M., Lowery, M. H., Rouy, D., Altman, P., Wong Po Foo, C., ... Lardo, A. (2012). Comparison of allogeneic vs autologous bone marrow-derived mesenchymal stem cells delivered by transcatheter injection in patients with ischemic cardiomyopathy: the POSEIDON randomized trial. *JAMA*, 308(22), 2369–2379. <https://doi.org/10.1001/jama.2012.25321>
- Haubner, B. J., Schneider, J., Schweigmann, U., Schuetz, T., Dichtl, W., Velik-Salchner, C., Stein, J. I., & Penninger, J. M. (2016). Functional Recovery of a Human Neonatal Heart after Severe Myocardial Infarction. *Circulation Research*, 118(2), 216–221. <https://doi.org/10.1161/CIRCRESAHA.115.307017>
- Heallen, T., Morikawa, Y., Leach, J., Tao, G., Willerson, J. T., Johnson, R. L., & Martin, J. F. (2013). Hippo signaling impedes adult heart regeneration. *Development*, 140(23), 4683–4690. <https://doi.org/10.1242/dev.102798>
- Hofmann, M., Wollert, K. C., Meyer, G. P., Menke, A., Arseniev, L., Hertenstein, B., Ganser, A., Knapp, W. H., & Drexler, H. (2005). Monitoring of bone marrow cell homing into the infarcted human myocardium.

- Circulation*, 111(17), 2198–2202. <https://doi.org/10.1161/01.CIR.0000163546.27639.AA>
- Honkoop, H., de Bakker, D. E. M., Aharonov, A., Kruse, F., Shakked, A., Nguyen, P. D., de Heus, C., Garric, L., J Muraro, M., Shoffner, A., Tessadori, F., Peterson, J. C., Noort, W., Bertozzi, A., Weidinger, G., Posthuma, G., Grün, D., van der Laarse, W. J., Klumperman, J., ... Bakkers, J. (2019). Single-cell analysis uncovers that metabolic reprogramming by ErbB2 signaling is essential for cardiomyocyte proliferation in the regenerating heart. *ELife*, 8, 1–27. <https://doi.org/10.7554/eLife.50163>
- Hou, D., Youssef, E. A.-S., Brinton, T. J., Zhang, P., Rogers, P., Price, E. T., Yeung, A. C., Johnstone, B. H., Yock, P. G., & March, K. L. (2005). Radiolabeled cell distribution after intramyocardial, intracoronary, and interstitial retrograde coronary venous delivery: implications for current clinical trials. *Circulation*, 112(9 Suppl), I150-6. <https://doi.org/10.1161/CIRCULATIONAHA.104.526749>
- Jopling, C., Sleep, E., Raya, M., Martí, M., Raya, A., & Belmonte, J. C. I. (2010). Zebrafish heart regeneration occurs by cardiomyocyte dedifferentiation and proliferation. *Nature*, 464(7288), 606–609. <https://doi.org/10.1038/nature08899>
- Kawamura, T., Miyagawa, S., Fukushima, S., Maeda, A., Kashiwama, N., Kawamura, A., Miki, K., Okita, K., Yoshida, Y., Shiina, T., Ogasawara, K., Miyagawa, S., Toda, K., Okuyama, H., & Sawa, Y. (2016). Cardiomyocytes Derived from MHC-Homozygous Induced Pluripotent Stem Cells Exhibit Reduced Alloeneic Immunogenicity in MHC-Matched Non-human Primates. *Stem Cell Reports*, 6(3), 312–320. <https://doi.org/10.1016/j.stemcr.2016.01.012>
- Kikuchi, K., Holdway, J. E., Werdich, A. A., Anderson, R. M., Fang, Y., Egnaczyk, G. F., Evans, T., Macrae, C. A., Stainier, D. Y. R., & Poss, K. D. (2010). Primary contribution to zebrafish heart regeneration by gata4(+) cardiomyocytes. *Nature*, 464(7288), 601–605. <https://doi.org/10.1038/nature08804>
- Kretzschmar, K., Post, Y., Bannier-Hélaouët, M., Mattiotti, A., Drost, J., Basak, O., Li, V. S. W., van den Born, M., Gunst, Q. D., Versteeg, D., Kooijman, L., van der Elst, S., van Es, J. H., van Rooij, E., van den Hoff, M. J. B., & Clevers, H. (2018). Profiling proliferative cells and their progeny in damaged murine hearts. *Proceedings of the National Academy of Sciences of the United States of America*. <https://doi.org/10.1073/pnas.1805829115>
- Leach, J. P., Heallen, T., Zhang, M., Rahmani, M., Morikawa, Y., Hill, M. C., Segura, A., Willerson, J. T., & Martin, J. F. (2017). Hippo pathway deficiency reverses systolic heart failure after infarction. *Nature*, 550(7675), 260–264. <https://doi.org/10.1038/nature24045>
- Li, F., Wang, X., Capasso, J. M., & Gerdes, A. M. (1996). Rapid transition of cardiac myocytes from hyperplasia to hypertrophy during postnatal development. *Journal of Molecular and Cellular Cardiology*. <https://doi.org/10.1006/jmcc.1996.0163>
- Loffredo, F. S., Steinhauser, M. L., Gannon, J., & Lee, R. T. (2011). Bone marrow-derived cell therapy stimulates endogenous cardiomyocyte progenitors and promotes cardiac repair. *Cell Stem Cell*, 8(4), 389–398. <https://doi.org/10.1016/j.stem.2011.02.002>
- Magadum, A., Singh, N., Kurian, A. A., Munir, I., Mehmood, T., Brown, K., Sharkar, M. T. K., Chepurko, E., Sassi, Y., Oh, J. G., Lee, P., Santos, C. X. C., Gaziel-Sovran, A., Zhang, G., Cai, C.-L., Kho, C., Mayr, M., Shah, A. M., Hajjar, R. J., & Zangi, L. (2020). Pkm2 Regulates Cardiomyocyte Cell Cycle and Promotes Cardiac Regeneration. *Circulation*, 141(15), 1249–1265. <https://doi.org/10.1161/CIRCULATIONAHA.119.043067>
- Patterson, M., Barske, L., Van Handel, B., Rau, C. D., Gan, P., Sharma, A., Parikh, S., Denholtz, M., Huang, Y., Yamaguchi, Y., Shen, H., Allayee, H., Crump, J. G., Force, T. I., Lien, C. L., Makita, T., Lusic, A. J., Kumar, S. R., & Sucov, H. M. (2017). Frequency of mononuclear diploid cardiomyocytes underlies natural variation in heart regeneration. *Nature Genetics*. <https://doi.org/10.1038/ng.3929>
- Porrello, E. R., Mahmoud, A. I., Simpson, E., Hill, J. A., Richardson, J. A., Olson, E. N., & Sadek, H. A. (2011). Transient regenerative potential of the neonatal mouse heart. *Science*. <https://doi.org/10.1126/science.1200708>
- Porrello, E. R., Mahmoud, A. I., Simpson, E., Johnson, B. A., Grinsfelder, D., Cansco, D., Mammen, P. P., Rothermel, B. A., Olson, E. N., & Sadek, H. A. (2013). Regulation of neonatal and adult mammalian heart regeneration by the miR-15 family. *Proceedings of the National Academy of Sciences of the United States of America*. <https://doi.org/10.1073/pnas.1208863110>
- Riegler, J., Tiburcy, M., Ebert, A., Tzatzalos, E., Raaz, U., Abilez, O. J., Shen, Q., Kooreman, N. G., Neofytou, E., Chen, V. C., Wang, M., Meyer, T., Tsao, P. S., Connolly, A. J., Couture, L. A., Gold, J. D., Zimmermann, W. H., & Wu, J. C. (2015). Human Engineered Heart Muscles Engraft and Survive Long Term in a Rodent Myocardial Infarction Model. *Circulation Research*, 117(8), 720–730. <https://doi.org/10.1161/CIRCRESAHA.115.306985>

- Shiba, Y., Fernandes, S., Zhu, W.-Z., Filice, D., Muskheli, V., Kim, J., Palpant, N. J., Gantz, J., Moyes, K. W., Reinecke, H., Van Biber, B., Dardas, T., Mignone, J. L., Izawa, A., Hanna, R., Viswanathan, M., Gold, J. D., Kotlikoff, M. I., Sarvazyan, N., ... Laflamme, M. A. (2012). Human ES-cell-derived cardiomyocytes electrically couple and suppress arrhythmias in injured hearts. *Nature*, 489(7415), 322–325. <https://doi.org/10.1038/nature11317>
- Soonpaa, M. H., Kim, K. K., Pajak, L., Franklin, M., & Field, L. J. (1996). Cardiomyocyte DNA synthesis and binucleation during murine development. *American Journal of Physiology - Heart and Circulatory Physiology*. <https://doi.org/10.1152/ajpheart.1996.271.5.h2183>
- Sultana, N., Zhang, L., Yan, J., Chen, J., Cai, W., Razzaque, S., Jeong, D., Sheng, W., Bu, L., Xu, M., Huang, G.-Y., Hajar, R. J., Zhou, B., Moon, A., & Cai, C.-L. (2015). Resident c-kit(+) cells in the heart are not cardiac stem cells. *Nature Communications*, 6, 8701. <https://doi.org/10.1038/ncomms9701>
- van Berlo, J. H., Kanisicak, O., Maillet, M., Vagnozzi, R. J., Karch, J., Lin, S.-C. J., Middleton, R. C., Marbán, E., & Molkentin, J. D. (2014). c-kit+ cells minimally contribute cardiomyocytes to the heart. *Nature*, 509(7500), 337–341. <https://doi.org/10.1038/nature13309>
- Wall, S. T., Yeh, C.-C., Tu, R. Y. K., Mann, M. J., & Healy, K. E. (2010). Biomimetic matrices for myocardial stabilization and stem cell transplantation. *Journal of Biomedical Materials Research. Part A*, 95(4), 1055–1066. <https://doi.org/10.1002/jbm.a.32904>
- Wang, W., Hu, C. K., Zeng, A., Alegre, D., Hu, D., Gotting, K., Granillo, A. O., Wang, Y., Robb, S., Schnittker, R., Zhang, S., Alegre, D., Li, H., Ross, E., Zhang, N., Brunet, A., & Alvarado, A. S. (2020). Changes in regeneration-responsive enhancers shape regenerative capacities in vertebrates. *Science*. <https://doi.org/10.1126/SCIENCE.AAZ3090>
- Weinberger, F., Breckwoldt, K., Pecha, S., Kelly, A., Geertz, B., Starbatty, J., Yorgan, T., Cheng, K.-H., Lessmann, K., Stolen, T., Scherrer-Crosbie, M., Smith, G., Reichenspurner, H., Hansen, A., & Eschenhagen, T. (2016). Cardiac repair in guinea pigs with human engineered heart tissue from induced pluripotent stem cells. *Science Translational Medicine*, 8(363), 363ra148. <https://doi.org/10.1126/scitransmed.aaf8781>
- Windmueller, R., Leach, J. P., Babu, A., Zhou, S., Morley, M. P., Wakabayashi, A., Petrenko, N. B., Viatour, P., & Morrissey, E. E. (2020). Direct Comparison of Mononucleated and Binucleated Cardiomyocytes Reveals Molecular Mechanisms Underlying Distinct Proliferative Competencies. *Cell Reports*. <https://doi.org/10.1016/j.celrep.2020.02.034>



APPENDICES

Acknowledgements

Curriculum vitae

List of publications

ACKNOWLEDGEMENTS

Over the past few years, I have had the pleasure of meeting and learning from a great number of people. Due to their enthusiasm and love for science, this thesis is now a reality.

First and foremost, I would like to thank **Jeroen Bakkers**, my supervisor and mentor. Jeroen, thank you so much for supporting me throughout my PhD project. You have always stimulated me to think for myself and express creativity in my work. Your obvious enthusiasm for science and excellent supervision have made my time in your research group one of the best experiences of my life. You have inspired me to pursue my own career in academia and form a great example of the type of scientist I would one day like to be (albeit with better table tennis and foosball skills!).

I would also like to thank the rest of the Bakkers people. The vibe in the group has always been excellent – helpful, cheerful and supportive – and it was a true pleasure working with you all. **Sonja**, sharing an office with you was so much fun! It was great to discuss our everyday lives and scientific frustrations, while sporadically enjoying the first-drawer delights together. **Federico**, you were always the first person for me to ask a question to, particularly when being confused about fresh-from-the-press results. The question “Can you have a look at this and tell me what you see” (without any context) was my favorite question to give and get – this is where true science happens! Now, it’s time to share my gratitude with the various members of the legendary R-squad! **Phong**, your arrival in the lab was a turning point for me. Through your critical look, vast knowledge, helpful spirit and often unique viewpoints, I think you played one of the most influential roles in the establishment of this thesis. Indeed, through your input I decided on how to interpret results, which candidate genes to follow up on (like Hmga1!) and which conferences to attend to. Malta was a definite highlight of my PhD! **Hessel**, I could of course say most of the same things about you. It was an absolute pleasure working with you every day. One of my first steps when interpreting results was to ask what you thought about it. Our discussions were where a lot of my ideas and interpretations were formed. In a way, you could say you were the Dirk Kuyt of my scientific soccer team! Next, I would like to mention the future of the R-squad: Olga and Mara. **Olga**, our overlap in the group has been short, but I think your energy and enthusiasm is going to benefit the group greatly! **Mara**, I am really grateful to have had you as my student. You really pushed the Prrx1b story to what it is today and I am truly impressed by your practical and theoretical excellence. I have no doubt you are going to do great in your own PhD project! The final member of the squad I would like to thank is its founder. **Fabian**, it has been a while since we worked together, but what I have learned from you in the beginning has formed the foundation of my work. I still vividly remember the first time you showed me how to perform cryoinjuries – I was thankful for having such a calm and expert instructor (in science and in the gym!). I always greatly enjoyed our CrossFit sessions, which of course we did together with Sven and Laurence. **Sven**, I remember us being completely destroyed by deadlifts (me) and squads (you). No

pain no gain! You are the true master of “that’s what she said” and I hope that becoming a responsible dad will not stop you from making your fantastically childish, awesome jokes. **Laurence**, I hope all is well in France and that you are able to make more people enjoy lying silently on the floor (the best part in any yoga session, right guys? ^^). Seriously though, thanks for yoga classes and the times we were invited into your apartment to eat cheese and chill! I also would like to thank **Silja** and **Emily**. I remember that as a student at the Hubrecht institute, you were the core of the Friday night drinks. I’m sad to say that after you guys left, we were not able to keep it going until 03.00 in the morning (at least not at the Hubrecht), but you showed me how it’s done for sure! I like to think that you guys inspired me to take an active part in the Friday drinks throughout my PhD! Next up on the thank you list is **Yesamin Bovenwater**. You really changed the atmosphere in the group with your cheerfulness and social skills! It was great to have you in the group and it was a pleasure supplying you with green ginger tea! **Melanie**, you are one of the most warm-hearted and kind people I know. It was always great to talk to you about personal stuff, and when I was a bit down you could always make me feel better with a talk and a hug. Thanks for that! I’m certain that like in your job as communication officer, you will truly excel at being a mom! When thinking about Melanie, of course her BFF **Lotte** comes to mind. I have always been a bit jealous of how well you have your stuff organized. So efficient! In my current job, I’m trying to “pull a Lotte” as many times as I can. Also, I miss having someone around to blurt out “blblblblblblbl!” to anytime I see them in the hallway! About hallway rituals. **Sarah**, we have probably fake-murdered each other over a 1000 times in the corridors, which I always took as a sign of intellectual connectedness. Or at least, dumbassery which I really enjoyed. I would also like to “thank” you for helping me grow as a person (physically, that is, due to your constant supply of chocolate and candy). Last, I would like to thank all of the students of the Bakkers group! Special notice go out to (of course) **Kim**, my first student who has genotyped more fish than I thought was possible and was a great presence in the group. Also, I’d like to thank **Daniël**, my first thesis-student. You have a great brain for science, you always impressed me with your excellent questions and theories. **Eva**, thanks for the music exchange and the zebrafish-pic, **Carlijn** for taking care of Hessel, **Iris** for taking care of Phong (in a different way) and all the other students that I remember but do not want to list in full in case I forget someone... Thanks guys!

Already from the start of my PhD project I worked closely together with members of the Christoffels group. First of all, I would like to thank **Vincent** himself of course. Thank you for your guidance throughout my projects, the feedback during the Cobra meetings and of course the reference letters you have written for me! I would also like to thank various members of the Christoffels group. **Rob**, you were my first collaborator outside of the Bakkers group and you helped to make the start of my project really exciting. **Karel**, you have been a great help with the bioinformatics throughout my project. It’s really great to have a bioinformatics expert like you around to ask for advice! **Marie**, thanks for the *in situ*’s

and all the fun surrounding the COBRA consortium. **Joyce**, I always enjoyed thinking and discussing about the enhancer project with you! I would also like to thank **Jan Ruijter** for his help with the qPCR statistics and the fun conversations about Australia!

I would also like to thank all the members of the COBRA3 consortium. Through our collaboration and shared meetings, I really felt a strong connection with the clinical side of the research. This has greatly impacted my work and my outlook on science in general, and I always felt a boost in motivation after our meetings. In particular, I would like to thank **Wim** for playing an important role in setting up the consortium and **Beatrijs** for her input on my work during our discussions. **Jelle, Guido, Marie, Eva** and **Vivian**: It was really great working together with you and going to the conference in Marseille together. This was a definite highlight of my PhD! **Jelle**, it was really great to help you organize the Masterclass. **Guido**, I loved our discussion on interpreting our data and science in general. **Eva** and **Vivian**, I'm really happy I got to work together with you guys! I still vividly remember the PULSE conference where you went on an active campaign to get the post votes for our poster: you got us close to winning!

For me, one of the most fun parts about working in academia are the collaborations. I had the pleasure of collaborating with a lot of great scientists, including **Esther Dronkers**. I still remember you coming to my poster at the retreat of the Heart Foundation and showing interest in the epicardial expression of *hmga1a*. With your enthusiasm you convinced me of the importance of the epicardium during regeneration and our ongoing (and fruitful) collaboration was a source of energy for me throughout my projects. Thank you so much for that! I also want to thank **Anke Smits** and **Marie-José Goumans** for their input on the Prrx1b story.

Leaving Leiden, I'd like to thank the people on the other side of the planet that really helped me initiate and realize the *hmga1a* chapter of the thesis: **Jan Kaslin** and **Danny Colquhoun** from Melbourne. Danny, it was great to collaborate with you and I really enjoyed meeting you during your visit to the Hubrecht! Thanks again for sharing the mutants and your valuable insights.

I would also like to give a special thanks to **Aryan Vink**, my go-to pathologists for human tissues at the UMCU. Your passion for research and your willingness to collaborate and hypothesize about clinical and fundamental concepts really gave an extra (and really cool) dimension to my research. **Petra**, thanks for the great interaction and all the technical support throughout the years! I would also like to thank **Naomi** for the collaboration on the tbx-story (this seems already decades ago!).

In my opinion, what makes the Hubrecht a great place to work at is the option to approach

almost anyone (for instance at the Friday drinks, after the lunch meetings or at the coffee machine) and ask them for their advice, input and potential help and reagents. I have had many great interactions like that, which really helped me to move my projects forward or sprouted interesting side projects. In that theme, I would like to thank half of the van Rooij group including **Eva** herself for the valuable input, **Danielle** for the huge amount of mouse work (thank you so much!), **Lieneke** for the qPCRs, **Martha** for the NRCM experiments, **Kees** for the help with the ATAC-seq optimization and general advice, **Monika** for the valuable input on making transgenic mice and immunohistochemistry and of course **Bas** for our intellectual deliberations on whether it should be fish > mouse or mouse < fish. I would also like to thank **Carolien** (thanks for the help with the ChiPI!), **Yorick, Johan**, the Bartscherer group members including **Kerstin** herself for the input on my projects during our shared lab meetings, **Henriette** (your positivity and enthusiasm is awesome, keep that going!) **Tim** (your project always intrigued me), **Elke, Vanessa, Rutger, Divyanshu** and **Antonio**. I also would like to thank all the (ex-)members of the de Laat group, I always enjoyed sharing a lab with you guys. In particular, I would like to thank **Peter** for his help with some of the cloning (not my favorite part!) and **Geert** for really helpful valuable advice on bioinformatics.

In the Netherlands, we have a saying: Better a good neighbor than a friend far away. This is definitely true if I consider the Hertog group. Although we never really collaborated on a project, I could always drop by for some sugar (= anything ranging from restriction enzymes to PCR machines). First of all, I would like to thank **Jeroen** for being on my advisory committee and providing me with valuable feedback. **Jelmer**, you are as modest as you are smart (which is very), I've always been impressed by your knowledge and expertise. **Sasja**, thanks for being my co-mentor and aquarium tour-guide – I always enjoyed our interactions (and thanks for not killing me when I was sitting on your injection machine when you were pregnant ^^'). I would also like to thank **Wouter** for the always uplifting vibes at the coffee machine, **Petra** for being Petra, **Maja** for keeping an eye on Phong in my absence, **Maike** for staying positive and showing great character after making a million non-phenotype mutants and **Xudong** for the friendly hello's in the corridors. Last but not least, I would like to thank **John** for his invaluable support, "can do" spirit and expertise on anything lab related, as well as our many great conversations!

I would also like to thank all of the Hubrecht supporting staff. Special thanks goes to the animal care takers keeping my fish alive and happy. **Erma**, thanks for the many years of patient advices and tips, pleasant conversations as well as keeping the baby facility organized and efficient! **Bert, Luuk** and **Martijn**, thanks for the great atmosphere and the grill-skills over the years! I really appreciated the conversations we had, it was always fun to go down to the aquarium! **Mark**, thanks for steering the boat, your support and positive attitude made working with animal models organized and practical.

Of course, I also need to thank the histology duo, Jeroen and Harry. **Harry**, thanks so much for all the help, advice and reagents over the years. Your expertise really helped bringing my research to the next level. **Jeroen**, thank you so much for all the practical help and advice. Your creativity and passion for the job are an inspiration to me and talking about the interface between art and science was a true pleasure. Also thanks to the IT-team, **Robin** in particular, for always being there when I needed support (which was a lot over the years!).

This brings me to the extensive list of people who I've met on the legendary TGIF's, many of which I now call my dear friends. I'm going to just do the shout-outs, otherwise this thesis will contain more acknowledgement pages than scientific ones. You know I love you all! **Rob de Bob** (Vieux is nog steeds smerig, maar thx voor alle hulp in het aquarium en de goede feestjes!), **Alex** (The Greek Chimney, you want to hug me...), **Alex** (de dude. Hoop dat alles goed gaat man!) **Anne** (de Leeuw, hoog gewaardeerde buurvrouw), **Clement** (Daft punk 4 ever), **Roxanne** (Sleeping beauty), **Iliana** (it was great seeing you in Athens! We miss you!), **Wessel** (wil weer terug naar zweden man!), **Erica** (Miss Fox. Miss you!), **Zunamys** (see you in east-Germany!) **Niels**, **Euclides** and **Lorenzo** (I miss our times in the open air), **Bart** (voor de vele goede gesprekken, de over-all bro-mance en het in de gaten houden van Peggy), **Juri** (Boardgames, city park sessions – the best of moments), **Merlijn** (Schulte-merker five), **Yara** (ga corona nou eens oplossen...), **Kim** en **Anna** (always a pleasure talking to you guys!), **Valerie** (fungi are awesome!), **Stijn** and **Deepak** (foosball colleagues) and **Tim** (foosball God and nemesis. You made me crawl too many times...), **Ajid** (woof woof, brother), **Mauro** (also for the help with the SCSeq and cool time travel riddle sessions), **Wouter** (for keeping Juri alive and the great beats), **Judith**, **Christian**, **Yike**, **Walter**, **Tim** (Boardgames and Pertubator!), **Jens**, **Bas** (PV held), **Bas** (Muis man) en **Bas** (Mariokart), **Susanne**, **Jelte**, **Antonio**, **Sanne Sunshine**, **Lotte** (paranymph scooper), **Corina**, **Annabel** (keep nurturing that inner science nerd!) **Guy**, **Christa** and all the Hubrecht PI's to join the TGIFs to give the right example and of course, the civil service team (shout out to **Elroy**) to help with the organization. I'm sure there are many others that I should thank for my awesome time at the Hubrecht. To those, I would like to say the following (based on a quote from Bilbo Baggins). Six years is far too short a time to live among such excellent and admirable scientists. I don't know half of you half as well as I should like, and I like less than half of you half as well as you deserve.

I would also like to thank my old mentors who helped forming me as a scientist and have instilled in me my passion for science. I did not make it easy for them at times, but they never gave up on me and pushed me to keep trying. You guys form the foundation of my view on science. **Ben Bouchet**, thank you so much for taking me on as a bachelor student and introducing me to the world of biomedical sciences. **Andreas van Impel**, thank you so much for introducing me to the zebrafish world and helping me develop myself into a scientist.

Furthermore, I would like to thank my new mentor **Dario** – I am so thankful that you accepted me in your group, it has been a great experience so far! I would also like to thank **Jan** and **Madelon** de Boer for the pleasant dinners, and for forming a great example of how to successfully mix the demanding science- and family-life!

With that, I will go to the acquired-family section of the acknowledgements. Shout-out to my brothers, **El-grandmaster_P**, **Yip-delux**, **Game-boy Joos**, **Bari** (MBN JWZ), **Meester Bas**, **waterpijp-Youri**, **de Gekker Ier**, **Ben-G**, **Wimme**, **Suki**, **Jonas-brother** and **Gregor Sheer Genius** (thanks so much for always being a mere button click away!).

(Ver)Ward, thanks so much for your help with the thesis cover! Also, thanks for the Groutars studio production donning the Hubrecht reception area, having you around at the Hubrecht was really great. I hope we can work together more in the future! **Sebasterd**, I really loved how close we were during our shared time in Utrecht. Our gym-sessions, boardgames and chill-sessions were true highlights of the past years. You played a central role in my life for the past years, which has made it so much better.

That brings me to my dear paranymphs. Thank you guys so much for your help with arranging everything surrounding the PhD ceremony, I could not have done it without you! **Erik**, it was bro-mance on first sight when I met you. I'm unable to not laugh at your jokes and I love how you have integrated into the boardgame-bros. Being at the TGIF and after parties together was really awesome. **Kinan**, the rough Diamond, getting you as my neighbor was such a blessing. We went through life together in a truly unique way – morning coffees, balcony sessions, evening series with food n stuff, romantic dramas, Dublin, Hassan's stay as well as many many others... I have met so many amazing people through you! Your hard work and vision are a true inspiration for me and I am very grateful to have you in my life!

With that, I would like to thank my amazing girlfriend **Peggy**. Thank you for all your support in the sometimes stressful times, you make my life so much brighter! I can't wait to start our adventure in Jena!

Dad, thank you so much for your support and your critical perspective. I like to think that I inherited your creativity and love for fish, which I needed to realize this thesis. I really like how our relationship has developed over the years! **Anouk**, you are my big example: both in life and in science. When I struggle with something big, I can always rely on your advice and help. I could not wish for a better big-sister! **Mom**, your love and support are always with me and give me strength when I need it. You are always with me, so I'm ready for whatever comes next!

CURRICULUM VITAE

Dennis Eduard Maria de Bakker was born on June 4th 1991 in Middelburg, the Netherlands. Dennis attended his secondary school at the CSW Elzenlaan, where he obtained his degree in 2009. In the same year, he enrolled into the Bachelor program Biology at the Utrecht University which he completed in 2013. Inspired by the courses in Cell biology and Developmental biology, as well as his Bachelor internship in the lab of Prof. dr. Anna Akhmanova, he decided to enroll into the research Master program Cancer, Stem cells and Developmental Biology at the University of Utrecht in 2013. For his first research internship, he joined the lab of Prof. dr. Stefan Schulte-Merker at the Hubrecht institute to investigate the process of vascularization during the embryonic development of zebrafish. For his second internship, he moved abroad to the lab of dr. Julie Canman at Columbia University in New York city, where he studied the cell divisions during *C. elegans* vulva precursor cell development. After obtaining his Master degree in 2015, he started his PhD in the group of Prof. dr. Jeroen Bakkers to study zebrafish and mammalian heart regeneration at the Hubrecht institute. His project was funded by the Dutch heart foundation as part of the COBRA3 consortium, which allowed him to work together with clinical researchers. Since 2021, Dennis is working as a post-doc in the group of dr. Valenzano, first at the Max Planck Institute for the Biology of Ageing (Cologne, Germany) and currently at the Leibniz Institute on Aging – Fritz Lipmann Institute (Jena, Germany), where he is conducting research into age-related neurodegeneration in killifish.

LIST OF PUBLICATIONS

de Bakker DEM*, Bouwman M*, Dronkers E, Simões FC, Vink A, Riley PR, Goumans MJ, Smits AM, & Bakkers J. (2021). Prrx1b restricts fibrosis and promotes Nrg1-dependent cardiomyocyte proliferation during zebrafish heart regeneration. *Development*, in press.

Nguyen PD*, **de Bakker DEM***, Bakkers J (2021). Cardiac regenerative capacity: an evolutionary afterthought? *Cellular and Molecular Life Sciences*, 1(3).

Tessadori F, **de Bakker, DEM***, Barske L*, Nelson N, Algra HA, Willekers S, Nichols JT, Crump JG and Bakkers J. (2020). Prrx1a is dispensable for cardiac looping morphogenesis in zebrafish. *Nature* 585, E14–E16.

Honkoop H*, **de Bakker DEM***, Aharonov A, Kruse F, Shakked A, Nguyen PD, de Heus C, Garric L, Muraro M, Shoffner A, Tessadori F, Peterson JC, Noort W, Bertozzi A, Weidinger G, Posthuma G, Grün D, van der Laarse WJ, Klumperman J, Jaspers RT, Poss KD, van Oudenaarden A, Tzahor T, Bakkers J. (2019). Single-cell analysis uncovers that metabolic reprogramming by ErbB2 signaling is essential for cardiomyocyte proliferation in the regenerating heart. *ELife*, 8, 1–27.

van Duijvenboden K*, **de Bakker DEM***, Man JCK*, Janssen R*, Günthel M*, Hill MC, Hooijkaas IB, van der Made I, van der Kraak PH, Vink A, Creemers EE, Martin JF, Barnett P, Bakkers J, & Christoffels VM. (2019). Conserved NPPB+ Border Zone Switches From MEF2- to AP-1-Driven Gene Program. *Circulation*, 140(10).

Chrispijn ND, Elurbe DM, Mickoleit M, Aben M, **de Bakker, DEM**, Andralojc KM, Huisken J, Bakkers J & Kamminga LM. (2019). Loss of the Polycomb group protein Rnf2 results in derepression of tbx-transcription factors and defects in embryonic and cardiac development. *Scientific Reports*, 9(1).

* these authors contributed equally to this work

MANUSCRIPTS IN PREPARATION

Günthel M, van Duijvenboden K, **de Bakker DEM**, Hooijkaas IB, Bakkers J, Barnett P, Christoffels VM. (2021). Epigenetic state changes underlie metabolic switch in mouse post-infarction border zone cardiomyocytes. Under review at *Journal of Cardiovascular Development and Disease*.

de Bakker DEM, Nguyen PD, Honkoop H, Colquhoun D, Vigil-Garcia M, Versteeg D, Kooijman L, Janssen R, Hooijkaas IB, Günthel M, Christoffels VM, Kaslin J, van Rooij E, Bakkers J. (2021). Interspecies comparison reveals Hmga1 as a driver of cardiac regeneration. In preparation.

